OXIDATIVE DAMAGE TO GUANINE IN DNA CAUSED BY REACTIVE OXYGEN SPECIES

Wenjie Ye

A dissertation submitted to the faculty of the University of North Carolina at Chapel Hill in partial fulfillment of the requirements for the degree of Doctor of Philosophy in the Department of Environmental Sciences and Engineering, Gillings School of Global Public Health.

Chapel Hill

2008

Approved by:

Dr. Louise M. Ball

Dr. Avram Gold

Dr. Karupiah Jayaraj

Dr. Stephen Chaney

Dr. Karl Koshlap

Dr. Carol Parker

ABSTRACT

WENJIE YE: Oxidative Damage to Guanine in DNA Caused by Reactive Oxygen Species
(Under the direction of Dr. Louise M. Ball)

Oxidative damage to DNA, a factor in cancer, mutation, and aging, is attributed to reactive oxygen species (ROS). The less well characterized ROS, organic peroxyl radicals and peracid are present during lipid peroxidation and also produced by peroxidases from organic hydroperoxides. Peracetic acid is also formed in mitochondria. Guanine (Gua) is the nucleobases most susceptible to oxidation due to its lowest electron potential. The study described here focuses on Gua oxidation by epoxidizing reagents including peroxyl radicals and organic peracids. Dimethyldioxirane (DMDO), peracetic acid and *m*-chloroperbenzoic acid selectively oxidizes the guanine moiety of dGuo, dGMP and dGTP to 5-carboxamido-5-formamido-2-iminohydantoin (2-Ih). Structures were established on mass spectrometry and NMR studies. Labeling studies support a mechanism involving initial epoxidation of the guanine 4-5 bond and contraction of the pyrimidine ring by a 1,2-migration of the guanine carbonyl C6 to form a transient dehydrodeoxyspiroiminodihydantoin followed by hydrolytic ring opening of the imidazolone ring. The 2-Ih is shown to be a major transformation in the oxidation of the single-stranded DNA 5-mer *d(TTGTT)* and the 5-base pair duplex *d*[*(TTGTT)·(AACAA)*]. 2-Ih has not previously been reported as an oxidative lesion in DNA. Consistent with the proposed mechanism, no 8-oxoguanine was detected as a product of the oxidations of the oligonucleotides or monomeric species mediated by the monooxygen

donors. The 2-Ih base thus appears to be a pathway-specific lesion and holds promise as a potential biomarker.

*N*9-(β-D-2-deoxyribofuranosyl)-N^2,3-ethenoguanine is a highly mutagenic DNA adduct arising from exposure to known occupational and environmental carcinogens and lipid peroxidation products *in vivo*. Chemical synthesis has proven to be challenging because of the reported lability of the glycosidic bond under conditions generally applicable to chemical synthesis. Enzymatic and chemical glycosylations of N^2,3-ethenoguanine were attempted as approaches to obtain this nucleoside under mild conditions. Both glycosylations led to nucleosides with ribosylation at positions corresponding to *N*7- and N^2 of the Gua framework. A minor product of the enzymatic ribosylation has tentatively been assigned as the α-anomer of the desired *N*3 riboside, and rigorous confirmation of this structure would demonstrate an unusual stereochemistry for the *trans* ribosylation.

ACKNOWLEDGEMENTS

I would like to acknowledge the advice and guidance of Dr. Louise M. Ball, committee chairman. I also thank the members of my Ph.D. committee, Dr. Karupiah Jayaraj, Dr. Stephen Chaney, Dr. Karl Koshlap, Dr. Carol Parker for their guidance and suggestions, especially Dr. Avram Gold for all his advice and encouragement. I also thank the members of the superfund groups in ESE, who contributed to the development of this work, particularly Dr. Ramiah Sangaiah, Diana E. Degen, Dr.Gunnar Boysen, Lina Gao and Leonard B. Collins, without whose knowledge and assistance this study would not have been successful.

I acknowledge the Superfund Basic Research Program for the financial support for this project.The important enzymes for this study were provided by Lannes Steven E. Ealick's Lab. in Department of Chemistry and Chemical Biology of Cornell University and Pierre Alexandre Kaminski in Institute Pasteur in Paris. I appreciate their support.

I would like to thank my family members, especially my mom, daddy and husband, Xinming Cai for supporting and encouraging me to pursue this degree. Without their encouragement, I would not have finished the degree. Finally, I have to say thank you to my little baby, Perry Cai.

TABLE OF CONTENTS

LIST OF TABLES

Table

LIST OF SCHEMES

Scheme

LIST OF CHARTS

Chart

LIST OF THE FIGURES

Figure

LIST OF ABBREVLATIONS

DGh	Dehydroguanidinohydantoin
dGuo	2'-Deoxyguanosine
dGMP	2'-Deoxyguanosine-5'-monophosphate
dGTP	2'-Deoxyguanosine-5'-triphosphate
DRTases	*N*-Deoxyribosyltransferases
-CH_2-	Methylene
dIz	2-Amino-5-(2-deoxyribosylamino) imidazolone
DMDO	Dimethyldioxirane
dZ	2,2-Diamino-5-(2-deoxyribosylamino)-5(2H)-oxazolone
ETC	Electron transport chain
Gh	Guanidinohydantoin
Gua	Guanine
Guo	Guanosine
H_2O_2	Hydrogen Peroxide
HOCl	Hypochlorous acid
2Ih	5-Carboxamido-5-formamido-2-iminohydantoin
*m*CPBA	*m*-Chloroperbenzoic acid
MS	Mass Spectrometry
N^2, 3-εdGuo	8,9-Dihydro-9-oxo-3-(*β*-D-2-deoxyribofuranosyl)-imidazo[2,1-b]purine
N^2, 3-εdGuo	*N9*-(β-D-2-deoxyribofuranosyl)-N^2,3-ethenoguanine

N^2, 3-εGua	N^2,3-ethenoguanine
NA	Nature abundance
NMR	Nuclear Magnetic Resonance
NO	Nitric oxide
$O_2^{\bullet-}$	Superoxide
$ONOO^-$	Peroxynitrite
PDT	Purine deoxyribosyltransferase
RO	Alkoxyl
ROO	Peroxyl
ROOH	Organic hydroperoxides
ROS	Reactive oxygen species
SOD	Superoxide dismutase
Sp	Spiroiminodihydantoin
VC	Vinyl chloride

I. Literature Review

1.1 Oxidation pressure in vivo

Oxidative stress is a physiological condition that occurs when there is a significant imbalance between production of reactive oxygen species and antioxidant defenses. In humans, oxidative stress is involved in many diseases, such as atherosclerosis, Parkinson's disease and Alzheimer's disease[Valko M. et al, 2005], but it may also be important in prevention of aging by induction of a process named mitohormesis. ROS can be beneficial, as they are used by the immune system as a way to attack and kill pathogens. ROS are also used in cell signaling. This is dubbed redox signaling. A particularly destructive aspect of oxidative stress is the production of ROS, which include free radicals and peroxides. Some of the less reactive of these species (such as superoxide) can be converted by oxidoreduction reactions with transition metals or other redox cycling compounds (including quinones) into more aggressive radical species that can cause extensive cellular damage. [Valko M. et al, 2005] The major portion of long term effects is inflicted by damage on DNA [Evans M.D. et al., 2004]. Most of these oxygen-derived species are produced at a low level by normal aerobic metabolism and the damage they cause to cells is constantly repaired.

1.1.1 Sources of the endogenous and exogenous oxidizing species

1.1.1.1 Sources of the endogenous oxidizing species

The production of oxidizing species occurs through a variety of endogenous processes which was summarized in the following paragraphs and Table 1.1[Williams, G. and Jeffrey, A.2000], [Frenkkel, 1992].

Oxidizing species are even produced daily during normal respiration by the mitochondrial respiratory chain and during the production of energy by each and every mitochondrion. Therefore, one may consider oxidative stress a necessary outcome of physiological functions such as respiration, digestion, and metabolism.

NADPH oxidase, the best characterized source of ROS, several other enzymes may contribute to ROS generation, including nitric oxide synthase, lipoxygenases, cyclo-oxygenases, xanthine oxidase and cytochrome P450 enzymes [Williams, G. and Jeffrey, A.2000].

In addition, metals and certain fatty substances can also cause oxidative stress. Metals (i.e., iron copper) acting as pro-oxidants and fatty substances (carbon-based molecules reacting with oxygen) undergoing lipid peroxidation are prime examples in which oxidative stress is accentuated.

1.1.1.2 Sources of the exogenous oxidizing species

Exogenous sources, like radiation, ozone, xenobiotics etc. [Williams, G. and Jeffrey, A., 2000], also can increase the level of the ROS. One cause of oxidative stress includes the redox cycling of toxins called xenobiotics. This occurs during drug or contamination metabolism and can cause oxidative stress from a variety of methods. Many inorganic

substances, particularly iron, chromium, cobalt(II), and nickel salts in the presence of hydrogen peroxide, have been long recognized as forming oxidized bases in DNA [Klein et al.,1991; Nackerdien et al., 1991; Standeven et al., 1991].Other cause of increased free radical generation occurs if the toxin increases damage by interfering with the antioxidant defenses. Finally, the toxin can also stimulate more free radical generation by damaging the mitochondrial electron transport system.

1.1.2 Types of ROS

1.1.2.1 Superoxide Radical

The $O_2^{\bullet-}$ is created by the reduction of oxygen to form superoxide (O_2 - e = O_2^-). This oxygen-centered free radical is formed by autoxidation reactions or by the mitochondrial electron transport chain (ETC). It is not reactive unless it comes in contact with other radicals, such as nitric oxide (NO), or certain metals, such as iron. O_2^- undergoes dismutation in the presence of superoxide dismutase (SOD) to form H_2O_2 (2 O_2^- + 2 H^+ = H_2O_2 + O_2). This radical is highly selective and has beneficial and damaging effects to tissues. It is considered a vital part of the cellular signaling pathways that provide important genetic information [Salo D.C., et al, 1990].

1.1.2.2 Hydrogen Peroxide

Many enzymes can generate H_2O_2, including xanthine, urate, and several protein oxidases. In fact, any biologic system that generates O_2^- also produces H_2O_2. Although H_2O_2 is considered a nonradical because it has paired electrons, it is an important biologic molecule. H_2O_2 can degrade certain haem proteins (ie, myoglobin, hemoglobin) to release iron. The reaction of H_2O_2 with metals like iron is called the Fenton reaction, and it can generate more dangerous free radicals. Furthermore, the additional reduction of Fe III by

O_2^- can accelerate the Fenton reaction, giving an O_2^--assisted Fenton reaction ($H_2O_2 + O_2^-$ (Fe/Catalyst) = $OH^- + OH + O_2$) [Halliwell B. 2003].

1.1.2.3 Hydroxyl Radical

This more potent hydroxyl radical ($^{\bullet}OH$) is often generated during the Fenton reaction, forming peroxynitrite ($ONOO^-$) from NO acid reacting with oxygen and from ionizing radiation. This radical attacks and damages most cellular components [Mandelker L., 2008].

1.1.2.4 Hypochlorous Acid

Hypochlorous acid (HOCl) is highly reactive and lipid soluble. It is formed from H_2O_2 and the enzyme myeloperoxidase. It is especially dangerous to protein constituents, in which it can oxidize and damage biomolecules [Mandelker L., 2008].

1.1.2.5 Alkoxyl Radicals/Peroxyl Radicals

Alkoxyl (RO) radicals/peroxyl (ROO) radicals are organic radicals formed from lipid peroxidation reactions. They are not stable; thus, they react readily with molecular oxygen, thereby creating a ROO or RO fatty acid radical. The new radicals are also unstable and can react with other free fatty acids molecules, producing more fatty acid radicals and H_2O_2. This is a chain reaction mechanism and stops only when forming a nonradical species. Certain antioxidants, such as vitamin E, can stop the "chain reaction" seen with the formation of these free radicals [Aikens J., et al, 1991], [Kyaw M.,et al, 2004].

1.1.2.6 Organic hydroperoxides

Organic hydroperoxides (ROOH) Formed by radical reactions with cellular components such as lipids and nucleobases, which will be discussed in detail at following text (3.1.3 Lipid peroxidation).

1.1.2.7 Peracid

Peracids (RC(O)OOH) may arise biologically during lipid peroxidation, through formation of triplet excited ketones and aldehydes by the Russell mechanism [Russell, G. et al, 1957] followed by β-cleavage and coupling with O_2, by peroxidase-catalyzed autoxidation of aldehydes [Adam, W., Kurz, A. et al, 1999], or by aldehyde oxidation catalyzed by transition metals [Nam, W. et al, 1996]. In mitochondria, three ThDP-dependent enzymes (S. typhimurium ALS II, Baker's yeast pyruvate decarboxylase and Zymomonas mobilis pyruvate decarboxylase) have been shown to catalyze the formation of peracetic acid [$CH_3C(O)OOH$] from pyruvate and O_2 under certain conditions [Abell, L. M. et al, 1991], [Bunik, V. I. et al, 2007], an observation that is significant because mitochondrial DNA repair capability appears to decrease with age [Ledoux, S. P. et al, 2007], [Croteau, D. L. et al, 1999] and accumulated of mutations are implicated in age related neuropathology and the ageing process in general [Dimauro, S. et al, 2005].

1.1.3 Lipid peroxidation

Lipid peroxidation refers to the oxidative degradation of lipids. It is the process whereby free radicals "steal" electrons from the lipids in cell membranes, resulting in cell damage. This process proceeds by a free radical chain reaction mechanism. It most often affects polyunsaturated fatty acids, because they contain multiple double bonds in between which lie methylene ($-CH_2-$) groups that possess especially reactive hydrogens. Lipid peroxidation, which may be initiated by radicals generated in both endogenous processes and

by metabolism of exogenous chemicals, has been recognized since the 1980s as an important contributor of reactive oxygen species involved in genotoxic endpoints. The primary species generated during lipid peroxidation are lipid hydroperoxides. From polyunsaturated lipids with 3 or more double bonds, cyclic peroxides and endoperoxides can also be generated [Yin, H. et al, 2005].

The hydroperoxides can yield alkylperoxyl and alkoxy radicals via redox reactions mediated by transition metals both within and external to the cellular environment [Aoshima, H. et al, 1997] (Scheme 1.1, eq 1, 2).

Peroxyl radicals also result from the coupling of allyl radicals with molecular oxygen following H• abstraction from lipids in the initiation step of lipid peroxidation (Scheme 1.1. , eq 3, 4). In addition, a variety of oxy radicals and other oxidizing species are generated during the peroxidation process. The reactions are summarized in (Scheme 1.1, eq 5–10). Coupling of peroxyl radicals in a chain terminating reaction can yield singlet oxygen or triplet excited ketones and aldehyded [Miyamoto, S. et al, 2006], [Miyamoto, S. et al, 2003] (Scheme 1.1 ,eq 6, 7) by the Russell mechanism[Russell, G. A. et al,1957]. The triplet ketones can, in turn, undergo α-cleavage to acyl radicals (Scheme 1.1 ,eq 8), and subsequent coupling with O_2 leads to peracyl radicals (Scheme 1.1. , eq 9) and peracids (Scheme 1.1, eq 10) [Adam, W. et al, 1999], [Adam, W. et al ,2001], [Adam, W., Nau, W.M. et al, 2001] .

1.2 Reactions between oxidizing species and guanine, guanosine and deoxyguanosine.

ROS can induce plenty of covalent modification to DNA, which encompass single-nucleobase lesions, strand breaks, inter and intrastrand cross-link, along with protein-DNA

cross-link [Evans, M.D. et al, 2004]. Since the focus of this proposal is damage to guanine, the Background review will not be concerned with the other kinds of damage to the DNA. Oxidation of dGuo by hydroxyl radical, one-electron abstraction and $^1O_2$ has been the focus of considerable work and the results covered in several recent reviews [Neeley W. L. et al, 2006], [Tudek, B. et al, 2003].

1.2.1 Oxidation of Guanine by hydroxyl radical

Products of reaction with hydroxyl radical are postulated to result from initial addition to the base, summarized in Scheme 1.2. Addition at C8 leads to 8-oxodGuo following oxidation or to a formamido pyrimidine (FAPyG) following reduction. Hydroxyl radical can also add to the C4-C5 bond. Addition at C4 is calculated by several methods to be favored over addition to C5 [Colson, A. et al, 1997]. Dehydration of the neutral radical adduct at C4, followed by oxidation, leads to 2-amino-5-(2-deoxyribosylamino) imidazolone (dIz) and subsequently to 2,2-diamino-5-(2-deoxyribosylamino)-5(2*H*)-oxazolone (dZ).

In addition to hydroxyl radical, one-electron abstraction from dGuo is accomplished by other radical species, including NO•, $SO_4^{\bullet/-}$, and a variety of transition metal complexes that have been investigated as probes for one-electron oxidation or as potential antineoplastic drugs. (Cr^{V} [Sugden, K. D. et al, 2002], Cr^{VI}, Mn^{II}, Fe^{III}, Co^{II}, Ni^{II} and Cu^{II} [Choi, S. et al, 2004]) and ionizing radiation. The radical cation resulting from one-electron oxidation of dGuo deprotonates at physiological pH to a neutral radical with substantial spin density calculated to reside at positions C5 and C8 [Hole, E. O. et al, 1987].

1.2.2 Oxidation of Guanine by superoxide anion

Addition of superoxide anion ($O_2^{\bullet/-}$) to the C8 or C5 followed by protonation gives the corresponding hydroperoxides. The C8-hydroperoxide leads to 8-oxodGuo under reducing conditions and the C5-hydroperoxide leads to dIz and dZ (Scheme 1.3.). Reaction of the Gua radical at C8 or C5 with O_2, gives the corresponding peroxyl radicals and, following hydrogen abstractions, the C8 or C5 hydroperoxides, which follow the respective pathways summarized in Scheme 1.3.

1.2.3 Oxidation of Guanine by singlet oxygen

dGuo undergoes a 2 + 4 cycloaddition with singlet oxygen to form a transient 4,8-endoperoxide, which rearranges to 8-hydroperoxy-dGuo. The hydroperoxide then reacts via two pathways (Scheme 1.4.) : (A) reduction to 8-oxodGuo and a 2+ 2 addition of a second molecule of $^1O_2$ to form the 4,5-endoperoxide [Neeley W. L. et al, 2006] which rearranges to 5-hydroperoxy-8-oxodGuo leading to dZ, via dehydroguanidinohydantoin (DGh); (B) decomposition to 8-oxodehydro-dGuo followed by addition of water leading to Sp and Gh through the transient 5-hydroxy-8-oxodG. It may be remarked that formation of the endoperoxides is formally a two-electron oxidation.

Recently, a diminoimidazole has been reported as a minor product [Suzuki, T. et al, 2003] directly from the reaction of dGuo with $^1O_2$.

1.2.4 Oxidation of Guanine by peracyl and peroxyl radicals

While research efforts have focused on the damage caused by the hydroxyl radical, $^1O_2$, and one-electron oxidations, other oxidizing species generated during the reactions that

produce ROS (Scheme 1.1. , eq 4, 6, 7, 9, 10) have received less attention. The proposed research is directed at elucidating the role of peracids in ROS-mediated DNA damage, through the characterization of base modifications and mechanisms of oxidation.

Oxidation of dGuo by a mixture of peracyl and peroxyl radicals generated either by photolysis of ketones or thermolysis of dioxetanes [Adam, W. et al, 2001] or by peroxyl radicals generated from hydroperoxides by the action of *Coprinus* or horseradish peroxidases [Adam, W. et al, 2000] yielded Sp (incorrectly identified as 4-OH-8-oxodGuo) and "guanidine releasing" products (not characterized further). 8-oxodGuo was identified in trace quantities, but was determined to be further oxidized under the reaction conditions, implying that it was an important intermediate [Adam, W. et al, 1995]. Interestingly, dGuo 4, 5-epoxide is a transient in the proposed mechanism [Adam, W. et al, 2001]. In the horseradish peroxidase-catalyzed oxidation of dGuo by isobutanal, the active oxidants were concluded to be the peracid and peracyl radical [Adam, W. et al, 1999]. Peroxyacyl radicals and peracids are also generated during the autoxidation of aldehydes. In support of this conclusion, *m*-chloroperbenzoic acid (*m*CPBA) alone or in the presence of the enzyme efficiently oxidized dGuo. dZ and dIz were the only products identified in this work, although they accounted for at most 50% of the dGuo consumed. Under the experimental conditions, no 8-oxodGuo was detected. *m*CPBA has been reported to modify dGuo and dAdo residues in ssDNA and to generate modified nucleotides having altered moblilities from dGMP and dAMP [Jacobsen, J. S. et al, 1986]. However, the investigators did not characterize either the DNA lesions or the modified bases. Although reaction schemes have been proposed for the oxidation of dGuo by peroxyacyl/peroxyl radicals, the mechanisms of oxidation are completely speculative. No mechanistic schemes have been proposed for the peracid-mediated oxidation.

1.2.5 Oxidation of Guanine by metal complexes

In addition to two-electron oxidations of dGuo by peracids and $^1O_2$, a two-electron oxidation of dGuo mediated by an oxoruthenium complex has been reported and of dGMP by Pt^{IV}(1,2-diaminocyclohexane). The latter oxidation yielded 8-oxodGuo via intramolecular donation of a phosphate oxygen to C8. Of interest with regard to the work proposed here is the oxidation of guanine in short dsDNA by a Mn^{III}(porphyrin)/$KHSO_5$ system. On the basis of mass spectrometric analysis of the modified DNA, the major product corresponded to a gain of 34 amu by Gua (G + 34), and was tentatively identified as 5,8-dihydroxy-7,8-dihydroGua via two-electron oxidation of Gua and deprotonation to a cation [Vialas C. et al, 2000]. Mechanistic studies of Foote [McCallum J.E.B et al., 2004], [Sheu C. et al, 1993], [Sheu C. et al, 1995] on the transients generated during oxidation of Gua and 8-oxoGua by $^1O_2$, argue strongly against the likelihood of the proposed structure because of the lability of 5-hydroxy-substituted guanine and 8-oxoguanine. An alternative structure for the G + 34 product is 4-carboxamido-4-formamido-2-iminohydantoin, identified by our laboratory as the two-electron oxidation product of Gua by dimethyldioxirane [Ye W. et al, 2006]. As discussed in the following section.

1.2.6 Oxidation of Guanine DMDO

Dimethlydioxirane (DMDO) is a three-membered cylic peroxide that efficiently transfers oxygen and reacts selectively [Adam W. et al., 1989]. The preparation method of DMDO reported in the literature yields a 0.1M solution [Adam W. et al., 1987]. DMDO demonstrates efficient transfer of oxygen through a single concentrated step [Edwards et al., 1979]. DMDO can be applied as a good model agent for 2-electron epoxidation in the

research of the DNA oxidation, not only because of the reasons mentioned above, but also the characteristic is low temperature, no residue of oxidant, short time and mild pH value which mimics the environment in vivo and provides the convenience for purification and analysis.

Oxidation of Gua and dGuo by DMDO has been studied with regard to its use in DNA sequencing by selectively introducing piperidine-labile lesions at guanine in both ss- and dsDNA [Davies J. R. et al, 2002], [Davies J. R. et al, 1990]. Following 2-minutes of DMDO treatment and appropriate workup, samples of ss- and ds-DNA underwent selective strand breakage at the guanine sites observed with the Maxam-Gilbert procedure, indicating efficient and selective oxidation of Gua bases. Preliminary oxidations of Gua and dGuo were carried out to characterize the lesions; however, the reaction mixtures were worked up by heating for 5 h at 85 ^{o}C prior to chromatographic isolation of products [Davies J. R. et al, 1990], [Ye W. et al, 2006]. Guo and dGuo both yielded 4-amadinocarbamoyl-5-hydroxyimidazole, but the product from dGuo was substituted at C2 with the deoxyribose-derived trihydroxy-*n*-butyl group. Both products are at the same oxidation level as the starting bases. Evidently, prolonged heating of the crude reaction mixture resulted in the reduction and, in the case of dGuo, rearrangement. The investigators proposed that DMDO initially epoxidized the C4-C5-bond of dGuo, by analogy with DMDO epoxidation of C5-C6 of the pyrimidine ring of 5′-*O*-trityl-dThyd [Lupatelli, P. et al, 1993].

Since peracids and the peroxyacyl and peroxyl radicals can epoxidize double bonds [Reed G.A. et al, 1990], [Dix T.A. et al, 1983] [Lang B. et al, 1986], we propose DMDO as a convenient model to investigate the role of epoxidation by these transient ROS in oxidations

of dGuo.

1.3 Basic information of the N^2,3-εGuanine

1.3.1 Formation of the etheno nucleobase in vivo

Among exocyclic DNA adducts, ethenobases have been most widely studied in the last 33 years, as this class of DNA lesions is formed by many genotoxic chemicals including the human carcinogen vinyl chloride (VC) and the multi-species carcinogen urethane [Bartsch H. et al, 1994]. Ethenobases were first described by Kochetkov et al. [Kochetkov N. K. et al, 1971] who identified them as reaction products of 2-chloroacetaldehyde with adenine and cytosine. Interest in the ε-lesions was renewed in 1975 when it was found that they were generated in vitro by the vinyl chloride metabolites, chloroethylene oxide and 2-chloroacetaldehyde (Scheme 1.5.) [Barbin A. et al, 1975], [Laib R.J. et al, 1977], [Laib R.J. et al, 1978]. Using replication and transcription fidelity assays and ε -modified oligo- or polynucleotides, it was established that εdA and εdC have miscoding or ambiguous base pairing properties [Barbin A.et al, 1981], [Hall J.A. et al, 1981], [Spengler S. et al, 1981] and thus could be involved in the mutagenic and carcinogenic effects of VC [IARC, 1979], [Barbin, H. et al, 1986].

In the 1990s, ε -adducts have received renewed attention, because background levels of etheno adducts have been detected in tissues from unexposed humans and rodents, suggesting an alternative, endogenous pathway of formation (Figure 1.1.) [Nair J., Barbin A. et al,1999]. This background which can be affected by dietary factors could arise from the reaction of lipid peroxidation products such as *trans*-4-hydroxy-2-nonenal via its 2,3-epoxy-intermediate with nucleic acid bases [Nair J., Vaca C.E. et al, 1997] (Scheme 1.6.).

Subsequently, it was shown that high intake of dietary ω-6 –polyunsaturated fatty acids by female volunteers greatly increased LPO-derived etheno-DNA adducts in white blood cells in vivo [Fang J.L., Vaca C.E. et al, 1996]. Further, elevated levels of ε -adducts were found in hepatic DNA from patients and rodents with genetic predisposition to oxidative stress, lipid peroxidation and increased risk of liver cancer due to metal storage disease [Nair J., Sone H., et al 1996]. Also, during inflammatory processes a cascade of reactive Oxygen/nitrogen intermediates can be generated, that could lead directly to oxidative DNA damage and/or to formation of ε -adduct via reaction of bifunctional 4-hydroxyalkenals and epoxides derived from LPO (Figure 1.2)

1.3.2 Significance of *N*9-(β-D-2-deoxyribofuranosyl)-N^2,3-ethenoguanine

N9-(β-D-2-deoxyribofuranosyl)-N^2,3-ethenoguanine(8,9-dihydro-9-oxo-3-(β-D-2-deoxyribofuranosyl)-imidazo[2,1-*b*]purine) is a one of highly mutagenic etheno DNA adduct both in vitro and in vivo research [Bartsch H., Barbin A. et al, 1994], [Kochetkov N.K. et al, 1971], [Nair J., Barbin A.et al, 1999]. 8,9-dihydro-9-oxo-3-(β-D-2-deoxyribofuranosyl)-imidazo[2,1-*b*]purine in DNA is therefore of considerable interest as a biomarker of exposure and in studies of molecular mutagenesis. Several labs have reported the level of N^2, 3-εG both in human and rat tissue. During the analyses of vinyl chloride induced DNA-adducts in rats, using a specific GC-MS method, a peak co-eluting with the internal standard identified as the pentaflurobenzyl derivative of N^2, 3-εG was detected as background in untreated rat liver at levels 60±40 fmols (9±6 adducts/10^8 G) [Fedtke, N. et al, 1990] assuming that the level reported was based on the analysis of 1 mg DNA. Using a LC-MS method, N^2, 3-εG was detected in one human liver sample at 60 fmol/mg DNA (9–10 adductsr$10^8/G^2$) [Yen, T.Y. et al, 1996] while a level of 70 fmol/μmol G (7 adducts/10^8 G)

[Scheller, N. et al, 1995] was reported, using a GC-MS method. However, the same laboratory reported that εG formed from endogenous sources occurred at a much higher level in 10/10 human liver samples (means of 3 and range from 0.7–7 per 10^7 G) [Swenberg, J.A. et al,1995].

1.3.3 Synthesis of *N*9-(β-D-2-deoxyribofuranosyl)-N^2,3-ethenoguanine

Quantitative analysis of DNA adducts requires both unambiguously characterized standards and on occasion, labeled isotopomers. Preparation of certain classes of deoxynucleoside adducts can be problematic because instability of intermediates under conditions of established synthetic routes, deglycosylation at low pH or elevated temperature often present particular difficulties. Chemical synthesis of 8,9-dihydro-9-oxo-3-(β-D-2-deoxyribofuranosyl)-imidazo[2,1-*b*]purine has proven to be challenging precisely because of the reported lability of the glycosidic bond under conditions generally applicable to chemical synthesis [Barbin A., Brěsil H.et al, 1975], [Laib R.J., Bolt H.M., 1977], [Laib R.J., Bolt H.M., 1978].

Several labs reported the synthetically routes of N^2,3-εdGuo (8,9-dihydro-9-oxo-3-(β-D-2-deoxyribofuranosyl)-imidazo[2,1-*b*]purine). Kuśmierek et al [Kuśmierek, J. T. et al, 1989] introduced an O^6-benzyl group to N^2,$O^{3'}$,$O^{5'}$-triacetyl-2'-deoxyguanosine by using the Mitsunobu reaction. After deacetylation with sodium methoxylate/methanol in dioxane, the resulting *O*6-benzyl-2'-deoxyguanosine was phosphorylated the target compound starting with O^6-benzyl-2'-deoxyguanosine-5'-phosphate. Then bromoacetaldehyde was drop inside at pH 8.5-7.5 which prevented significant loss of the sugar. Finally, the monophosphate derivative was treated by phosphatase to gain the corresponding nucleoside. The routes of synthesis were shown in the Scheme1.7. However, the overall yield of this method is only

1% if we try to use the labeled dGuo as the starting material to synthesize the internal standard for quantitative analysis.

Johnson's Group [Khazanchi R. et al, 1993] described a route starting in the riboside series. O^6-Benzylguanosine when treated with bromoacetaldehyde under conditions of continuous buffering gives the N^2,3-etheno derivative in 48% yield. The 3',5'-*O*-(1,1,3,3-tetraisopropyldisiloxa-l,3-diyl) derivative when allowed to react with phenyl chlorothionoformate led to the corresponding 2' ester**.** 2'-Deoxygenation of **10** by the Barton procedure then afforded 65 % of **11,** and deprotection of the latter (BuN+F^-) gave **12** quantitatively. Catalytic hydrogenation of **12** then produced pure N^2,3-εdGuo in 86% yield.(see scheme 1.8.). The overall yield of this route is still lower than 5%. The synthetic route of this procedure is too long which will lead the synthesis of internal standard unpractical because of the high price of the labeled starting material.

N-Deoxyribosyltransferases (DRTases) [Anand, R. et al, 2004] catalyze the transfer of a 2'-deoxyribosyl group from a donor deoxynucleoside to an acceptor nucleobase. DRTases can be divided into two classes on the basis of their substrate specificity. The DRTase I class (also called purine deoxyribosyltransferase (PDT)) is specific for the transfer of deoxyribose between two purines. The DRTase II class (also called nucleoside deoxyribosyltransferase) catalyzes the transfer of deoxyribose between either purines or pyrimidines, but has a strong preference for deoxypyrimidines as the donor. DRTase was applied in the synthesis of *N9*-(β-D-2-deoxyribofuranosyl)-N^2,3-ethenoguanine in Guengerich' s Lab[Müller, M. et al, 1996]. A mixture of 25 μg of partially purified *trans*-*N*-deoxyribosylase protein and 5.3 mM dCyd (as the deoxyribose donor) in a total volume of 1.0 mL of 0.1−0.5 M potassium 2-(*N*-morpholino)ethanesulfonate buffer (pH 6.0) and

containing 0.3−0.5 mM N^2,3-ethenoguanine, dissolved either in 50−100 μL of 0.1−1 N HCl. Incubations proceeded for 15 h (under Ar), then products were separated by HPLC and analyzed by UV, ^{1}H NMR and mass spectrometry. They reported the difference between the N9:N7 (using the numbering system for Gua) coupling ratios is 92:8 for N^2,3-ε-dGuo. However, the apparent fraction linked at the N9 atom instead of N7 was only estimated from ^{1}H NMR measurements, using the chemical shifts of the sugar protons as a guide.

Scheme 1.1 Generation of oxidizing species in vivo

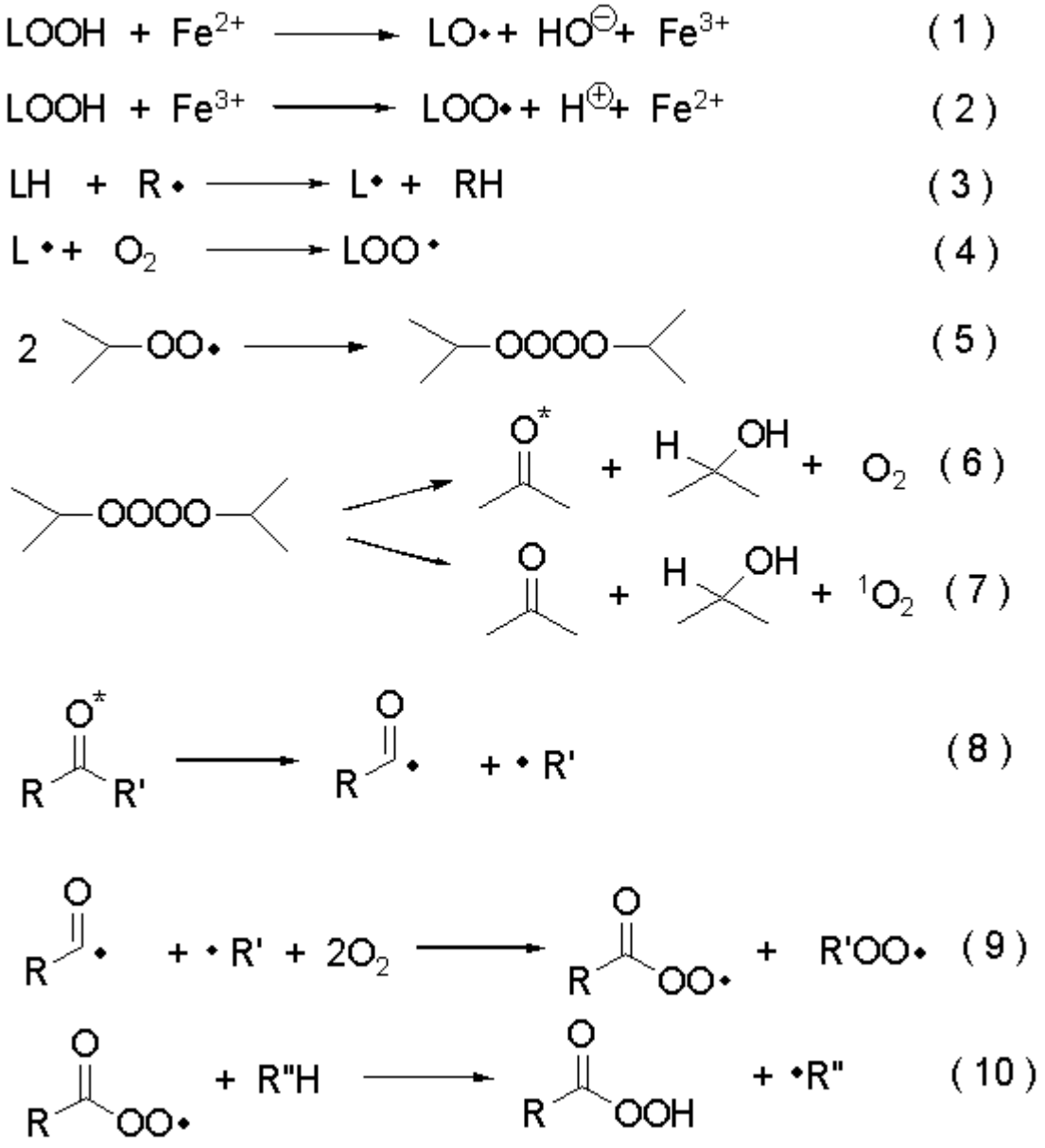

Scheme 1.2 Oxidation of Guanine by hydroxyl radical

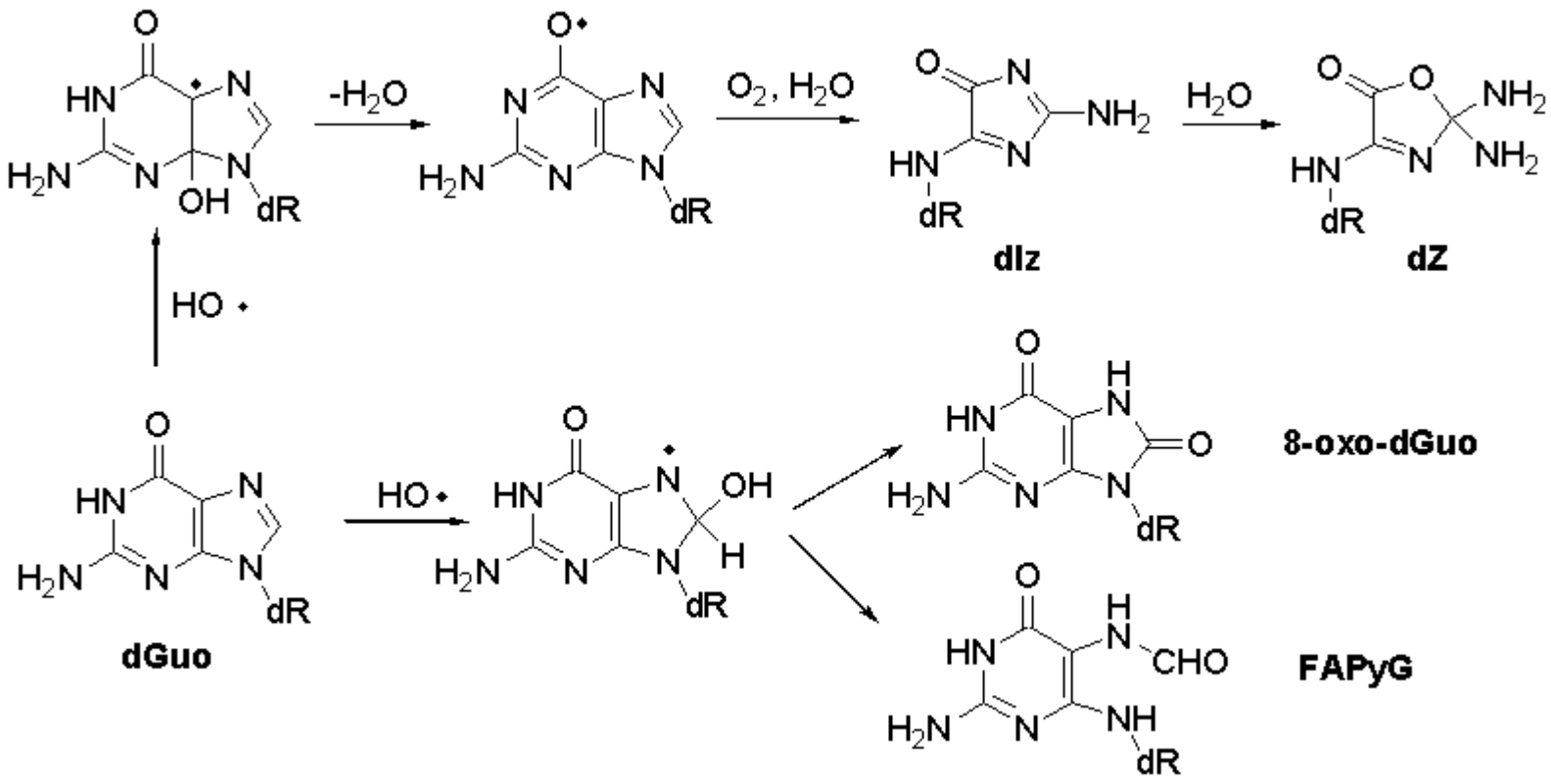

Scheme 1.3 Oxidation of Guanine by superoxide anion

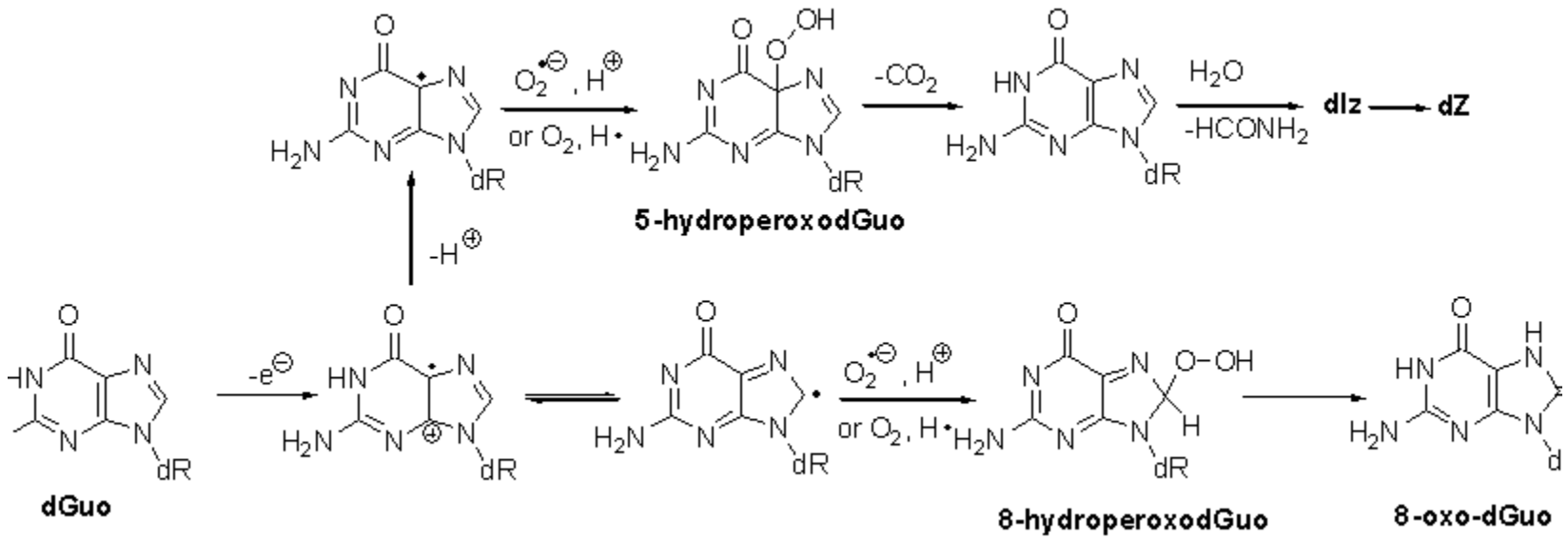

Scheme 1.4 Mechanism of oxidation of guanine by singlet oxygen

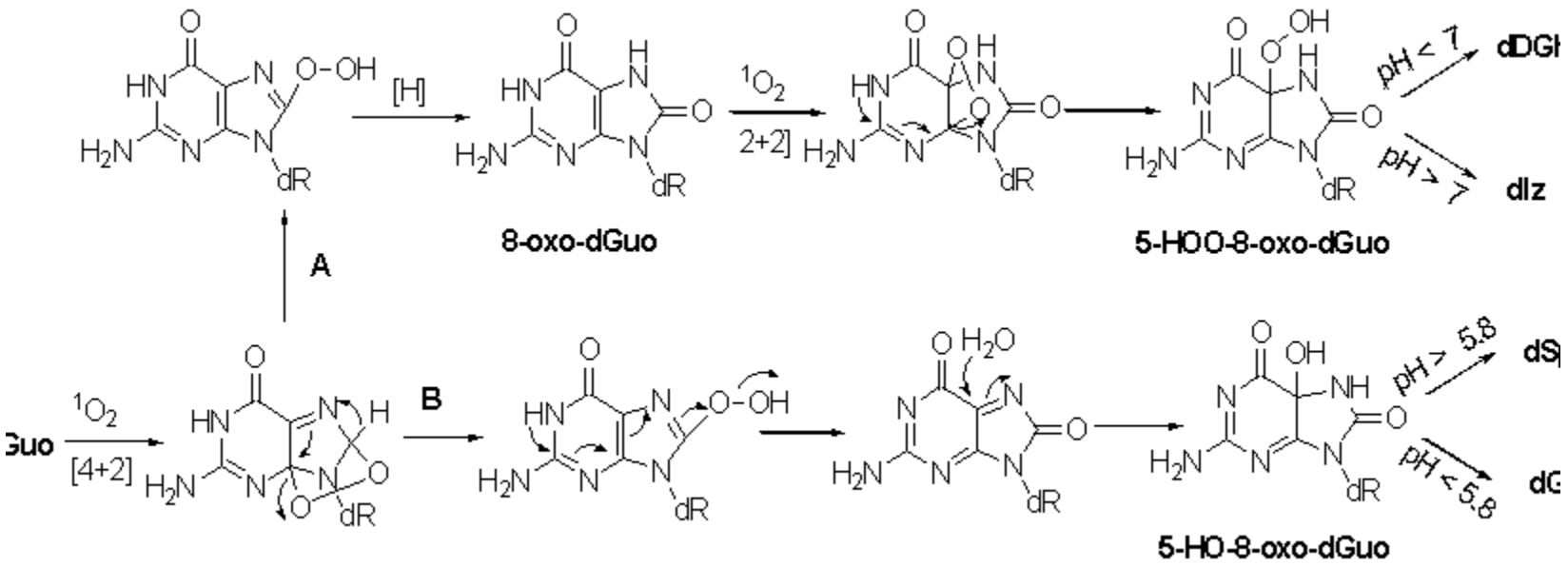

Scheme 1.5 Enzymatic oxidation of vinly chloride to 2-chlorooxirane and rearrangement to $ClCH_2CHO$ and design of experiments for in situ destruction of reactive intermediates

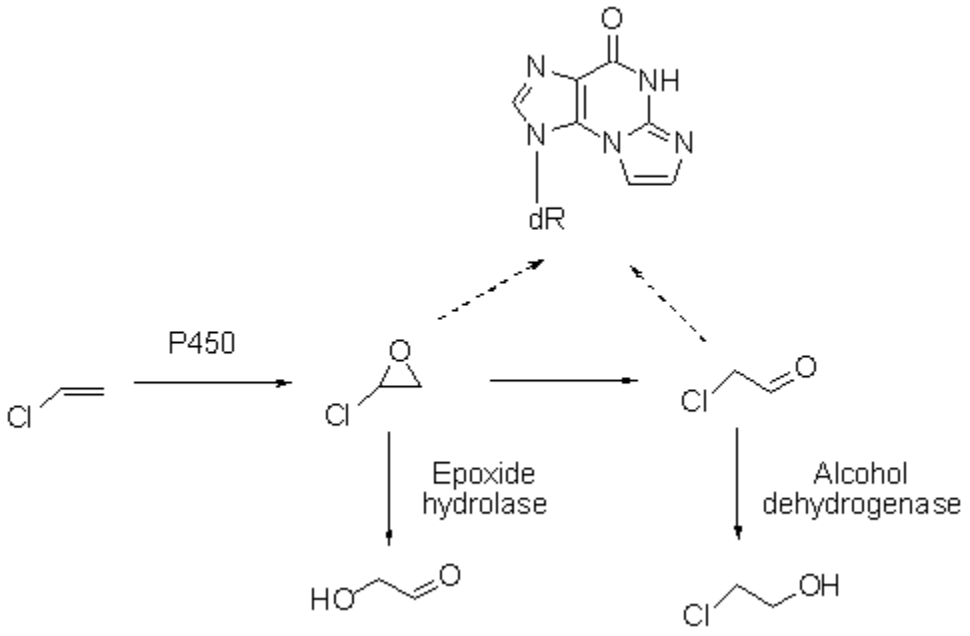

Scheme 1.6 Possible Mechanism of Formation of N^2,3-εGua from 2-Substituted Oxiranes

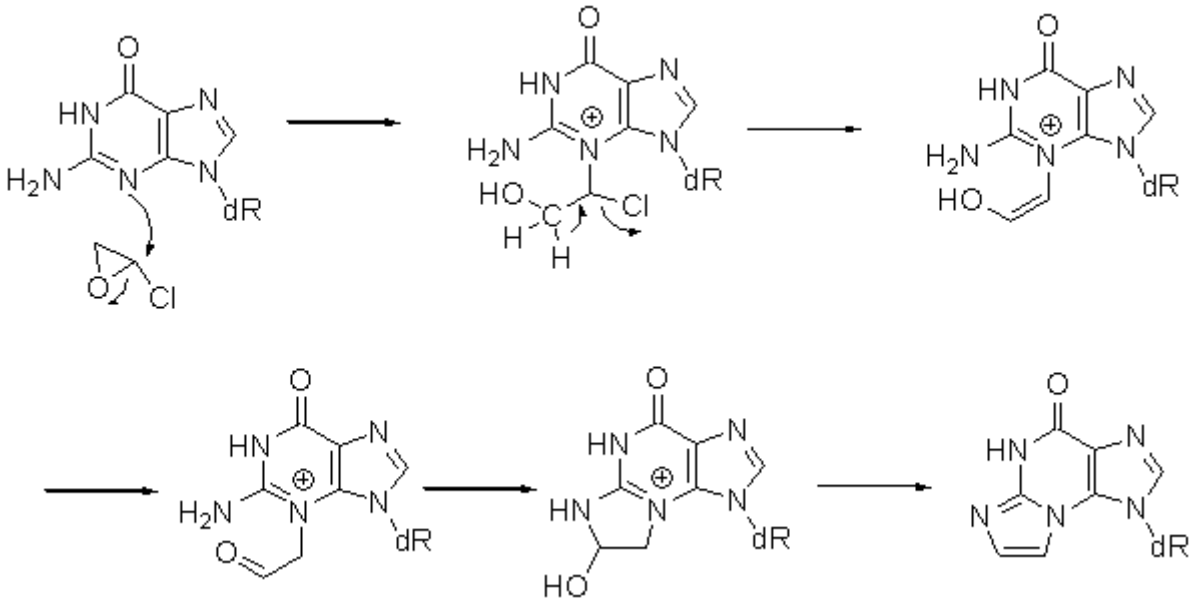

Scheme 1.7 Kuśmierek's synthetic routes of N^2,3-εdGuo [Kuśmierek, J. T. et al, 1989]

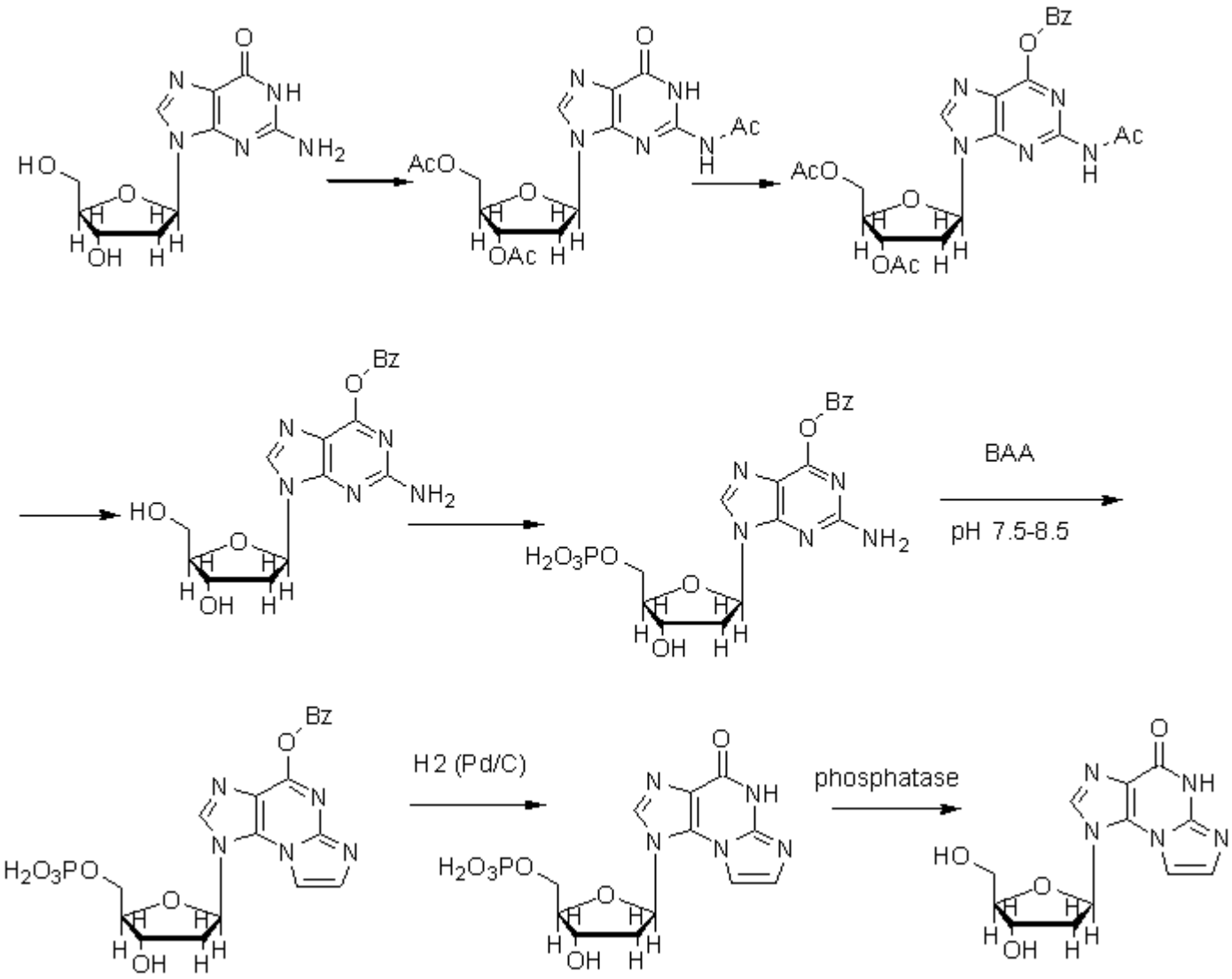

Scheme 1.8 Khazanchi's synthetic routes of N^2,3-εdGuo [Khazanchi R. et al, 1993]

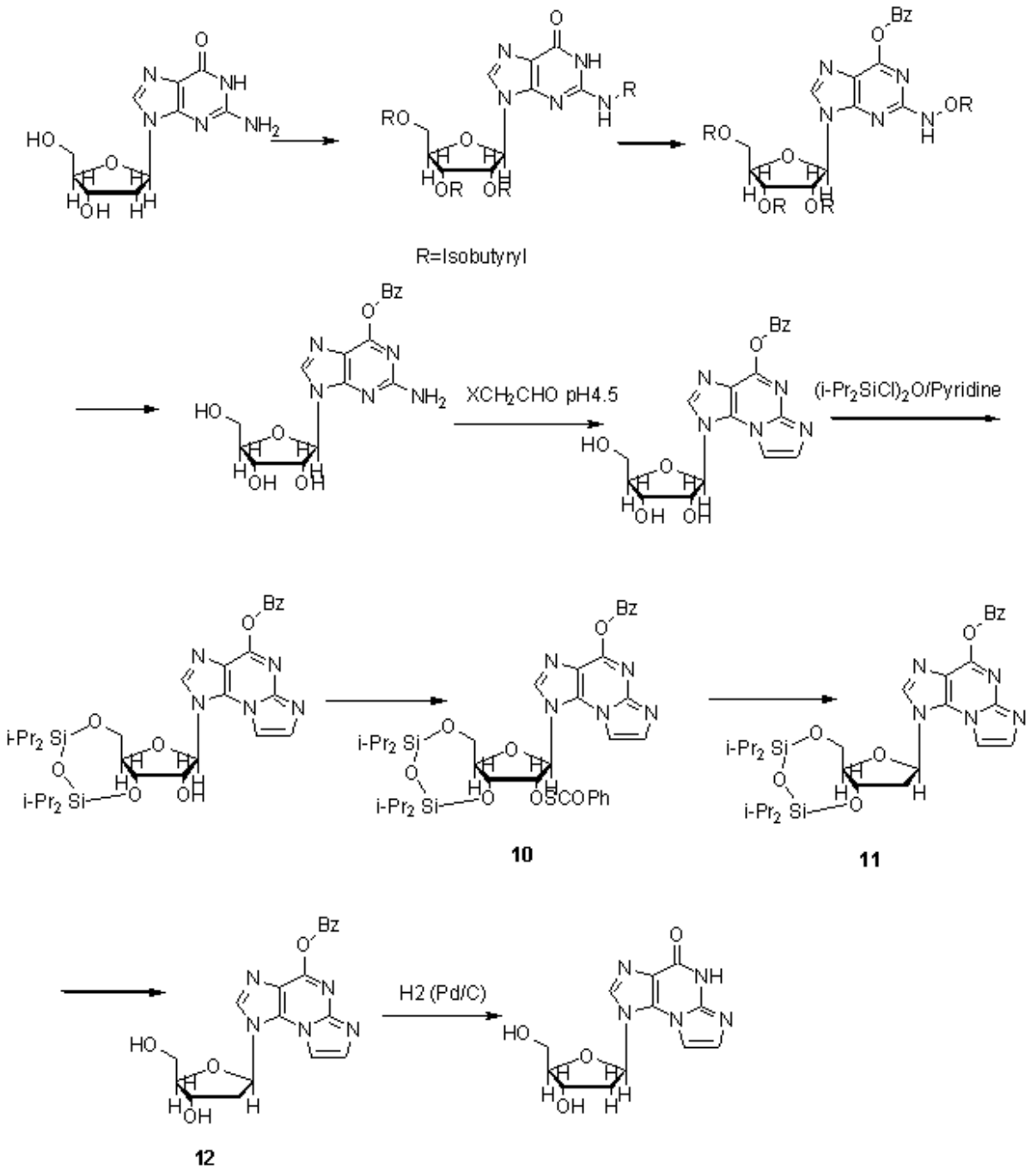

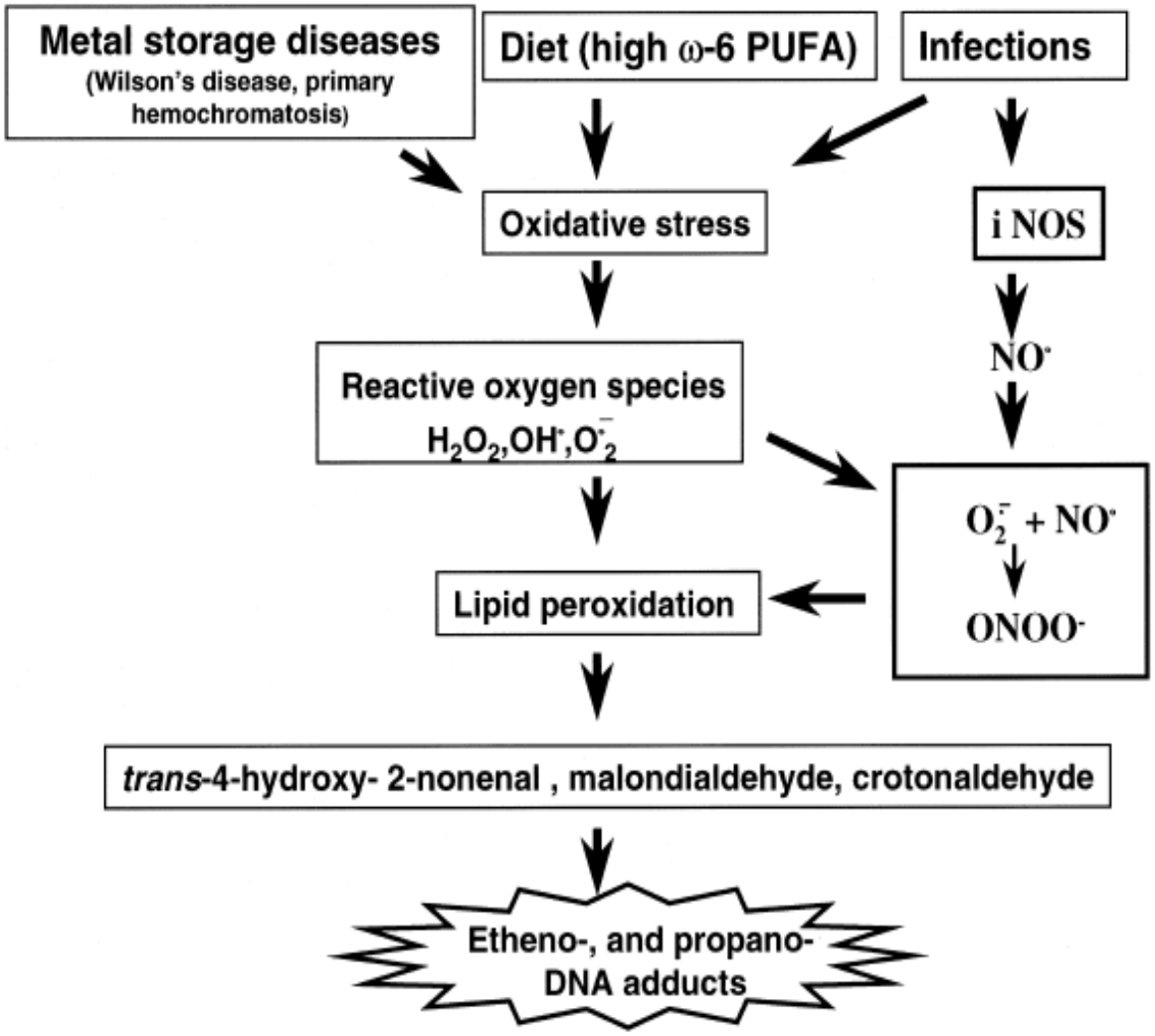

Figure 1.1 A hypothetical scheme for carcinogenic factors leading to endogenous species and exocyclic DNA-base damage [Nair J., Barbin A. et al,1999]

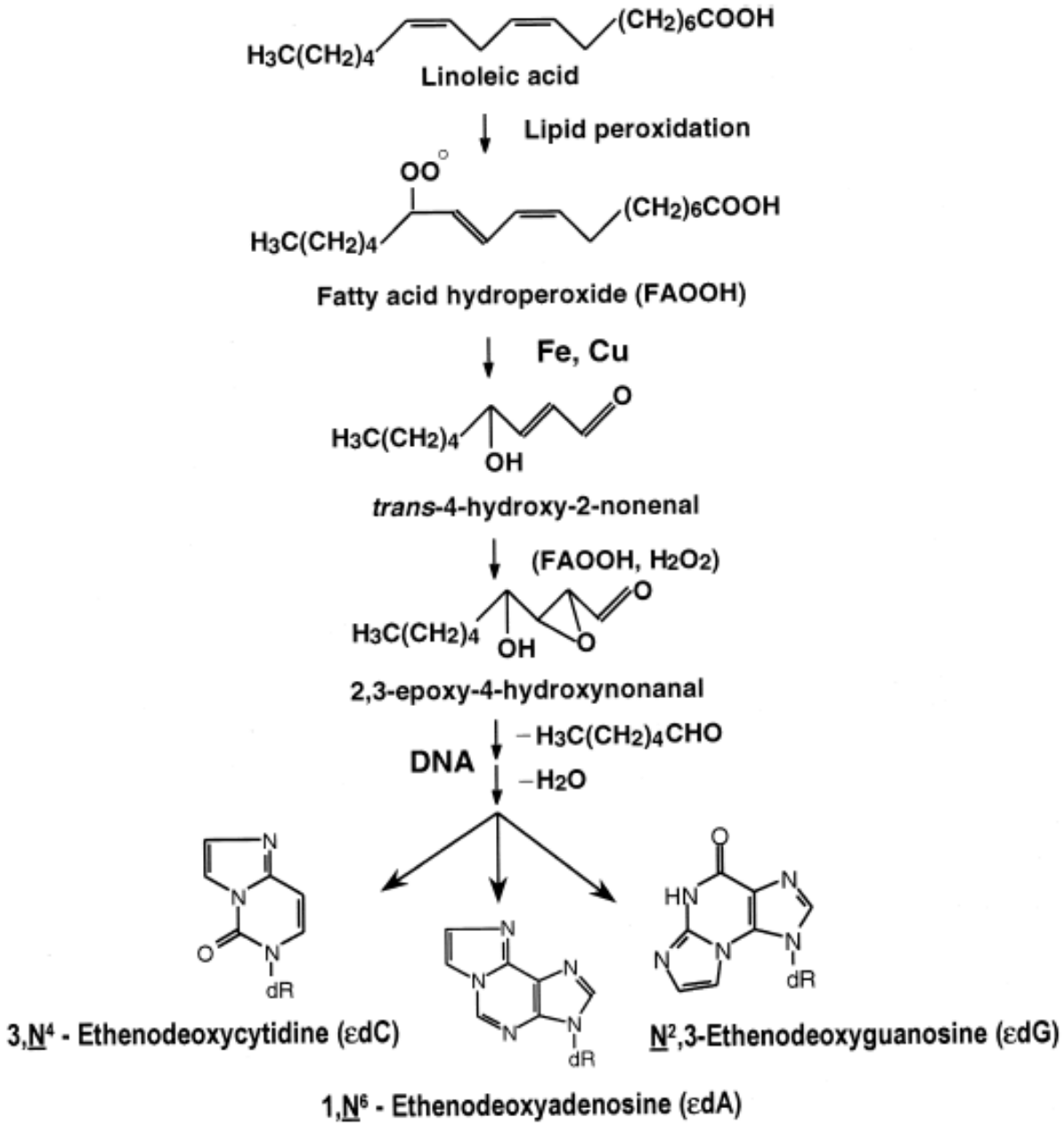

Figure 1.2 Suggested mechanism for the formation of etheno adducts from DNA nucleosides and LPO products such as trans-4-hydroxy-2-nonenal derived from PUFAs, as exemplified fro linoleic acid, a ω-6 PUFA (dR=deoxyribose)

Table 1.1 Process leading to generation of ROS [Williams, G. and Jeffrey, A.2000], [Frenkkel, 1992]

1. Cellular Respiration
—Mitochondrial electron transport
—Hexose monophosphate shunt
2. Biosynthetic and biodegrading processes of normal intermediary metabolism
—Arachidonic acid metabolism
—b-Oxidation of high-molecular-weight fatty acids (fatty acid CoA oxidase)
—Amino acid oxidation (D-amino acid oxidase, tyrosine oxidase, etc.)
—Iron metabolism
—Ascorbic acid biosynthesis (L-gulonolactone oxidase: absent inhumans)
—Polyamine oxidation
—Steroidogenesis
—Purine oxidation (urate oxidase: absent in humans, xanthine oxidase)
3. Biotransformation of xenobiotics
—Microsomal electron transport (cytochrome P450 and b_3)
—Other mixed function oxidases
—Peroxidative oxidation (myeloperoxidase, prostaglandin H synthetase)
4. Activation of phagocytic cells by natural stimuli
—Peripheral blood leukocytes
—Tissue macrophages
—Kupffer cells (liver)
—Clara Cells (lung)

II. Oxidation of Guanine by Epoxidizing Reagents

2.1 Abstract

Oxidative damage to DNA, of concern as a factor in cancer, mutation, and aging, is attributed to reactive oxygen species. Organic peroxyl radicals, known to be present during lipid peroxidation and also products of the action of peroxidases on organic hydroperoxides, have received much less attention. Guanine (Gua) is the most susceptible to oxidation due to the lowest electron potential in all of nucleobases. This chapter focuses on Gua oxidation by epoxidizing reagents. The structure of the product of Gua oxidized by epoxidizing model agent, dimethyldioxirane (DMDO), 5-carboxamido-5-formamido-2-iminohydantoin (2-Ih, Chart 2.1) was established on the basis of mass spectrometry and NMR studies on 2-Ih and its isotopomers generated by the oxidation of [4-^{13}C] and [7-^{15}N] guanine. The mononeric species dGuo, dGMP and dGTP were oxidized to study the reaction mechanism and to characterize fully the oxidation products. The DMDO selectively oxidizes the guanine moiety of dGuo, dGMP and dGTP to 2-Ih (see Chart 2.1 and Scheme 2.2), peracetic acid and *m*-chloroperbenzoic acid also oxidize the base moiety of dGuo to 2-Ih. The presence of the glycosidic bond results in the stereoselective induction of an asymmetric center to give a mixture of diastereomers, with each diastereomer in equilibrium with a minor conformer through rotation about the formamido C-N bond. Labeling studies with $^{18}O_2$-*m*-CPBA as oxidant and with DMDO as oxidant in the presence of $H_2{}^{18}O$, in concert with the study of the DMDO oxidation of [4-^{13}C] and [7-^{15}N]-labeled guanine, support a mechanism involving

initial epoxidation of the guanine 4-5 bond and contraction of the pyrimidine ring by a 1,2-migration of the guanine carbonyl C6 to form a transient dehydrodeoxyspiroiminodihydantoin followed by hydrolytic ring opening of the imidazolone ring. The 2-Ih is shown to be a major transformation in the oxidation of the single-stranded DNA 5-mer *d(TTGTT)* by *m*-CPBA and DMDO and in the oxidation of the 5-base pair duplex *d*[*(TTGTT)·(AACAA)*] with DMDO. 2-Ih has not previously been reported as an oxidative lesion in DNA. The lesion is stable to DNA digestion and chromatographic purification suggesting that 2-Ih may be generated as a stable lesion in vivo in DNA by peracids and possibly other epoxidizing agents. Consistent with the proposed mechanism, no 8-oxoguanine was detected as a product of the oxidations of the oligonucleotides or monomeric species mediated by the monooxygen donors. The 2-Ih base thus appears to be a pathway-specific lesion and holds promise as a potential biomarker.

2.2 Introduction

Oxidative damage to DNA, of concern as a factor in cancer, mutation, aging, and degenerative diseases is attributed to reactive oxygen species [Klaunig, J. E., et al, 2004], [Hoeijmakers, J. H. J. et al, 2001]. Processes initiated by one-electron oxidations mediated by hydroxyl radical, ionizing radiation and transition metals have been extensively characterized [Burrows, C. J. et al, 1998], [Neeley W. L et al, 2006], [Dedon, P. C., 2008] resulting in identification of numerous products from the oxidation of guanine, the most easily oxidized of the nucleobases. Of these, only 8-oxo-7,8-dihydroguanine (8-oxoGua) and its further oxidation products guanidinohydantoin and spiroiminohydantoin (Sp) have been reported in vivo. 8-Oxo-Gua, found in vivo at background levels of $1 – 2 \times 10^{-6}$ guanines [Gedick, C. M.et al, 2002] is widely used as a biomarker of oxidative stress although it is not highly

mutagenic [Neeley W. L et al, 2006],. By contrast, DNA damage by initial two-electron processes, whether direct or via rapid sequential one-electron oxidations, has only recently come into focus [Neeley W. L. et al, 2006], [Dedon, P. C. et al, 2008], [Gedick, C. M.et al, 2002], [Hong, I. S. et al, 2007], [Xu, X. et al, 2008]. The project is examining oxidation of DNA by peracids and by dimethyldioxirane (DMDO) as a model congruent in mechanism to peracids [Bach, R.D. et al] [Porter, N. A. et al]. These compounds function as monooxygen donors by formally concerted, two-electron oxidations. Peracids may arise biologically during lipid peroxidation, through formation of triplet excited ketones and aldehydes by the Russell mechanism [Russell, G. et al, 1957] followed by β-cleavage and coupling with O_2, by peroxidase-catalyzed autoxidation of aldehydes [Adam, W., Kurz, A. et al, 1999], or by aldehyde oxidation catalyzed by transition metals [Nam, W. et al, 1996]. In mitochondria, 2-oxoacid decarboxylases have been shown to generate peracids under certain conditions [Abell, L. M. et al, 1991], [Bunik, V. I. et al, 2007], an observation that is significant because mitochondrial DNA repair capability appears to decrease with age [Ledoux, S. P. et al, 2007], [Croteau, D. L. et al, 1999] and accumulated of mutations are implicated in age related neuropathology and the ageing process in general [Dimauro, S. et al, 2005].

In both single and double stranded DNA, guanine appears to be the predominant target of both peracids and DMDO [Adam, W., Kurz, A. et al, 1999], [Jacobsen, J. S. et al, 1986], [Davies, J. R. et al, 1990]. The action of *m*-CPBA on DNA appears to be associated with damage targeted to purines that is strongly blocking to replication, particularly in loop regions [Jacobsen, J. S. et al, 1986].

2.3 Materials and methods

2.3.1 Nuclear magnetic resonance and mass spectrometric analyses

NMR spectra were recorded on a Varian Inova NMR spectrometer operating at for 500 MHz ^{1}H and at 125 MHz for ^{13}C. ^{13}C shifts were obtained from HSQC and HMBC spectra $^{1}J_{C\text{-}H}$ were derived from unsuppressed 1-bond coupling in the heteronuclear shift correlation spectra. Low resolution electrospray ionization-mass spectrometry (ESI-MS) and tandem mass spectrometry (ESI-MS/MS) were performed on a Finnigan DECA ion trap system. Liquid chromatography ESI-MS (LC-ESI-MS) and LC-ESI-MS/MS were performed on a Finnigan TSQ Quantum system. Exact mass measurements were acquired on an IonSpec HiRes QFT ion cyclotron resonance mass spectrometer (Lake Forest, CA) equipped with a 9.4 T superconducting magnet and a Waters/Micromass Z-spray source. Samples were injected at a flow rate of 500 nL/min. The instrument was employed in the positive ion and broadband modes with a probe voltage of 3.2 kV, a cone voltage of 45 V, an accumulation in Q3 of 5000 ms, and quadrupole ion guide burst optimized to transmit ions in the 200 *m*/*z* mass range. Matrix-assisted laser desorption/ionization-MS (MALDI-MS) data were acquired on a Bruker Ultraflex II MALDI-time of flight (TOF)/TOF mass spectrometer (Bruker Daltonics, Billerica, MA). Samples were dissolved in 50:50 MeOH: 0.1% TFA, and MALDI spectra were acquired in the negative ion reflectron mode, using α-cyano-4-hydroxy-cinnamic acid as the matrix. Spectra were acquired over the mass range 500 to 2500 Da, using ACTH(1-17) and ACTH(18-39) as calibration standards.

2.3.2 Chemicals

Guanine, [2-^{13}C] bromoacetic acid, Na$^{15}NO_2$, 2,4-diamino-4-hydroxypyrimidine, dGuo, dGMP, dGTP, 77 % *m*-chloroperbenzoic acid (*m*-CPBA) and 32 % peracetic acid

purchased from Sigma-Aldrich (Milwaukee, WI) were used as received. DMDO was generated by potassium monopersulfate oxidation of acetone and was analyzed by iodometric titration immediately prior to use [Murray, R. W., and Jeyaraman, R., 1985]. *d(TTGTT)* and *d(AACAA)* were synthesized by the Oligonucleotide Synthesis Core Facility at UNC – Chapel Hill and purified by HPLC on a reverse phase Vydac C18 250 x 4.6mm column eluted with a linear gradient 8 to 15% MeOH in water over 10 min at flow rate of 1ml/min monitored at a detector wavelength of 260nm.

$^{18}O_2$-*m*-CPBA was synthesized as follows (personal communication, Spiro, T. G.). A flask containing methylene chloride (35 mL) and *m*-chlorobenzaldehyde (3 mL) was degassed by 3 freeze-thaw cycles on a high-vacuum manifold, frozen in liquid nitrogen under vacuum ($1x10^{-3}$ mm) and then $^{18}O_2$ (500 mL, >95 %) from a break-seal vessel was condensed into the reaction flask. The reaction flask was isolated, removed from the vacuum line and irradiated with a Fisher Biotech UV lamp at 365 nm with vigorous stirring for 8 h at -20 ^{o}C. Following transfer to a round bottom flask, the reaction mixture was reduced in volume under aspirator pressure to 10 mL and the precipitate collected by filtration and washed with cold hexane, yielding 700 mg $^{18}O_2$-*m*-CPBA, activity 55 % by iodometric titration.

2.3.3 Synthesis of [4-^{13}C]-and [7-^{15}N]Gua

Syntheses of [4-^{13}C]Gua and [7-^{15}N]Gua were based on Scheme 2.1 [Scheller, N. et al, 1995], using the appropriately labeled synthons. For [4-^{13}C]Gua, Scheme 2.1 was followed in its entirety starting with [2-^{13}C]bromoacetic acid to give the ^{13}C-labeled product in 21% overall yield. [7-^{15}N]Gua was synthesized from 2,4-diamino-6-hydroxypyrimidine as the

starting point and $Na^{15}NO_2$ as the labeled synthon to give the ^{15}N-labeled product in 30% overall yield.

2.3.4 Oxidation of Gua

To a suspension of Gua (15 mg, 0.1 mmol) in 2 mL of distilled H_2O, 2 mL of a solution of NaOH (1% w/v) and 14.2 mg of Na_2CO_3 were added with stirring until the Gua completely dissolved. The solution was diluted with an additional 6 mL of distilled H_2O and cooled to 0 °C in an ice bath, and 1 mL of a 0.11 mM solution of DMDO was added with stirring. After 30 min, the reaction was allowed to warm to ambient temperature (final pH 7.5) and adjusted with acetic acid to pH 7.0. The solvent was removed under a stream of Ar, and the solid residue was lyophilized overnight to give 81.1 mg of a mixture of 2-Ih and salts as an off-white powder. HPLC separation of a 13.6 mg aliquot of the mixture on a 250 mm × 9.4 mm ZORBAX C8 column eluted isocratically with 70% H2O: 30% MeOH gave pure 2-Ih (retention time, ~8.6 min) in the amount of 2.2 mg (71%, calcd from aliquot). UV: ~max (H2O) 229 nm. ESI-MS, natural abundance isotopomer (NA-2-Ih) (Figure 2.1): m/z 186 $[MH]^+$. ESI-MS/MS^+ (Figure 2.2), NA-2-Ih: m/z 186 $[MH]^+$, 169 $[MH - NH_3]^+$, 158 [MH -CO]+, 141 [MH -formamide]$^+$. ESI-MS, [7-^{15}N]-2-Ih: *m*/*z* 187 $[MH]^+$. ESI-MS/MS [7-^{15}N]2-Ih: *m*/*z* 187 $[MH]^+$, 169 $[MH - {}^{15}NH_3]^+$, 159 $[MH - CO]^+$, 142 [MH-formamide]$^+$. ESI-MS, [4-^{13}C]2-Ih: *m*/*z* 187 $[MH]^+$. ESI-MS/MS, [4-^{13}C]2-Ih: *m*/*z* 187 $[MH]^+$, 170 $[MH - NH_3]^+$, 159 $[MH - CO]^+$, 142 [MH -formamide]$^+$. High-resolution mass determined as the protonated dimer by ESI FT-ICR: calcd for $[C_5H_7N_5O_3]2H^+$, 371.11760; found, 371.11783 (mass error) 0.6 ppm). ^{1}H and ^{13}C NMR data are described in detail below.

2.3.5 Oxidation of d(TTGTT) by DMDO

d(TTGTT) (1 μmol) in 0.5 mL of 0.1 M bicarbonate buffer (pH 8.1) was cooled in an ice bath and treated with 80 μL of 0.09 M DMDO in acetone for 30 min and total reaction mixture was then lyophilized. The total crude reaction mixture was analyzed by MALDI-TOF and positive- and negative ion ESI-MS. The reaction mixture was then separated by HPLC on a Vydac C18 250 x 2.1 mm, 5 μm column under the following conditions: 0 to 10 % MeOH in 10 mM TEAA over 20 min at a flow rate of 1 mL/min and showed one major peak at 9.5 min. ESI-MS data on the collected peak were acquired by loop injection under the following conditions: 25 % methanol/75 % 10 μM aqueous ammonium formate (pH 6.0) at an injector flow rate of 50 μL/min.

2.3.6 Digestion of oxidized d(TTGTT)

D(TTGTT) (2 μmole) was oxidized as described above. An aliquot of the crude reaction mixture (~ 400 nmole) was dissolved in 1050 μL of a solution of 20 mM $MgCl_2$ in 80 μM Tris-HCl buffer (pH 7.4) to which 50 μL Dnase I (bovine pancreas, 4000U/mL) was added. Doubly distilled water was added to bring the total volume to 2100 μL, the sample was vortexed and incubated at 37 °C for 10 min. Alkaline phosphatase (50 μL, type VII-T, from bovine intestinal mucosa, 200U/mL) and phosphodiesterase I (50 μL, type II, from *Crotalus ademanteus* venom, 0.26U/mL) were added, the sample vortexed and incubated at 37 ^{o} for 60 min. Protein was removed by Centricon-10 filtration for 90 min at 4 °C, and the filters rinsed by addition of H_2O followed by centrifugation for a further 90 min. The combined filtrates were lyophilized and the product separated by HPLC on an Econosphere C8 column (9.4 x 250 mm) eluted at 2 mL/min using a gradient of 5% to 40% MeOH in water over 30min.

2.3.7 Oxidation of d(TTGTT) by m-CPBA

To *d(TTGTT)* (3.8mg, 2.29μmol) dissolved in 5 mL 0.1 mM ammonium acetate buffer at pH 4.65, 0.5 mL of a methanol solution of *m*-CPBA (5.1 mg, 22.9 μmol) was added dropwise with stirring. After 48 hours, the reaction mixture was extracted with 3 x 5 mL dichloromethane. The aqueous portion was lyophilized and the residue analyzed by ESI-MS/MS following desalting by ZIPTIP C_{18} (Millipore Corp., Billerica, MA).

2.3.8 Oxidation of d[(TTGTT)·(AACAA)]

One μmole of *d(AACAA)* in 500 μL of 50 mM NaCl and 0.1 M $NaHCO_3$ (pH 6.5) was mixed with 0.9 μmole *d(TTGTT)* in 465 μL of 50 mM NaCl and 0.1 M $NaHCO_3$ (pH 6.5), heated to 90 ^oC and slowly cooled in to 0 ^oC (estimated T_m of duplex, 12 ^oC [Kibbe, W. A., 2007]). The duplex was oxidized and digested as described above. The mixture obtained from lyophilization of the Centricon-10 filtrates was separated on an Econosphere C8 column (9.4 x 250 mm) eluted at 2 mL/min using a gradient of 0% to 30% MeOH in water over 20min.

2.3.9 Oxidation of dGuo by Peracetic Acid

A solution of 0.1 mmol dGuo and 50 μL 32 % peracetic acid (0.2 mmol) in 10 mL H_2O was stirred at ambient temperature, with further additions of 0.2 mmol peracetic acid at 24, 48 and 68 h. Ammonium carbonate (27 mg) was added during the reaction to maintain a pH of ~3.9. After 72 h, most of the volatiles were removed under a stream of Ar and the residue lyophilized overnight. The resulting solid residue was separated by semi-preparative HPLC on an Econosphere C8 column (9.4 × 250 mm) eluted isocratically at 2mL/min with 13% methanol in deionized water. Peaks at 6.4 min (spiroiminodihydantoin nucleoside; Sp-dR), 6.6 min (spiroiminodihydantoin base; Sp), 7 min (2-Ih) and 15.8 min (dGuo) were

collected and characterized by NMR and ESI-MS. A yield of 2-Ih = 25 % was estimated from the chromatographic trace at 230 nm by comparing the peak areas (adjusted for ε_{230}) (2-Ih)/(Sp-dR + Sp + 2-Ih + dGuo).

2.3.10 Oxidation of dGuo by m-CPBA

dGuo (0.1 mmol) and 0.1 mmol *m*-CPBA in 10 mL 9:1 aqueous buffer (0.1 M NH_4OAc, pH 4.5)/methanol was stirred at ambient temperature with a further addition of 0.1 mmol *m*-CPBA at 36 h. After 72 h, *m*-CBA and residual *m*-CPBA were extracted with 3 × 5 mL CH_2Cl_2 and the aqueous reaction layer lyophilized overnight. The resulting residue was separated by semi-preparative HPLC on an Econosphere C8 column (9.4 × 250 mm) eluted isocratically at 2mL/min with 10% methanol in deionized water. Peaks at 7 min (2-Ih-dR /2-Ih, 3:1, 80 % resolved) and 15.8 min (dGuo) were collected. A combined yield 2-Ih-dR + 2-Ih = 79 % was determined from the chromatographic trace at 230 nm by comparing the peak areas (adjusted for ε_{230}) (2-Ih-dR + 2-Ih)/(2-Ih-dR + 2-Ih + dGuo).

2.3.11 Oxidation of dGuo by $^{18}O_2$-m-CPBA

Oxidation of dGuo with ^{18}O-*m*-CPBA was performed as described above, except that $^{18}O_2$-*m*-CPBA was used in place of natural abundance *m*-CPBA.

2.3.12 Incorporation of ^{18}O into 2-Ih from $H_2{}^{18}O$

Gua (0.001 mmol) was suspended in 0.2 mL H_2O and dissolved by slow addition of 0.2 mL 1 % (w/v) aqueous NaOH. Then 0.4 mL $H_2{}^{18}O$ was added, the reaction mixture was cooled in an ice bath and 0.15 mL 0.1 M DMDO in acetone was added. After stirring for 30 min, the solvents were evaporated under a stream of Ar, and the solid analyzed by ESI-MS.

2.3.13 Oxidation of dGuo by DMDO

dGuo (0.1 mmol) was dissolved in 10 mL $NaHCO_3$ buffer (pH 8.1) cooled in an ice bath. To this solution was added with stirring DMDO in acetone (1.2 mL, 0.10 M) and after 30 min, acetone was evaporated under a stream of Ar. The remaining aqueous solution was lyophilized overnight to give a mixture of products and salts as an off-white powder. The diastereomers were desalted by semi-preparative HPLC on an Econosphere C8 column (9.4 x 250 mm) eluted isocratically with 30% MeOH in water at 2 mL/min and the product mixture collected as a single peak at retention time ~8.25 min. UV: λ_{max} (H_2O) 230 nm. Positive ion ESI-MS: *m/z* 302 ($[MH]^+$). Positive ion ESI-MS/MS: *m/z* 302 ($[MH]^+$), 284 ($[MH - H_2O]^+$), 186 ([MH – deoxyribose]$^+$), 141 ([MH – deoxyribose – formamide]$^+$). Positive ion high resolution Fourier transform-ICR-ESI-MS (as protonated dimer): calcd for $[C_{10}H_{15}N_5O_6]_2H^+$, 603.21229, found 603.21511. ^{1}H NMR (500 MHz, D_2O, 5 ^{o}C): **1a**, 8.59 (s, 1H, H9), 5.62 (ψt, 1H, *J*= 7.06 Hz, H1'), 4.35 (m, 1H, H3'), 3.93 (m, 1H, H4'), 3.82, 3.72, m, H5', H5" overlapping with other isomers), 2.61 (m, >1H, H2", overlapping with H2"-1b), 2.31 (m, 1H, H2') ppm; **1b**, 8.65 (s, 1H, H9), 5.57 (ψt, 1H, *J*= 6.61 Hz, H1'), 4.43 (m, 1H, H3'), 3.98 (m, 1H, H4'), 3.70 – 3.64, m, H5', H5", overlapping with other isomers), 2.61 (m, >1H, H2", overlapping with H2"-1a), 2.45 (m, 1H, H2') ppm; **1a'**, 8.36 (s, 1H, H9), 5.72 (1H, H1'), 4.39 (m, 1H, H3'), 2.59 (m, 1H, H2") ppm; **1b'**, 8.31 (s, 1H, H9), 5.68 (1H, H1'), 4.46 (m, 1H, H3') ppm. ^{13}C NMR (125 MHz, D_2O, 5 ^{o}C) **1a**, 164.2 (C6), 163.8 ($^1J_{C9\text{-}H9}$ = 206.3 Hz, C9), 85.5 ($^1J_{C1'\text{-}H1'}$ = 170.4 Hz, C1'), 83.3 ($^1J_{C4'\text{-}H4'}$ = 148.0 Hz, H4'), 76.2 (C5), 67.8 ($^1J_{C3'\text{-}H3'}$ = 152.8 Hz, H3'), 58.9 (C5'), 37.2 ($^1J_{C2'\text{-}H2''}$ = 148.5 Hz, C2') ppm; **1b**, 163.8 ($^1J_{C9\text{-}H9}$ = 207.0 Hz, C9), 85.2 ($^1J_{C1'\text{-}H1'}$ = 171.6 Hz C1'), 84.1 ($^1J_{C4'\text{-}H4'}$ = 149.2 Hz, H4'), 76.7 (C5), 68.1 ($^1J_{C3'\text{-}H3'}$ = 152.3 Hz, H3'), 64.1 (C5'), 35.5 ($^1J_{C2'\text{-}H2''}$ = 138.4 Hz, C2') ppm.

2.3.14 Separation of diastereomers 1a and 1b

Diastereomers **1a** and **1b** from the oxidation of dGuo described above were separated by semi-preparative HPLC on an AQUASIL C18 column (10 x 250 mm) eluted isocratically with 1.5 % acetonitrile in 17 mM ammonium acetate. Peaks were collected at 8.84 min (**1b**) and 9.40 min (**1a**). Proton shifts of **1a** and **1b** observed in ^{1}H NMR, NOESY and ROESY spectra (500 MHz, D_2O, 5 ^{o}C) were identical to those assigned to **1a** and **1b** in the mixture above.

2.3.15 Oxidation of dGMP by DMDO

dGMP (0.1mmol) was dissolved in 10 mL of 0.1 M $NaHCO_3$ buffer (pH 8.1) with stirring in an ice bath. To this solution was added 1.2 mL of 0.10 M DMDO in acetone with stirring. After 30 min, the acetone was evaporated under a stream of Ar, and the residue lyophilized overnight to give an off-white powder. Desalting was accomplished by semi-preparative HPLC on an Econosphere C8 column (9.4 × 250 mm) eluted isocratically with 30% MeOH in H_2O at 2mL/min. The mixture of diastereomers was collected as a single peak, with retention time ~ 4.7 min. UV: λ_{max} (H_2O) 230 nm. Negative ion ESI-MS: *m*/*z* 380 $[MH]^-$. Negative ion ESI-MS/MS: *m*/*z* 380 $[MH]^-$, 337 [MH – formamide] $^-$, 240 [MH – (5-formamido-2-iminohydatoin)] $^-$. Positive ion high resolution Fourier transform-ICR-ESI-MS (as protonated dimer): calcd for $[C_{10}H_{15}N_5O_6]_2H^+$, 763.14495; found, 763.14832. ^{1}H NMR (500 MHz, D_2O, 5 ^{o}C) **2a**: 8.21 (s, 1H, H9), 5.70 (ψt, 1H, *J* ~ 6.7 Hz, H1'), 4.35 (m, 1H, H3'), 3.95 (m, 1H, H4'), 3.73 – 3.56 (m, overlapping with other isomers, H5',H5"), 2.36 (m, 1H, H2"), 1.91 (m, 1H, H2') ppm; **2b**: 8.50 (s, 1H, H9), 5.38 (ψt, 1H, *J* ~ 5.5 Hz, H1'), 4.39 (m, 1H, H3'), 3.79 (m, 1H, H4'), 3.73 – 3.56 (m, overlapping with other isomers, H5',H5"), 2.55 (m, 1H, H2"), 2.20 (m, 1H, H2') ppm; **2a'**: 8.38 (s, 1H, H9), 5.47 (ψt, 1H, *J* ~ 5.4 Hz, H1'), 4.27 (m, 1H, H3'), 3.83 (m, 1H, H4'), 3.73 – 3.56 (m, overlapping with other isomers,

H5',H5"), 2.41 (m, 1H, H2"), 2.17 (m, 1H, H2') ppm; **2b'**: 8.32 (s, 1H, H9), 6.01 (dd, 1H, , *J* ~ 4.8, 9.4 Hz, H1'), 4.31 (m, 1H, H3'), 3.88 (m, 1H, H4'), 3.73 – 3.56 (m, overlapping with other isomers, H5',H5"), (H2", H2' not resolved) ppm. ^{13}C NMR (125 MHz, D_2O, 5 ^{o}C) **2a**: 180.5 (C4), 171.9 (C2), 167.1 (C6), 164.6 ($^{1}J_{C9\text{-}H9}$ = 206.9 Hz, C9), 88.3 (C1'), 87.7 ($^{3}J_{P\text{-}C4'}$ = 8.6 Hz, C4'), 79.0 (C5), 71.8 (C3'), 64.2 ($^{3}J_{P\text{-}C5'}$ = 4.5 Hz, C5'), 42.0 ($^{1}J_{C2'\text{-}H2''}$ = 136.8 Hz, C2') ppm; **2b**: 181.9 (C4), 171.8 (C2), 167.3 (C6), 166.5 ($^{1}J_{C9\text{-}H9}$ = 207.9 Hz, C9), 88.7 (C1'), 86.3 ($^{3}J_{P\text{-}C4'}$ = 9.0 Hz, C4'), 79.6 (C5), 71.7 (C3'), 64.4 ($^{3}J_{P\text{-}C5'}$ = 4.2 Hz, C5'), 39.0 (C2') ppm; **2a'**: 181.8 or 182.6 (C4), 172.1 (C2), 167.5 (C6), 165.6 ($^{1}J_{C9\text{-}H9}$ = 208.2 Hz, C9), 88.6 (C1'), 85.9 ($^{3}J_{P\text{-}C4'}$ = 8.7 Hz, C4'), 78.7 (C5), 71.5 (C3'), 65.3 ($^{3}J_{P\text{-}C5'}$ = 4.6 Hz, C5') ppm, C2', not resovled; **2b'**: 182.4 (C4), 171.4 (C2), 163.8 (C9), 85.4 ($^{3}J_{P\text{-}C4'}$ = 7.9 Hz, C4'), 84.7 (C1'), 79.0 (C5), 72.3 (C3') ppm, C2', C5' signals could not be resolved.

2.3.16 Oxidation of dGTP by DMDO

dGTP (0.05 mmol) was dissolved in 0.1 mM $NaHCO_3$ buffer (pH8.1) at 0 ^{o}C. To this solution was added 0.75 mL of 0.081 M DMDO in acetone with stirring. After stirring 30 min at 0 ^{o}C, acetone was removed under a stream of Ar and the reaction mixture lyophilized and stored at -80 ^{o}C. The product mixture was characterized without further purification. Negative ion ESI-MS: *m/z* 584 ($[MNa_2 - H]^-$), 562 ($[MNa - H]^-$), 540 ($[M - H]^-$), 460 ($[M - H_2PO_3]^-$], 387 ($[MNa - HP_2O_7]^-$). ^{1}H NMR (500 MHz, D_2O, 0 ^{o}C) 8.45 (s), 8.43 (s), 8.42 (s), 8.18 (s), 5.90 (m), 5.75 (m), 5.59 (m), 4.51 (m), 4.48 (m), 4.36 (m), 4.24 (m), 4.16 (m), 4.04 – 3.83 (m), 2.60 – 2.44 (unresolved), 2.32 (m), 2.17 (m) ppm.

2.4 Results

2.4.1 Oxidation of guanine

The structure of 2-Ih has been established on the basis of mass spectrometry and NMR studies on NA-2-Ih and its isotopomers generated by the oxidation of [4-^{13}C] and [7-^{15}N]Gua, which yield [5-^{13}C]-2-Ih and [7-^{15}N]-2-Ih, respectively. By ESI-MS in the positive mode, the protonated molecular ion of NA-2-Ih was observed at *m*/*z* 186, a gain of 34 amu relative to Gua (Figure 2.1). In the ESI-MS/MS^{+} of NA-2-Ih (Figure 2.2) and [7-^{15}N]2-Ih, a product ion at *m*/*z* 169 in both fragmentation patterns indicated loss of NH_3 and $^{15}NH_3$, respectively, from the carboxamido group, as expected for ^{15}N at position 7. The high-resolution mass of NA-2-Ih, obtained as the protonated dimer $[M_2H]^+$ by HR ESI/ FT-ICRMS^{+}, corresponds to the required composition $[C_5H_8N_5O_3]2H^+$.

By comparison of ^{1}H NMR spectra acquired on NA-2-Ih in $^{2}H_2O$ and DMSO-d_6, a single nonexchangeable proton resonance was identified at 7.94 ppm (DMSO-d_6) (Figure 2.3a). Assignment of this signal to the 5-formyl C*H* is confirmed by the ^{1}H,^{13}C heteronuclear single quantum coherence (HSQC) spectrum, in which a single cross-peak is observed between the nonexchangeable proton and a carbon signal at 161.5 ppm in the region reported for formamido carbon [Ferris, T. D. et al, 1997], [Breitmaier, E. et al, 1973], and therefore assigned to C9 (data not shown). Relatively sharp proton signals present in DMSO-d_6 at 7.19, 7.29, and 8.77 ppm (Figure 2.3a) represent three protons undergoing slow exchange with residual H_2O at ambient temperature.

On the basis of the strong cross-peaks observed in the double quantum-filtered COSY (DQFC) spectrum (Figure 2.4) between the signals of the slowly exchanging protons at 7.19 and 7.29 ppm, these resonances are assigned to nonequivalent 5-carboxamido protons N*H*$_a$ and N*H*$_b$, confirmed in the proton spectrum of [7-^{15}N]-2-Ih (Figure 2.3b) by $^{1}J_{N\text{-}H}$ coupling of

89.7 and 88.8 Hz, respectively. The splittings are identical to $^{1}J_{\text{N-H}}$ coupling reported for the amido protons of acetamide, propiolamide, and formamide, with the smaller coupling constant assigned to NH_{b} trans to the carbonyl oxygen [Ferris, T. D. et al, 1997]. Magnetic nonequivalence of NH_{a} and NH_{b} is expected because of hindered rotation around the amido C-N bond [Ferris, T. D. et al, 1997]. In the ^{1}H NMR spectrum of [5-^{13}C]-2-Ih (Figure 2.3c), a three-bond coupling with $^{3}J_{\text{C-H}}$) 7.1 Hz is resolved for the signal assigned as NH_{b} providing further confirmation of amido proton non-equivalence. Additionally, a three-bond coupling with $^{3}J_{\text{C-H}}$ 6.3 Hz (Figure 2.3c) is resolved for the signal assigned as H9 consistent with structure 2-Ih.

In the proton-decoupled ^{13}C NMR spectrum of NA-2-Ih (Figure 2.5a), carbon signals at 181.3 and 172.9 ppm and a quaternary carbon at 74.3 ppm have shifts similar to the iminohydantoin ring carbons of the Gua oxidation product spiroiminodihydantoin [Adam, W.et al, 2002], [Niles, J. C. et al, 2001]. By comparison with the ^{13}C NMR chemical shifts reported for neutral 5,5-disubstituted iminohydantoin bases [Olofson, A. et al, 1998], the signals at 181.3 and 172.9 ppm can be assigned to C4 and C2, respectively, and the upfield signal at 74.3 ppm can be assigned to the quaternary carbon C5, which is the only carbon in an sp^{3} hybridization state. The resonances at 172.9, 167.4, and particularly 161.5 ppm display broadening and some structure, the possible origins of which are discussed below.

The ^{13}C NMR spectrum of the ^{15}N isotopomer of 2-Ih (Figure 2.5b) is consistent with the presence of the ^{15}N label at position 7 and is helpful in confirming the remaining carbon resonances. The signals at 167.4 and 74.3 ppm appear as doublets, with splittings of 17.6 and 7.8 Hz, respectively. The splitting of 17.6 Hz is within the range reported for the one-bond

C(=O)-N coupling in amides [Stothers, J. B., 1972] and the signal can therefore be assigned to carboxamido carbon C6. The splitting of 7.8 Hz is in the range reported for two-bond C-N couplings [Otting, G., 1996] consistent with the assignment of the signal at 74.3 ppm to the quaternary carbon of 2-Ih made above. In agreement with the single peak observed in HSQC spectrum, the remaining carbon signal at 161.5 ppm belongs to formamido C9.

The weak off-diagonal peak x (approximately aligned with H8) is due to a minor impurity with signals that are overlapping H8 and the broad exchangeable NH proton resonance of 2-Ih between 8.2 and 8.5 ppm. The exchange-broadened peaks on the diagonal are not observed at the contour level of the DQF COSY spectrum.

In the ^{13}C NMR spectrum of 2-Ih from oxidation of [4-^{13}C]Gua (Figure 2.5c), the ^{13}C label appears as the quaternary carbon C5. The ^{13}C-^{13}C couplings in Figure 2.5c are in accord with the structure [5-^{13}C]-2-Ih and support carbon assignments made from the ^{13}C NMR spectra of the NA and ^{15}N isotopomers. The 38.3 Hz coupling of the signal at 181.3 ppm assigned to C4 is in good agreement with $^{1}J_{\text{C-(C=O)}}$ coupling reported for five-membered cyclic ketones, and the 55.1 Hz coupling of the signal at 167.4 ppm assigned to C6 corresponds to $^{1}J_{\text{C-(C=O)}}$ reported for acyclic amides [Stothers, J. B., 1972]. As in NA-2-Ih and [7-^{15}N]-2-Ih, resonances assigned to C2 and C9 are broadened, with the result that ^{2}J coupling with ^{13}C5 is not resolved.

The ^{1}H,^{13}C heteronuclear multiple bond correlation (HMBC) spectrum (Figure 2.6) shows cross-peaks expected from the ^{1}H and ^{13}C assignments. Formamido carbon C9 at 161.5 ppm shows an unsuppressed $^{1}J_{\text{C-H}}$ coupling of 194.5 Hz with the C9*H* at 7.94 ppm.

This coupling is in the range reported for $^{1}J_{C\text{-}H}$ of the formamido group [Ferris, T. D.et al, 1997], [Breitmaier, E. et al, 1973] and is significantly smaller than one-bond C,H coupling of ≥ 200 Hz reported for intact imidazole rings at C8 of purines (pH 5.6) [Read, J. M., and Goldstein, J. H., 1965]. A two-bond coupling is also observed between the C9 and the slowly exchanging proton at 8.77 ppm, which is accordingly assigned to the formamido H8. Quaternary carbon C5 at 74.2 ppm has the expected cross-peaks with H9, H8, and carboxamido $H7_b$. In accord with hindered rotation about the carboxamido C-N bond and different HNCC torsion angles, as well as the coupling pattern observed in the ^{1}H NMR spectrum (Figure 2.3c), no cross-peak is present between C5 and $H7_a$. Carboxamido carbon C6 at 167.2 ppm has cross-peaks with NH_a and NH_b as well as with H8. C4 has a cross-peak only with H8, since the other slowly exchanging protons and nonexchanging H9 are four bonds distant. No cross-peaks were observed for C2, which is separated by four bonds from the nearest slowly exchanging proton.

In the NOESY spectrum of NA-2-Ih (Figure 2.7), the expected cross-peaks were observed between the nonexchangeable formyl H9 and the slowly exchanging protons formamido H8 and carboxamido $H7_a$ and $H7_b$.In addition, exchange cross-peaks were observed between the exchangeable protons and between the exchangeable protons and the water. On the basis of exchange cross-peaks with H_2O, three broad signals around 9.2, 8.1, and 7.8 ppm in Figure 2.3a can be identified with N*H*1, N*H*3 and the exocyclic imino-N*H*, although specific assignments are not possible.

In the ^{13}C NMR of NA-2-Ih,HCl recorded in 9:1 $H_2O/^{2}H_2O$, C2 and C4 showed upfield shifts reported to be diagnostic for the iminohydantoin ring [Olofson, A. et al, 1998].

As indicated above, the ^{13}C NMR signals of C2, C6, and C9 show broadening and/or structure, with C9 being most significantly affected. In the ^{13}C NMR spectrum of the hydrochloride salt, the C9 resonance displayed well-resolved structure (Figure 2.8), with one predominant narrow line flanked by low intensity peaks (spread over ~ 0.5 ppm) over which well-resolved multiplets were superimposed.

The pattern observed is similar to patterns reported in ^{13}C NMR spectra of amides and is ascribed to a distribution of rotational conformers [Johnston, E. R. et al, 2000], [Bulai, A. et al, 1997], [Bulai, A. et al, 1996], [Hamilton, J. G. et al, 1976]. Analogous rotational isomerism has been observed in formamidopyrimidine derivatives of dGuo [Gates, K. S. et al, 2004], [Tomasz, M. et al, 1987]. In 2-Ih, steric hindrance and H-bonding between the *gem* substituents on C5 and the ring carbonyl oxygen are expected to contribute to multiple conformers. Equilibration between carbonyl and hydrated forms of the formamido substituent could cause additional complication of the C9 signal. For the spectrum of NA-2-Ih,HCl recorded in $H_2O/^2H_2O$, further complexity is anticipated from ^2H isotope effects and $^{13}C,^2H$ coupling in the partially ^2H-exchanged compound [Reuben, J., 1985], [Garcia-Martín, M. L. et al, 2002].

2.4.2 Oxidation of d(TTGTT)

Following treatment of the 5-mer with a 7-fold excess of DMDO, the total crude reaction mixture was analyzed directly by NMR, MALDI-TOF and ESI-MS. In the ^1H NMR spectrum of the total reaction mixture (Figure 2.9), pairs of signals are present at 8.72/5.84 ppm and 8.68/5.57 ppm with a 1:4 ratio. The resonances at 5.57 and 5.84 ppm are in the region associated with H1' signals while those at 8.68 and 8.72 ppm are singlets in the region

where the formyl H9 of 2-Ih is expected [Davies, J. R. et al, 1990]. The pattern observed in Figure 2.9 is consistent with formation of 2-Ih diastereomers in the oxidized 5-mer in a 1:4 ratio. Based on integrated signals from unreacted 5-mer and the 2-Ih diastereomers, > 95 % of the 5-mer was oxidized, with at least 40 % conversion to 2-Ih-containing product. The MALDI-TOF mass spectrum in the negative ion mode showed a strong ion at *m/z* 1516, corresponding to a gain of 34 mass units as expected for formation of the 2-Ih lesion, in addition to unmodified 5-mer (Figure 2.10). The negative ion ESI-MS acquired by loop injection (Figure 2.11) shows strong ions at *m/z* 1516 and 758 as expected for the $[M - H]^-$ and $[M - H]^{2-}$ ions, respectively, of the 5-mer containing the 2-Ih modification. In the ESI-MS, ions corresponding to unmodified 5-mer are not observed, consistent with the estimate from the NMR spectrum that only 5 % of the 5-mer was unreacted and that a substantial proportion of the 5-mer was converted to the 2-Ih-modified oligonucleotide. ESI-MS/MS of the ion at m/z 1516 (Figure 2.12) yielded a product ion at *m/z* 1376 corresponding to loss of a 2-iminoimidazole fragment (2-imino-5-oxo-2,5-dihydro-1H-4-imdazole-4-carboxamide) to yield a ribosyl formamide-containing 5-mer anion, a fragmentation pattern consistent with oxidation of the Gua to 2-Ih. The positive ion ESI-MS (Figure 2.13) by loop injection, was entirely in accord with this result, having ions at *m/z* 1518 ($[MH]^+$) and 1540 ($[MNa]^+$), along with product ions at *m/z* 1400 for loss of 2-iminoimidazole from $(MNa)^+$, 729 [sodium adduct of 5'-*O*-(2-methylene-2,3-dihydrofuran-3-yl)-pdTpdT), 671 (disodium adduct of $(pdT)_2$) and 649 (sodium adduct of $(pdT)_2$) and no protonated molecular ion corresponding to the unmodified 5-mer. ESI-MS/MS of $(MH)^+$ (Figure 2.14) yielded a product ion at m/z 1378 ($[MH]^+$ - 2-iminoimidazole). The HPLC trace of the reaction mixture showed a major peak at 9.5 min (Figure 2.15). In the positive ion ESI-MS of this collected peak, a major ion at *m/z*

1540 was identified as the sodium adduct $(MNa)^+$ of the 2-Ih-modified 5-mer by ESI-MS/MS, which gives a product ion at *m/z* 1400, corresponding to the sodium adduct of the 5-mer containing ribosyl formamide following loss of the 2-iminoimidazole fragment (Figure 2.16). The slight inflection at the leading edge of the 9.5 min peak in Figure 2.15 may represent the unoxidized 5-mer (5 % by ^{1}H NMR, not detected in the ESI-MS of the collected peak) or partially resolved diastereomeric product. In the mixture of mononucleosides resulting from digestion of the oxidized 5-mer, 2-Ih-dR was definitively identified both by HPLC retention time (vide infra) and protonated molecular ion (*m/z* 302) in the ESI-MS. These data establish transformation of guanine to 2-Ih as the major oxidation pathway of the 5-mer. Treatment of the 5-mer with *m*-CPBA yields a product mixture having an ion at *m/z* 1518 by positive ion ESI-MS, confirmed as 2-Ih by ESI-MS/MS which yields the expected product ion at *m/z* 1378.

2.4.3 Oxidation of d[(TTGTT)·(AACAA)

d(TTGTT) complexed to its complement *d(AACAA)* was oxidized by DMDO under the same conditions as the single-stranded 5-mer and the reaction mixture was digested to nucleosides. The presence of 2-Ih-dR in the digest was confirmed by retention time and ESI-MS/MS of the collected peak (Figure 2.17).

2.4.4 Oxidation of dGuo by peracids

Figure 2.18a, b shows the HPLC traces of reaction mixtures from peracetic acid and *m*-CPBA oxidations of dGuo. 2-Ih aglycone, Sp aglycone and Sp-dR were identified by ESI-MS and chromatographic retention times in the peracetic acid oxidation. The yields of 2-Ih and total spiroiminodihydantoins (aglycone + nucleoside) were estimated to be ~ 25 % and 50 %, respectively, from integration of the HPLC peaks in Figure 2.18a adjusted for

extinction coefficients, assuming approximately equivalent extinction coefficients for the broad absorption maximum of the three oxidation products at 230 nm. Oxidation of dGuo by *m*-CPBA, gave 2-Ih and 2-Ih-dR in a combined yield of 79 % and Figure 2.18b shows that they are the only products present in significant yield. The mass spectrum of the broad, low peak eluting at 4 min (Figure 2.18b) shows traces of *m*-chlorobenzoic acid and Sp/Sp-dR. No 8-oxo-dGuo was detected in the HPLC and ESI-MS analysis of the peracid oxidation mixtures.

2.4.5 ^{18}O Labeling reactions

We addressed the origins of the added oxygens in two experiments: (1) by oxidizing guanine with DMDO in 1:1 $H_2{}^{18}O/H_2O$ and (2) by oxidizing deoxyguanosine with $^{18}O_2$-*m*-CPBA (>95 % $^{18}O_2$). The use of deoxyguanosine for oxidation with $^{18}O_2$-*m*-CPBA was dictated by the insolubility of guanine in aqueous medium at pH 4.5 required for activity of the peracid. Negative ion ESI-MS analysis of the oxidation mixture obtained with DMDO in 1:1 $H_2O/H_2{}^{18}O$ yielded the ion chromatogram in Figure 2.19.a in which the ratio ^{16}O-2-Ih/^{18}O-2-Ih is > 40 %. Making allowances for contamination of the reaction with natural-abundance water from the acetone solution of DMDO and from atmospheric condensate during transfer of the cold (-80 ^{o}C) DMDO, the ion chromatogram is in accord with incorporation of 50 % of one atom of ^{18}O. Comparison of the negative ion ESI-MS/MS of the $[M - H]^-$ ions of the labeled and unlabeled 2-Ih shows that the ^{18}O is lost with the formamide fragment (Figure 2.19.b, 2.19.c).

Exchange of the formamido oxygen with $H_2{}^{18}O$ during work-up was ruled out by determining that no ^{18}O-incorporation could be detected on stirring natural abundance 2-Ih in $H_2{}^{18}O$ under the reaction conditions for 2 h. In the positive ion ESI-MS of the product from

oxidation of deoxyguanosine with $^{18}O_2$-*m*-CPBA, the protonated molecular ion shifts from *m/z* 302 to *m/z* 304, indicating complete incorporation of a single ^{18}O label. The major product ions in the positive ion ESI-MS/MS (Figure 2.20) of the ion at *m/z* 304 corresponded to loss of the deoxyribose (*m/z* 188), loss of deoxyribose along with natural abundance CO (*m/z* 160) and loss of natural abundance deoxyribosylformamide (*m/z* 143). As shown in Figure 2.20, ^{18}O label is retained in the product ions corresponding to loss of deoxyribose, CO and deoxyribosylformamide.

2.4.6 Oxidation of dGuo by DMDO

Product from desalting the DMDO oxidation mixture by semi-preparative HPLC was collected as a single peak which, by accurate mass measurement, corresponded in composition to the protonated dimer $(2\text{-Ih-dR})_2H^+$. ESI-MS/MS of the protonated molecule (MH^+) yielded the same product ions as shown in Figure 2.20a for 2-Ih-dR from oxidation of dGuo by natural abundance *m*-CPBA. Multiple signals in the ^1H NMR spectrum of the total reaction mixture (Figure 2.21) were identified at chemical shifts expected for formyl H9 [Ye, W. et al, 2006] of the 2-Ih base and H1' of the deoxyribose [Ippel, J. H.et al, 1996], indicating the presence of diastereomers. In all, the reaction mixture appeared to contain two major and two minor species. The diastereomer mixture was confirmed by the ROESY spectrum (Figure 2.22) which contained independent sets of NOESY connectivities (Tables 2.1, 2.8). By virtue of the NOESY connectivities between H9 and H1' signals (Figure 2.22; Tables 2.1, 2.2), sugar-base connectivity was established for the two major components **1a** and **1b** of the product mixture, demonstrating the presence of nucleosides rather than a mixture of modified nucleobases bases and sugars. Exchange cross peaks permitted **1a** and **1b** to be correlated with the minor components, **1a'** and **1b'**, respectively (Figure 2.22).

Based on observations of rotational isomerism around the N8-C9 formamido bond of the 2-Ih base[24] and the formyl C-N bond of *N*-(2'-deoxyribosyl)formamide [Guy, A.et al, 1991], [Maufrais, C. et al, 2003], rotational isomerism can be ascribed as the exchange mechanism and **1a'** and **1b'** are assigned as the minor rotational isomers around the formamido N8-C9 bond of the respective major nucleoside components. A signal present in the ^{1}H NMR spectrum at 5.72 ppm partially overlaps H1' assigned to **1a'** (Figures 2.21 and 2.22) and shows NOESY connectivity to a signal overlapping H9 of **1b** at 8.65 ppm. However, this set of signals (indicated by "X" in Figure 2.21) lacks exchange or NOESY connectivity to any other component of the sample, and must therefore be an impurity or oxidation side-product. To discount the effect of the impurity, the ratio of diastereomers (**1a** + **1a'**)/(**1b** + **1b'**) was estimated from integrated signals of **1a'** and **1b'** in the H9 region and **1a** and **1b** in the H1' region and found to be ~ 2:1, while the ratios **1a**/**1a'** (estimated from **1a'**-H9/**1a**-H9) and **1b**/**1b'** (estimated from **1b'**-H1'/**1b**-H1') are ~ 10, indicating that a single rotamer is strongly favored for both diastereomers.

Consistent with the ROESY spectrum, the HMBC spectrum of the oxidation mixture (Figure 2.23) shows the two independent sets of correlations derived for **1a** and **1b**. The HMBC spectrum of the diastereomer mixture confirms sugar-base connectivities for the major rotational isomers **1a** and **1b** observed in the ROESY spectrum and allows assignment of the deoxyribose carbon shifts as well as the shifts of formyl C9 and *spiro* C5 of the hydantoin ring. $^{3}J_{C,H}$ Sugar-base couplings observed for **1a** are between C9-H1' and H1'-C5. Both H1' and H9 are coupled to a carbon at 76.2 ppm having no attached proton (no C/H cross peak observed at the corresponding carbon shift in the HSQC spectrum (Figure 2.24)) which is therefore assigned to *spiro* C5 (Table 2.3). A carbon shift of 76.2 ppm is within the

range of shifts reported for the *spiro* carbons of the 2-Ih [Ye, W. et al, 2006] and spiroiminodihydantoin bases and the diastereomeric spiroiminodihydantoin deoxynucleosides [Adam, W. et al, 2002], [Niles, J. c. et al, 2001]. A similar set of sugar-base couplings are observed for **1b** (Table 2.4). All remaining deoxyribose C/H cross peaks of **1a** and **1b** could be assigned by a similar analysis of the HMBC and HSQC spectra of the product mixture. The low concentrations of minor rotamers **1a'** and **1b'** precluded observation of C,H coupling in the heteronuclear shift correlation spectra.

Diastereomers **1a** and **1b** could be separated with ~ 90 % efficiency by semi-preparative HPLC. The later-eluting product proved to be **1a**. The ROESY spectra of the resolved diastereomers (Figures 2.25, 2.26) permitted the deoxyribose NOESY connectivities to be identified for the major rotational isomers (Table 2.1, 2.2).

2.4.7 Oxidation of dGMP by DMDO

Exact mass measurement of the single molecule ion from the mixture dGMP oxidation products corresponded in composition to the protonated 2-Ih-dRP dimer $(2\text{-Ih-dRP})_2H^+$. The ^1H NMR spectrum (Figure 2.27) was qualitatively similar to that of the mixture of 2-Ih nucleosides and shows two major components **2a**, **2b** along with two minor components **2a'**, **2b'**. The components of the dGMP oxidation mixture were identified by applying the same strategy described above for the nucleosides. Signals in the H9 – H1' and H2' – H2'' regions were well-resolved. In the ROESY spectrum (Figure 2.28), independent sets of NOESY connectivities were determined for **2a** and **2b**, as well as for one of the minor components, which we have assigned as a rotational isomer of **2a'** by virtue of exchange connectivity with **2a** (Tables 2.5 – 2.7). An expansion of the H9 - H1' region of the ROESY spectrum (Figure 2.29) shows exchange connectivity of both minor components **2a'** and **2b'**

to corresponding major components **2a** and **2b**. With the exception of the H5', H5'' region, where signals of all species in the product mixture overlap, resolution of signals in the ^{1}H NMR and ROESY spectra was sufficient to permit unambiguous assignment of proton signals for three of the four species present. The concentration of **2b'** was too low to allow assignment of signals aside from H1' and H9. By summing integral ratios in the H1' region, the ratio (**2a** + **2a'**)/(**2b** + **2b'**) is ~ 2:1, in line with the results from dGuo oxidation, while the ratio of rotamers **2a**/**2a'** is ~ 3:1 and **2b**/**2b'** is > 5:1. For **2a**, **2a'** and **2b**, NOESY cross peaks between formyl H9 and sugar H1' signals demonstrate the required connectivity between the base and sugar (Figure 2.29).In the case of **2b'**, the connectivity between sugar and base can be inferred from the observation that **2b'** is generated from **2b** by rotational exchange.

For **2a**, **2a'** and **2b**, assignment of cross-peaks in the heteronuclear shift correlation spectra was determined from the HMBC, HSQC and ^{13}C spectra (Figures 2.30 – 2.32). ^{1}H and ^{13}C assignments derived from these data are given in Tables 2.8 – 2.10. The ^{1}H assignments are in complete accord with those derived from the ROESY spectrum. Base – sugar connectivity was confirmed by the 3-bond couplings H9-C1', C9-H1' and C5-H1' observed for **2a**, **2a'** and **2b**. The chemical shifts of the *spiro* carbons were assigned from the HMBC spectrum on the basis of ^{13}C cross peaks at shifts of ~ 80 ppm with H1' protons and the absence of signals from carbons in this region of the HSQC spectrum. The assignment of carbon signals to C4' and C5' are established by observation of the ^{31}P-^{13}C coupling in the ^{13}C NMR spectrum (Figure 2.32). Because of the low concentration of **2b'** in the mixture, only the H1'/C5 cross peak in the HMBC spectrum could be assigned. Nevertheless, this

assignment is important because it unequivocally establishes the sugar-base connectivity of **2b'**.

2.4.8 Oxidation of dGTP by DMDO

Because of the lability of the phosphates in dGTP, the oxidation mixture was maintained at 0 ^{o}C and the products were characterized in the total reaction mixture without attempting further purification. The major ions in the negative ion ESI-MS corresponded to mono- and disodium adducts of the deprotonated molecular ion $[M - H]^-$: $[MNa - H]^-$ and $[MNa_2 - H]^-$, along with product ions $[M - H_2PO_3]^-$ and $[MNa - HP_2O_7]^-$. The ^{1}H NMR spectrum of the crude reaction mixture (Figure 2.33) was qualitatively similar to those of the product mixture from oxidation of dGuo and dGMP. In the HMBC spectrum (Figure 2.34), one set of connectivities could be unambiguously ascribed to one 2-Ih-dRTP diastereomer. A component of a multiplet at ~ 5.75 ppm in the H1' region couples with a carbon resonance at 164.0 ppm which can be assigned to C9 of the 2-Ih base by virtue of unsuppressed 1-bond coupling to a formyl H9 signal at 8.43 ppm. The H1' and formyl H9 signals both couple to a carbon at 78.3 ppm having no attached proton and identified on this basis as *spiro*-C5 of the 2-Ih base. The formyl H9 also couples to a carbon signal in the C1' region at 88.4 ppm which in turn couples to a proton in the H2' region at 2.11 ppm. Two additional products in the HMBC spectrum have signals within the H9 region of 2-Ih which show unsuppressed 1-bond coupling to carbons at shifts consistent with 2-Ih formyl C9 and also coupling to carbons in the 2-Ih *spiro* C5 region. However, connectivity between the base moieties and a sugar cannot be definitively established for these components from the HMBC data.

2.5 Discussion

2.5.1 Oxidation of Guanine

We propose 2-Ih as an alternative structure to the isomeric 5,8-dihydroxy-7,8-dihydro-Gua, tentatively identified by mass spectrometry as the major oxidative lesion in double-stranded DNA generated by treatment with the tetrakis(1-methyl-4-pyridiniumyl)manganese porphyrin/$KHSO_5$ oxidation system [Vialas, C. et al,2000]. The manganese porphyrin/$KHSO_5$ oxidant, like DMDO, is known to epoxidize double bonds [Bernadou, J. et al, 1994], and 5-*O*-substituted Gua derivatives have been observed only as transients at low temperature [McCallum, J. E. B. et al, 2004]. This structural reassignment supports the suggestion that iminohydantoin 2-Ih may be a primary oxidative DNA lesion.

2.5.2 Oxidation of DNA

Of paramount interest was whether peracids and DMDO would transform guanine to 2-Ih in single- and double-stranded DNA. We approached this question by DMDO oxidation of the 5-mer *d(TTGTT)* and the short duplex *d*[*(TTGTT)·(AACAA)*]. The single-stranded 5-mer *d(TTGTT)* treated with ~ 7-fold excess of DMDO was 95 % oxidized, with at least 40 % conversion to 2-Ih-modified oligonucleotides estimated from ^{1}H NMR analysis based on integration of signals identified as H1' and H9. Negative ion MALDI-TOF MS of the crude oxidation mixture showed a strong ion at *m/z* 1516, a gain of 34 mass units relative to the deprotonated molecular ion of the unmodified sequence and consistent with formation of the 2-Ih lesion. Fragmentation of this ion, observed by ESI-MS/MS, provided further support for the oxidation of Gua to 2-Ih, showing a collision-induced fragmentation pattern consistent with breaking of the C5-N8 bond to yield ions of the oligonucleotide containing the deoxyribosyl formamide group in both positive and negative ion modes (Figures 2.13, 2.11). The HPLC trace of the reaction mixture indicates a single major product, having an ESI-MS consistent with the 2-Ih-modified 5-mer. 2-Ih in the oxidized 5-mer was definitively

confirmed by digestion and identification of 2-Ih-dR in the mixture of mononucleosides. Oxidation of *d(TTGTT)* annealed to its complement also resulted in generation of 2-Ih, unequivocally identified as the nucleoside by retention time in the HPLC of the digest and by positive ion ESI-MS/MS of the ion corresponding to $[MH]^+$ (Figure 2.14). Significantly, the 2-Ih lesion is sufficiently stable to withstand both digestion and chromatographic separation. This observation, and the stability of the glycosidic bond under acid conditions as evident from the isolation of 2-Ih nucleoside from *m*-CPBA oxidation of dGuo, indicate that 2-Ih, if formed in vivo, might be expected to persist as a stable lesion. Oxidation of DNA by *m*-CPBA has been reported to target purines, particularly in loop regions, with generation of blocking lesions[22]. The lesions were not structurally characterized, but our determination that 2-Ih is a product of Gua oxidation in DNA by *m*-CPBA suggests that 2-Ih may in part account for the reported interference of the oxidative lesions with replication.

Gua + 34 species have been reported from the oxidation of Gua in DNA by a Mn-porphyrin/$KHSO_5$ system, which can function as a monooxygen transfer catalyst [Vialas, C. et al, 2000], and by a dicopper-phenolate complex, via a putative hydroperoxo dicopper(II) transient [Li, L. et al, 2005]. A putative mechanism for the formation of this product with the Mn-porphyrin catalyst has been proposed which involves the trapping of water by a transient guanine cation, formation of dehydrodeoxyspiroiminodihydantoin followed by hydrolytic opening of the imidazolone ring by breaking the bond between imino carbon and the nitrogen attached to the deoxyribose to give an *N*-formylamido-substituted structure rather than the *N*-formylamino-substituted structure of Scheme 2.2. However, the assignment of the *N*-formyl carboxamido structure was speculative, while we have rigorously established the *N*-

formylamino substitution of 2-Ih by a combination of labeling and NMR studies discussed below. We therefore suggest the *N*-formylamino structure of 2-Ih as a plausible alternative.

2.5.3 Oxidation of dGuo by peracids

Peracetic acid is representative of low molecular weight alkyl peracids that might be generated in biological processes[Russell, G. et al, 1957], [Adam, W., Kurz, A. et al, 1999], [Nam, W. et al, 1996], [Abell, L. M. et al, 1991], [Bunik, V. I. et al, 2007], and is also a convenient model oxidant because the acetic acid by-product of oxidation can be removed from reaction mixtures under vacuum, avoiding the need for chromatographic separation of products from spent oxidant. A drawback of aqueous peracetic acid is the presence of hydrogen peroxide as a ~ 6 % equilibrium component [Dul'neva, L. V., Moskvin, A. V., 2005], raising the possibility of concurrent oxidation via an alternative hydroxyl radical pathway. Indeed, Sp and Sp-dR, products of dGuo oxidation by hydroxyl radicals [Lou, W., et al, 2000], [Cadet, J. et al, 2003], were identified in the reaction mixture and can most likely be attributed to hydroxyl radical oxidation. Deglycosylation of the 2-Ih and Sp nucleosides evident in Figure 2.18.a is not surprising in view of the lengthy reaction time at pH < 4 required to maintain peracetic acid in the active, protonated form. The choice of *m*-CPBA as a peracid oxidant rested on the availability in our laboratory of $^{18}O_2$- *m*-CPBA with an ^{18}O content >95 %, allowing us to determine the number and site of oxygen atoms incorporated from the peracid. The *m*-CPBA oxidation yielded 2-Ih-dR and a minor amount of the aglycone as virtually exclusive oxidation products (Figure 2.18.b) supporting the suggestion that Sp observed in the oxidation of Gua with peracetic acid was generated by hydroxyl radical. Only trace quantities of Sp-dR and its aglycone were detected in the *m*CPBA oxidation, possibly products of a minor radical pathway via O-O homolysis of *m*-

CPBA [Ryu, E. K., MacCoss, M., 1981], [Bravo, A. et al, 1996]. The product profile generated by *m*-CPBA oxidation strongly supports 2-Ih as the product of the peracid oxidation of dGuo in protic solvents, and the predominance of the nucleoside as a product at pH 4.5 indicates that the glycosidic bond is robust and should be stable under physiological conditions.

2.5.4 Labeling studies and oxidation mechanism

A mechanism for the oxidation of Gua consistent with the positions of the ^{13}C and ^{15}N labels in the isotopomeric iminohydantoin products is given in Scheme 2.2. Epoxidation of the 4,5-double bond is followed by a 1,2-acyl migration and hydrolytic opening of the imidazole ring [Vialas, C. et al, 1998] to give 2-Ih. As required by the 1,2-carbonyl shift, the ^{13}C label at position 4 of guanine becomes *spiro* carbon C5 of 2-iminohydantoin. Also in accord with Scheme 2.2, oxidation of [7-^{15}N]guanine yielded 2-Ih with ^{15}N label at the carboxamido nitrogen [Ye, W., et al]. Hydrolytic opening of the transient imidazolone ring via dehydrodeoxyspiroiminodihydantoin (**4**, Scheme 2.2) is then predicted to give 2-Ih. Ring cleavage of **4** to 2-Ih according to Scheme 2.2 has been definitively established by the presence of two inequivalent carboxamido N*H* signals in the ^1H NMR spectrum of 2-Ih, which show $^1J_{N\text{-}H}$ coupling of ~ 90 Hz in the 7-^{15}N isotopomer These observations rule out an *N*-formylamido structure which, as discussed above, has been proposed to result from the hydrolytic ring opening of transient **4** in the Mn-porphyrin-catalyzed persulfate oxidation of Gua in DNA [Pratviel, G.; Meunier, B., 2006]. Along with the ^{18}O-incorporation studies, which show that the carboxamide oxygen is derived from oxidant and the formamide oxygen from water, definitively establish the oxidation mechanism proposed in Scheme 2.2. The high yield of 2-Ih-dR on oxidation of dGuo by *m*-CPBA along with the absence of 8-oxo-

dGuo or other products that have been identified in radical-mediated oxidation of dGuo, support Scheme 2.2 as the predominant oxidation pathway by peracids and DMDO and also support the high level of conversion of guanine to 2-Ih in the oxidation of DNA, as implied by the analysis of the oxidized single and double stranded oligonucleotides.

2.5.5 Structural Analysis of the DMDO Oxidation of dGuo, dGMP and dGTP

Oxidations with DMDO as oxidant were carried out on a scale permitting rigorous structural characterization of the product profiles. The presence of the N9 sugar substituent would be expected to result in enantioselective induction of the asymmetric center at *spiro* C5. The DMDO oxidations of dGuo and dGMP conform to expectation; both starting compounds yield two diastereomers in a ~ 2:1 mixture. In addition, slow rotation around the N8-C9 formamido bond resulted in resolution of two rotational isomers for each diastereomer, analogous to behavior reported for the 2-Ih base [Ye, W., 2006] and the *N*-(2'-deoxyribosyl)formamide lesion [Guy, A. et al, 1991], [Maufrais, C. et al, 2003]. The major rotational isomers of the 2-Ih deoxynucleoside diastereomers were favored by an order of magnitude over the minor rotamers, with the result that only the major components **1a** and **1b** gave detectable NOESY interactions in homonuclear shift correlation spectra and C,H cross peaks in the heteronuclear shift correlation spectra. Exchange cross peaks in the ROESY spectrum permitted the proton signals of minor rotamers **1a'** and **1b'** to be correlated with those of the corresponding major rotamers **1a** and **1b**, respectively (Figure 2.22). Rotamer preference was less pronounced for the deoxynucleotide diastereomers, with ratios being 3:1 for the major diastereomer **2a** and ~ 5:1 for the minor diastereomer **2b**. In the ROESY spectrum, two sets of NOESY peaks could be related by exchange and were assigned to the major diastereomer (**2a** and **2a'**). One set of NOESY cross peaks was assigned to **2b** (Table

2.3). The signals assigned to diastereomer **2b** were related by exchange to the remaining minor component **2b'** which was too dilute for detection of NOESY cross peaks. Sugar-base connectivities were established for all deoxynucleoside and 5'-monophosphate diastereomers.

Chart 2.1 Structure of 5-carboxamido-5-formamido-2-iminohydantoin (2-Ih) and 2-Ih-containing products **1a**, **b** (2-Ih-dR); **2a**, **b**(2-Ih-dRP); **3a**, **b**(2-Ih-dRTP).

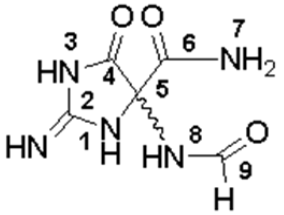

2-Ih

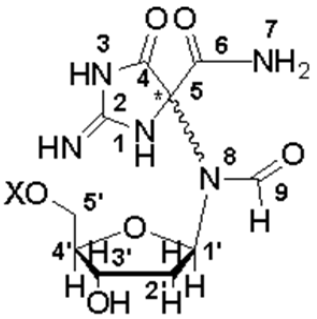

1a, **b**, X=H
2a, **b**, X=PO_3H_2
3a, **b**, X= triphosphate

Scheme 2.2 Mechanism of guanine epoxidation by DMDO or peracid

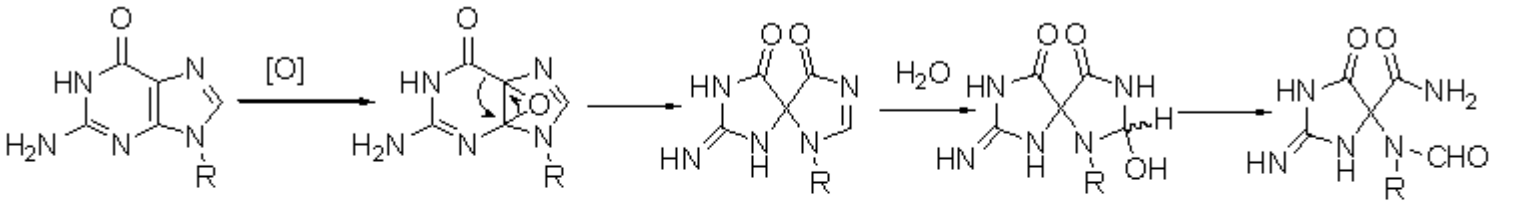

dehydrodeoxyspiroimino-dihydantoin (**4**)

2-Ih or 2-Ih derivatives

Note: R can be assigned to H, 2'-deoxyribose, 2'-deoxyribose monophosphate, 2'-deoxyribose triphosphate or DNA backbond

Scheme 2.1 Synthetic scheme of labeled Guanine

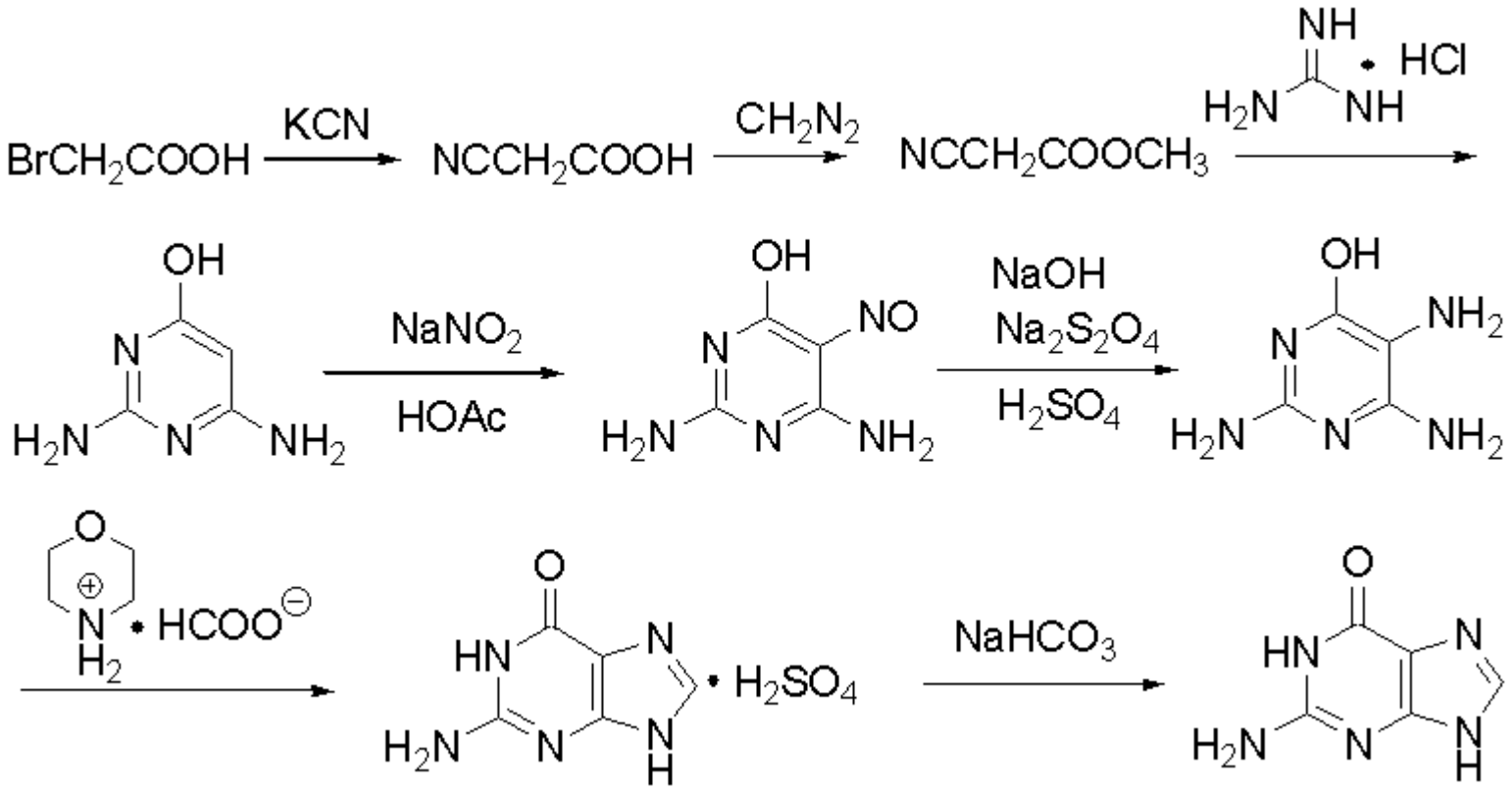

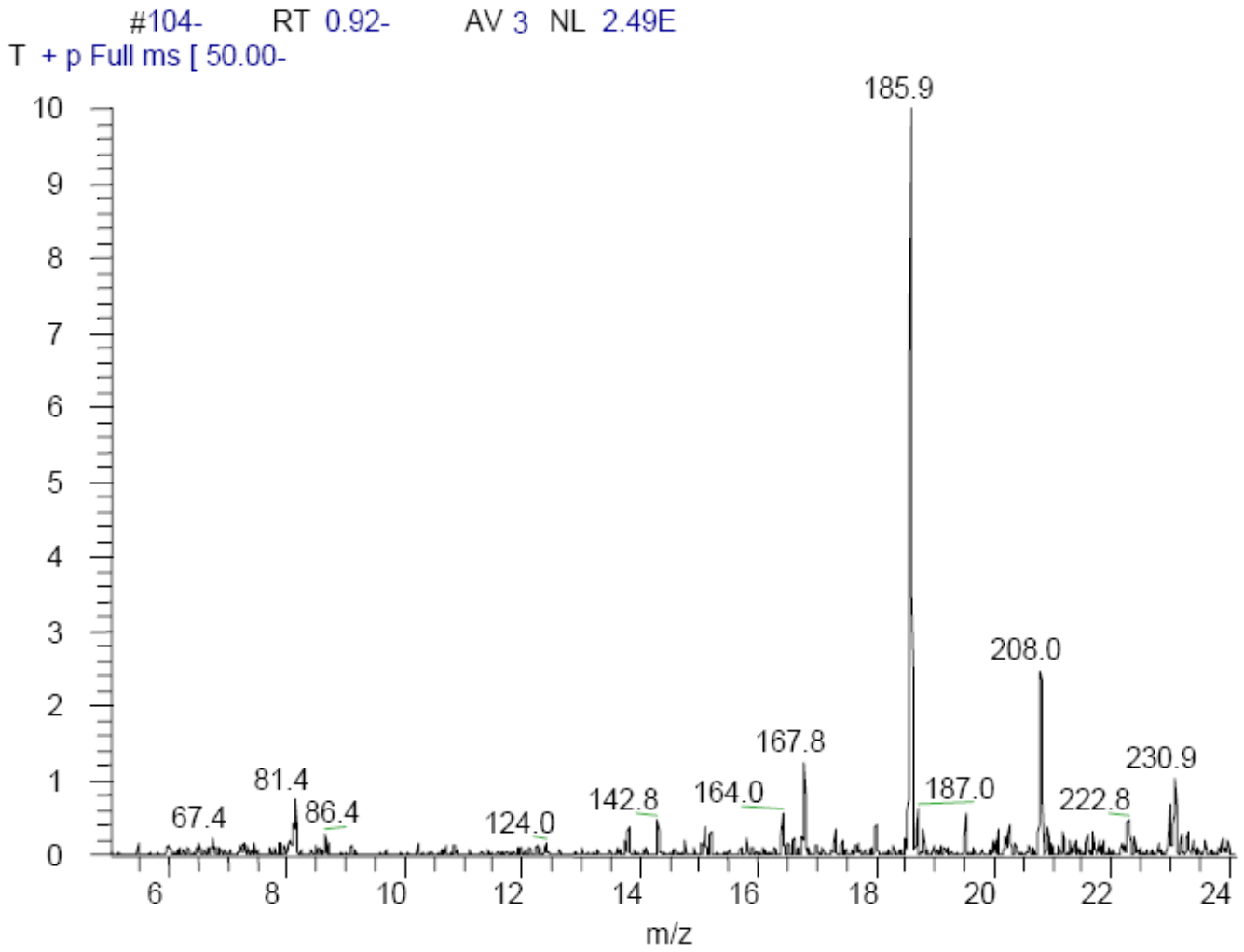

Figure 2.1 Full scan ESI-MS$^+$ of NA-2-Ih: m/z 186 $[MH]^+$, 208 $[M + Na]^+$.

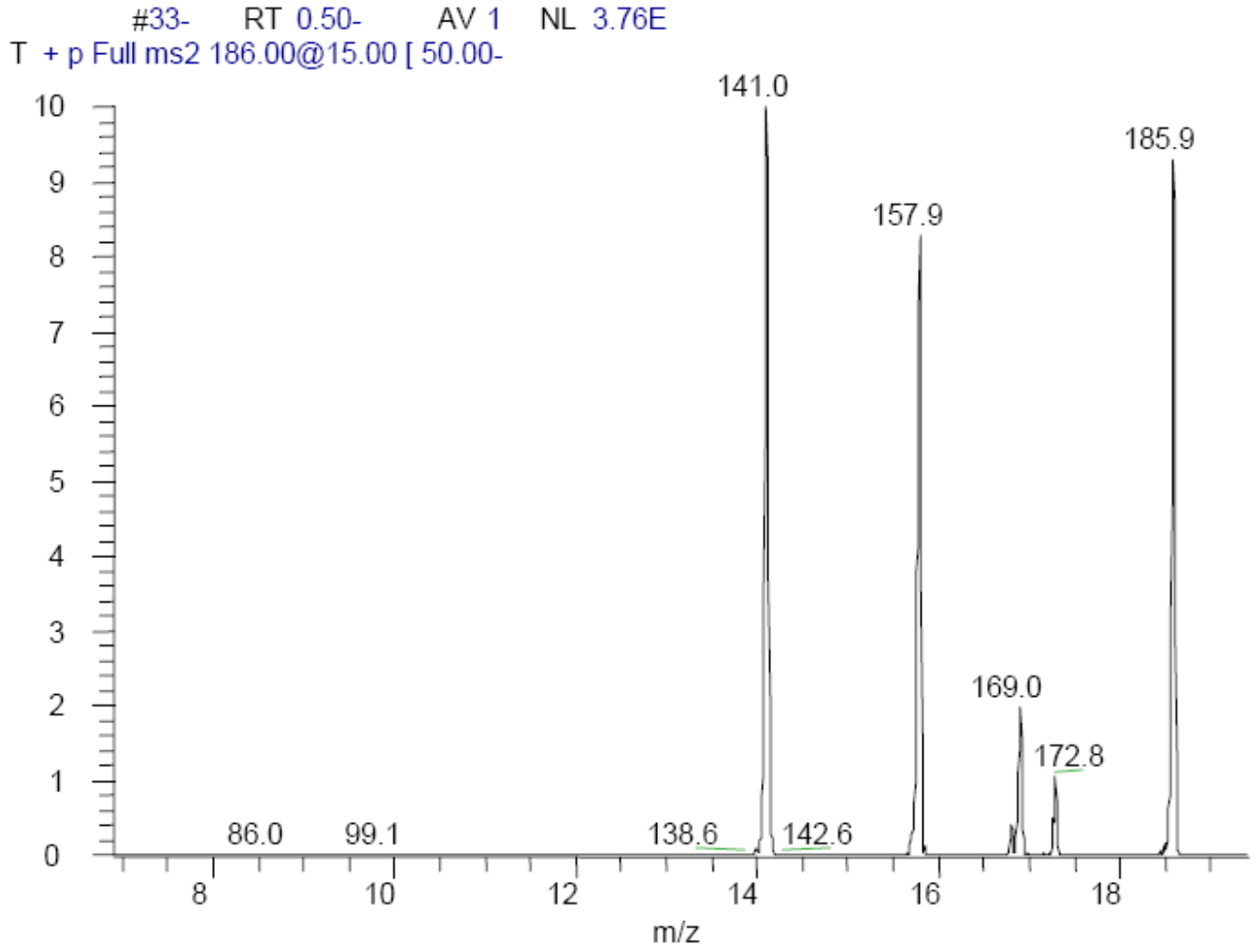

Figure 2.2 ESI-MS/MS$^+$ of NA-2-Ih: m/z 186 $[MH]^+$, 169 $[MH\text{-}NH_3]^+$, 158 $[MH\text{-}CO]^+$, 141 [MH-formamide]$^+$.

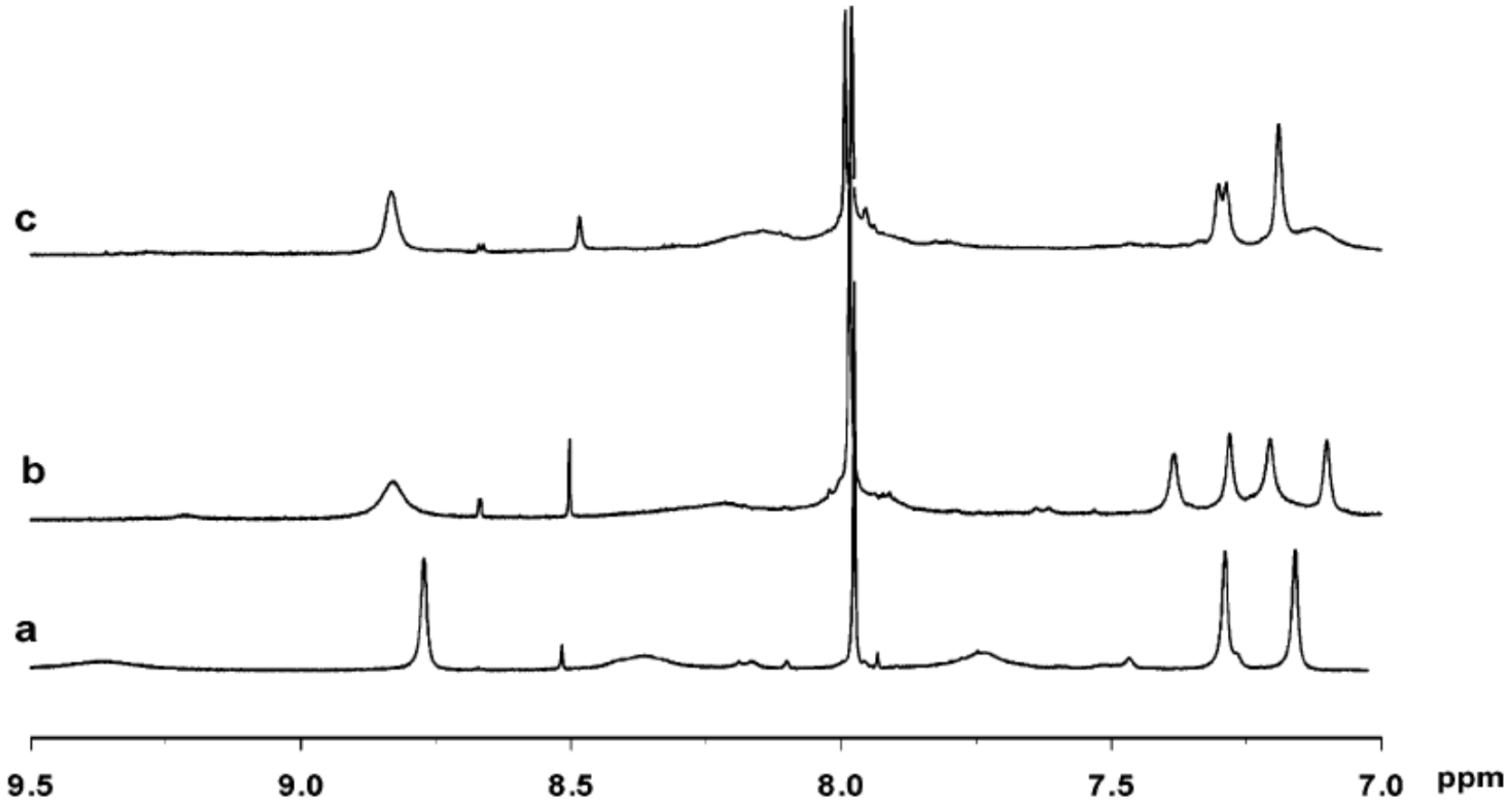

Figure 2.3 ^{1}H NMR (500 MHz, DMSO-d_6) of (a) NA-2-Ih, (b) [7-^{15}N]-2-Ih, and (c) [5-^{13}C]-2-Ih. Signal assignments are discussed in the text. The dependence of the chemical shifts of rapidly exchanging protons on sample concentration and residual water is evident.

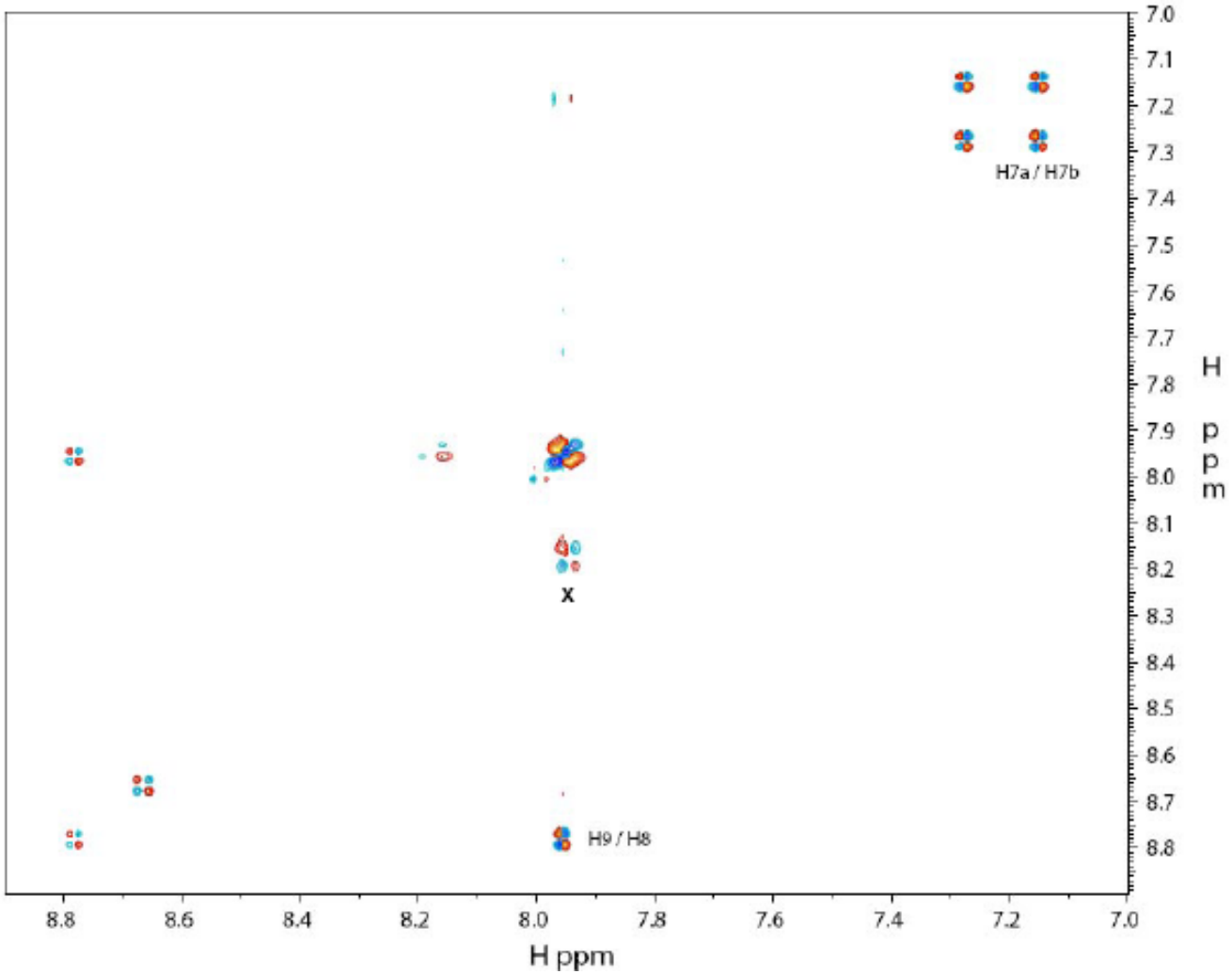

Figure 2.4 DQF COSY spectrum of NA-2-Ih. Cross peaks between the signals of the slowly exchanging carboxamido protons at 7.19 (NH_a) and 7.29 (NH_b) ppm and between the formyl proton H9 at 8.77 ppm and the formamido proton H8 at 7.94 ppm are indicated in the figure.

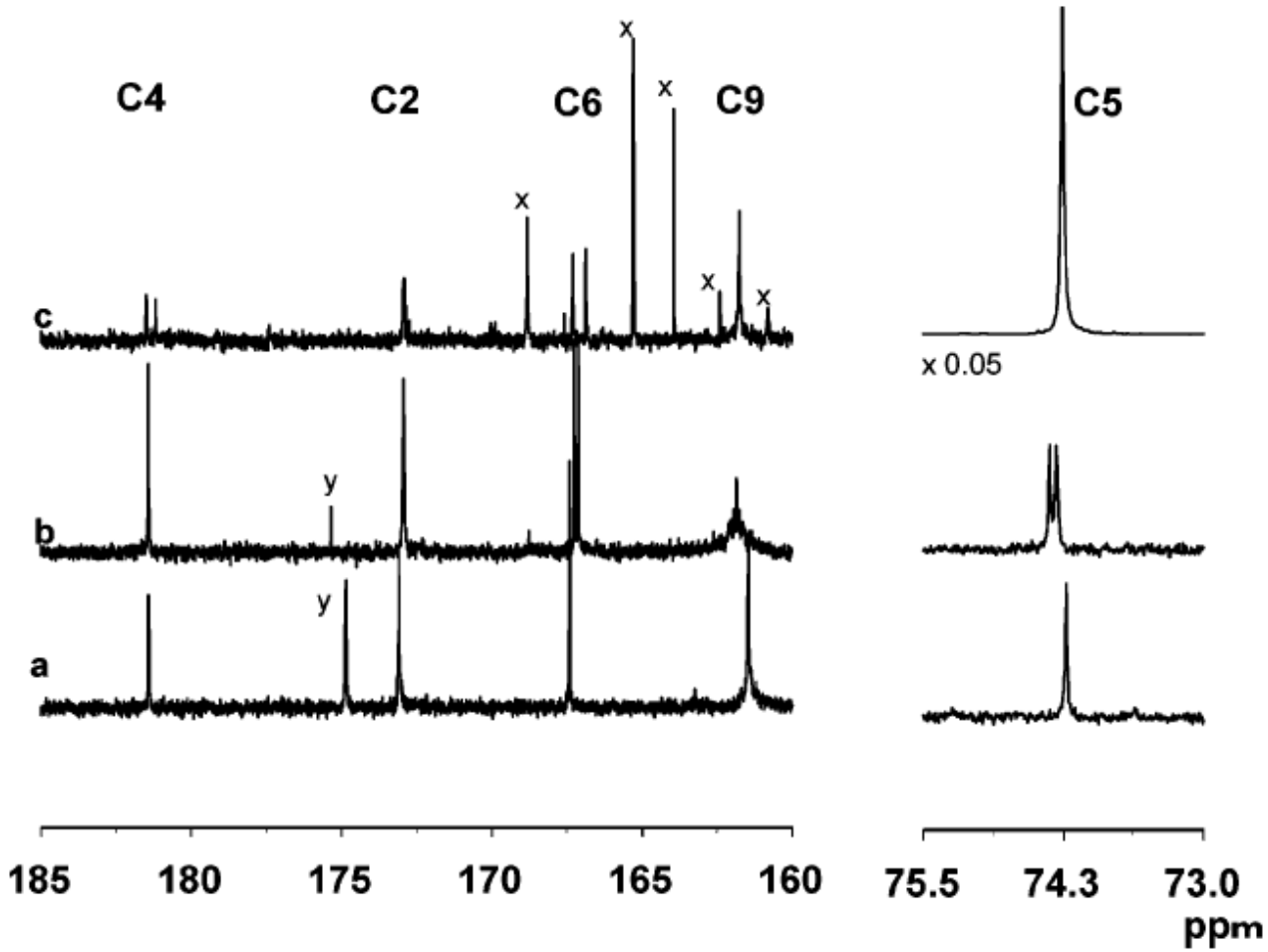

Figure 2.5 Proton-decoupled ^{13}C NMR (125 MHz, DMSO-d_6) of (a) NA-2-Ih, (b) [7-^{15}N]-2-Ih, and (c) [5-^{13}C]-2-Ih. Signal assignments are shown above the top panel. Peaks denoted *x* are impurities; peaks denoted *y* are acetate from buffer.

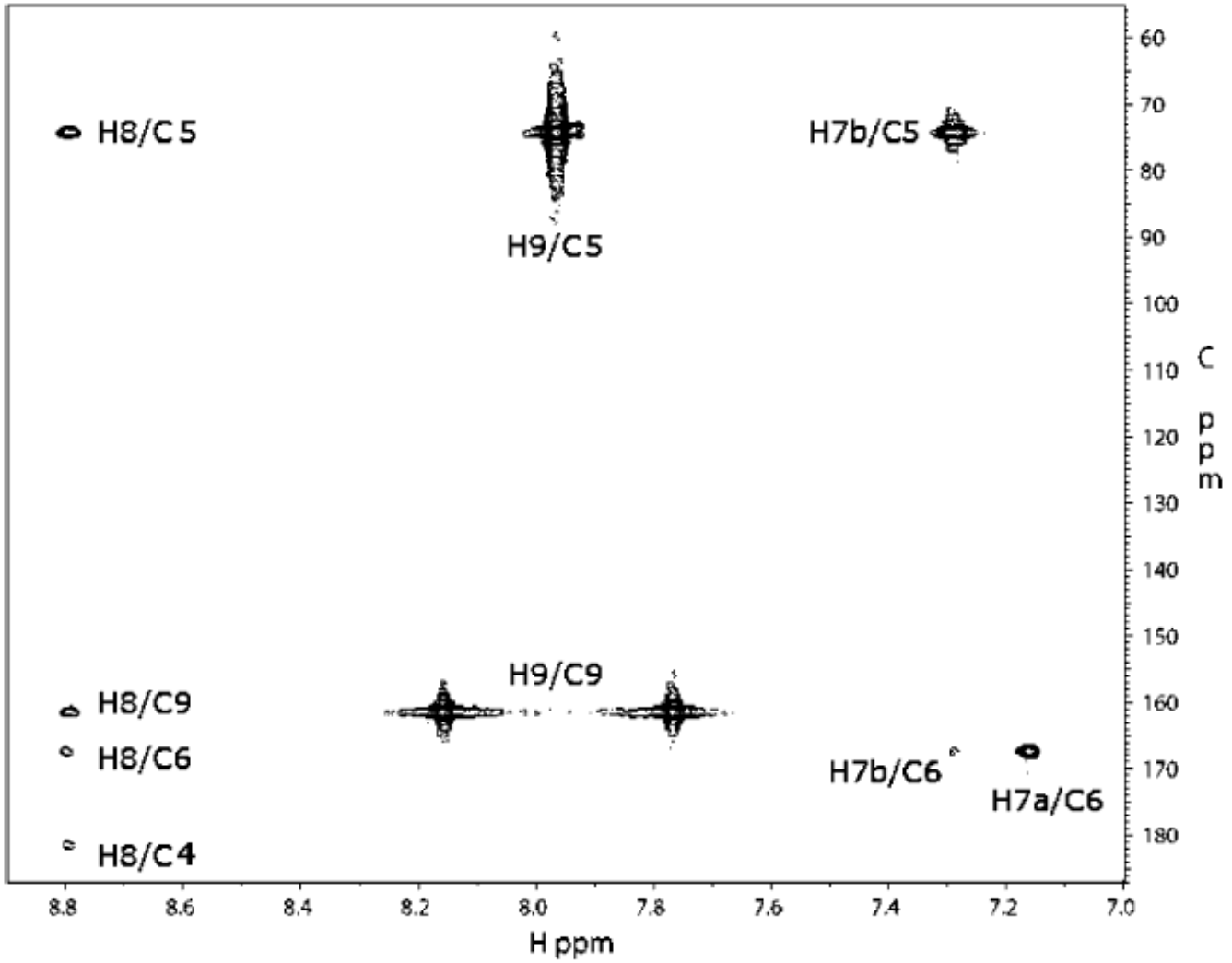

Figure 2.6 HMBC spectrum of NA-2-Ih. C,H cross-peaks are indicated on the spectrum.

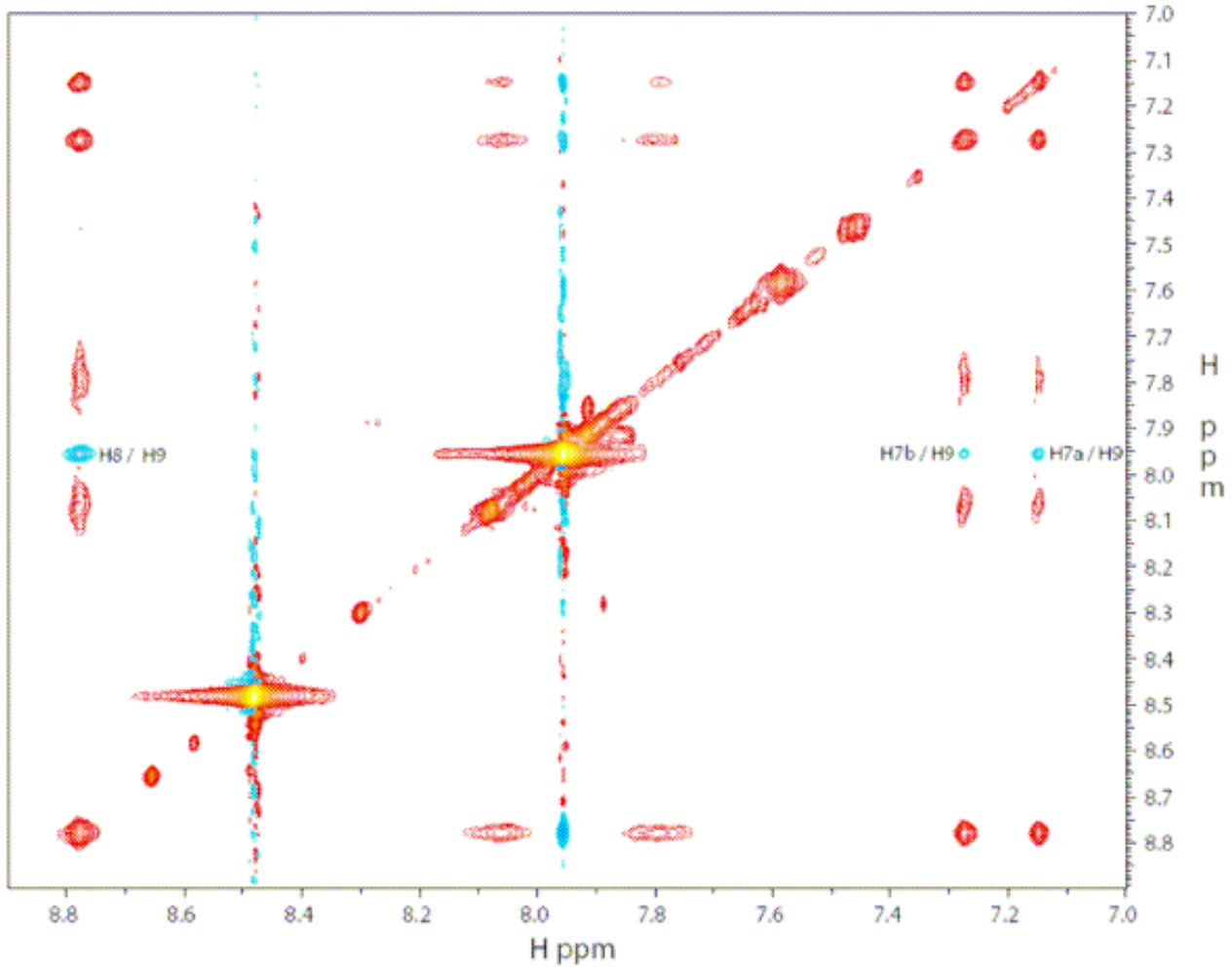

Figure 2.7 NOESY spectrum of NA-2-Ih. True NOESY cross peaks (blue contours) between the 4-carboxamido protons $H7_a$ and $H7_b$ and between and the formyl C*H* at 7.94 ppm and between the formyl proton and the slowly exchanging N*H* at 8.77 ppm are indicated on the spectrum. Cross peaks between the exchangeable protons as well as between the exchangeable protons and residual water (red contours) are also observed.

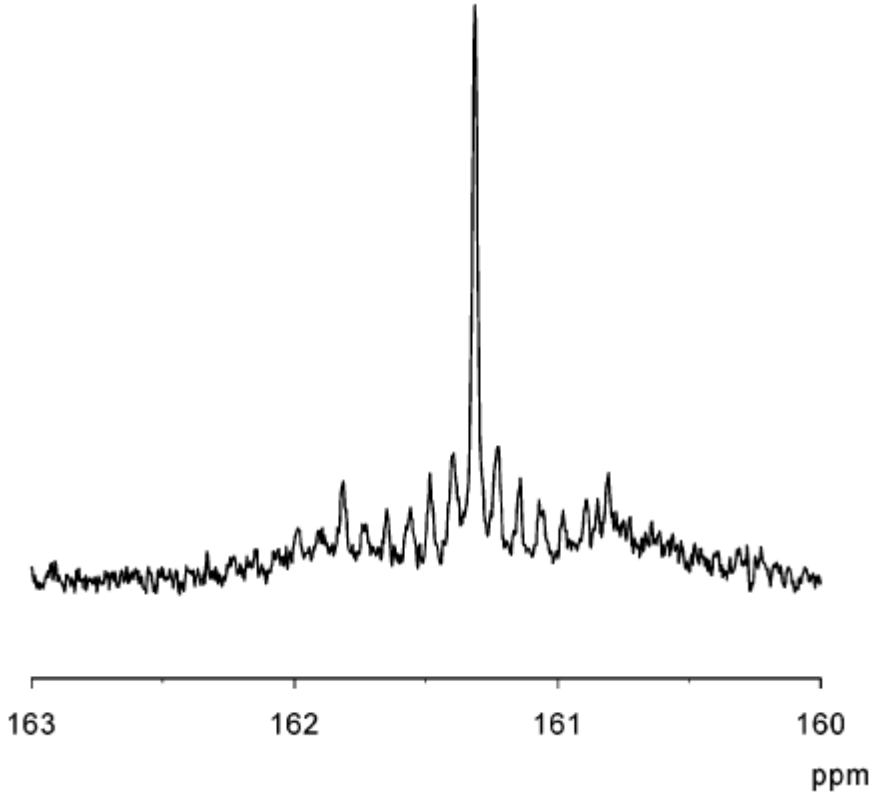

Figure 2.8 ^{13}C NMR (125 MHz, 9:1 $H_2O/^2H_2O$) of NA-2-Ih, HCl showing the structure of the signal assigned to formamido carbon arising from rotational isomers and deuterium exchange.

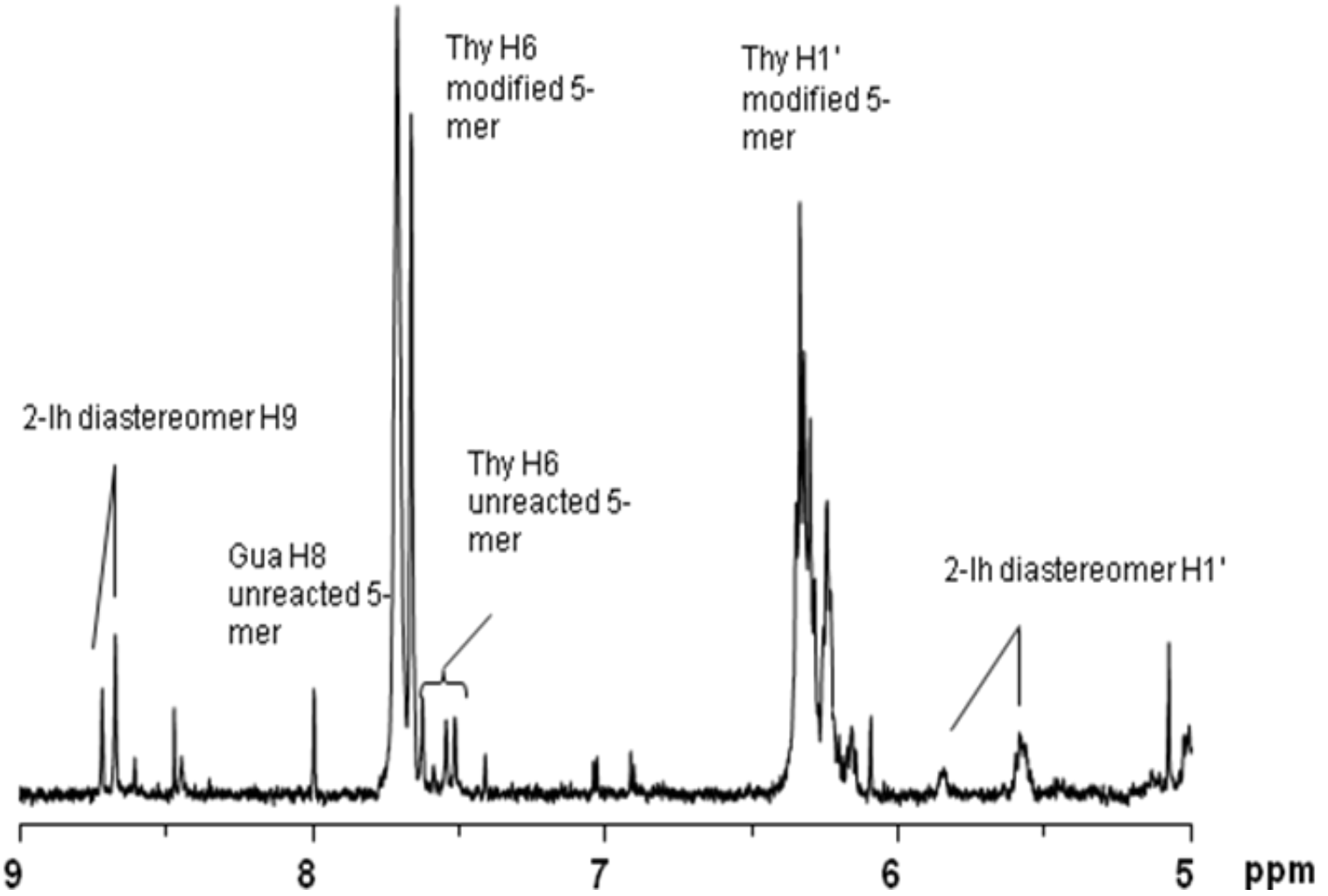

Figure 2.9 ^{1}H NMR (500 MHz, D_2O) of oxidized d(TTGTT) in the H1′ - H9 range. Signals identified with 2-Ih are identified on trace.

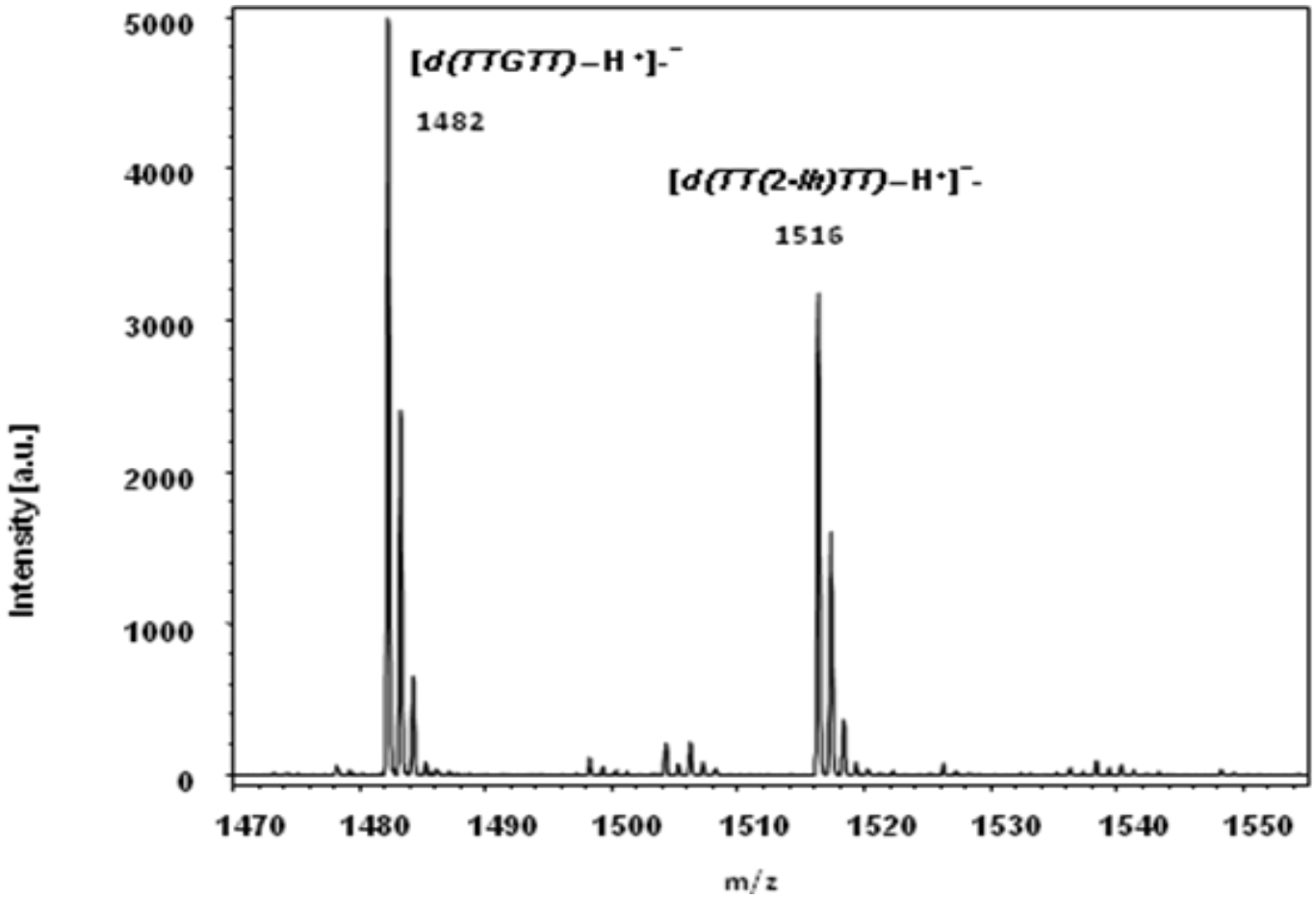

Figure 2.10 Negative ion MAL DI-TOF mass spectrum of total reaction mixture of oxidized *d(TTGTT)* showing unoxidized 5-mer (*m/z* 1482) and product at +34 mass units (*m/z* 1516).

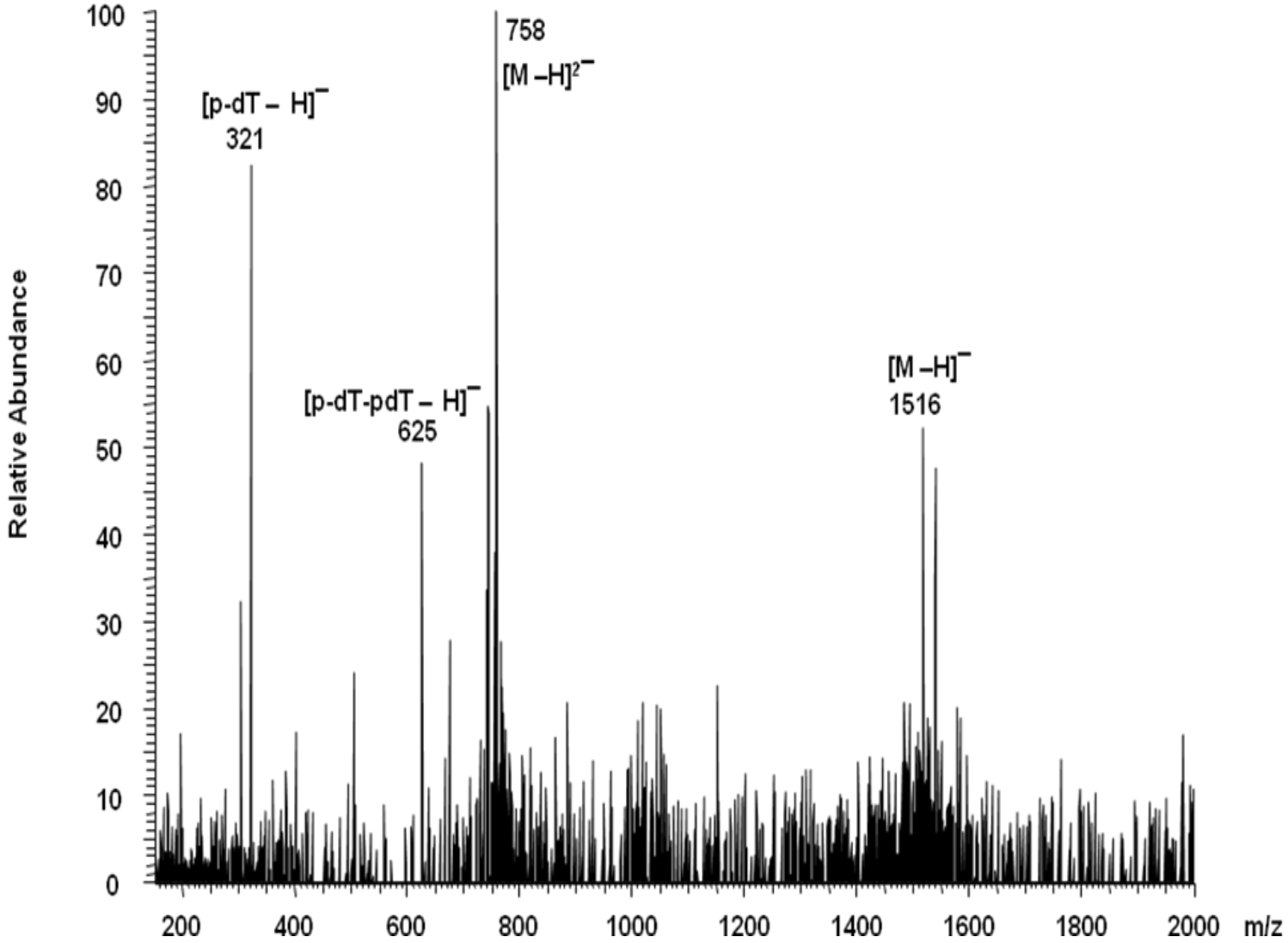

Figure 2.11 Negative ion ESI-MS of oxidized 5-mer.

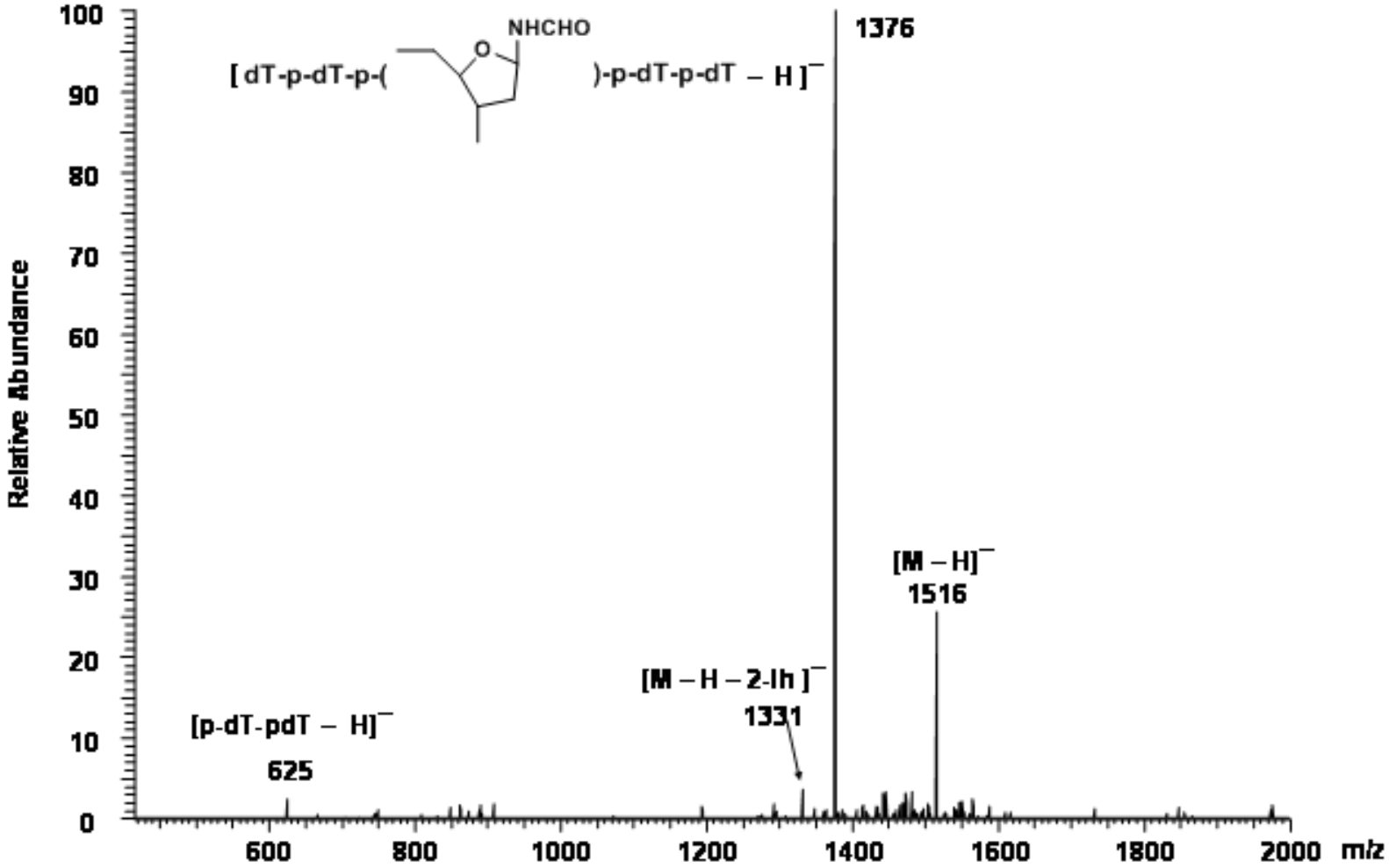

Figure 2.12 Negative ion ESI-MS/MS of ion *m/z* 1516 of oxidized 5-mer.

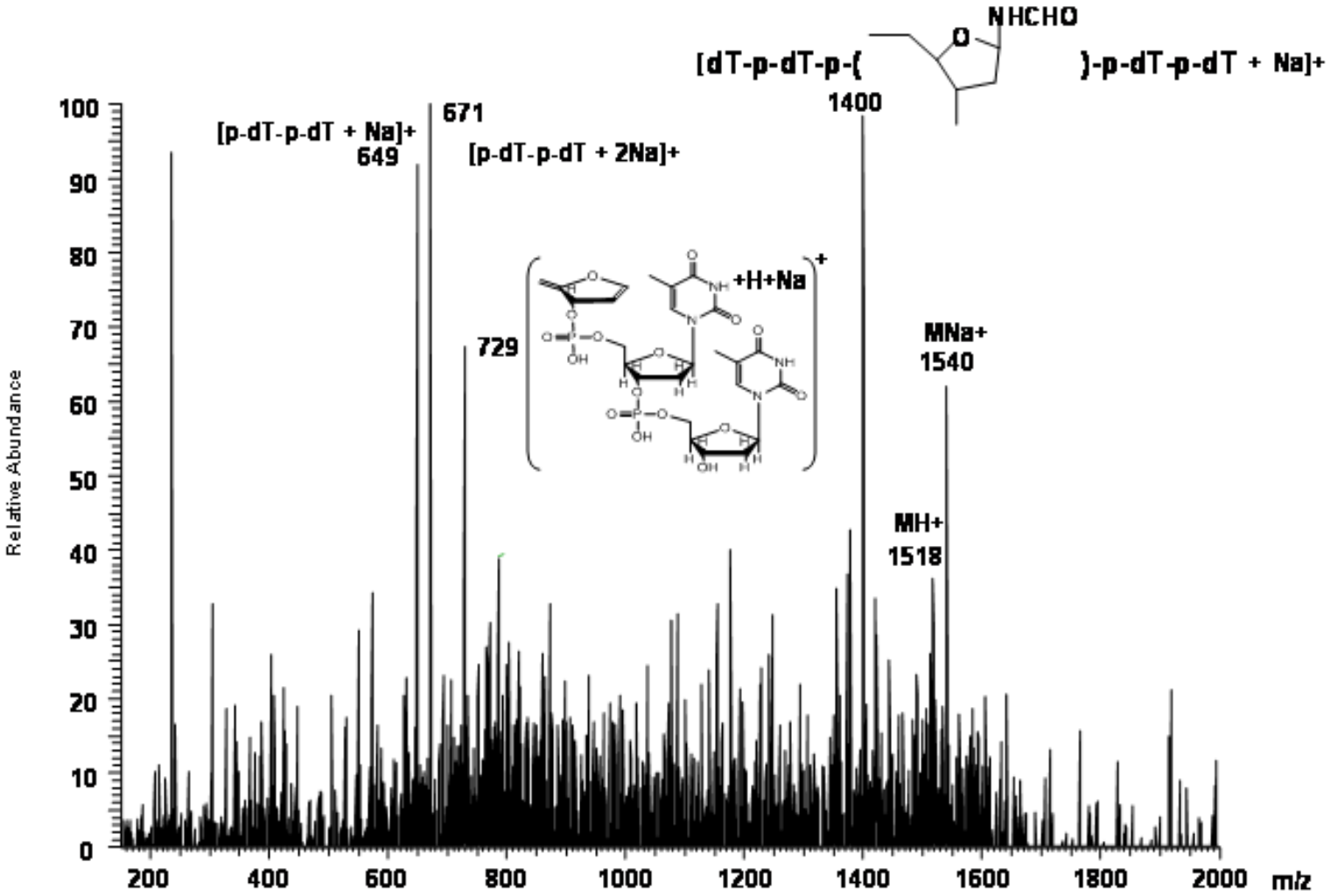

Figure 2.13 Positive ion ESI-MS of oxidized 5-mer.

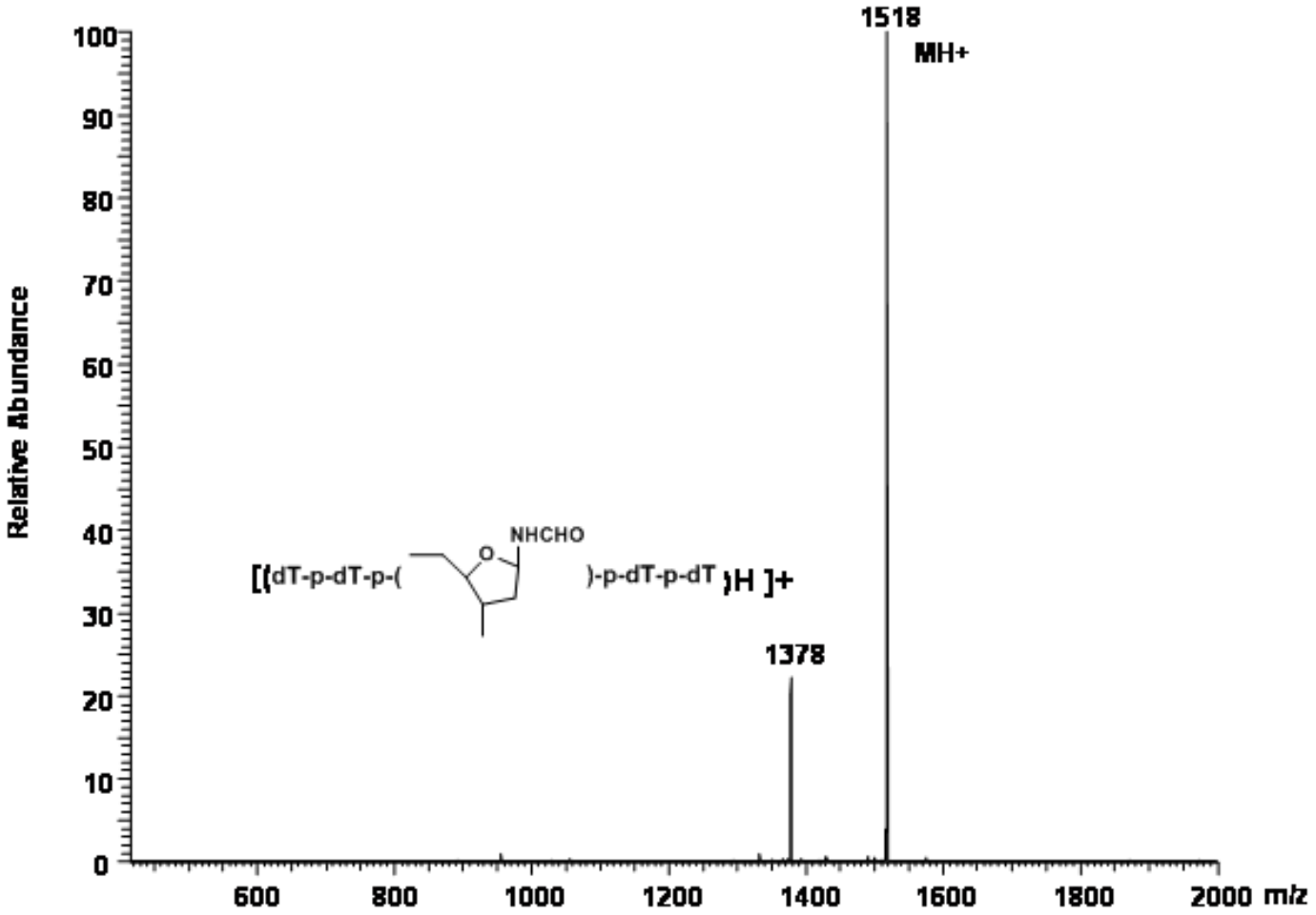

Figure 2.14 Positive ion ESI-MS/MS of ion at *m/z* 1518, 9 min peak in HPLC of oxidized 5-mer.

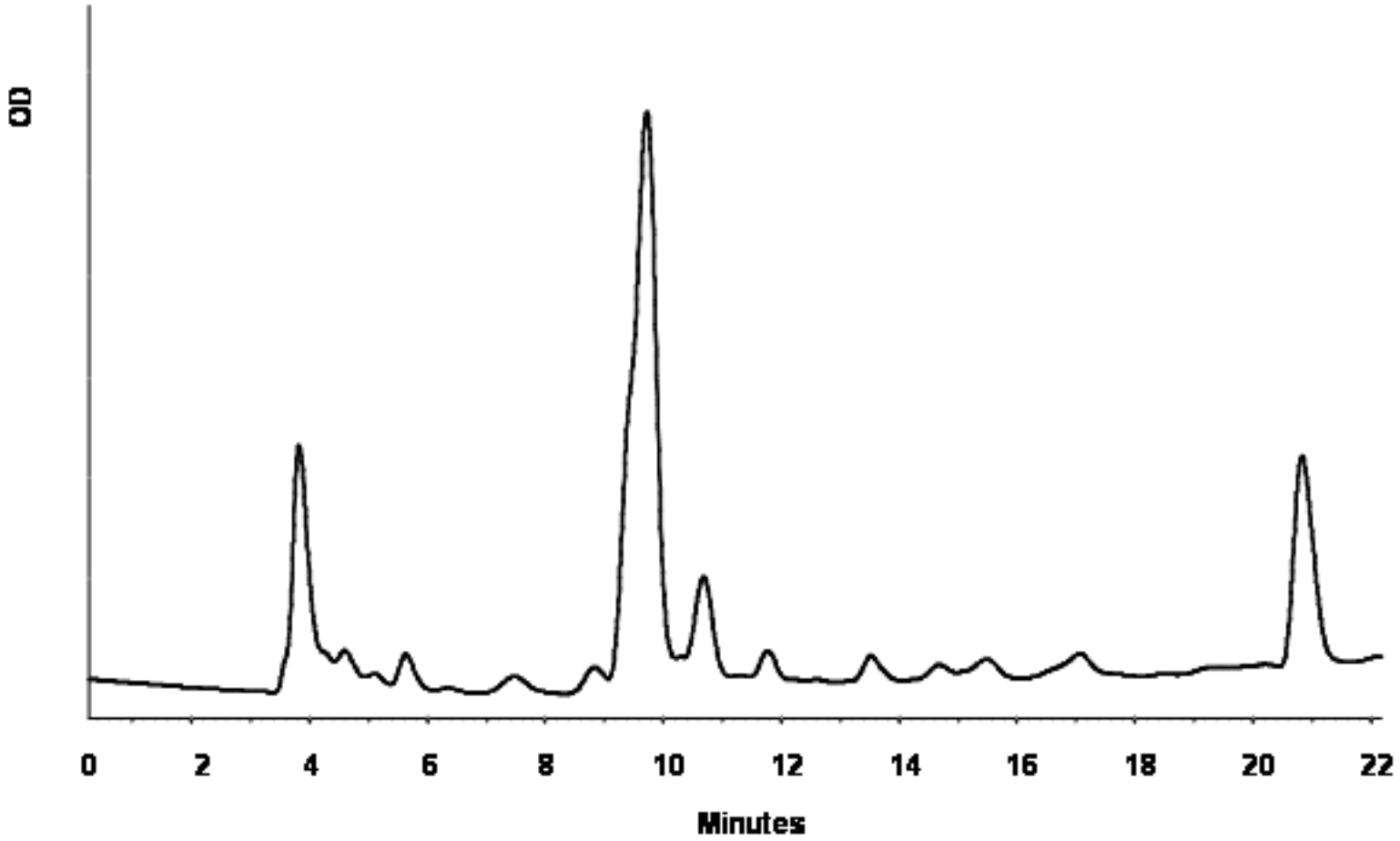

Figure 2.15 HPLC trace (detector at 260 nm) of reaction mixture from DMDO oxidation of 5-mer.

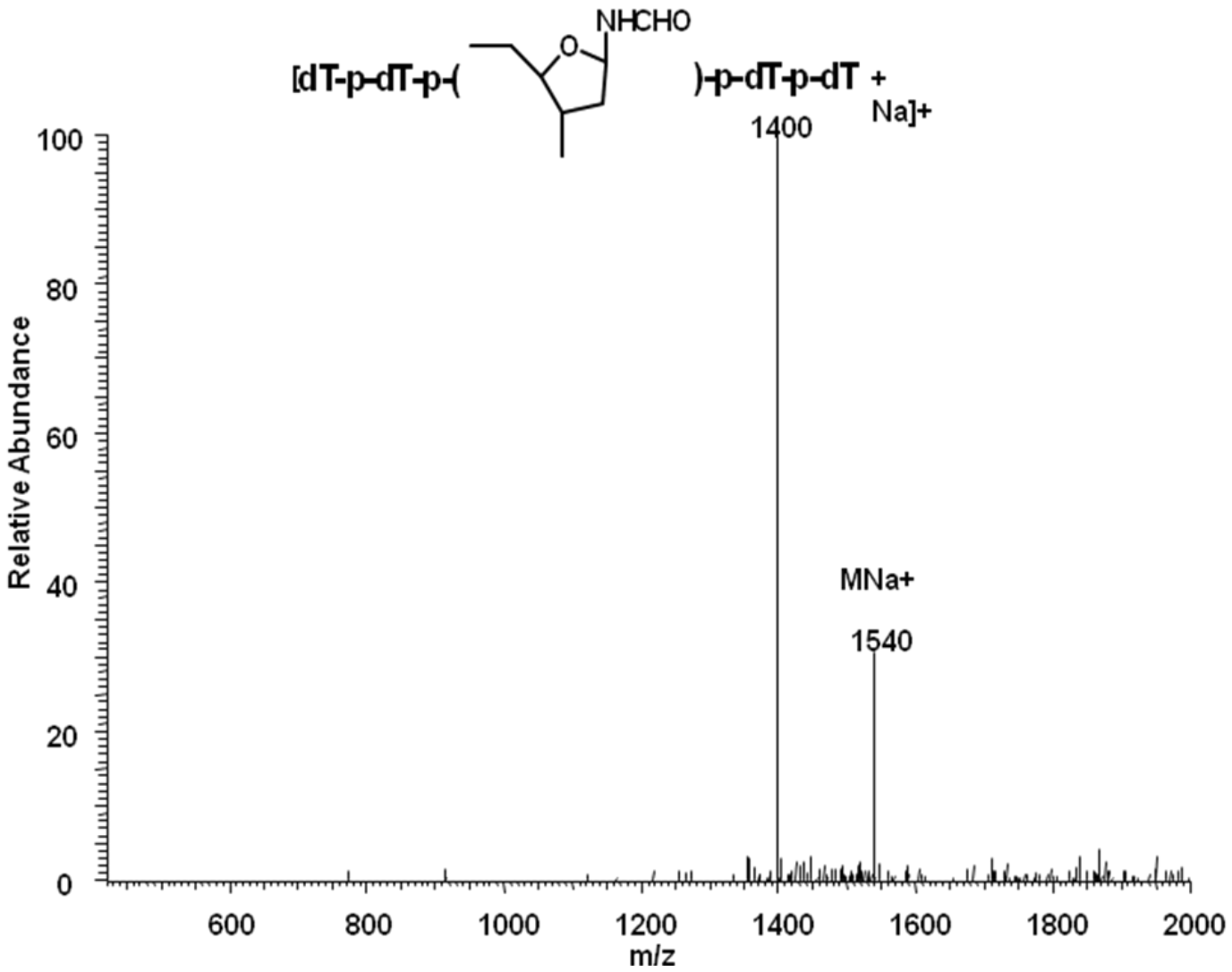

Figure 2.16 Positive ion ESI-MS/MS of m/z 1540 ($[MNa]^+$) from peak at 9.5 min in HPLC of oxidized 5-mer.

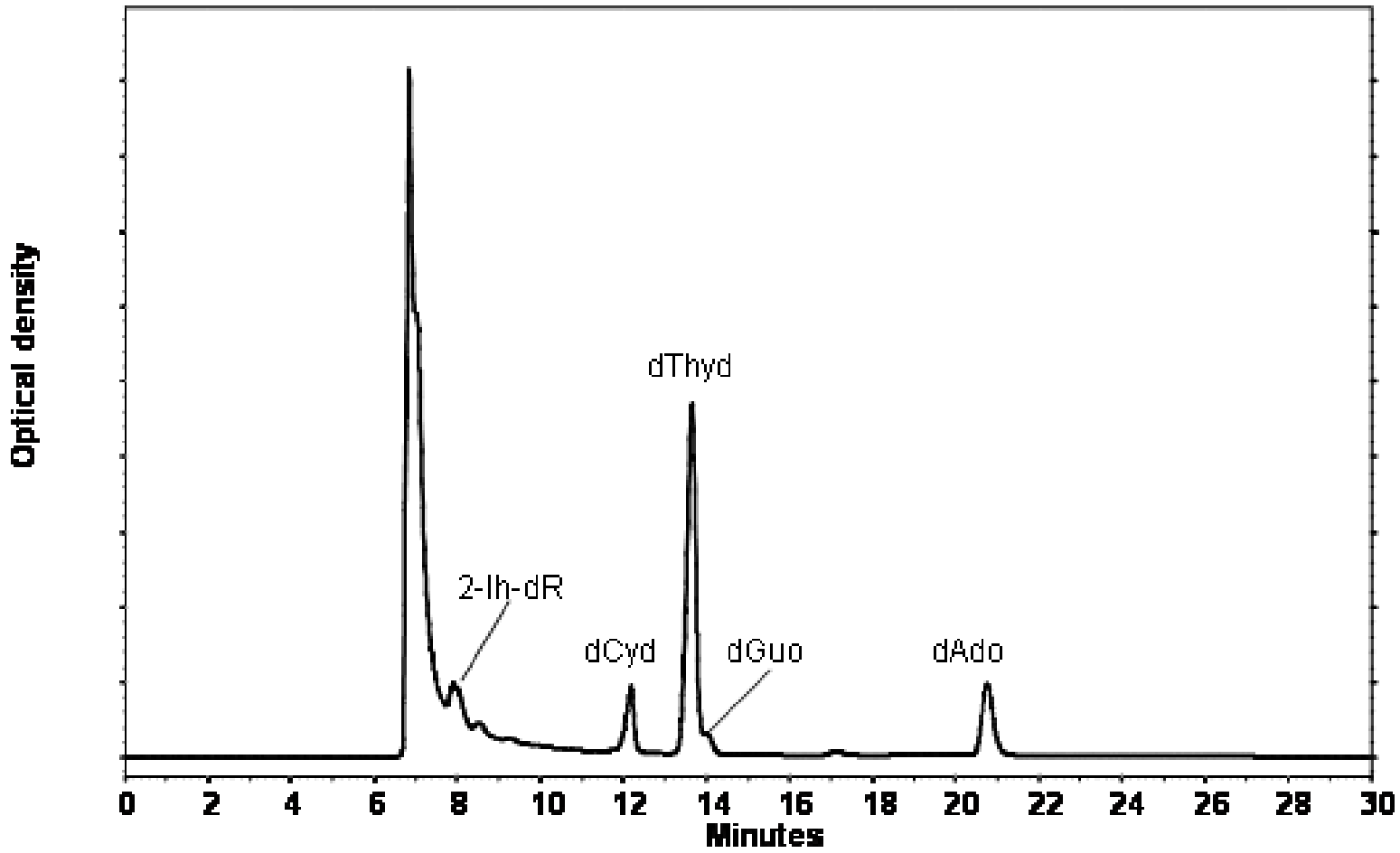

Figure 2.17 HPLC (UV detector set at 252 nm) of digest of oxidized 5-mer. Peaks are identified on trace.

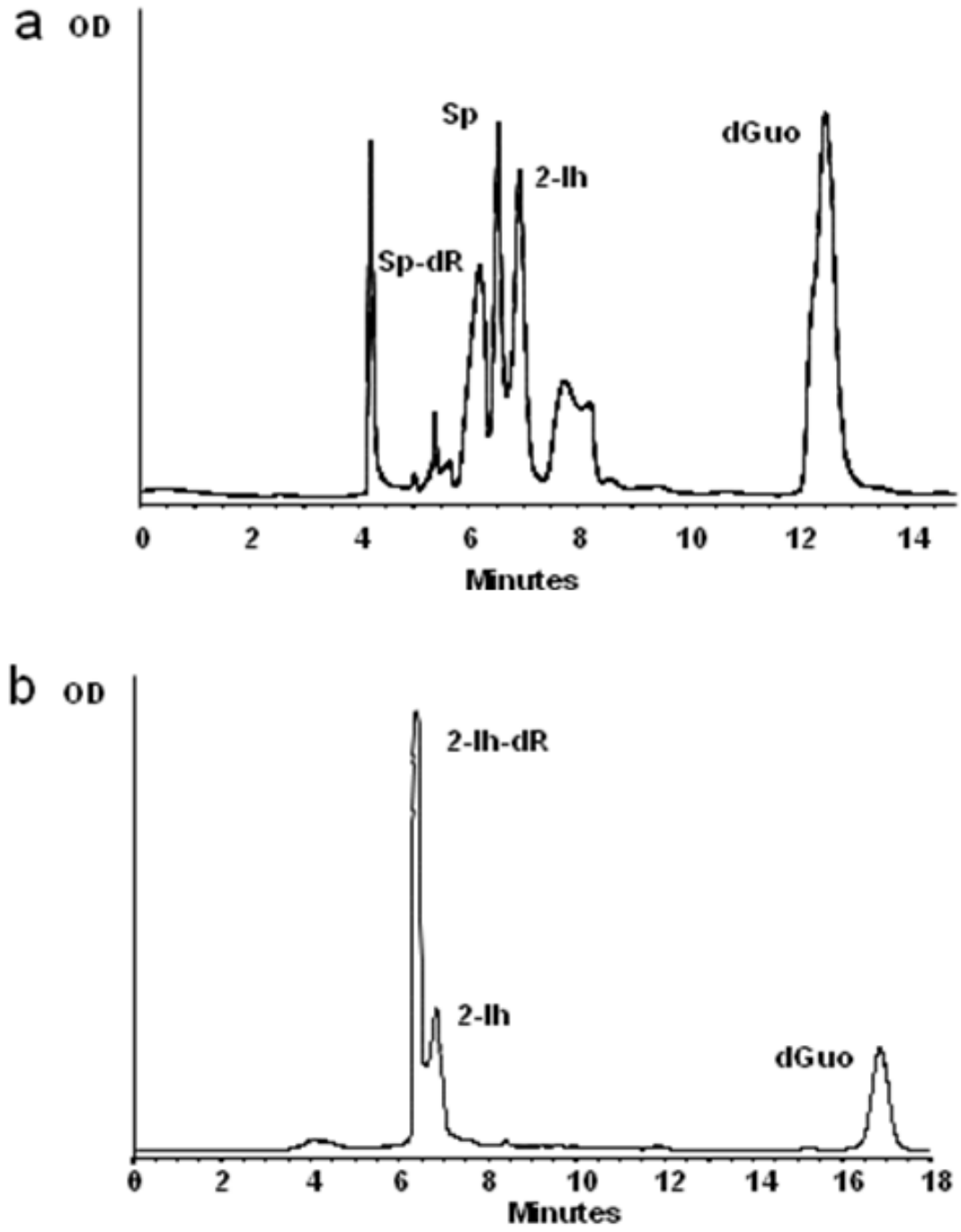

Figure 2.18 HPLC traces (detector set at 230 nm) of reaction mixtures from dGuo oxidation by (a) peracetic acid and (b) *m*-CPBA, following extraction of spent oxidant. Products identified are indicated on traces.

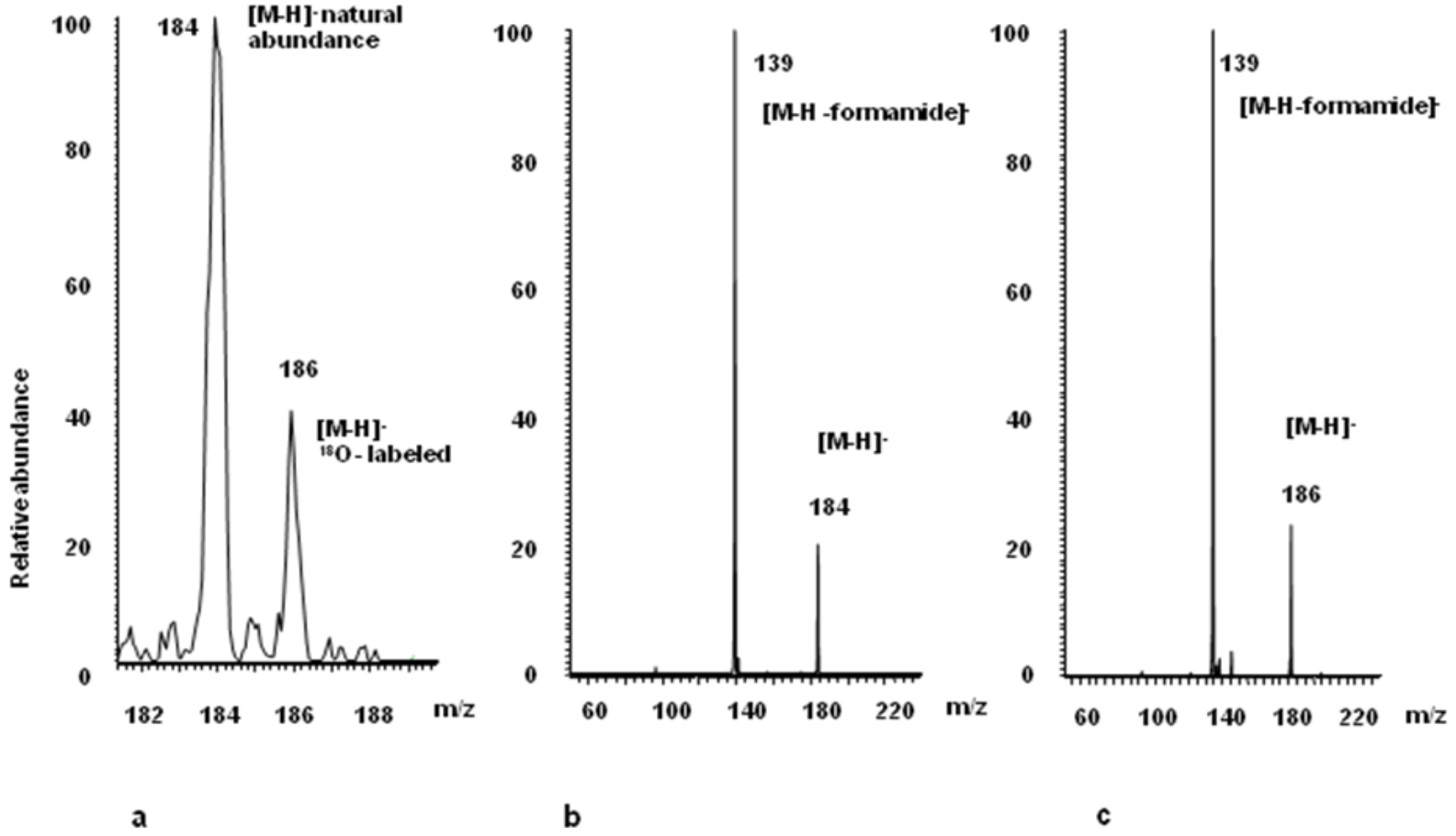

Figure 2.19 (a) Negative ion ESI-MS showing $^{16}O/^{18}O$ distribution in 2-Ih base from DMDO oxidation of Gua in 1:1 mixture of $H_2{}^{16}O/H_2{}^{18}O$, (b) Negative ion ESI-MS/MS of molecular ion of natural abundance 2-Ih and (c) Negative ion ESI-MS/MS of molecular ion ^{18}O-labeled 2-Ih showing loss of the label with the formamide moiety.

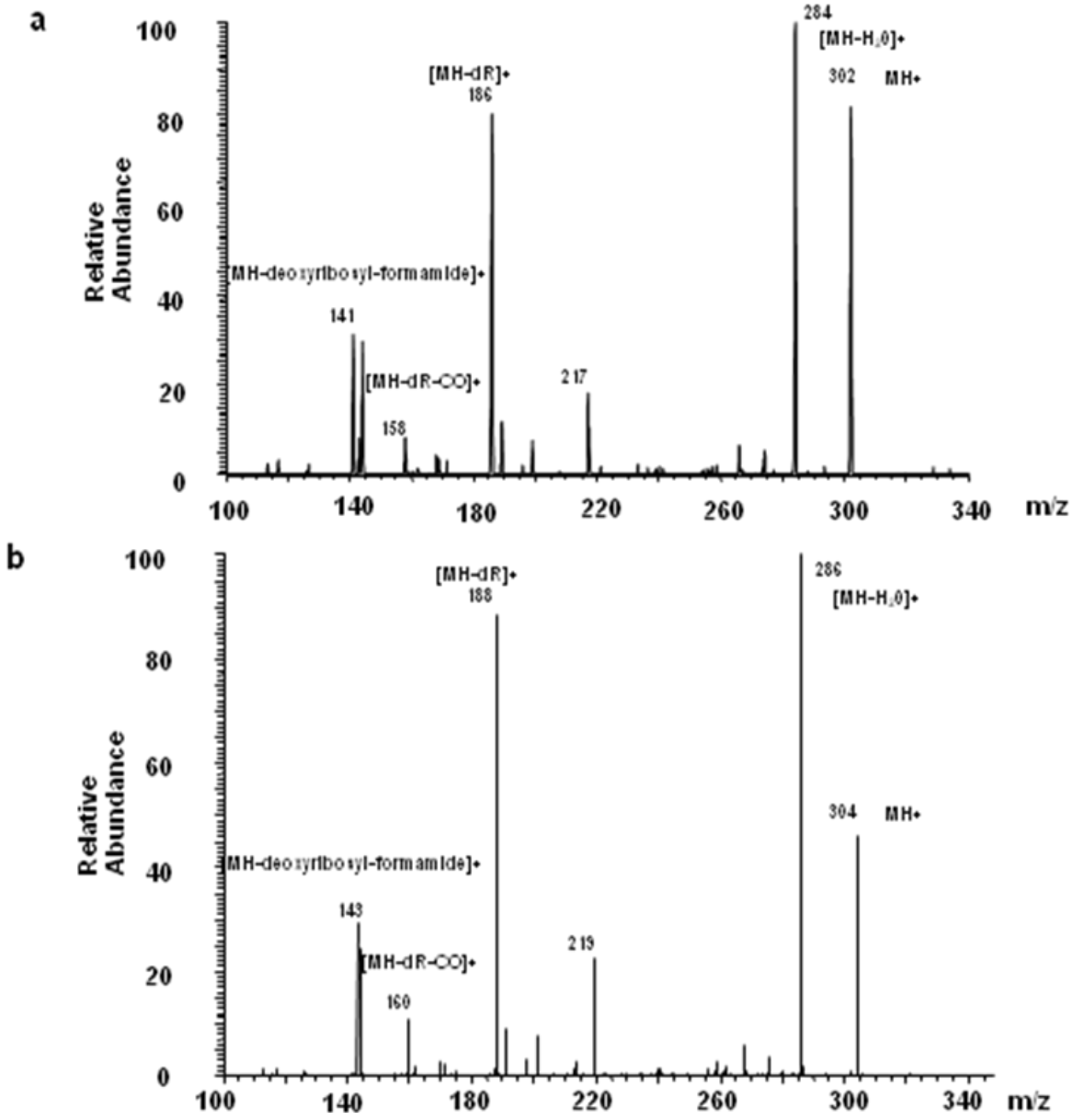

Figure 2.20 Positive ion ESI-MS of 2-Ih-dR from oxidation of dGuo with (a) natural abundance *m*-CPBA and (b) $^{18}O_2$-*m*-CPBA, indicating retention of ^{18}O label in the product ion at *m/z* 143 from loss of deoxyribosylformamide.

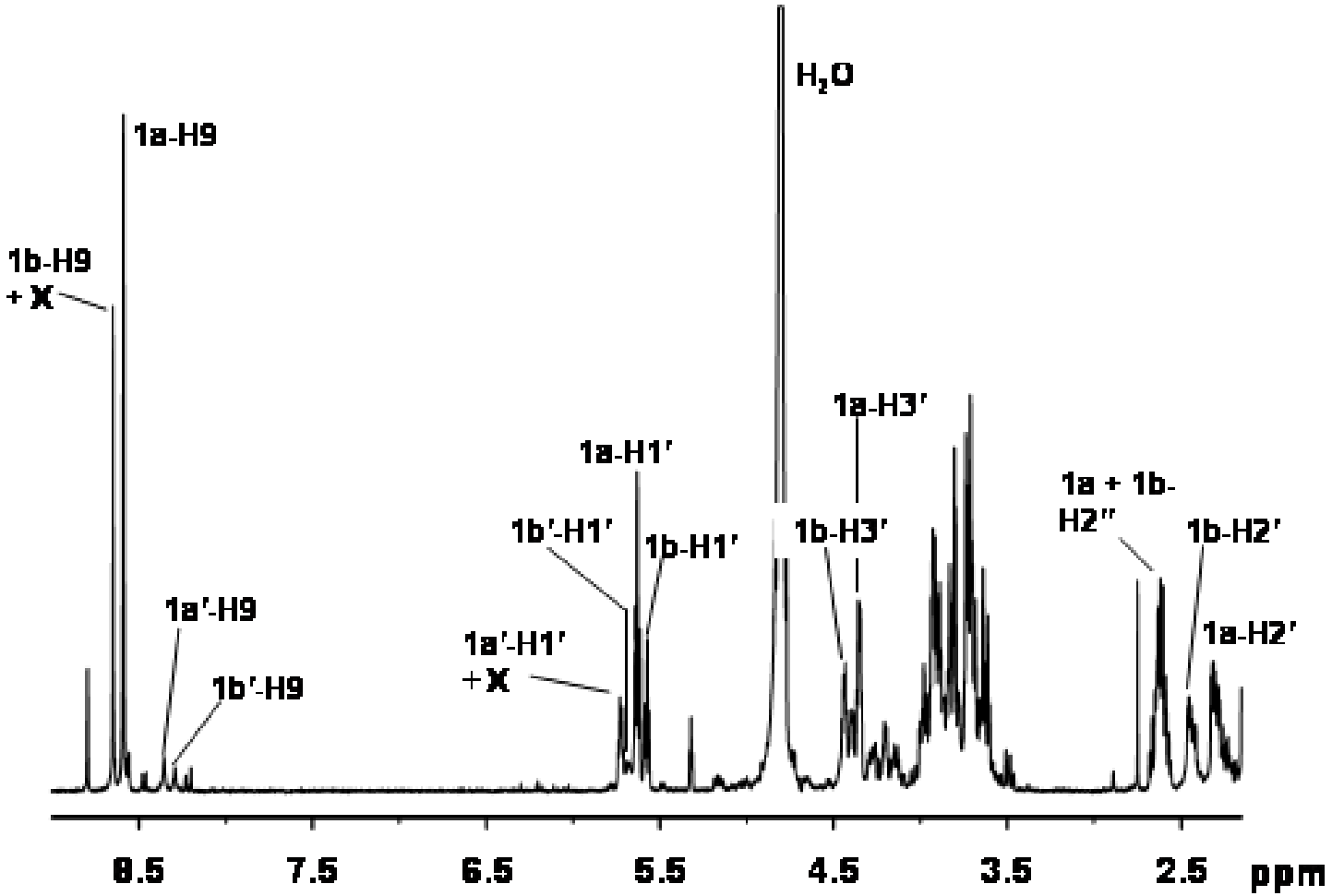

Figure 2.21 ^{1}H NMR (500 MHz, D_2O) of mixture of 2-Ih-dR diastereomers and rotamers **1a**, **1b**, **1a′**, **1b′** from the oxidation of dGuo by DMDO. For clarity, only well-resolved signals are identified on trace. An impurity in the H1′ region is indicated by "X".

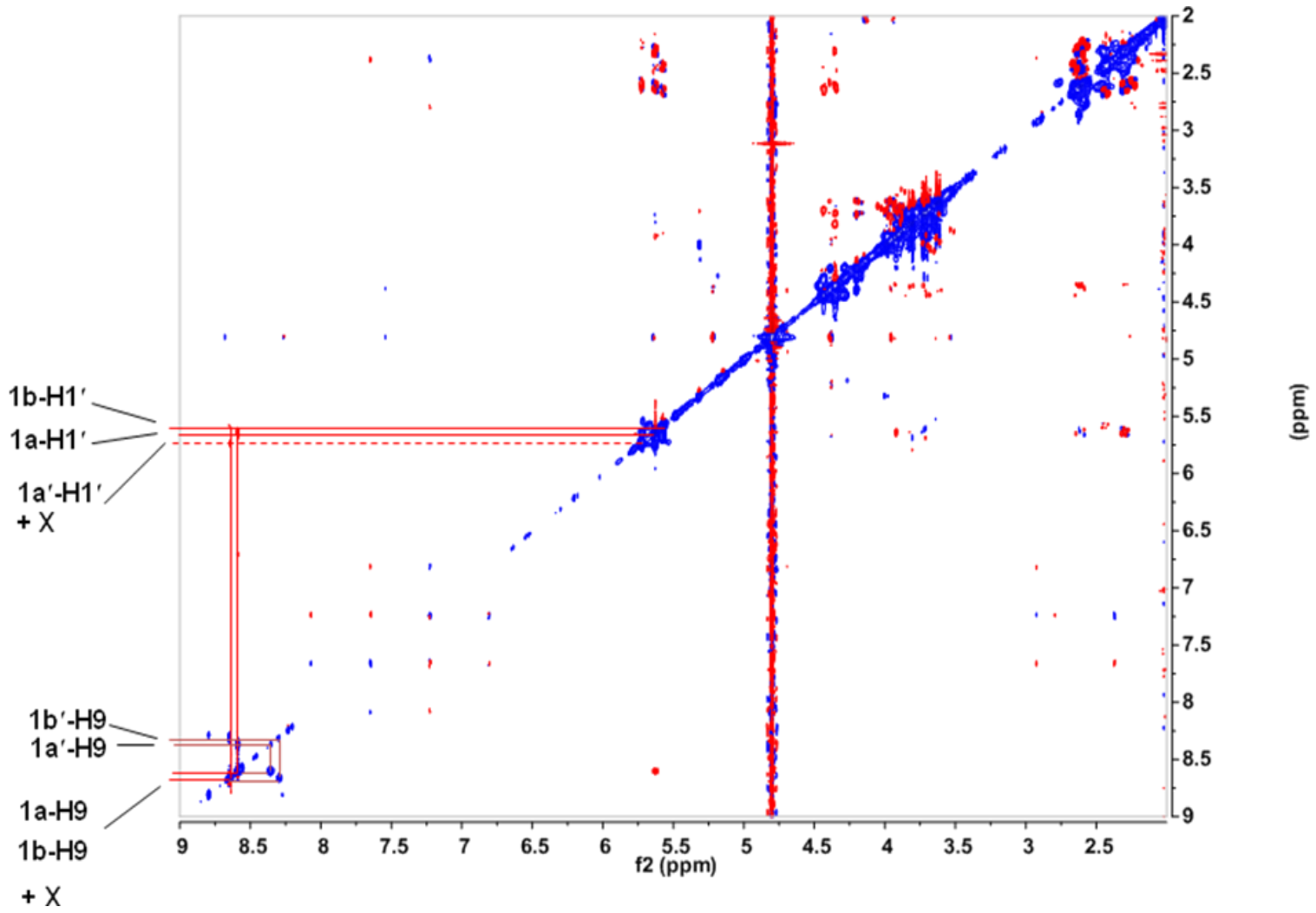

Figure 2.22 ROESY spectrum of diastereomer mixture from oxidation of dGuo. H9-H1′ NOESY connectivities are detected for the major rotamers (red). The dashed line indicates an impurity having a NOESY cross peak with a signal in the H9 region. Minor rotamers are identified by exchange cross peaks (blue).

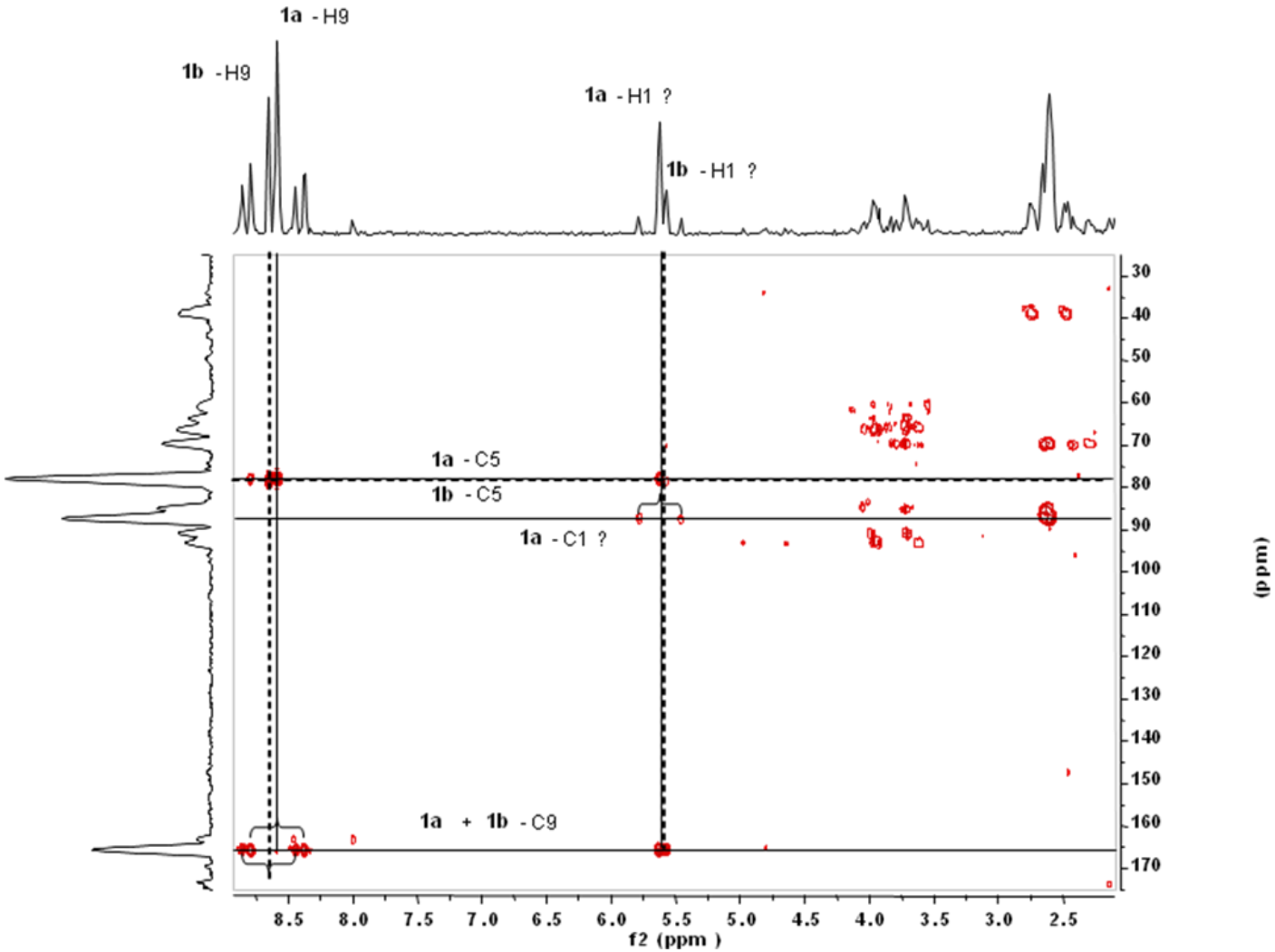

Figure 2.23 HMBC spectrum of diastereomer mixture from the oxidation of dGuo. For major rotamers, the coupling of H1‘ and H9 with C5 and C9 (solid lines) and coupling of H1‘ with C1‘, C9 and C5 (dashed lines) are indicated. Brackets indicate unsuppressed 1-bond couplings.

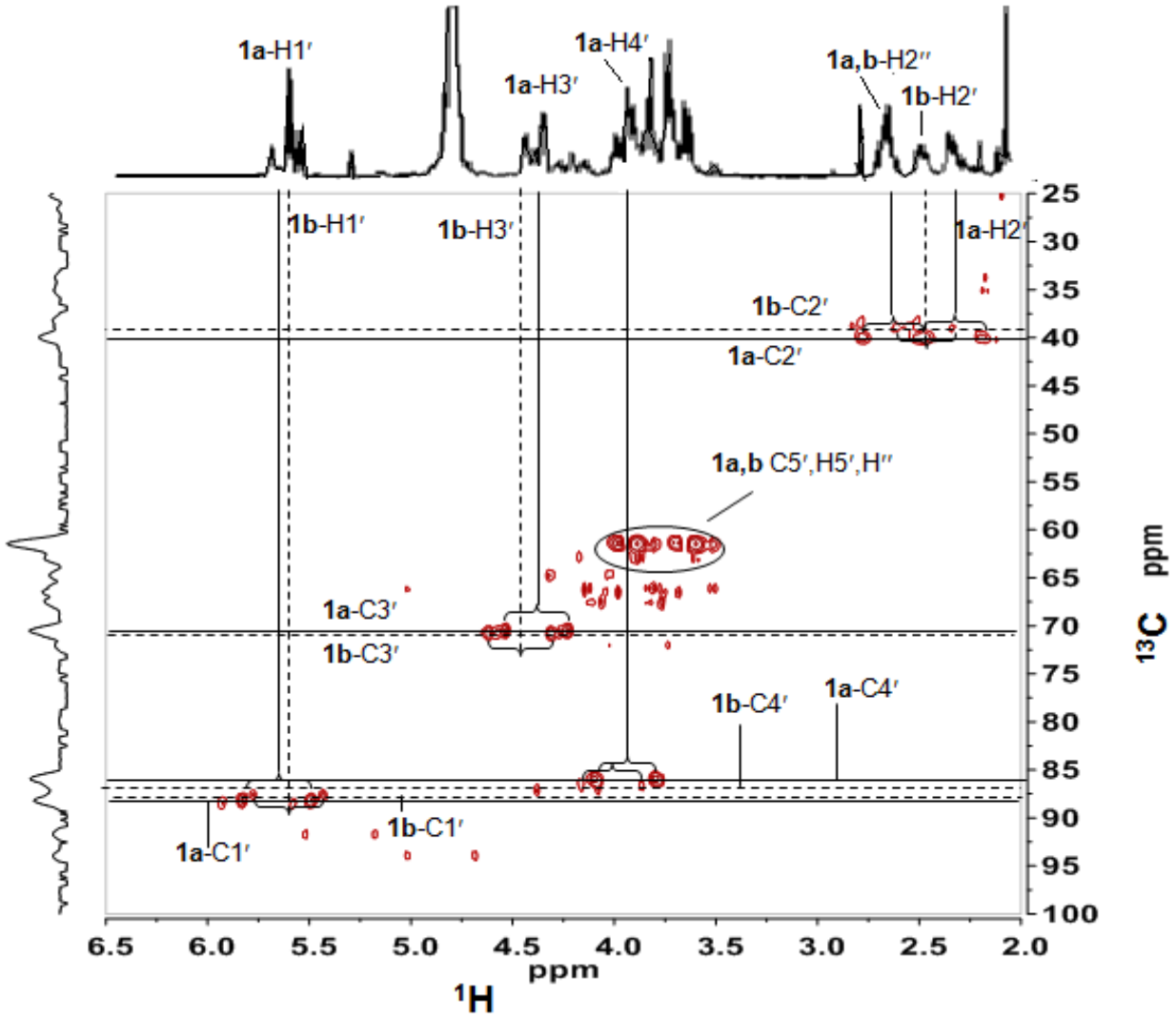

Figure 2.24 HSQC spectrum of diastereomer mixture from oxidation of dGuo. C,H coupling detected for major rotamers of **1a** (solid lines) and **1b** (dashed lines) is indicated on spectrum.

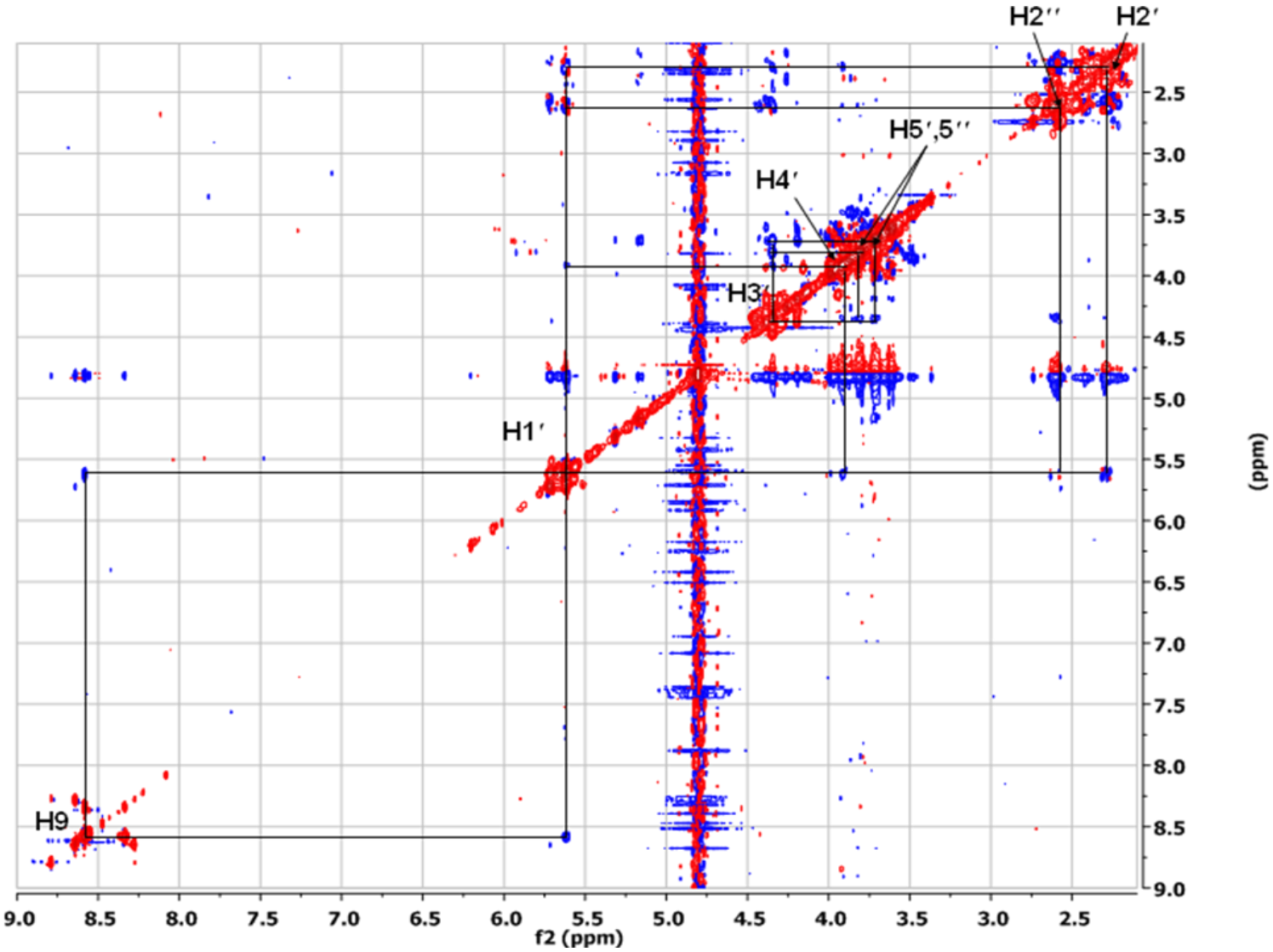

Figure 2.25 ROESY spectrum of diastereomer **1a**. Proton signals and cross peaks of major rotamer are indicated on the spectrum.

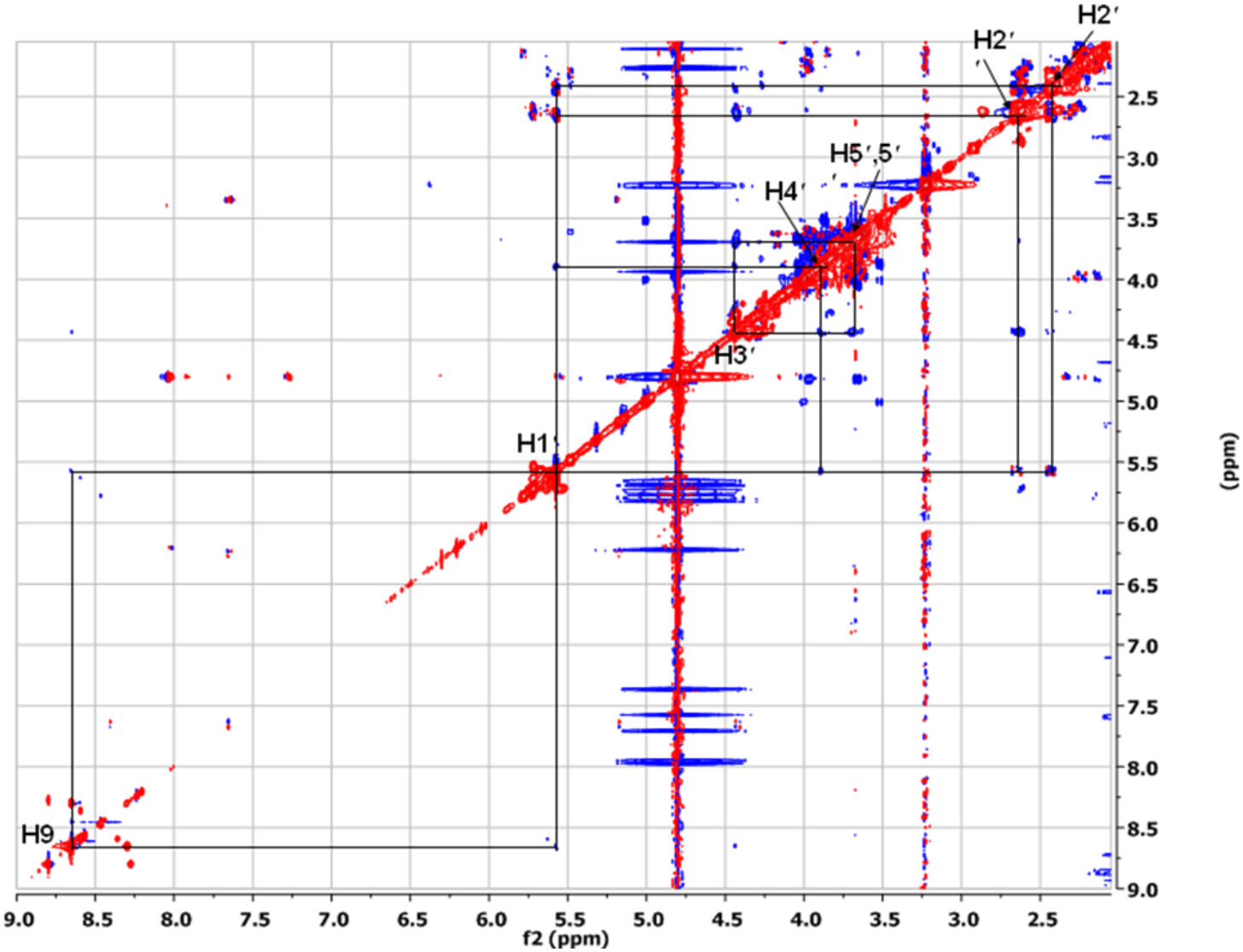

Figure 2.26 ROESY spectrum of diastereomer **1b**. Proton signals and cross peaks of major rotamer are indicated on the spectrum.

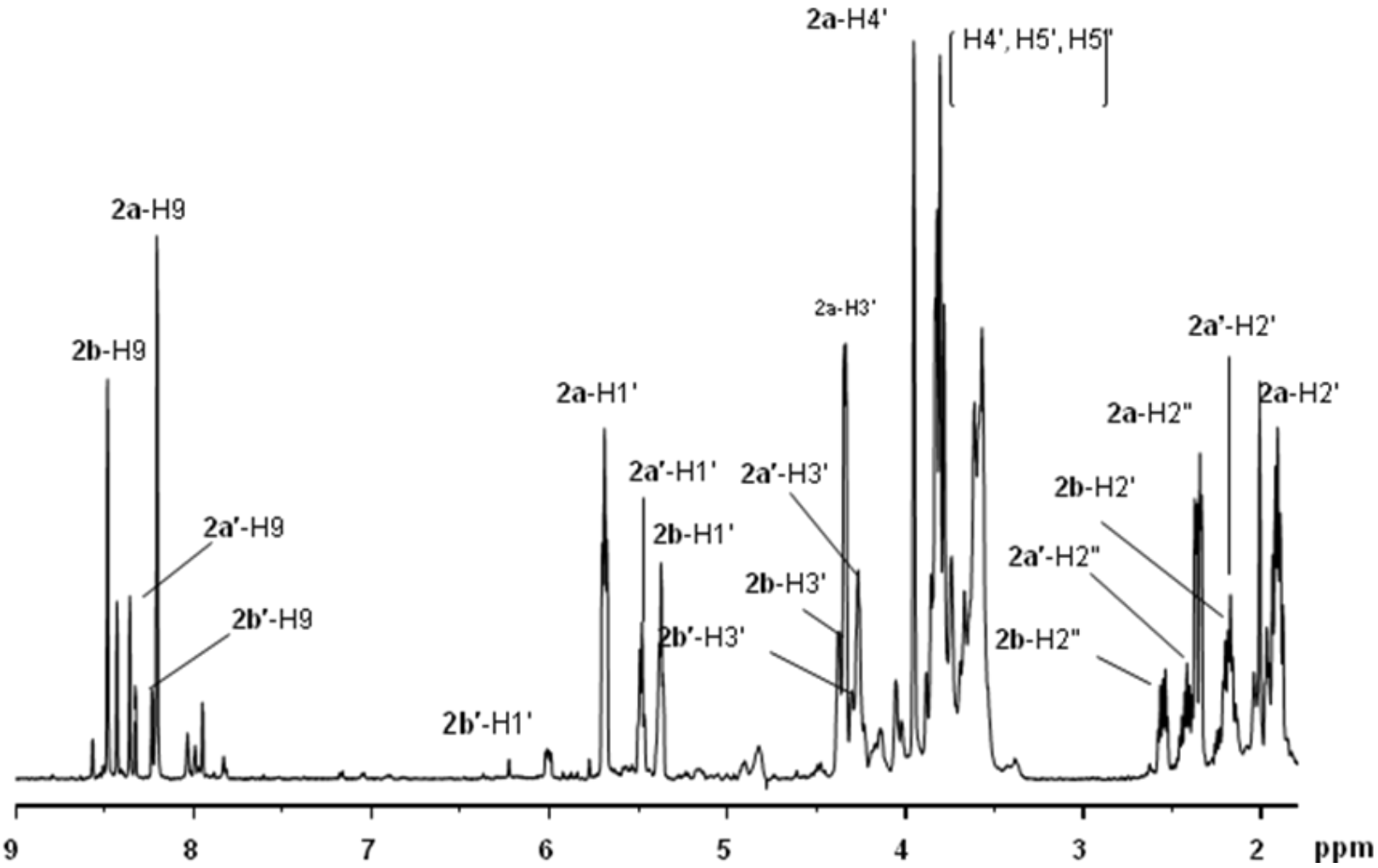

Figure 2.27 ^{1}H NMR (500 MHz, D_2O) of mixture of 2-Ih-dRP diastereomers and rotamers **2a**, **2a′**, **2b**, **2b′** from the oxidation of dGMP by DMDO. Signal assignments are given on the trace.

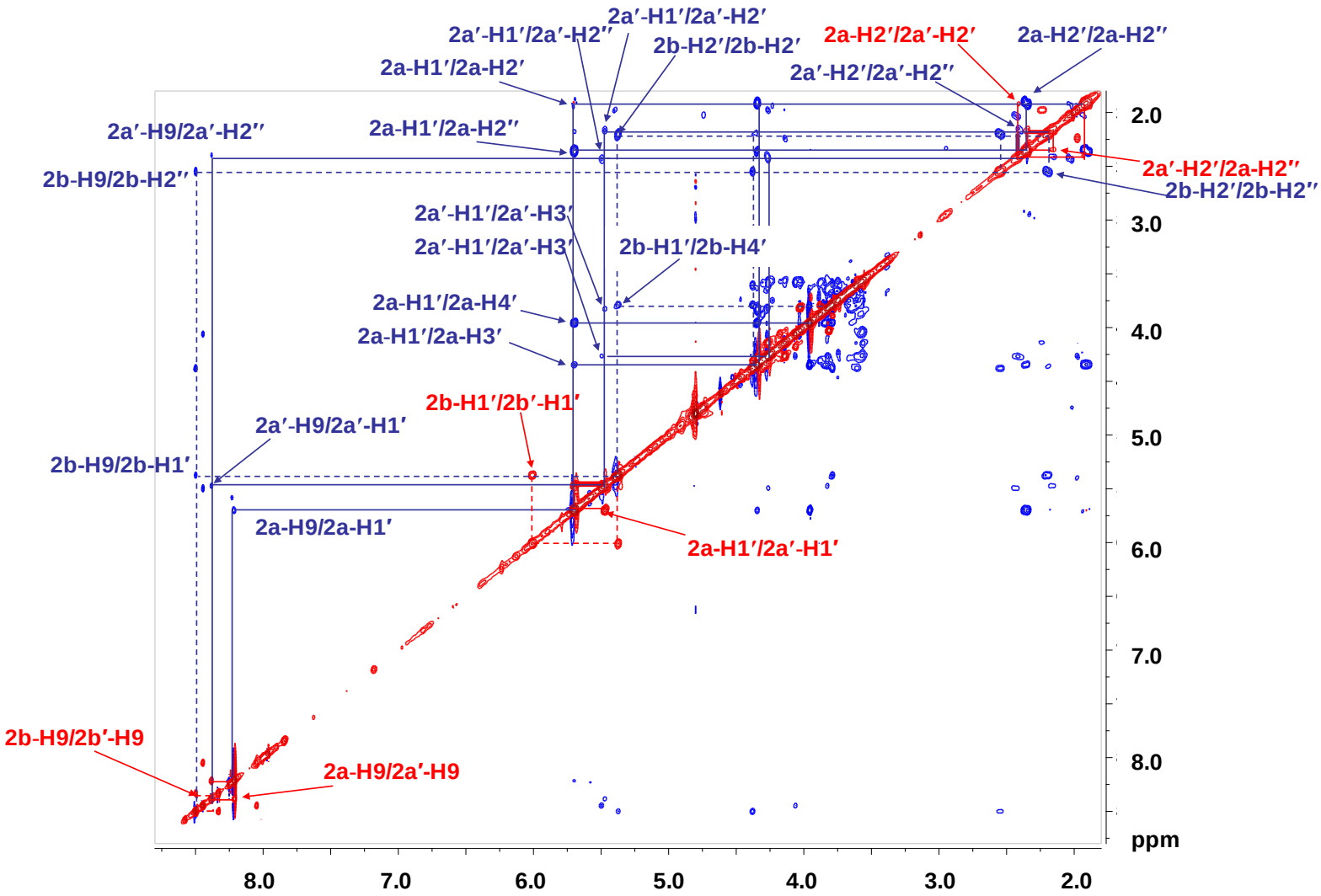

Figure 2.28 ROESY spectrum of diastereomer mixture from oxidation of dGMP. NOESY connectivities are indicated in blue, and exchange connectivities in red. Cross peak assignments are shown on spectrum. Connectivities of minor rotamers are indicated by dashed lines.

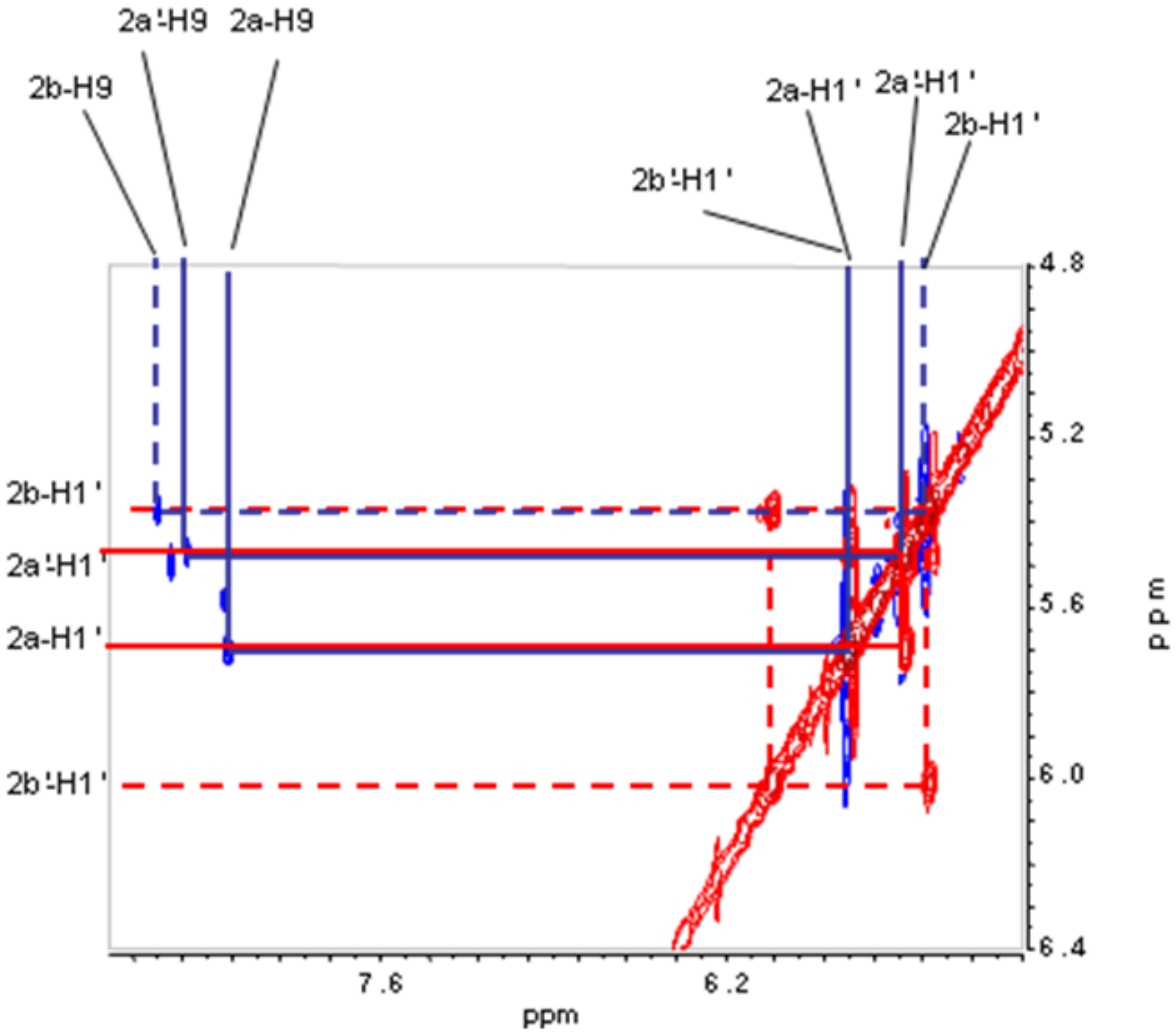

Figure 2.29 ROESY NMR spectrum of the H1′ - H9 region of the mixture of diastereomers and rotamers from the oxidation of dGMP by DMDO. Cross peaks of signals related by rotational exchange are red, and NOESY cross peaks blue. Exchange and NOESY connectivities between **2a** and **2a′** are indicated by solid lines and between **2b** and **2b′** by dashed lines.

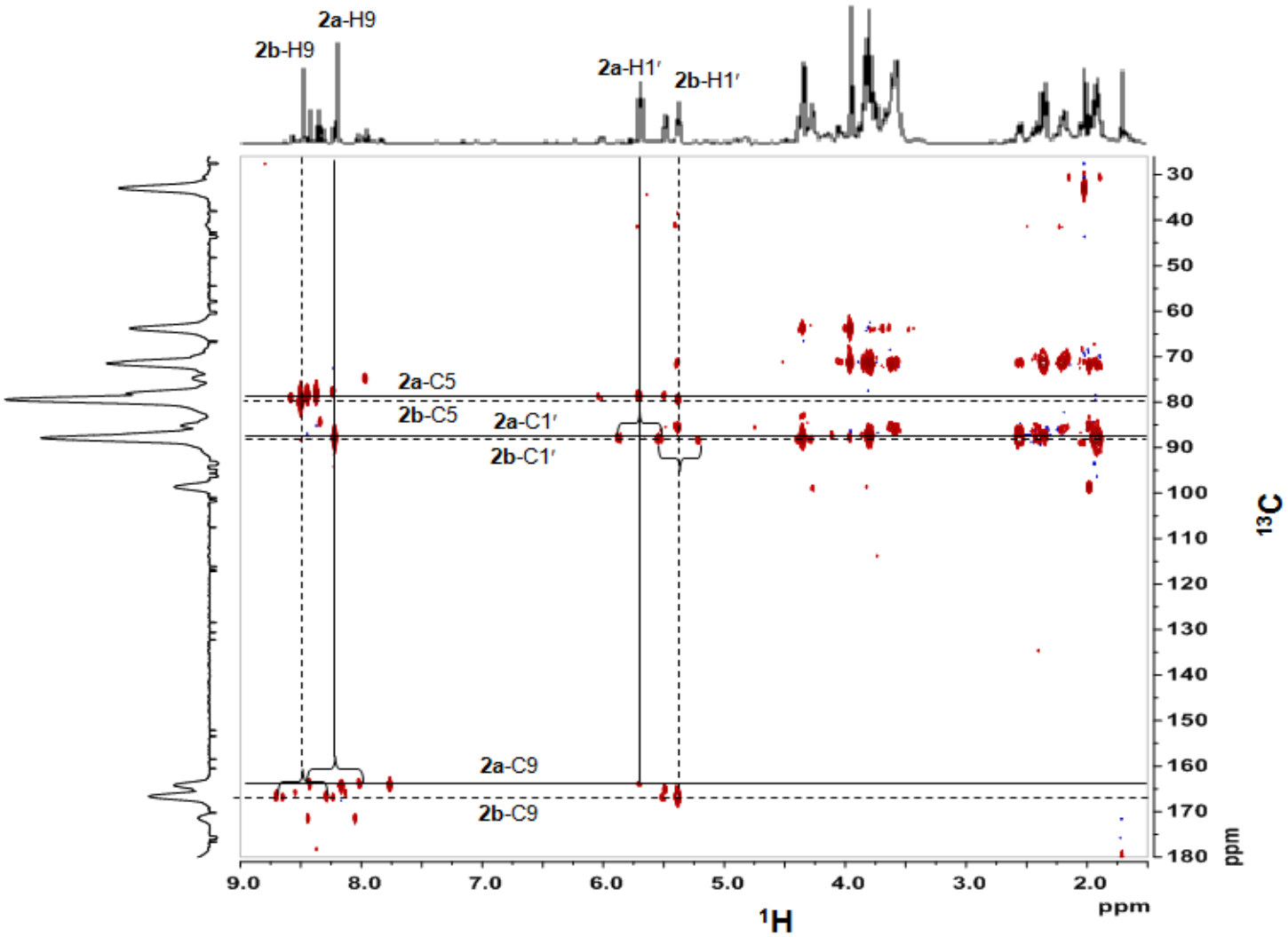

Figure 2.30 HMBC spectrum of diastereomer mixture from oxidation of dGMP. C,H coupling is indicated for major rotamers **2a** (solid lines) and **2b** (dashed line) are: H1‘ with C1‘, C9 and C5; H9 with C1‘, C5 and C9. Unsuppressed 1-bond couplings are indicated by brackets.

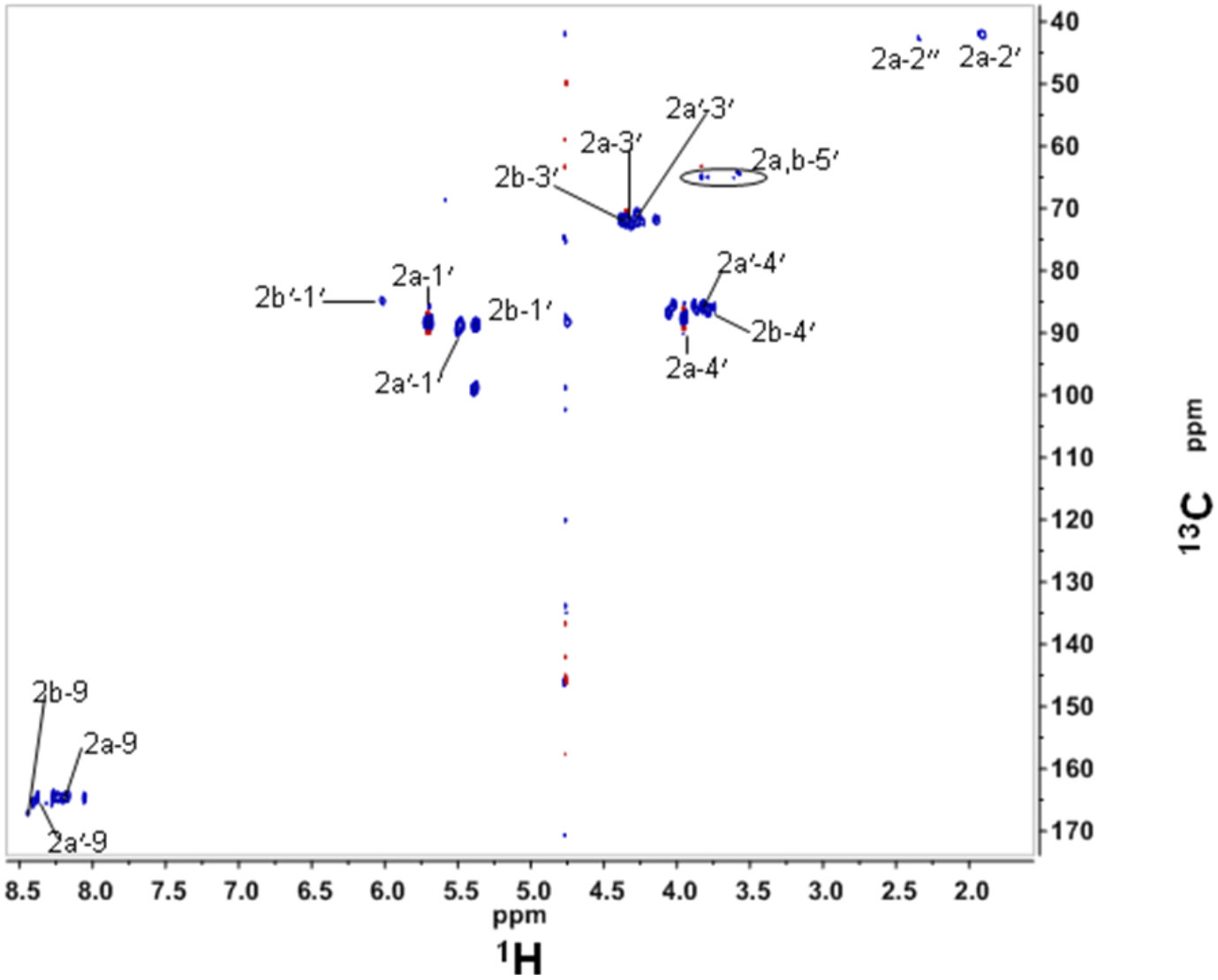

Figure 2.31 HSQC spectrum of diastereomer mixture from oxidation of dGMP. C,H cross peaks are identified on spectrum.

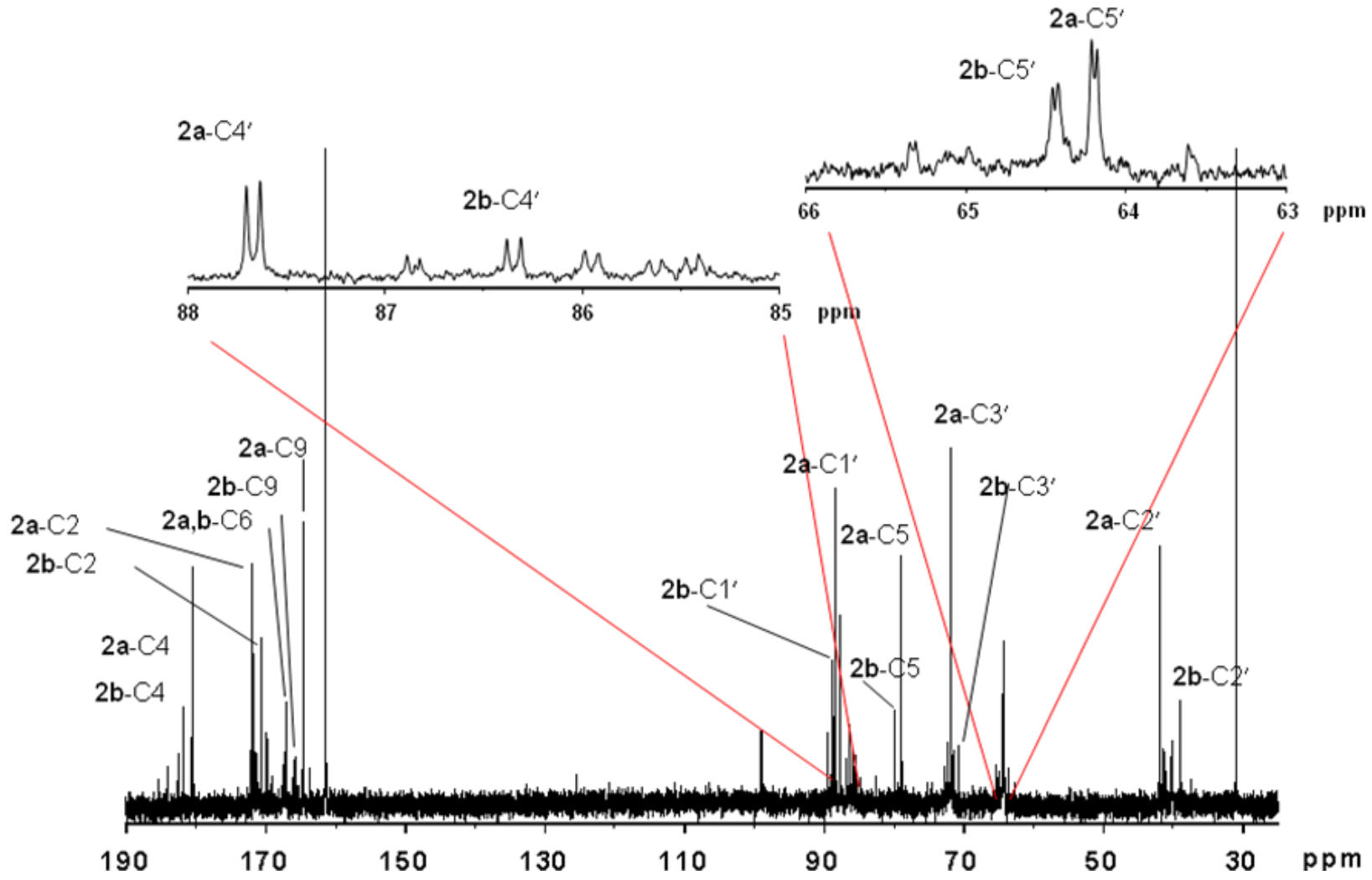

Figure 2.32 ^{13}C NMR spectrum (125 MHz, D_2O) of diastereomer mixture from oxidation of dGMP. Carbon signals are identified on trace. Expansions show ^{31}P,13C coupling.

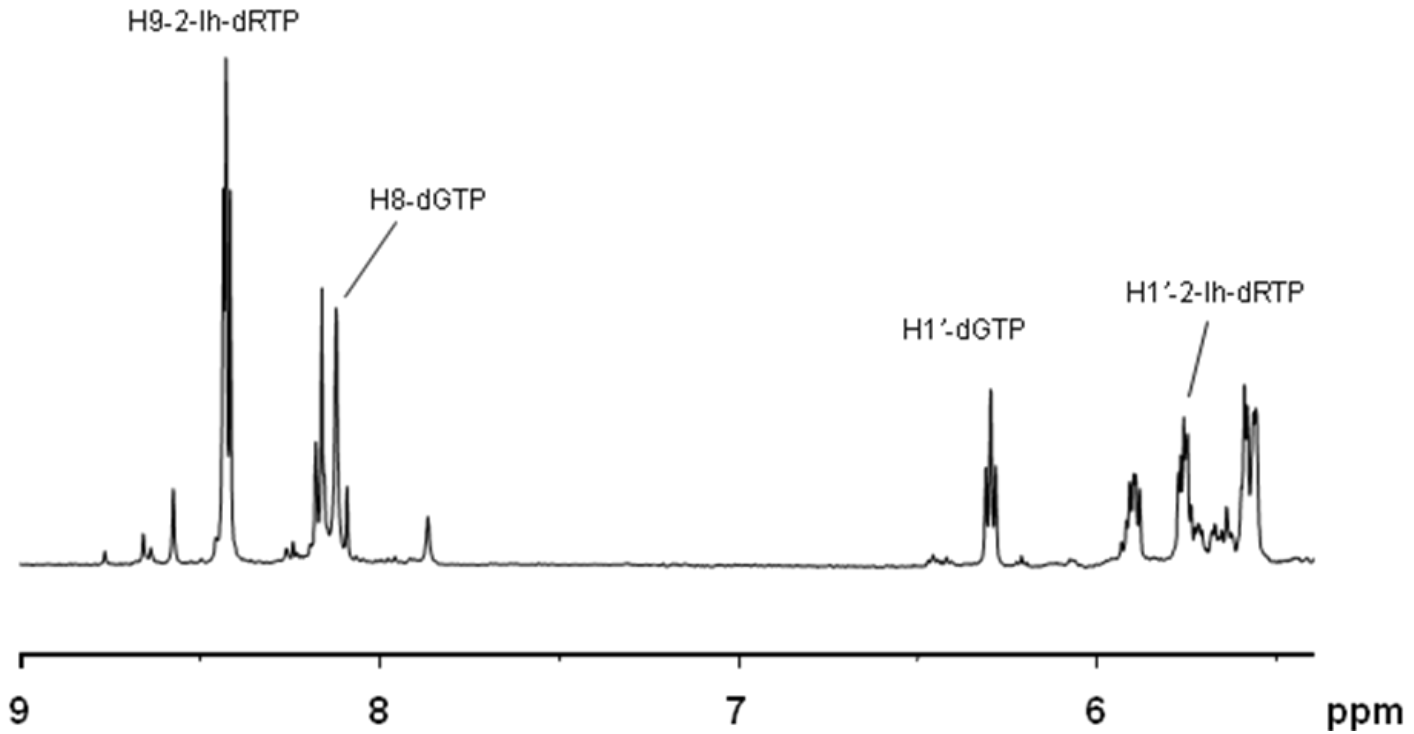

Figure 2.33 ^{1}H NMR (500 MHz, D_2O) of the H1' – H9 region of the product mixture from oxidation of dGTP. Signals of the major rotamer of the major diastereomer of the 2-Ih-dRTP and of residual dGTP are indicated on trace.

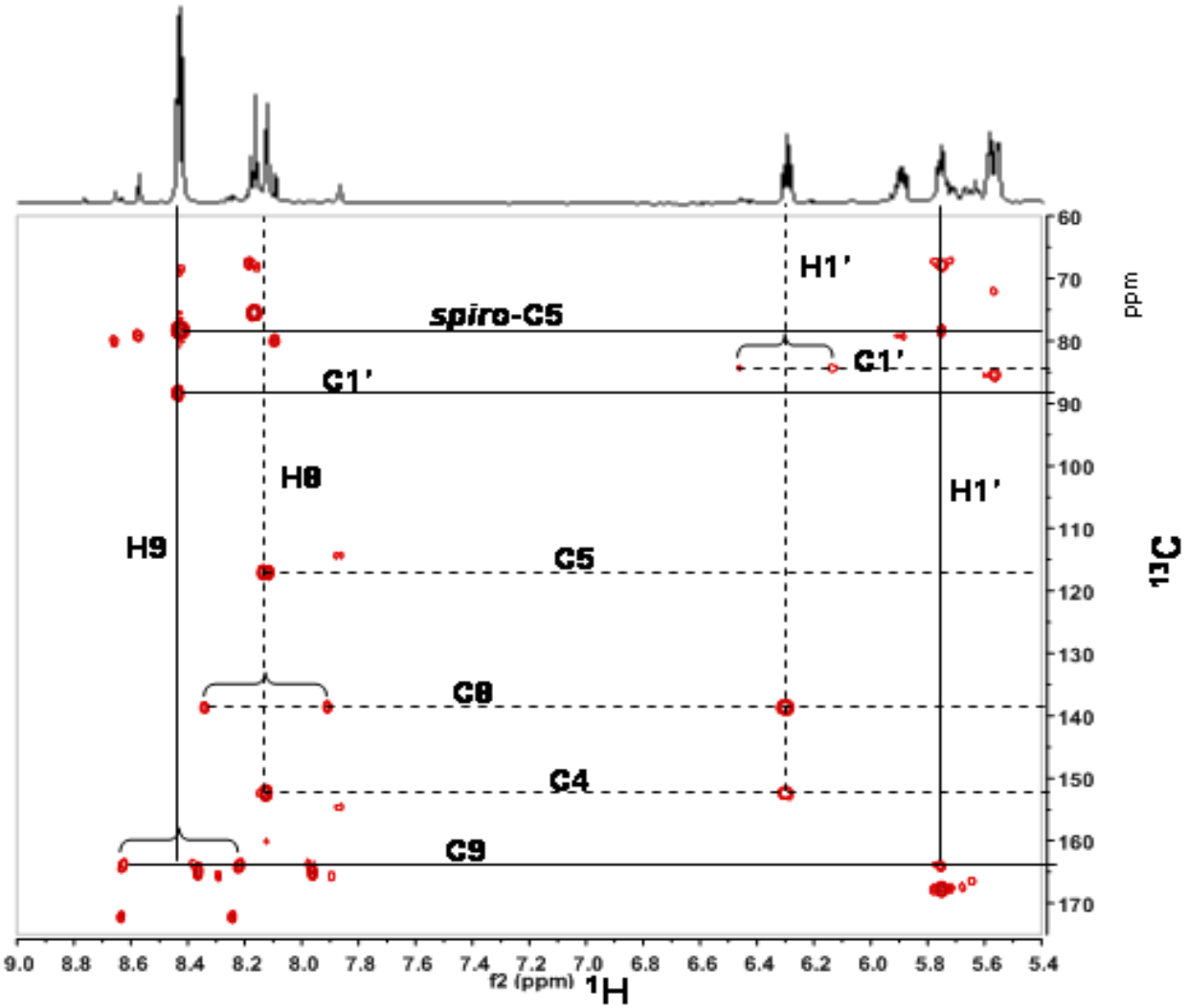

Figure 2.34 HMBC spectrum of oxidation mixture of dGTP in the C1‘ – H9 region. C,H couplings for the major 2-Ih-dRTP species (solid lines) and residual dGTP (dashed lines) are identified on the spectrum. Unsuppressed 1-bond couplings are indicated by brackets.

Table 2.1 Proton signal assignments and NOESY interactions (●) for **1a**.

		H9	H1′	H3′	H4′	H2″	H2′
		8.21	5.70	4.35	3.95	2.36	1.91
H9	8.21		●				●
H1′	5.70	●		●	●	●	●
H3′	4.35		●		●	●	●
H4′	3.95		●	●		●	
H2″	2.36		●	●			●
H2′	1.91	●	●	●		●	

Table 2.2 Proton signal assignments and NOESY interactions (●) for **1b**.

		H9	H1′	H3′	H4′	H2″	H2′
		8.50	5.38	4.39	3.79	2.55	2.20
H9	8.50		●	●		●	
H1′	5.38	●			●		●
H3′	4.39	●			●	●	●
H4′	3.79		●	●			●
H2″	2.55	●		●			●
H2′	2.20		●	●	●	●	

Table 2.3 Proton signal assignments and NOESY interactions (●) for **1a′**.

		H9	H1′	H3′	H4′	H2″	H2′
Shift (ppm)		8.38	5.47	4.27	3.83	2.41	2.17
H9	8.38		●	●		●	
H1′	5.47	●		●		●	●
H3′	4.27	●	●			●	
H4′	3.83						●
H2″	2.41	●	●	●			●
H2′	2.17		●		●	●	

Table 2.4 C,H cross peaks resolved in the HMBC spectrum of **1a**.

		H9	1′	3′	4′	5′,5″	2″	2′
	Shift	8.21	5.70	4.35	3.95	3.73-3.76	2.36	1.91
C9	164.6	●	●					
C1′	88.3	●	●	●	●			●
C3′	71.8				●	●	●	●
C4′	87.7				●	●	●	
C5′	64.2			●	●	●		
C2′	42.0		●				●	
C2	171.9							
C4	180.5							
C5	79.0		●					
C6	167.1							

Table 2.5 C,H cross peaks resolved in the HMBC spectrum of **1b**.

		H9	1′	3′	4′	5′,5″	2″	2′
		8.50	5.38	4.39	3.79	3.73-3.56	2.55	2.20
C9	166.5	●	●					
C1′	88.7		●	●			●	
C3′	71.7		●		●		●	●
C4′	86.3		●			●		
C5′	64.4							
C2′	39.0							
C2	171.8							
C4	181.9							
C5	79.6	●	●					
C6	167.3							

Table 2.6 C,H cross peaks resolved in the HMBC spectrum of **1a′**.

		H9	1′	3′	4′	5′,5″	2″	2′
		8.38	5.47	4.27	3.83	3.73-3.56	2.41	2.17
C9	165.6	●	●					
C1′	88.6			●				
C3′	71.5				●			●
C4′	85.9							
C5′	65.3							
C2′								
C2	172.1							
C4	181.8/182.6							
C5	78.7	●	●					
C6	167.5							

Table 2.7 NOESY cross peaks for **2a**.

		H9	H1′	H3′	H4′	H5′,5″	H2″	H2′
		8.59	5.62	4.35	3.93	3.82, 3.72	2.61	2.31
H9	8.59		●					
H1′	5.62	●			●		●	●
H3′	4.35				●	●	●	●
H4′	3.93		●	●			●	●
H5′,5″	3.82, 3.72			●				
H2″	2.61		●	●				●
H2′	2.31		●	●			●	

Table 2.8 NOESY cross peaks for **2b**.

		H9	H1′	H3′	H4′	H5′,5″	H2″	H2′
		8.65	5.57	4.43	3.98	3.70-3.64	2.61	2.45
H9	8.65		●	●				
H1′	5.57	●			●		●	●
H3′	4.43	●			●	●	●	●
H4′	3.98		●	●				●
H5′,5″	3.70-3.64			●				
H2″	2.61		●	●				●
H2′	2.45		●	●	●		●	

Table 2.9 Multiple-bond (x) and one-bond (y) C,H cross peaks for **2a**.

		H9	H1′	H3′	H4′	H5′,5″	H2″	H2′
		8.59	5.62	4.35	3.93	3.82, 3.72	2.61	2.31
C9	163.8	y	x					
C5	76.2	x	x					
C1′	85.5	x	y	x			x	
C2′	37.2						y	y
C3′	67.8			y	x	x	x	x
C4′	83.3				y	x		x
C5′	58.9			x		y		

Table 2.10 Multiple-bond (x) and one-bond (y) C,H cross peaks for **2b**.

		H9	H1′	H3′	H4′	H5′,5″	H2″	H2′
		8.65	5.57	4.43	3.98	3.70-3.64	2.61	2.45
C9	163.8	y	x					
C5	76.7	x	x					
C1′	85.2		y	x			x	
C2′	35.5						y	y
C3′	68.1		x	y			x	x
C4′	84.1				y	x		
C5′	64.1			x		y		

III. Investigation of ribosylation routes to 8,9-dihydro-9-oxo-3-(β-D-2-deoxyribofuranosyl)-imidazo[2,1-b]purine (*N*9-β-deoxyribosyl-N^2, 3-εdGuo)

3.1 Abstract

*N*9-(β-D-2-deoxyribofuranosyl)-N^2,3-ethenoguanine (8,9-dihydro-9-oxo-3-(β-D-2-deoxyribofuranosyl)imidazo[2,1-*b*]purine) is a highly mutagenic DNA adduct arising from exposure to known occupational and environmental carcinogens and is also generated under conditions associated with oxidative stress. *N*9-β-deoxyribosyl-N^2, 3-εGua is therefore of considerable interest for quantitation in DNA as a biomarker of exposure both *in vivo* and *in vitro* in studies of molecular mutagenesis. Chemical synthesis has proven to be challenging because of the reported lability of the glycosidic bond under conditions generally applicable to chemical synthesis. We investigated enzymatic glycosylation and chemical glycosylation of N^2, 3-ethenoguanine as approaches to obtaining this nucleoside under mild conditions. We report that both enzymatic and chemical glycosylation of N^2, 3-εGua led to nucleosides having spectroscopic data compatible with ribosylation at positions corresponding to *N*7- and N^2 of the Gua framework. A minor product of the enzymatic ribosylation had a C,H coupling pattern in the HMBC spectrum that was consistent with ribosylation at the target Gua *N*9, but the HPLC retention time and NMR data ruled out the target structure. This product has tentatively been assigned as the α-anomer of the desired *N*3 riboside, and rigorous

confirmation of this structure would demonstrate an unusual stereochemistry for the *trans* ribosylation. We re-investigated a route to 8,9-dihydro-9-oxo-3-(β-D-2-deoxyribofuranosyl)imidazo[2,1-*b*]purine via cycloaddition of bromoacetaldehyde to O^6-benzyl-protected dGuo, which gave the target compound, albeit in only 6 % overall yield. Despite the low overall yield, cycloaddition appears to be the only unambiguous route to 8,9-dihydro-9-oxo-3-(β-D-2-deoxyribofuranosyl)imidazo[2,1-*b*]purine.

3.2 Introduction

*N*9-(β-D-2-deoxyribofuranosyl)-N^2,3-ethenoguanine (8,9-dihydro-9-oxo-3-(β-D-2-deoxyribofuranosyl)imidazo[2,1-*b*]purine) is a highly mutagenic DNA adduct arising from exposure to known occupational and environmental carcinogens, including vinyl chloride and chloroacetaldehyde [Guengerich, F. P. et al, 1979], [Guengerich, F. P. et al, 1992] and is also generated under conditions associated with oxidative stress [Gros, L. et al, 2003].

Among exocyclic DNA adducts, ethenobases have been most widely studied in the last 33 years, as this class of DNA lesions is formed by many genotoxic chemicals including the human carcinogen vinyl chloride (VC) and the multi-species carcinogen urethane [Bartsch H. et al, 1994]. Ethenobases were first described by Kochetkov et al. [Kochetkov N. K. et al, 1971] who identified them as reaction products of 2-chloroacetaldehyde with adenine and cytosine. Interest in the ε-lesions was renewed in 1975 when it was found that they were generated in vitro by the vinyl chloride metabolites, chloroethylene oxide and 2-chloroacetaldehyde [Barbin A. et al, 1975], [Laib R.J. et al, 1977], [Laib R.J. et al, 1978]. Using replication and transcription fidelity assays and ε-modified oligo- or polynucleotides, it was established that εdA and εdC have miscoding or ambiguous base pairing properties [Barbin A.et al, 1981], [Hall J.A. et al, 1981], [Spengler S. et al, 1981] and thus could be

involved in the mutagenic and carcinogenic effects of VC [IARC, 1979], [Barbin, H. et al, 1986].

In the 1990s, ε -adducts have received renewed attention, because background levels of etheno adducts have been detected in tissues from unexposed humans and rodents, suggesting an alternative, endogenous pathway of formation [Nair J., Barbin A. et al,1999]. This background which can be affected by dietary factors could arise from the reaction of lipid peroxidation products such as *trans*-4-hydroxy-2-nonenal via its 2,3-epoxy-intermediate with nucleic acid bases [Nair J., Vaca C.E. et al, 1997]. Subsequently, it was shown that high intake of dietary ω-6 –polyunsaturated fatty acids by female volunteers greatly increased LPO-derived etheno-DNA adducts in white blood cells in vivo [Fang J.L., Vaca C.E. et al, 1996]. Further, elevated levels of ε -adducts were found in hepatic DNA from patients and rodents with genetic predisposition to oxidative stress, lipid peroxidation and increased risk of liver cancer due to metal storage disease [Nair J., Sone H., et al 1996]. Also, during inflammatory processes a cascade of reactive oxygen/nitrogen intermediates can be generated, that could lead directly to oxidative DNA damage and/or to formation of ε -adduct via reaction of bifunctional 4-hydroxyalkenals and epoxides derived from LPO.

(8,9-dihydro-9-oxo-3-(β-D-2-deoxyribofuranosyl)imidazo[2,1-*b*]purine) in DNA is therefore of considerable interest as a biomarker of exposure and in studies of molecular mutagenesis. Quantitative analysis of DNA adducts requires both unambiguously characterized standards and on occasion, labeled isotopomers. Preparation of certain classes of deoxynucleoside adducts can be problematic because instability of intermediates under conditions of established synthetic routes, deglycosylation at low pH or elevated temperature often present particular difficulties. Chemical synthesis of (8,9-dihydro-9-oxo-3-(β-D-2-

deoxyribofuranosyl)imidazo[2,1-*b*]purine) has proven to be challenging precisely because of the reported lability of the glycosidic bond under conditions generally applicable to chemical synthesis [Kusmierek, J. et al, 1989], [Khazanchi, R. et al, 1993], [Müller, M. et al, 1996]. We investigated both enzymatic glycosylation and chemical glycosylation of N^2,3-ethenoguanine (N^2,3-εGua) as approaches to obtaining this nucleoside adduct under mild conditions. Deoxyribosyl transferases serve for preparation of therapeutic nucleoside analogues [Anand, R. et al, 2004]. Enzymatic or chemical glycosylation would also be highly advantageous for synthesis of product multiply labeled with ^{13}C and/or ^{15}N because of the availability of labeled N^2,3-εGua aglycone from labeled Gua [Scheller, N., Sangaiah, R., etal, 1995] in high yield and furthermore, has the distinct advantage of being readily adaptable to small scale reactions for synthesis of labeled standards. We report that both enzymatic and chemical glycosylation of N^2,3-εGua led to nucleosides having spectroscopic data compatible with ribosylation at positions corresponding to *N*7- and N^2 of Gua. A minor product of the enzymatic ribosylation had C,H coupling pattern in the HMBC spectrum that was consistent with ribosylation at the target Gua *N*9, but the HPLC retention time and NMR data appear to rule out the target structure. Consequently, we re-investigated an unambiguous route to (8,9-dihydro-9-oxo-3-(β-D-2-deoxyribofuranosyl)imidazo[2,1-*b*]purine) via cycloaddition of bromoacetaldehyde to O^6-benzyl-protected dGuo [Kusmierek, J. et al, 1989]. Conducted on a small scale, the cycloaddition pathway gave the target compound, albeit in only 6 % over all yield. Although we use the nomenclature N^2,3-ε-Gua for convenience, we will refer to the heterocyclic system as 8,9-dihydro-9-oxoimidazo[2,1-*b*]purine when elaborating the structural characterization of the ribosylated products described below.

3.3 Materials and methods

3.3.1 Instrumentation

NMR spectra were recorded on a Varian Inova NMR spectrometer at 500 MHz for acquisition of ^{1}H data and 125 MHz for ^{13}C data with cold probe. Low resolution ESI-MS/MS data were acquired on a Finnigan DECA system. High resolution mass measurements were performed on a Bruker FT-ICR-MS equipped with an capillary ESI source by flow injection of 4-6 μL samples. The calibration standard was Angiotensin I solution (0.02 mg/mL). UV-vis spectra were recorded on a Cary 300, with Cary Win UV software. HPLC was performed using a Thermo LC with an Altech detector and Ezstar software (EZCHROM). Both analytical and semi-preparative separations were achieved on a reverse phase Eclipse XDB C18 column (250×10mm) at a flow rate of 2 ml/min, using gradient programs described below.

Analytical thin-layer chromatography (TLC) was performed on silica-coated aluminum plates (particle size 17 μm thickness) purchased from Sigma-Aldrich and preparative TLC, on silica-coated glass plates (particle size 40-63 μm, 500 or 1000 μm thickness), purchased from Analtech Inc.

3.3.2 Chemicals

Solvents were HPLC grade and were purchased from Fisher Scientific Co. or Mallinckrodt Baker, Inc., with the exception of ethanol, purchased from AAPER Alcohol and Chemical Co. The following reagents were purchased from Fisher Scientific Co.: ammonium hydroxide, sodium bicarbonate, HCl, acetic acid, acetic anhydride, and potassium monohydrogen phosphate. 2′-Deoxyguanosine was purchased from USB Corp. and benzyl

alcohol, from J. T. Baker. All other reagents were purchased from Sigma-Aldrich. Hydrogen gas was purchased from National Welders Supply Co.

3,5-Di-*O*-(*p*-toluyl)-2-deoxy D-ribofuranosyl chloride was synthesized according to a published procedure [Hoffer. M., 1960], as was O^6-benzylguanine [Barth, C. et al, 2004].

3.3.3 Enzymes

Lactobacillus helveticus (*L. helveticus*) purine *N*-2′-deoxyribosyl transferase type I [Anand, R. et al, 2004] and *Lactobacillus fermentum* (*L. fermentum*) nucleoside deoxyribosyl transferase type II were a gift from the laboratory of Steven Ealick. *Lactobacillus leichmanni* (*L. leichmanni*) nucleoside deoxyribosyl transferase type II was a gift from the laboratory of Pierre Kaminski.

3.3.4 Synthesis of 8,9-dihydro-9-oxoimidazo[2,1-b]purine (N^2, 3–ethenoguanine) (Scheme 3.1)

O^9-benzyl-8,9-dihydro-9-oxoimidazo[2,1-b]purine (O^6-benzyl-N^2,3-εGua). O^6-benzylguanine [Barth C. et al, 2004] (241mg, 1mmol) was dissolved in 15ml EtOH at 37ºC. 5ml of 1M pH4.5 sodium acetate buffer and 0.628ml of 50%(w/v) (4mmol) aqueous chloroacetaldehyde solution were added in to flask with stirring at 48ºC [Sattsangi, P. D. et al, 1977]. After 60hr, the mixture was evaporated; the residue was triturated with 5ml of water. Following the pH was adjusted to neutral; the light yellow precipitate was collected by filtration (237.7mg, yield 89.7%). UV (MeOH) λ_{max1}=220nm, λ_{max2}=274 nm; ESI-MS *m/z* 266 ($[M+H]^+$, 100), *m/z* 284 ($[M+H+H_2O]^+$, 50); ESI-MS/MS *m/z* 266$[M+H]^+$, 188[M+H-phenyl]$^+$, 91$[M+1-\varepsilon G]^+$; ^{1}H NMR [DMSO-d_6] δ 13.91(bs, 1H, *N3*H), 8.33(s, 1H, H2), 7.91 (s, 1H, H-5), 7.59 (d, J=7.3Hz, 2H, phenyl H), 7.43 (s, 1H, H6), 7.35-7.14(M, 3H, phenyl H), 5.62(s, 2H, Methylene H in Benzyl).

8,9-dihydro-9-oxoimidazo[2,1-b]purine (N^2, 3–ethenoguanine). 64mg O^6-Bz-N^2,3-εG was dissolved in solution of 10ml H_2O, 8ml MeOH, 3 ml conc. NH_3 aqueous solution. 74 mg 10% Pd/C was suspended in the reaction solution under 1.1 ATM H_2 at room temperature for 24hr. After filtration of the Pd/C and blow off the MeOH under Ar, the clear solution was neutralized with formic acid, then cooled at 4 ºC over night. The suspension of solution was filtered and washed with water, MeOH and ether, then dried with lyophilization to gain off white powder (37.5mg, yield 88%): UV (H_2O, pH7) λ_{max1}=273nm, λ_{max2}=251 nm; ESI-MS *m/z* 176 ($[M+H]^+$, 83), *m/z* 351 ($[2M+H]^+$, 100); ^{1}H NMR [DMSO-d_6] δ 7.11 (d, J=1.2Hz, 1H, H-6), 7.61 (d, J=1.5Hz, 1H, H-5), 8.15(s, 1H, H-2).

3.3.5 Unambiguous synthesis of 8,9-dihydro-9-*oxo*-3-(2-deoxy-*β*-D-ribofuranosyl)-imidazo[2,1-b]purine (Scheme 3.2)

3′,5′-Di-O-acetyl-2′-deoxyguanosine. 3′,5′-Di-*O*-acetyl-2′-deoxyguanosine was synthesized by slight modification of a published procedure (*12*). dGuo (267 mg, 1 mM) and tetraethylammonium bromide (770 mg) were dissolved in distilled water and then lyophilized. The residue was stirred with acetic anhydride in anhydrous pyridine for 18 hr protected from light. Excess acetic anhydride was destroyed by addition of 5 mL ethanol, the solvents removed under vacuum and pure 3′,5′-di-*O*-acetyl-2′-deoxyguanosine was purified by crystallization from methanol (330mg, 95%). UV-vis (MeOH) λ_{max}=251 nm; positive ion ESI-MS *m/z* (rel intensity) 725 (100) $[M_2Na]^+$, 703 (50) $[M_2H]^+$, 352 (28) $[MH]^+$,152 (42) [MH- deoxyribose]$^+$. ^{1}H NMR (methanol-d_4) 7.90 (s, 1H), 6.30 (ψt, 1H, J = 6.6 Hz), 5.47 (m,1H), 4.35-4.44 (m, 2H), 4.33 (m, 1H), 3.02(m, 1H), 2.59(ddd, 1H, J = 14.5, 6.2, 2.5 Hz), 2.15 (s, 3H), 2.09 (s, 3H) ppm.

O^6-benzyl-3′,5′-di-O-acetyl-2′-deoxyguanosine. To a suspension of 3′,5′-di-*O*-acetyl-2′-deoxyguanosine (200 mg) under Ar in dry tetrahydrofuran (8 mL), were added triphenylphosphine (194.8 mg) and benzyl alcohol (102.4 μL). Diisopropyl azodicarboxylate (65.2 mg) was added drop wise with stirring in an ultrasonic bath at 25 °C. After 48 hr, the reaction solution was evaporated under reduced pressure. Semipreparative TLC over SiO_2 eluted with 3: 97 by vol. CH_3OH/CH_2Cl_2, yielded crystalline of O^6-benzyl-3′,5′-di-*O*-acetyl-2′-deoxyguanosine (35 mg, 14%, R_f 0.31). Positive ion ESI-MS *m/z* (rel intensity) 464 (100) $[MNa]^+$, 442 (58) $[MH]^+$, 242 (94) [MH-deoxyribose]$^+$. ^{1}H NMR (methanol-d_4) 7.88 (s, 1H), 7.31 (t, 2H, J = 7.4 Hz), 7.24 (m, 3H), 6.27 (dd, J = 7.5, 6.6 Hz 1H), 5.44 (m, 1H), 5.31 (s, 2H), 4.39 (dd, 1H, J =11.7, 4.5 Hz), 4.33 (dd, 1H, J = 11.7, 4.5 Hz), 4.29 (m, 1H), 3.03 (m, 1H), δ 2.55 (ddd, 1H, J = 14.2, 6.6, 2.6, Hz) 2.10 (s, 3H), 2.03 (s, 3H) ppm.

O^6-Benzyl -2′-deoxyguanosine. O^6-benzyl-3′,5′-di-*O*-acetyl-2′-deoxyguanosine (20 mg) was dissolved in methanolic 2M ammonium hydroxide (8mL) and stirred overnight at room temperature. Following the evaporation of solvent, the residue was purified by semipreparative TLC over SiO_2 eluted with 15: 85 CH_3OH/CH_2Cl_2 to give O^6-benzyl -2′-deoxyguanosine (15.9mg, 98%, R_f 0.6). UV (MeOH) λ_{max}=256 nm. Positive ion ESI-MS *m/z* (rel intensity) 380 (100) $[MNa]^+$, 358 (8) $[M+H]^+$. ^{1}H NMR (methanol-d_4) 7.98 (s, 1H), 7.31 (ψt, 2H, J = 7.4 Hz), 7.25 (t, 1H, J = 7.4 Hz), 7.22 (d, 2H, J = 7.3 Hz), 6.28 (ψt, 1H, J = 7.0 Hz), 5.32 (s, 2H), 4.52 (td, 1H, J = 5.9, 2.9 Hz), 3.99 (dd, 1H, J = 6.7, 3.5 Hz), 3.79 (dd, 1H, J = 12.0, 3.6 Hz), 3.72 (dd, 1H, J = 12.0, 3.6 Hz), 2.71 (ddd, 1H, J = 13.5, 7.2, 6.2 Hz), 2.35 (ddd, 1H, J = 13.5, 6.9, 3.1 Hz) ppm.

8,9-Dihydro-9-oxo-3-(2-deoxy-β-D-ribofuranosyl)-imidazo[2,1-b]purine.

O^6-Benzyldeoxyguanosine (18.0 mg) was dissolved in saturated aqueous $NaHCO_3$ (6 mL) and bromoacetaldehyde (1 mL, ~1.3 M) solution and ethanol (2 mL) added at room temperature. The mixture was stirred at 50 °C for 48 h, lyophilized and the residue purified by HPLC, eluting with the gradient program: 40% to 70% MeOH in water over 15 min to give O^9-benzyl-8,9-dihydro-9-oxo-3-(2-deoxy-*β*-D-ribofuranosyl)-imidazo[2,1-*b*]purine (0.6 mg, 3.1 %, retn time,12min). Positive ion ESI-MS *m/z* (rel intensity) 382 (100) $(MH)^+$, 266 (41), $(MH\text{-deoxyribose})^+$. Unreacted starting material (retention time 10.5 min) was collected for repetition of the cycloaddition reaction to accumulate 2.2 mg of the intermediate, which was used directly in the next reaction.

O^9-Benzyl-8,9-dihydro-9-oxo-3-(2-deoxy-*β*-D-ribofuranosyl)-imidazo[2,1-*b*]purine (2.2 mg) was dissolved in a mixture of conc. NH_4OH (0.5 mL), D.I. water (1 mL), ethanol (2.5 mL) and methanol (1 mL) and stirred over 2.2 mg 10% Pd/C catalyst (containing 50% water) under 1.1 atm H_2 at 25 °C for 30h. The reaction was monitored by HPLC using a gradient program: 25% to 30% MeOH in H_2O over 5min, then 30% to 90% MeOH in H_2O over the next 9 min. Material eluting at a retn time of 5.4 min was collected. Volatiles were removed under a stream of Ar, and the remaining aqueous solution lyophilized. The residue was purified by HPLC, using the above gradient program to give 8,9-dihydro-9-oxo-3-(2-deoxy-*β*-D-ribofuranosyl)-imidazo[2,1-*b*]purine (1.6 mg, 95% yield). Over all yield based on O^6-benzyl-dGuo consumed was estimated to be 6 %. UV λ_{max} (MeOH) 228, 263 nm. Positive ion ESI-MS *m/z* (rel intensity) 314 (100) $(MNa)^+$, 292 (57) $(MH)^+$,176 (32) $(MH\text{-deoxyribose})^+$. Positive ion ESI-MS/MS *m/z* 292 $(MH)^+$, 176 (MH- deoxyribose)$^+$. ^1H NMR (DMSO-d_6) 7.94 (s, 1H, H2), 7.44 (bs, 1H, H5), 6.96 (bs, 1H, H6), 6.40 (t, 1H, J = 6.2 Hz, H1′), 4.26 (dd, 1H, J = 10.1, 4.4 Hz, H3′), 3.89 (q, 1H, , J = 4.4 Hz, H4′), 3.49 (dd, 1H, J =

11.8, 4.4 Hz, H5′ or H5″), 3.43 (dd, 1H, partially overlapping H_2O, H5′ or H5″), 2.70 (dt, 1H, *J* = 12.9, 6.2 Hz, H2'), 2.39 (m, 1H, H2") ppm. (Figure 3.1)

3.3.6 Chemical Glycosylation of 8,9-dihydro-9-oxoimidazo[2,1-b]purine (N^2, 3-ethenoguanine) (Scheme 3.3)

Chemical glycosylation of O^9-benzyl-8,9-dihydro-9-oxoimidazo[2,1-b]purine (O^6-benzyl-N^2,3-εGua). To a stirred suspension of 75 mg of O^9-benzyl-8,9-dihydro-9-oxoimidazo[2,1-*b*]purine in 10 mL of acetonitrile (distilled from P_2O_5), 20 mg NaH was added and stirring continued for 2 h at ambient temperature. The reaction was then cooled in ice for 10 min and 120 mg 3,5-di-*O*-(*p*-toluyl)-2-deoxy-D-ribofuranosyl chloride added in one portion. Stirring was continued overnight, allowing the reaction to warm to ambient temperature. The reaction mixture was filtered from solid, the filter washed with ether and the combined filtrate and washings taken to dryness under vacuum. The oil was purified by semi-preparative TLC on SiO_2 eluted with 6 % methanol in chloroform. Bands were collected with R_f values 0.44 (F1, 30 mg, 17 %) and 0.2 (F2, 28 mg, 16 %). F1 ^{1}NMR (chloroform-*d*) 8.15 (s, 1H), 7.82 (q, 4H, *J* = 5.83 Hz), 7.78 (d, 1H, *J* = 1.4 Hz), 7.56 (d, 1H, *J* = 1.4 Hz), 7.48 (d, 2H, *J* = 7.8 Hz), 7.44 – 7.29 (m, overlapping with chloroform-*d*), 7.17 (d, 2H, *J* = 7.8 Hz), 6.63 (dd, 1H, *J* = 7.3, 6.3 Hz), 5.70 (d, 1H, *J* = 12.0 Hz), 5.62 (d, 1H, *J* = 12.0 Hz), 5.58 (m, 1H), 4.70 (m, 1H), 4.68 – 4.63 (m, 2H), 2.83 (ddd, 1H, *J* = 14.1, 6.3, 1.9 Hz), 2.53 (m, 1H), 2.47 (s, 3H), 2.36 (s, 3H) ppm. F2 ^{1}NMR (chloroform-*d*) 8.05 (s, 1H), 8.01 (d, 2H, *J* = 8.11 Hz), 7.81 (d, 2H, *J* = 8.11 Hz), 7.74 (d, 1H, *J* = 2.3 Hz), 7.53 (d, 2H, *J* = 7.7 Hz), 7.41 (d, 1H, *J* = 2.3 Hz), 7.33 – 7.26 (m, 5H), 7.16 (d, 2H, *J* = 7.7 Hz), 6.64 (dd, 1H, *J* = 7.4, 6.0 Hz), 5.78 – 5.70 (m, 3H), 4.79 (dd, *J* = 12.1, 3.3), 4.69 (m, 1H), 4.64 (dd, 1H, *J* = 12.1, 3.3), 2.84 (ddd, 1H, *J* = 14.2, 6.0, 2.2 Hz), 2.71 (m, 1H), 2.44 (s, 3H), 2.36 (s, 3H) ppm.

3',5'-Deprotection of glycosylated F1 and F2. F1 and F2 were each stirred in ammonia-saturated methanol (15 mL) overnight at ambient temperature. The solvent was evaporated under a stream of Ar, the resulting solids triturated with methylene chloride, filtered and the

filters washed with methylene chloride. Evaporation of the collected filtrates yielded F1-1 (12.6 mg, 68 %) and F2-1 (13.0 mg, 70 %). F1-1 ^{1}NMR (DMSO-d_6) 8.68 (s, 1H), 7.94 (d, J = 0.8 Hz, 1H), 7.56 (d, 2H, J= 7.37 Hz), 7.49 (d, 1H, J = 0.8 Hz), 7.41 (ψt, 2H, J = 7.4 Hz), 7.35 (t, 1H J = 7.3 Hz), 6.55 (t, 1H, J = 5.8 Hz), 5.63 (q, 2H, J = 13.0 Hz), 5.32 (d, 1H, J = 4.4 Hz), 5.07 (t, 1H, J = 5.2 Hz), 4.31 (dd, 1H, J = 10.2, 5.2), 3.87 (q, 1H, J = 3.9), 3.62 (dd, 1H, J = 11.9, 4.0 Hz), 3.54 (dd, 1H, J = 11.9, 4.0 Hz), 2.52 (m, overlap with DMSO-d_6), 2.36 (m, 1H) ppm. F2-1 ^{1}NMR (DMSO-d_6) 8.19 (d, J = 1.8 Hz), 8.12 (d, 1H, J = 1.8 Hz), 7.87 (bs, 1H), 7.58 (d, 2H, J = 7.4 Hz), 7.43 (ψt, 1H, J = ~7.2 Hz), 7.38 (t, 2H, J = 7.4 Hz) 6.62 (t, 1H, J = 6.4 Hz), 5.71 (s, 2H), 5.43 (d, 1H, J = 4.2 Hz), 5.07 (t, 1H, J = 5.1 Hz), 4.43 (m, 1H), 3.92 (dd, 1H, J = 7.1, 3.8 Hz), δ 3.68-3.55 (m, 2H), 2.56 (m, 1H), 2.39 (m, 1H) ppm.

Hydrogenolysis of O^9-benzyl-F1-1 and -F2-1. O^9-Benzyl-protected compound (F1-1 or F2-1, 10 mg) was dissolved in methanol (6 mL) and stirred for 2 h with 2 mg 10 % Pd/C under an atmosphere of H_2. The reaction mixture was filtered, the filter washed with additional methanol (5 mL) and the combined washings and filtrate taken to dryness under a stream of Ar followed by evacuation under oil pump vacuum. F1-2, 8,9-dihydro-9-oxo-1-(*β*-D-2-deoxyribofuranosyl)-imidazo[2,1-*b*]purine (6.7 mg, 88 %), UV-vis (H_2O): λ_{max} (ε) 217 (20867), 263 (9066) nm; ESI-MS m/z 176 ([M+H-deoxyribose]$^+$, 50), 292([M+H]$^+$,18), 314 ([M+Na]$^+$, 20), 330 ([M+K]$^+$, 100); ESI-MS/MS m/z 292 [M+1]$^+$, 176 [M+H- deoxyribose]$^+$; NMR (DMSO-d_6) (Figure 3.2) 12.38 (bs, 1H, N*H*8), 8.51 (s, 1H, H2), 7.63 (d, 1H, J = 1.6 Hz, H5), 7.15 (d, 1H, J = 1.6 Hz, H6), 6.68 (t, 1H, J = 6.2 Hz, H1'), 5.35 (bs, 1H, 3'-OH), 5.07 (bt, 1H, 5'-OH), 4.33 (m, 1H, H3'), 3.89 (q, 1H, J = 4.0 Hz, H4'), 3.58 (m, 2H, H5', H5''), 2.42 (m, 2H, H2', H2'') ppm. F2-2, 8,9-dihydro-9-oxo-7-(*β*-D-2-deoxyribofuranosyl)-imidazo[2,1-*b*]purine (6.0 mg, 79 %): UV-vis (H_2O): λmax (ε) 218 (22342), 263 (11056) nm; NMR (DMSO-

d_6) (Figure 3.3) 13.52 (bs, 1H, N*H*3), 8.09 (s, 1H, H2), 7.76 (d, 1H, *J* = 2.7 Hz, H5), 7.65 (d, 1H, *J* = 2.7 Hz, H6), 6.32 (ψt, 1H, *J* = 6.8 Hz, H1'), 5.33 (d, 1H, *J* = 3.7 Hz, 3'-OH), 5.08 (bt, 1H, 5'-OH), 4.35 (m, 1H, H3'), 3.84 (dd, 1H, *J* = 6.9, 4.0 Hz, H4'), 3.56 (m, 2H, H5', H5''), 2.43 (m, 1H, H2'), 2.22 (ddd, 1H, *J* = 13.2, 6.8, 3.1 Hz, H2'') ppm. The high-resolution mass of both of samples obtained as the Potassiumated monomer $[MK]^+$, corresponds to the required composition $C_{12}H_{13}N_5O_4K^+$ (Gained 330.0599, Calced 330.0599, see Figure 3.4 and Figure 3.5).

3.3.7 Enzymatic glycosylation of N^2,3 –ethenoguanine

The enzymatic glycosylations were conducted under the following general conditions. N^2,3-εGua (25.2 μmol) and deoxynucleoside donor (75.6 μmol) were dissolved in buffer at pH 7.5 (phosphate) or 8.0 (2-(*N*-morpholino)ethanesulfonic acid) and the transglycosylase was added (reaction volume 10 mL). Reactions were incubated overnight at 45 ^oC, filtered and the products isolated from the filtrate by HPLC, eluted with methanol/1 mM phosphate buffer (pH 8) using a gradient program: 5% methanol/buffer - 12 % methanol/buffer over 20 min.. For incubations with *L. helveticus* type I, 40 μg of enzyme were added with dGuo as donor, with type II *L. fermentum* and *L. leichmanni*, 40 μg of enzyme were added with dCyd as donor. For glycosylation with the Thyd phosphorylase (*E. coli*)/nucleoside phosphorylase, 0.846 IU phosphorylase and 2.536 unit purine nucleoside phosphorylase were incubated with 25.5 μmol N^2,3-εGua and dThyd in 10 mL phosphate buffer (pH 8.0) at 41 ^oC.

The Lactobacillus incubations were filtered, lyophilized, redissolved in ~ 2 mL H_2O and the products separated by HPLC on an Eclipse XDB C18 column (250 X 10 mm) at a flow rate of 2 mL/min, using the gradient program: 5 % methanol in 95 % 1 mM phosphate buffer (pH 8.0) to 12 % methanol in buffer over 20 min. The incubation mixture from Thyd

phosphorylase/nucleoside phosphorylase incubation mixture was filtered, reduced ~ 50 % in volume on the lyophilizer and then separated by HPLC as described for the Lactobacillus incubations. Products were collected at 12.0, 16.4 and 18.3 min. Under these conditions, the authentic 8,9-dihydro-9-oxo-3-(2-deoxy-*β*-D-ribofuranosyl)-imidazo[2,1-*b*]purine eluted at 5.4 min. Fraction collected at 12 min: UV-vis (H_2O): λmax (ε) 218 (22342), 263 (11056) nm. NMR was identical to 8,9-dihydro-9-oxo-7-(*β*-D-2-deoxyribofuranosyl)-imidazo[2,1-*b*]purine. Fraction collected at 16 min: UV-vis (H_2O): λmax (ε) 217 (20867), 263 (9066) nm. NMR was identical to 8,9-dihydro-9-oxo-1-(*β*-D-2-deoxyribofuranosyl)-imidazo[2,1-*b*]purine. Fraction collected at 18 min, tentatively assigned as 8,9-dihydro-9-oxo-3-(α-L-2-deoxyribofuranosyl)-imidazo[2,1-*b*]purine: UV-vis (H_2O): λmax (ε) 226 (15863), 284 (5318) nm. NMR (D_2O) 8.11 (s, 1H, H2), 7.62 (d, 1H, J = 2.4 Hz, H5), 7.32 (d, 1H, J = 2.4 Hz, H6), 6.41 (ψt, 1H, J = 6.9 Hz, H1′), 4.63 (dt, 1H, J = 6.4, 3.4 Hz, H3′), 4.13 (dd, 1H, J = 7.5, 3.6 Hz, H4′), 3.81 (dd, 1H, J = 12.5, 4.1 Hz, H5′ or H5″), 3.75 (dd, 1H, J = 12.5, 4.1 Hz, H5″ or H5′), 2.85 (m, 1H, H2'), 2.51 (ddd, 1H, J = 14.1, 6.3, 3.5 Hz, H2") ppm. NMR (DMSO-d_6) (Figure 3.6) 7.81 (s, 1H, H2), 7.39 (d, 1H, J = 0.9 Hz, H5), 7.05 (d, 1H, J = 0.9 Hz, H6), 6.22 (dd, 1H, J = 8.4, 6.0 Hz, H1′), 5.82 (bs, 1H, OH3′), 5.22 (d, 1H, J = 3.6 Hz, OH5′), 4.38 (m, 1H, H3′), 3.87 (m, 1H, H4′), 3.61 (dt, 1H, J = 11.7, 3.6 Hz, H5′ or H5″), 3.52 (m, 1H, H5″ or H5′), 2.76 (m, 1H, H2'), 2.13 (ddd, 1H, J = 12.3, 6.0, 1.8 Hz, H2") ppm. The high-resolution mass of both of samples obtained as the Potassiumated monomer $[MK]^+$, corresponds to the required composition $C_{12}H_{13}N_5O_4K^+$ (Gained 330.0598, Calced 330.0599, see Figure 3.7).

3.4 Results and Discussion

The glycosylation pathways shown in Scheme 3.1 were developed for eventual application to synthesis of a standard containing a labeled Gua moiety. Therefore Scheme 3.1

includes synthesis of O^6-benzylguanine, although this compound is available commercially as the natural abundance isotopomer.

3.4.1 Enzymatic glycosylations

Glycosylation of N^2,3-εGua by *trans N*-deoxyribosylase partially purified from *L. helveticus* has been reported give the *N*3/*N*1-nucleosides (*N9/N7* in terms of the Gua skeleton) with a selectivity of 98:2 at pH 8 decreasing to 50:50 at pH 6, the optimal pH for *L. helveticus* [Müller, M.et al, 1996], suggesting that with N^2,3-ε-Gua as substrate, the basic pH favored formation of the target nucleoside in addition to helping prevent degradation of the product by deglycosylation. We investigated glycosylation of N^2,3-ε-Gua by purified Type I *trans N*-deoxyribosyltransferase from *L. helveticus*, the Type II transferases from *L. leichmanni* (structurally similar to the transferase from *L. helveticus* [Anand, R. et al, 2004] and *L. fermentum* and by commercially available *E. coli* purine nucleoside phosphorylase. Glycosylations with the *trans N*-deoxyribosyltransferase enzymes were performed at pH 7.5 and 8.0 to determine the effect of pH on product formation and distribution. The *Lactobacillus trans N*-deoxyribosyltransferase enzymes generated major products having HPLC retention times (Figure 3.8 of ~ 12 and 16 min and one minor product with a retention time of ~ 18 min. The chromatographic trace of the transglycosylation mixture from *L. fermentum* at pH 7.5 shown in Figure 3.8 typifies the resolution of the products. The total extent of conversion was high and independent of pH for *L. fermentum* and *L. leichmanni*, but the product profiles at lower pH show an increase in the 16 min peak at the expense of the 12 minute peak. Transribosylation by *L. helveticus* is more efficient at lower pH, and the effect of lower pH on the product profile is reversed, with the 12 minute peak increasing at the expense of the 16 minute peak. The *E. coli* phosphorylase generated the same three

products, but at a very low level of conversion, and in contrast to the deoxyribosyl transferases, the 18 min peak was the predominant product.

By high-resolution mass spectrometry, all products of enzymatic glycosylation correspond to addition of the 2-deoxyribosyl moiety to N^2,3-εGua. Since the chemical shifts of the etheno protons in ^{1}H NMR spectra have been reported to depend strongly on solvent environment [Guengerich, F. P. et al, 1993] , we established the structures of the enzymatic ribosylation products by heteronuclear multiple bond shift correlation (HMBC) and NOESY NMR studies. The HMBC and NOESY spectra of the nucleoside eluting at 12 minutes are presented in Figure 3.9 and 3.10, respectively. Key features of the HMBC spectrum are H1′/C7a and H1′/C6 coupling, which are consistent with sugar substitution at *N*7 and the absence of H1′/C3a, H1′/C9a, H1′/C2 or H2/C1′ coupling, which rule out ribosylation at *N*1 or *N*3. *N*7 ribosylation is confirmed by the NOESY spectrum, where a cross peak between H1′ and H6 is observed and no NOESY interactions are detected between H2 and any of the deoxyribose protons.

In the HMBC spectrum of the nucleoside eluting at 16 min (Figure 3.11), ribosylation at *N*1 is established by H1′/C2, H2/C1′ and H1′/C9a coupling and the absence of H1′/ C3a coupling. A NOESY cross peak between H1′ and H2 (Figure3.12) is the only NOESY interaction between H1′ and the base, consistent with *N*1 ribosylation assigned by the HMBC spectrum.

In the HMBC spectrum of the minor product eluting at 18 min (Figure 3.13), H1′/C3a and H1′/C2 couplings are observed, indicative of ribosylation at *N*3. Because of the small quantity of sample collected, however, neither the reciprocal H2/C1′ nor unsuppressed

H1′/C1′ one-bond coupling, characteristically observed for deoxyribonucleosides, were detected. Although the HMBC spectrum requires attachment of the ribosyl group at *N*3, chemical shifts of the etheno protons as well as deoxyribose protons H1′, H5′, H5″ and H2′ in the NMR spectrum in DMSO-d_6 do not match the shifts of the corresponding protons of 8,9-dihydro-9-oxo-3-(*β*-D-2-deoxyribofuranosyl)-imidazo[2,1-*b*]purine in the NMR spectrum acquired in DMSO-d_6 in this work or in work reported by others [Khazanchi, R. et al, 1993]. The significance of differences in the chemical shifts of the etheno proton signals may be questionable because of the variability of etheno proton shifts with solvent environment cited above [Guengerich, F. P. et al, 1993]. In contrast to the etheno proton shifts, however, the chemical shifts of the deoxyribose protons and the coupling pattern of H1′ with H2′,H2″ do not appear to vary from sample to sample. In particular, the difference in the shift and splitting pattern of H1′, which appears as a doublet-of-doublets, centered at 6.22 ppm in the spectrum of the enzymatic product and as a pseudo triplet centered at 6.40 ppm in the NMR spectra of 8,9-dihydro-9-oxo-3-(*β*-D-2-deoxyribofuranosyl)-imidazo[2,1-*b*]purine determined in this and other reports, argues strongly against assignment of the enzymatically *N*3-coupled product as the desired β-anomer. In the NOESY spectrum (Figure 3.14), an H1′,H2 interaction was present but an expected H1′,H5 interaction was absent [Guengerich, F. P. et al, 1993]. Finally, the 18 min retention time of the enzymatic ribosylation product is significantly longer than that of the authentic sample of 8,9-dihydro-9-oxo-3-(*β*-D-2-deoxyribofuranosyl)-imidazo[2,1-*b*]purine (described below) under identical conditions. We considered formation of the *N*3 α-anomer, and inspected the NOESY spectrum for an H1′, H3′ interaction, since a strong cross peak would support this assignment. Unfortunately, observation of a NOESY interaction between H1′ and H3′ was precluded by suppression of

the water peak, which resulted in a significant decrease in the intensity of the nearby H3′ signal along with any possible cross peaks. Based on the site of ribosylation at *N*3 determined by the HMBC spectrum and both NMR and HPLC properties that argue against the 8,9-dihydro-9-oxo-3-(*β*-D-2-deoxyribofuranosyl)-imidazo[2,1-*b*]purine structure, we tentatively assign the minor ribosylation product as the α-anomer. Table 1 presents relative efficiencies in terms of per cent N^2,3-εGua substrate converted as well as product profiles for the *trans N*-deoxyribosyltransferase enzymes and the *E. coli* phosphorylase.

3.4.2 Chemical glycosylation

Glycosylation in solution might be expected to impose less rigorous steric constraints than glycosylation within the active sites of the enzymes. However, chemical glycosylation of N^2,3-εGua did not yield the target 8,9-dihydro-9-oxo-3-(*β*-D-2-deoxyribofuranosyl)-imidazo[2,1-*b*]purine, but gave products identical by NMR and NOESY spectra to the *N*1 and *N*7 ribosides generated by the enzymes.

3.4.3 Unambiguous synthesis of 8,9-dihydro-9-*oxo*-3-(2-deoxy-*β*-D-ribofuranosyl)-imidazo[2,1-b]purine

Since neither enzymatic nor chemical glycosylation of N^2, 3-εGua gave the target compound, we reinvestigated an unambiguous synthetic route based on cycloaddition of bromoacetaldehyde to O^6-protected dGuo followed by deprotection Kusmierek, J. T. et al, 1989], [Khazanchi, R. et al, 1993] (see Scheme 3.2) .

Two steps in the procedure proved to be problematical. In anticipation of applying this route to synthesis of 8,9-dihydro-9-oxo-3-(2-deoxy-*β*-D-ribofuranosyl)-imidazo[2,1-*b*]purine using labeled dGuo, we synthesized O^6-benzyl dGuo, although the natural abundance isotopomer is available commercially. While a 91 % yield for benzylation of Gua

using this procedure has been reported (*10*), the relatively small scale benzylation of 3′,5′-di-*O*-acetyl-dGuo gave the desired O^6-benzyl-protected derivative in only 14 % yield. The yield can undoubtedly be improved, but for this work, we did not attempt to optimize conditions. The penultimate step, cycloaddition of bromoacetaldehyde to O^6-benzyldeoxyguanosine, also proved to be refractory. The basic conditions required to avoid deglycosylation of the product resulted in low conversion (3.1 %). However, unreacted O^6-benzyldeoxyguanosine could be recovered in high yield and recycled. We did not continue the recycling process until O^6-benzyldeoxyguanosine was completely consumed, nor make a systematic effort to optimize the cycloaddition conditions. However, it is likely that this step could also be improved, increasing the over all yield of this scheme.

Comparison of the NMR spectrum acquired on our sample with spectra reported for the two other published syntheses [Kusmierek, J. et al, 1989], [Khazanchi, R. et al, 1993] is in accord with the cited variability of etheno proton chemical shifts [Guengerich, F. P. et al, 1993]. However, the chemical shifts of the deoxyribose protons and the appearance of H1′ as a pseudo triplet are identical for all samples. The ^{1}H NMR spectrum of our synthetic product is thus in accord with published data [Kusmierek, J. et al, 1989], [Khazanchi, R. et al, 1993]. Since nuclear overhauser effect data has been reported for O^9-ethyl-8,9-dihydro-9-oxo-3-(*β*-D-ribofuranosyl)-imidazo[2,1-*b*]purine [Guengerich, F. P. et al, 1993] but not for 8,9-dihydro-9-oxo-3-(*β*-D-2-deoxyribofuranosyl)-imidazo[2,1-*b*]purine, we also acquired the NOESY spectrum and confirmed the expected H1′,H5 interaction (Figure 3.15). An interesting feature of the NOESY spectrum is the absence of an H1′, H2 interaction.

Scheme 3.1 Synthesis of N^2, 3–εGua and chemical and enzymatic glycosylation of N^2, 3–εGua

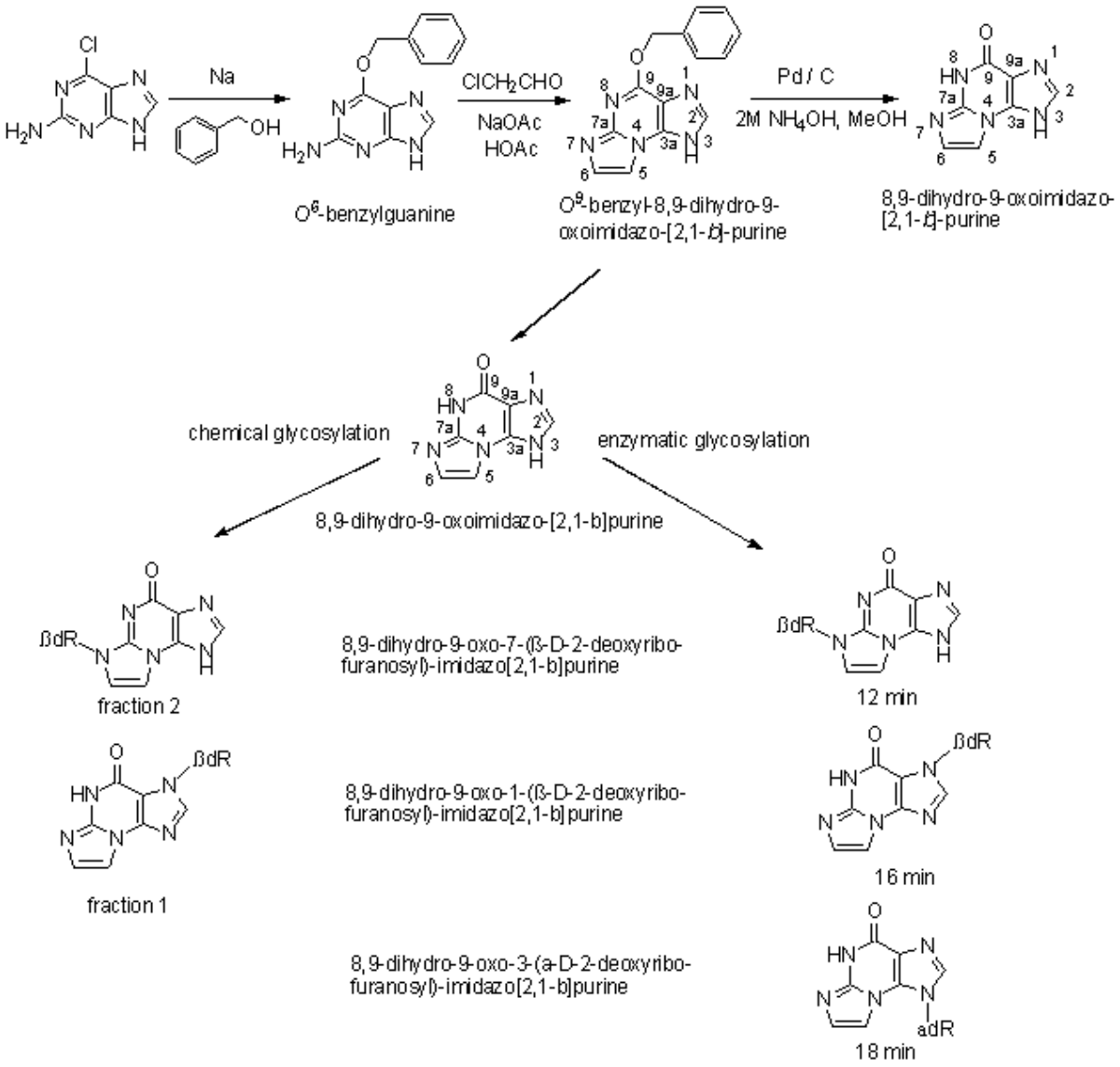

Scheme 3.2 Designed route for chemical synthesis of 8,9-dihydro-9-oxo-3-(β-D-2-deoxyribofuranosyl)-imidazo[2,1-*b*]purine *via* cycloaddition of bromoacetaldehyde to O^6-benzyl-protected dGuo

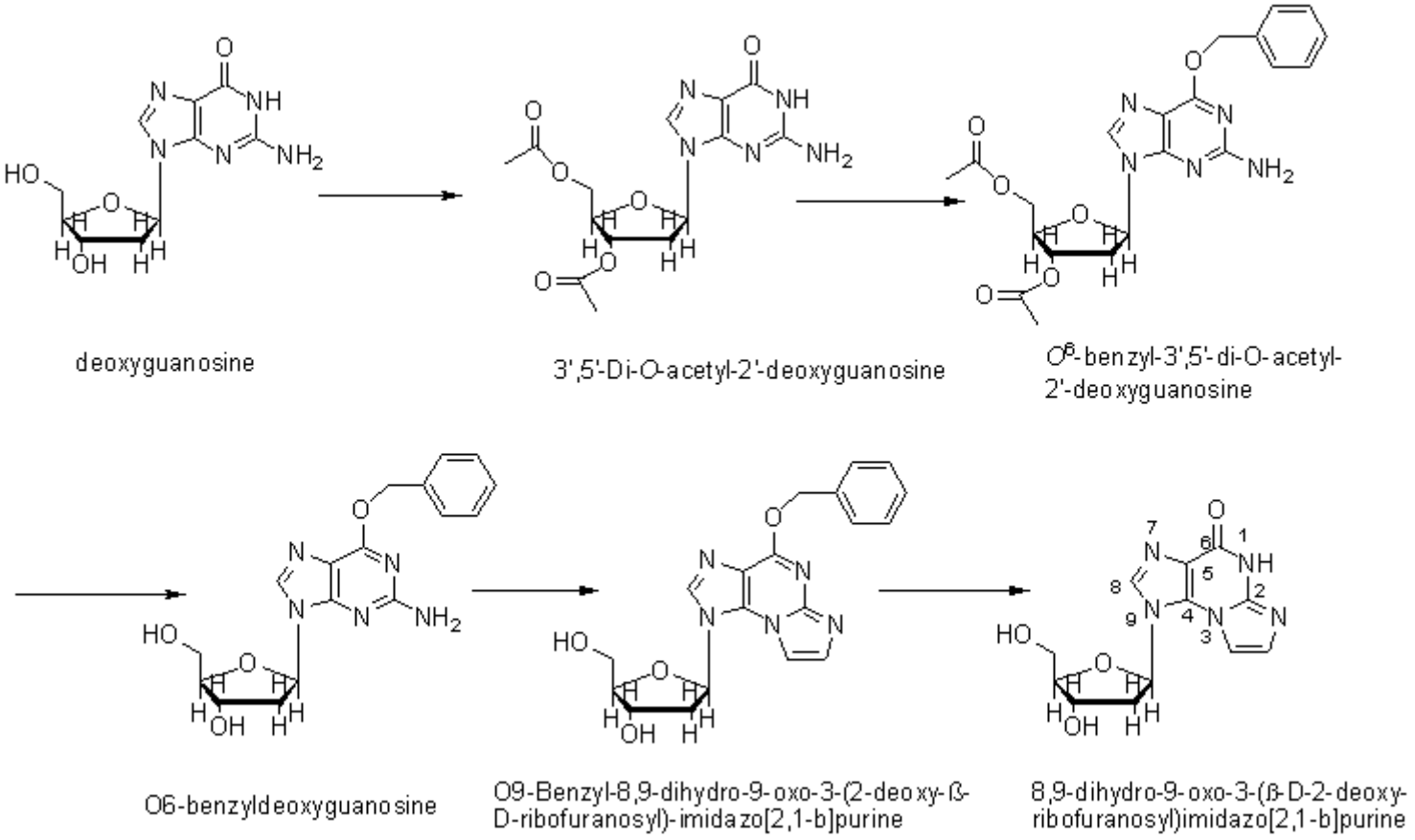

Scheme 3.3 Chemical Glycosylation of N^2, 3-εGua

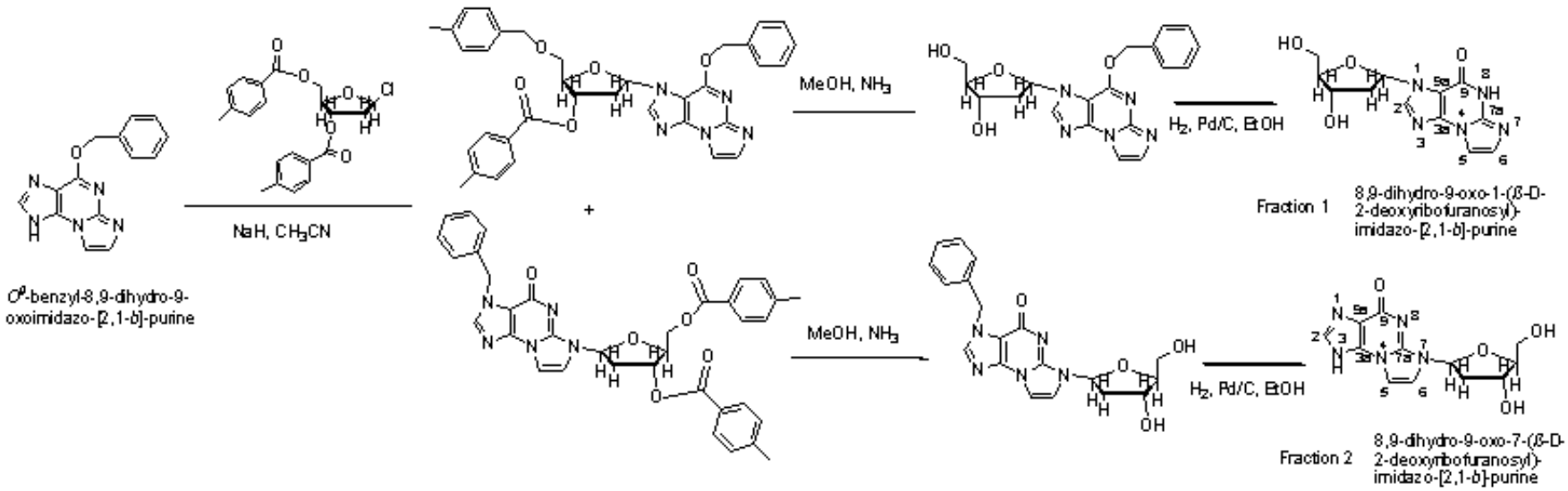

O^6-benzyl-8,9-dihydro-9-oxoimidazo-[2,1-*b*]-purine

8,9-dihydro-9-oxo-1-(β-D-2-deoxyribofuranosyl)-imidazo-[2,1-*b*]-purine

8,9-dihydro-9-oxo-7-(β-D-2-deoxyribofuranosyl)-imidazo-[2,1-*b*]-purine

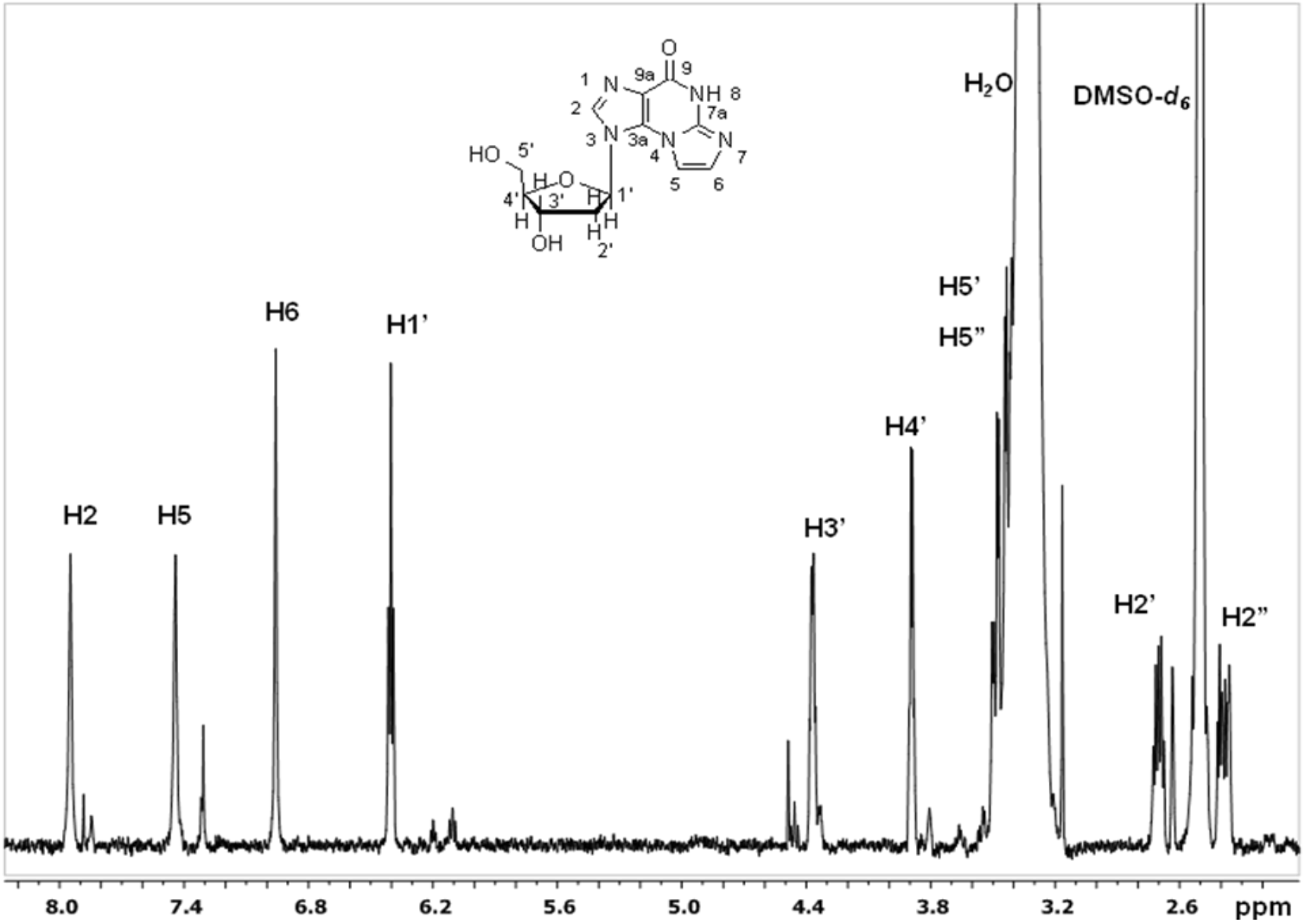

Figure 3.1 ^{1}H NMR of 8,9-dihydro-9-oxo-3-(β-D-2-deoxyribofuranosyl)-imidazo-[2,1-*b*]purine.

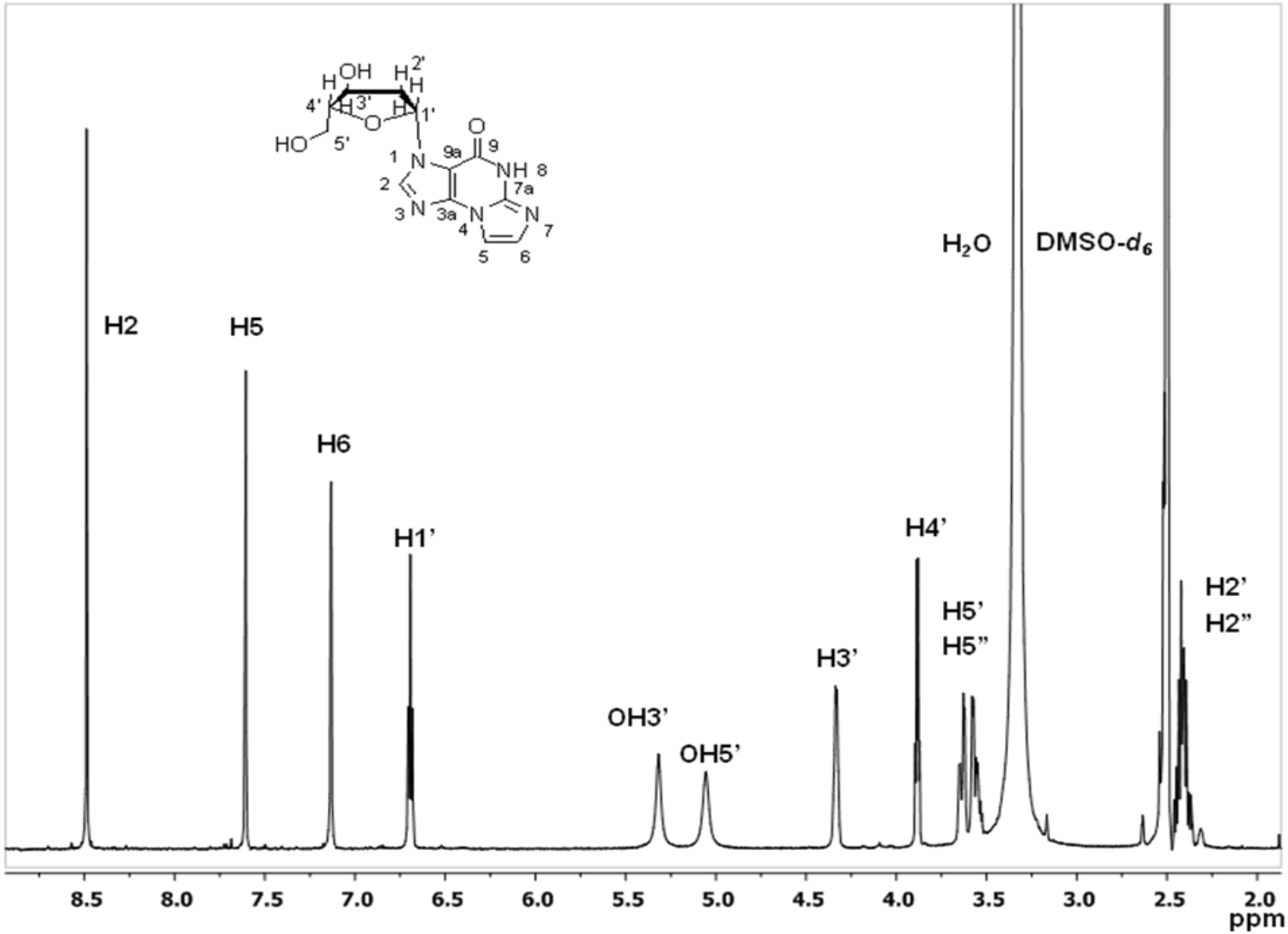

Figure 3.2 [1]H NMR of 8,9-dihydro-9-oxo-1-(β-D-2-deoxyribofuranosyl)-imidazo-[2,1-*b*]purine.

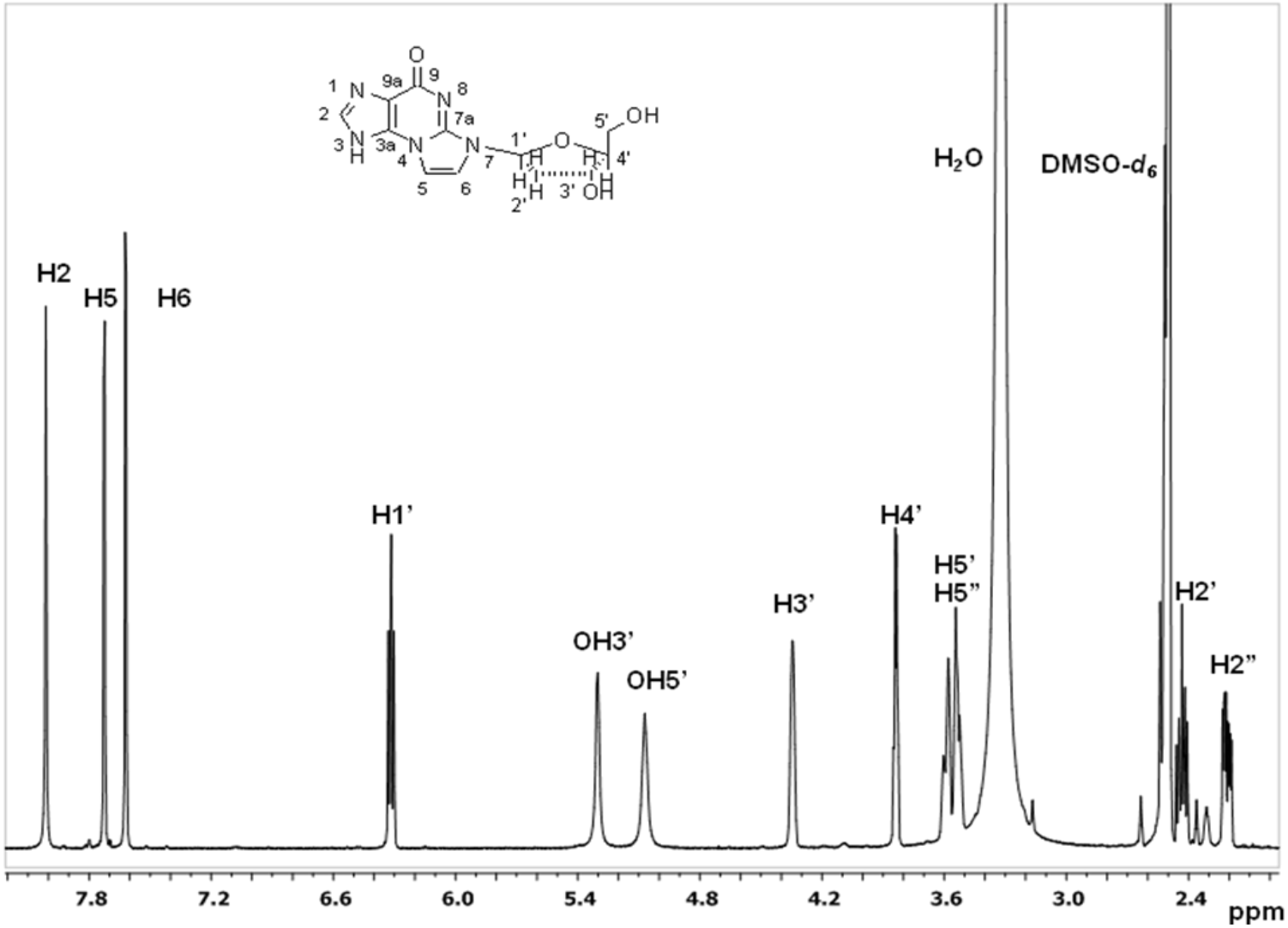

Figure 3.3 [1]H NMR of 8,9-dihydro-9-oxo-7-(β-D-2-deoxyribofuranosyl)-imidazo-[2,1-*b*]purine.

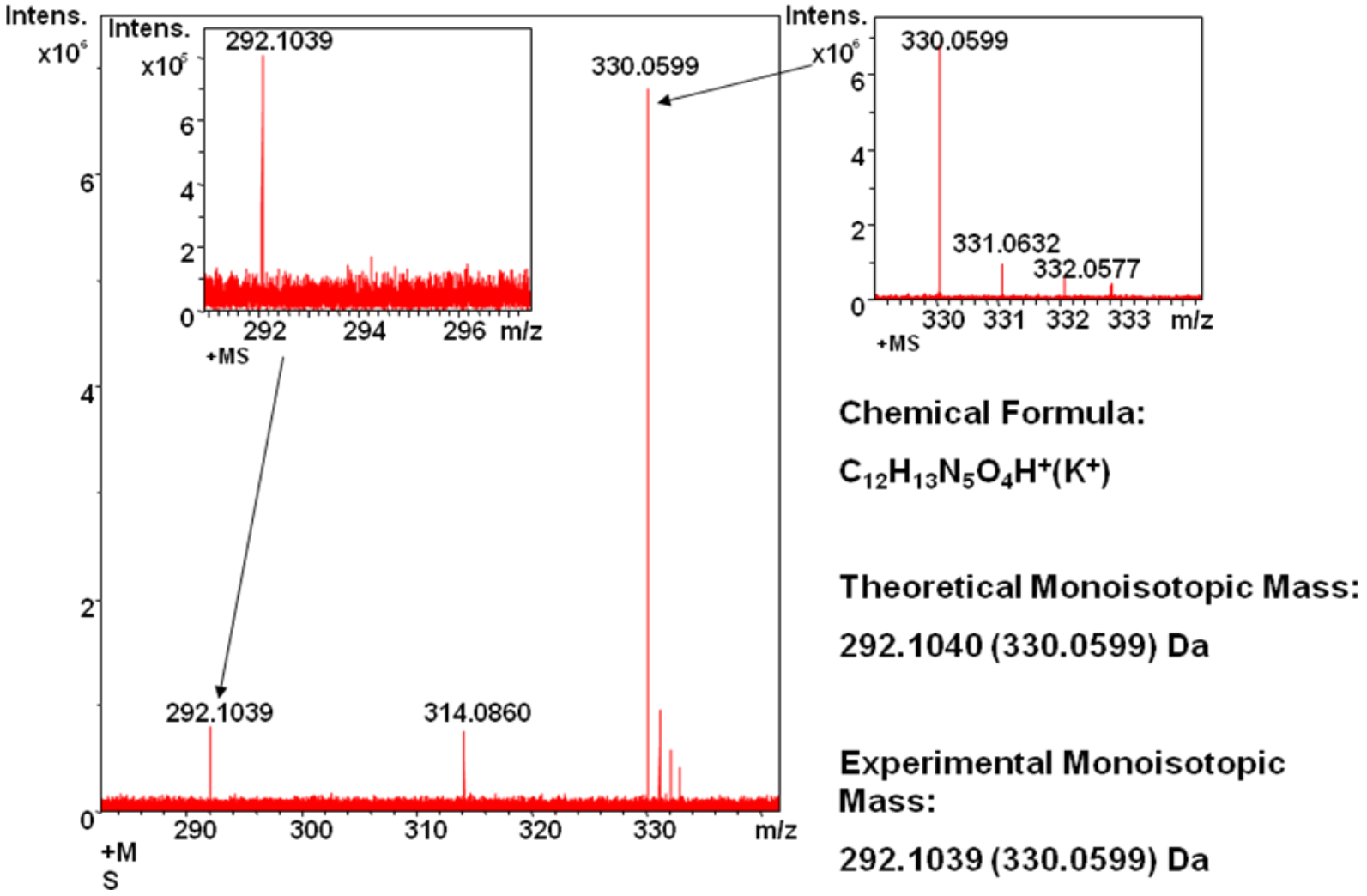

Figure 3.4 Exact Mass of 8,9-dihydro-9-oxo-1-(β-D-2-deoxyribofuranosyl)-imidazo[2,1-*b*]purine(K^+).

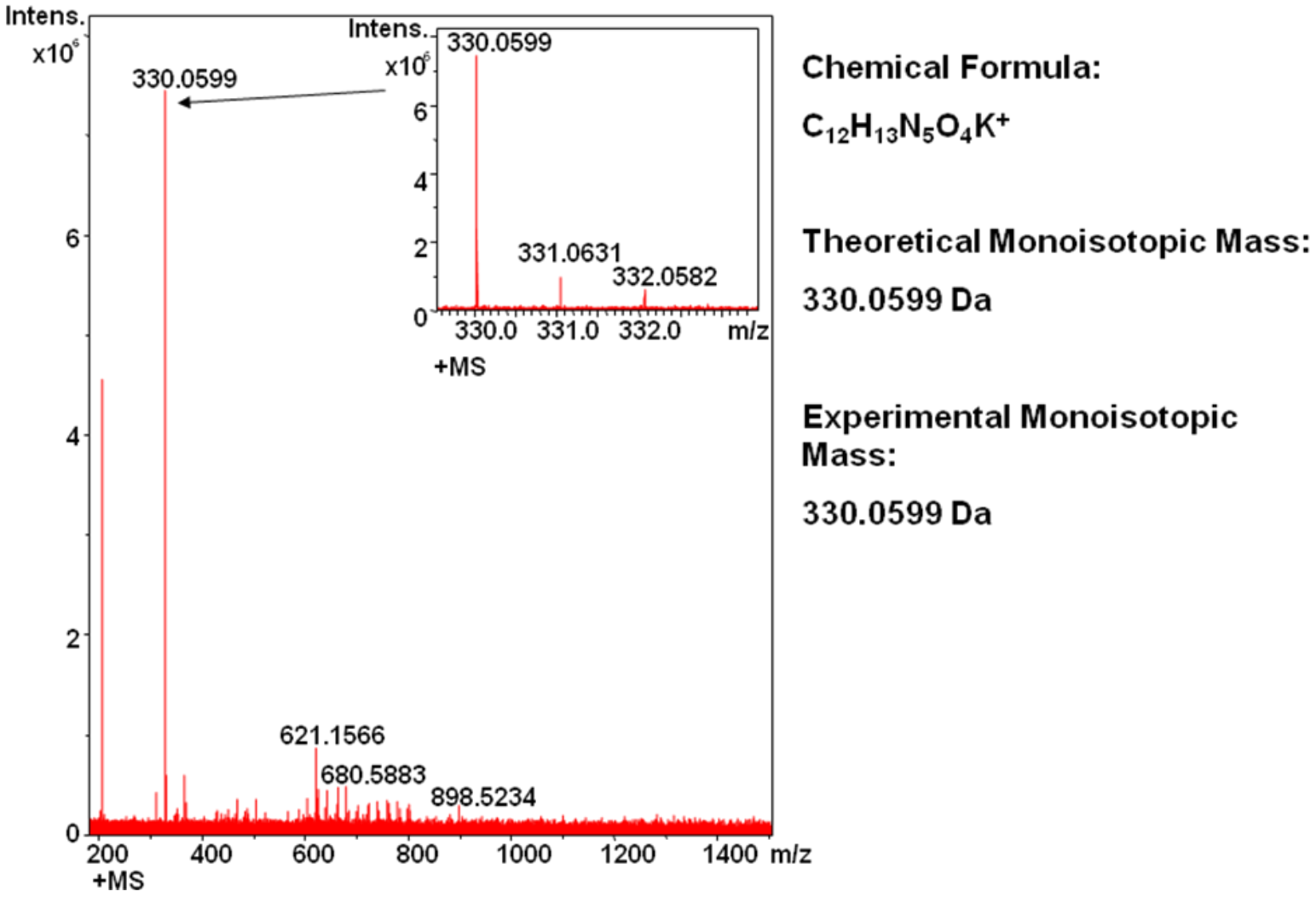

Figure 3.5 Exact Mass of 8,9-dihydro-9-*oxo*-7-(*β*-D-2-deoxyribofuranosyl)-imidazo[2,1-*b*]purine(K^+).

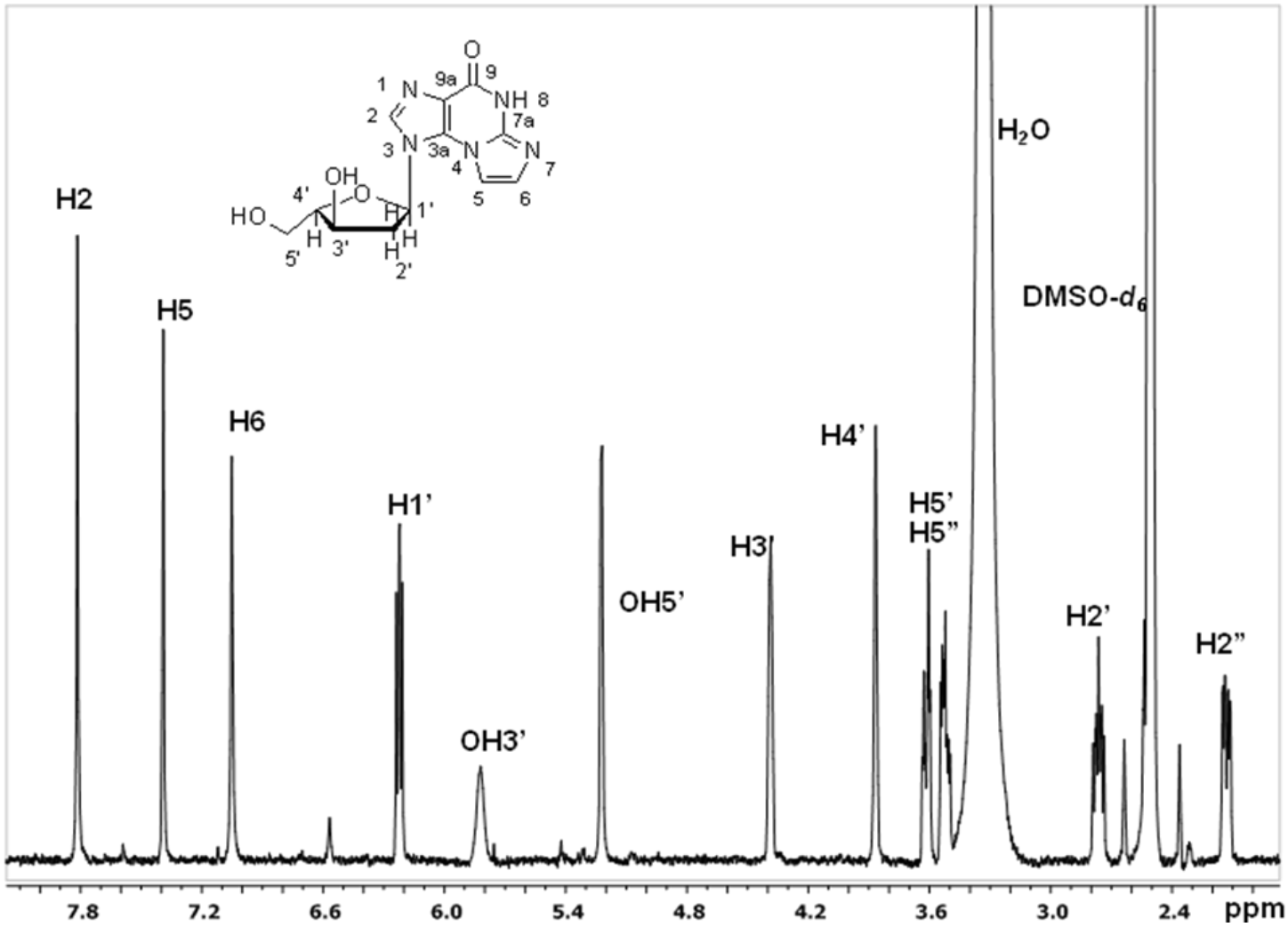

Figure 3.6 ^{1}H NMR of minor product at 18 min. Possible structure: 8,9-dihydro-9-oxo-3-(α-D-2-deoxyribofuranosyl)-imidazo-[2,1-*b*]purine.

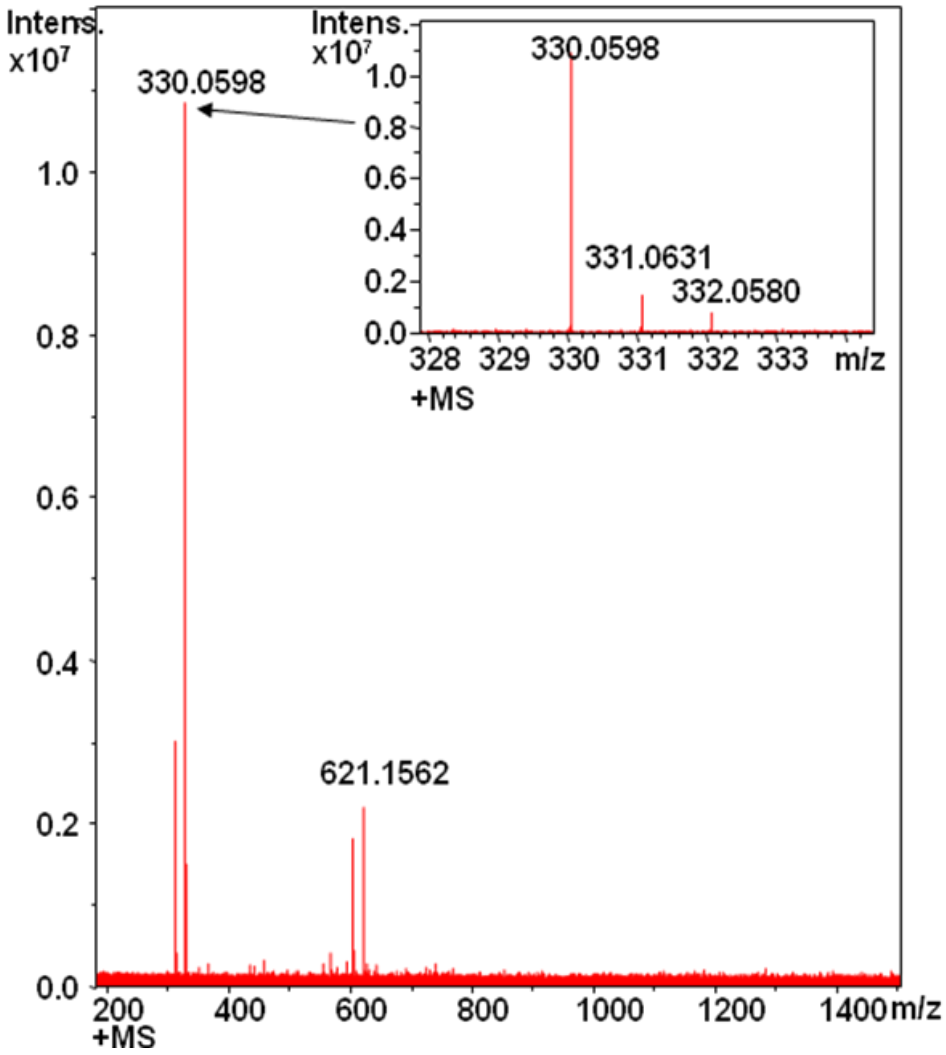

Chemical Formula:

$C_{12}H_{13}N_5O_4K^+$

Theoretical Monoisotopic Mass:

330.0599 Da

Experimental Monoisotopic Mass:

330.0598 Da

Figure 3.7 Exact Mass of minor product at 18 min. Possible structure: 8,9-dihydro-9-oxo-3-(α-D-2-deoxyribofuranosyl)-imidazo[2,1-*b*]purine(K^+).

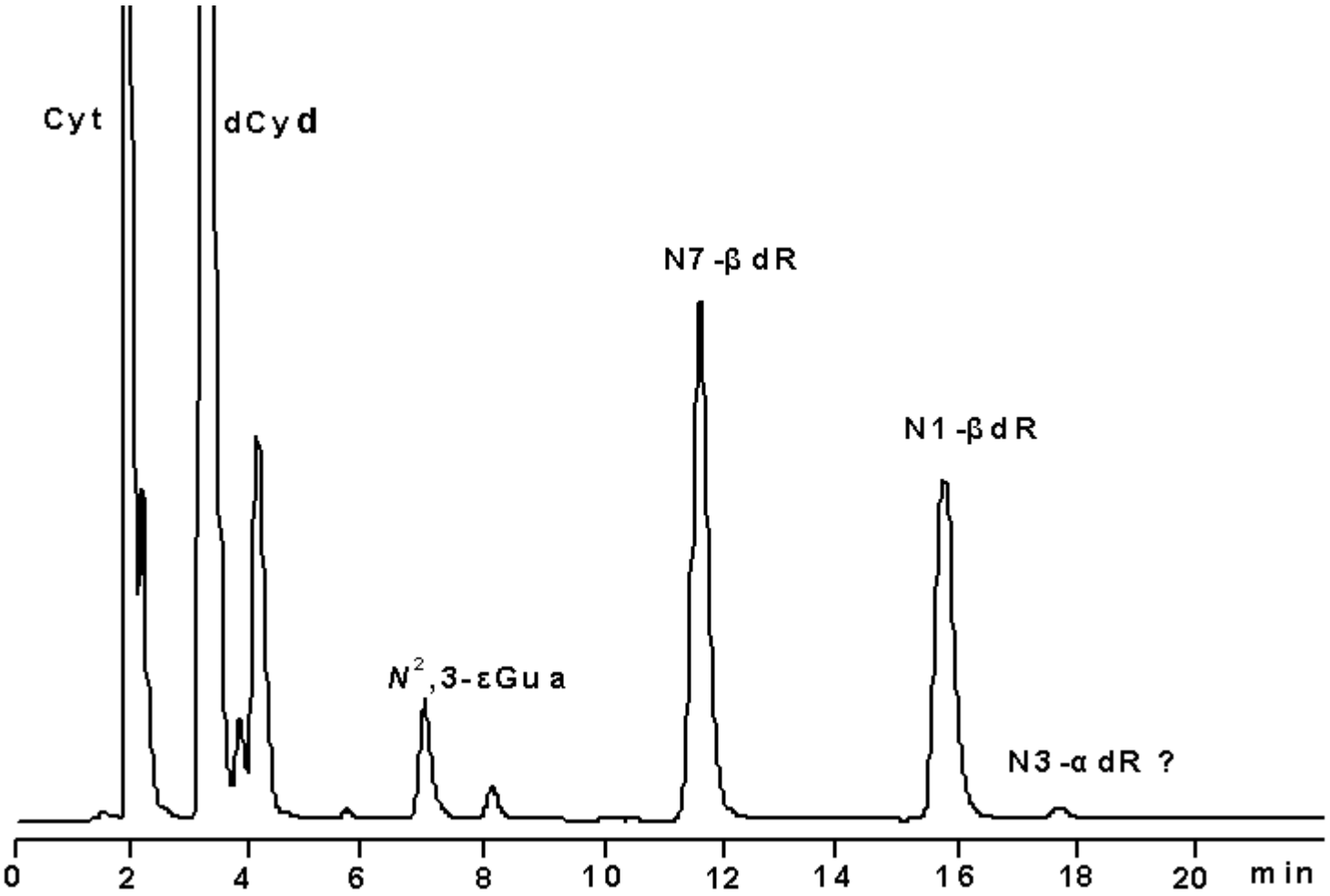

Figure 3.8 HPLC trace monitored at 260 nm, of mixture from ribosylation of N^2,3-εGua by *L. fermentum* transribosylation at pH 7.5.

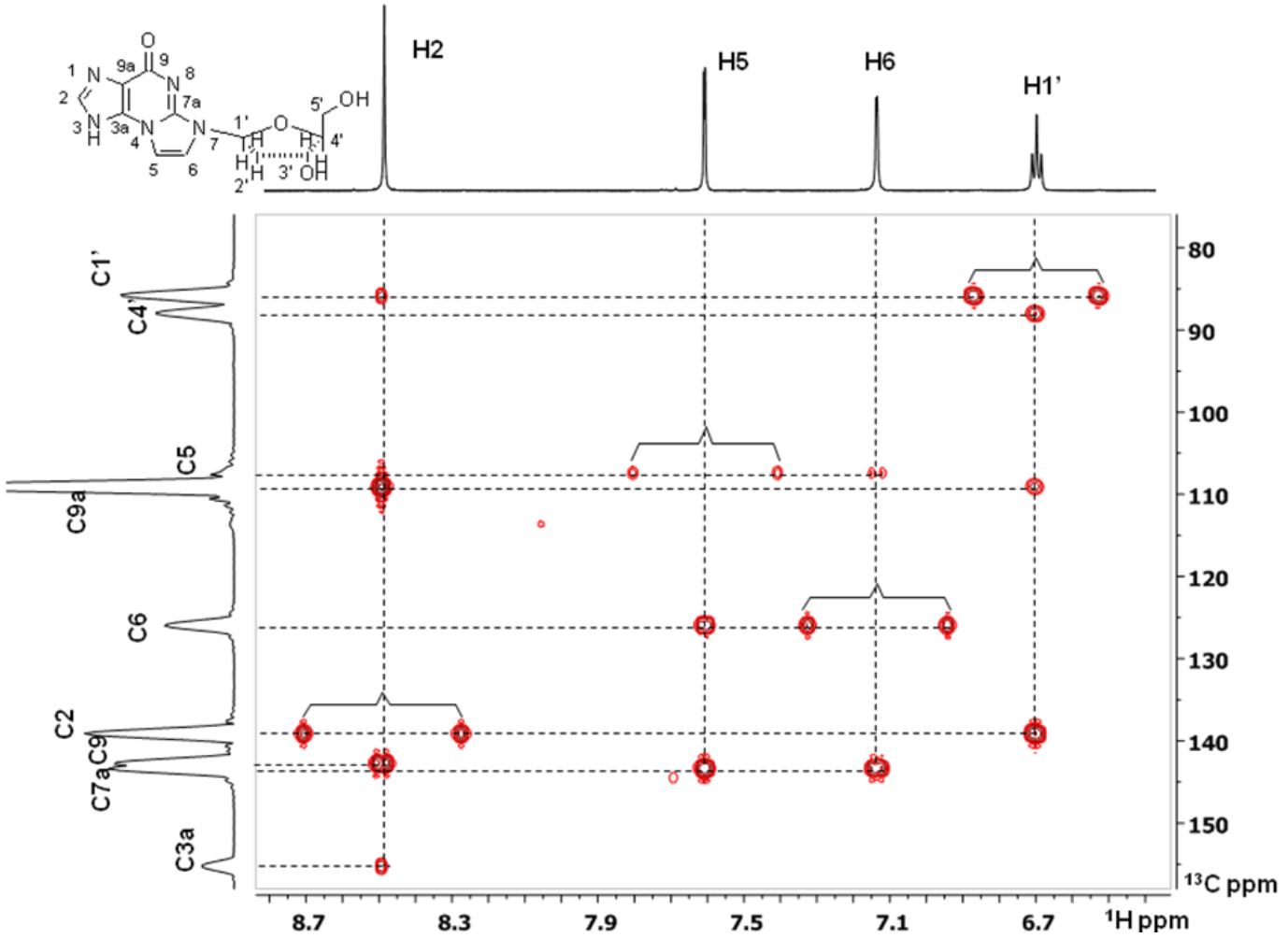

Figure 3.9 HMBC NMR spectrum (DMSO-d_6) of 8,9-dihydro-9-oxo-7-(β-D-2-deoxyribofuranosyl)-imidazo[2,1-*b*]purine spanning the region of H1'-enthenoguanine interaction. Protons are identified on spectrum. Unsuppressed $^{1}J_{C\text{-}H}$ coupling are indicated by brackets**.**

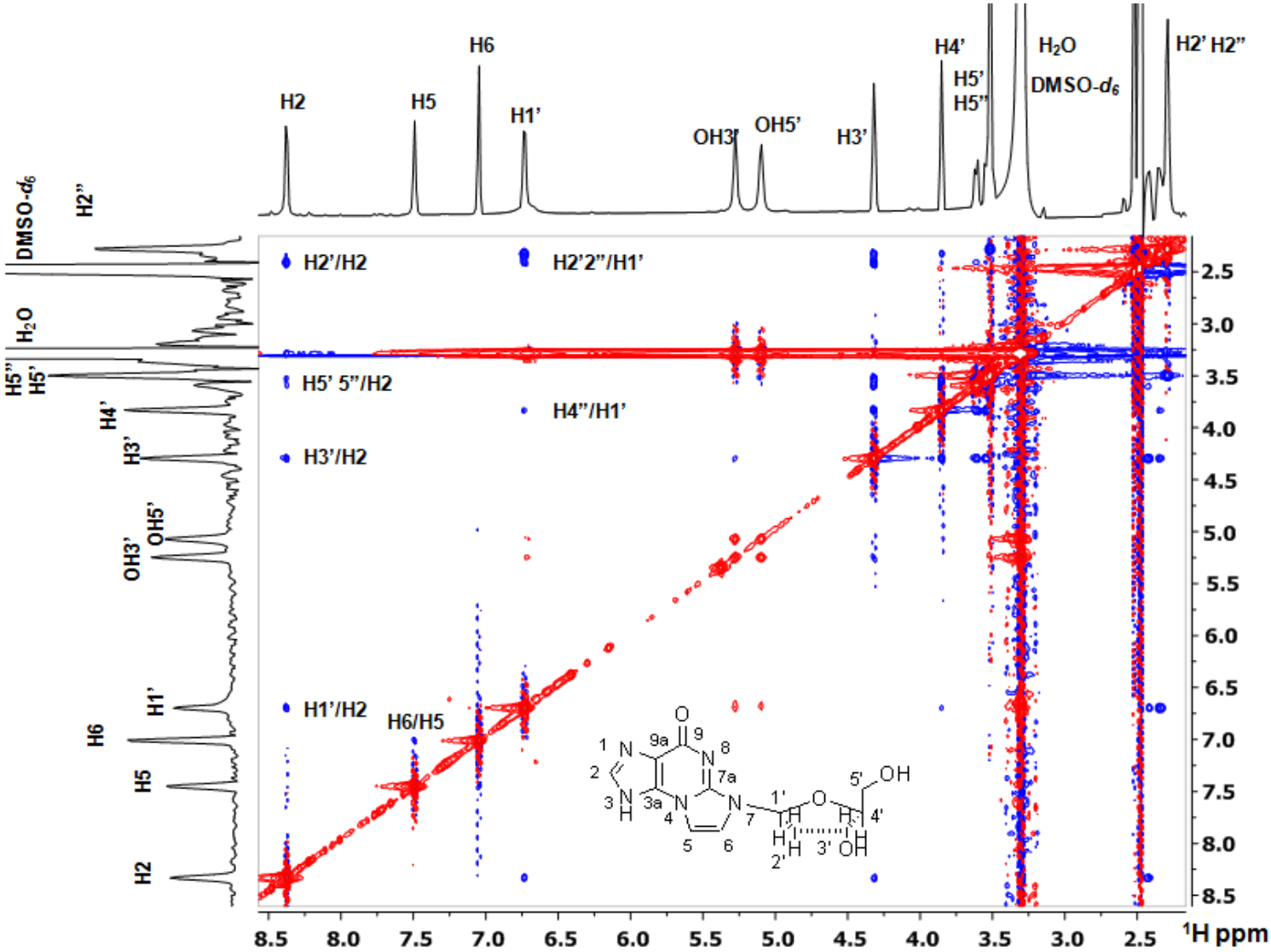

Figure 3.10 NOESY NMR spectrum (DMSO-d_6) of 8,9-dihydro-9-oxo-7-(β-D-2-deoxyribofuranosyl)-imidazo[2,1-*b*]purine spanning the region of H1'-enthenoguanine interaction. Protons are identified on spectrum.

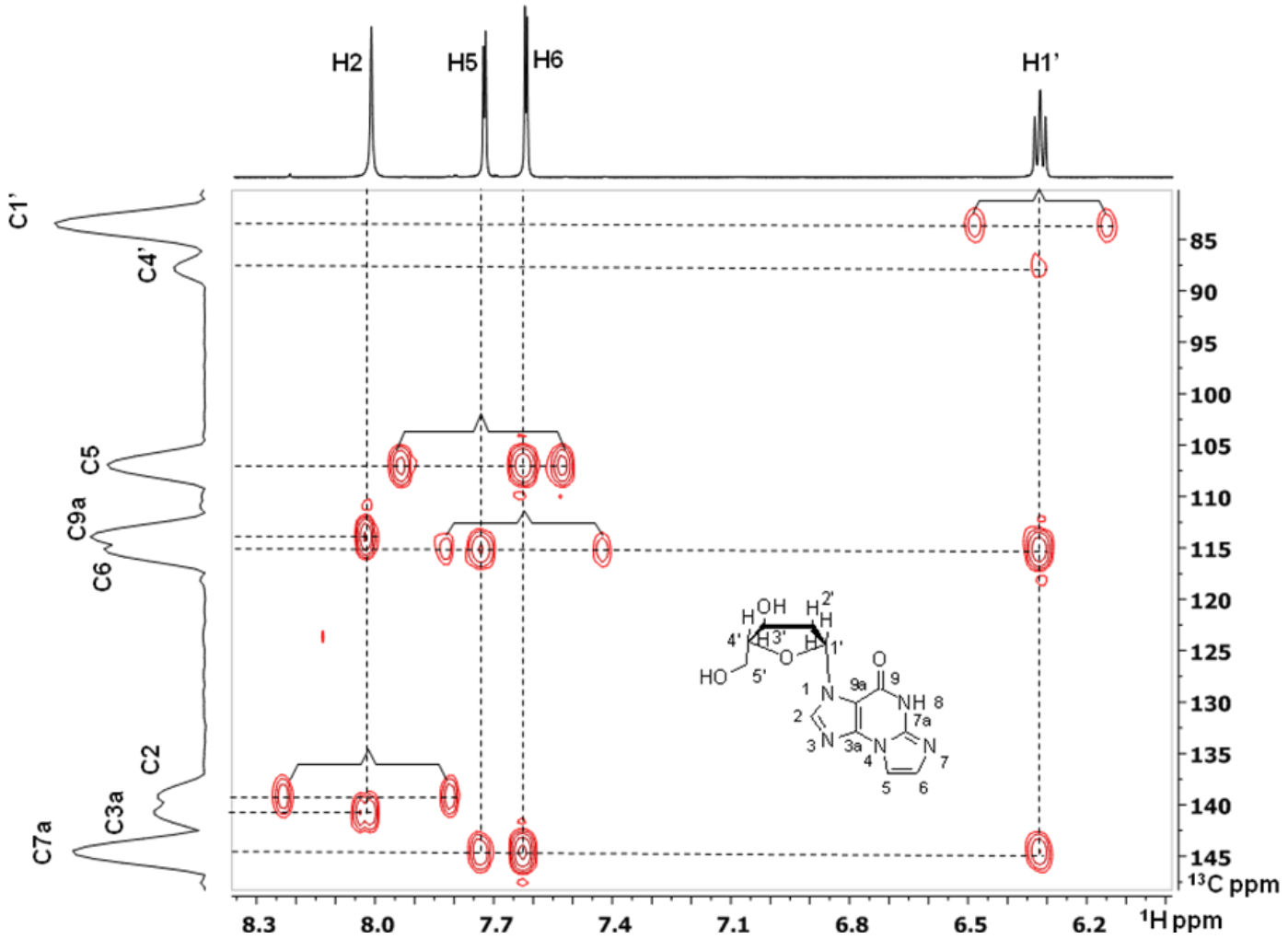

Figure 3.11 HMBC NMR spectrum (DMSO-d_6) of 8,9-dihydro-9-oxo-7-(β-D-2-deoxyribofuranosyl)-imidazo-[2,1-*b*]purine spanning the region of H1'-enthenoguanine interaction. Protons are identified on spectrum. Unsuppressed $^{1}J_{C\text{-}H}$ coupling are indicated by brackets.

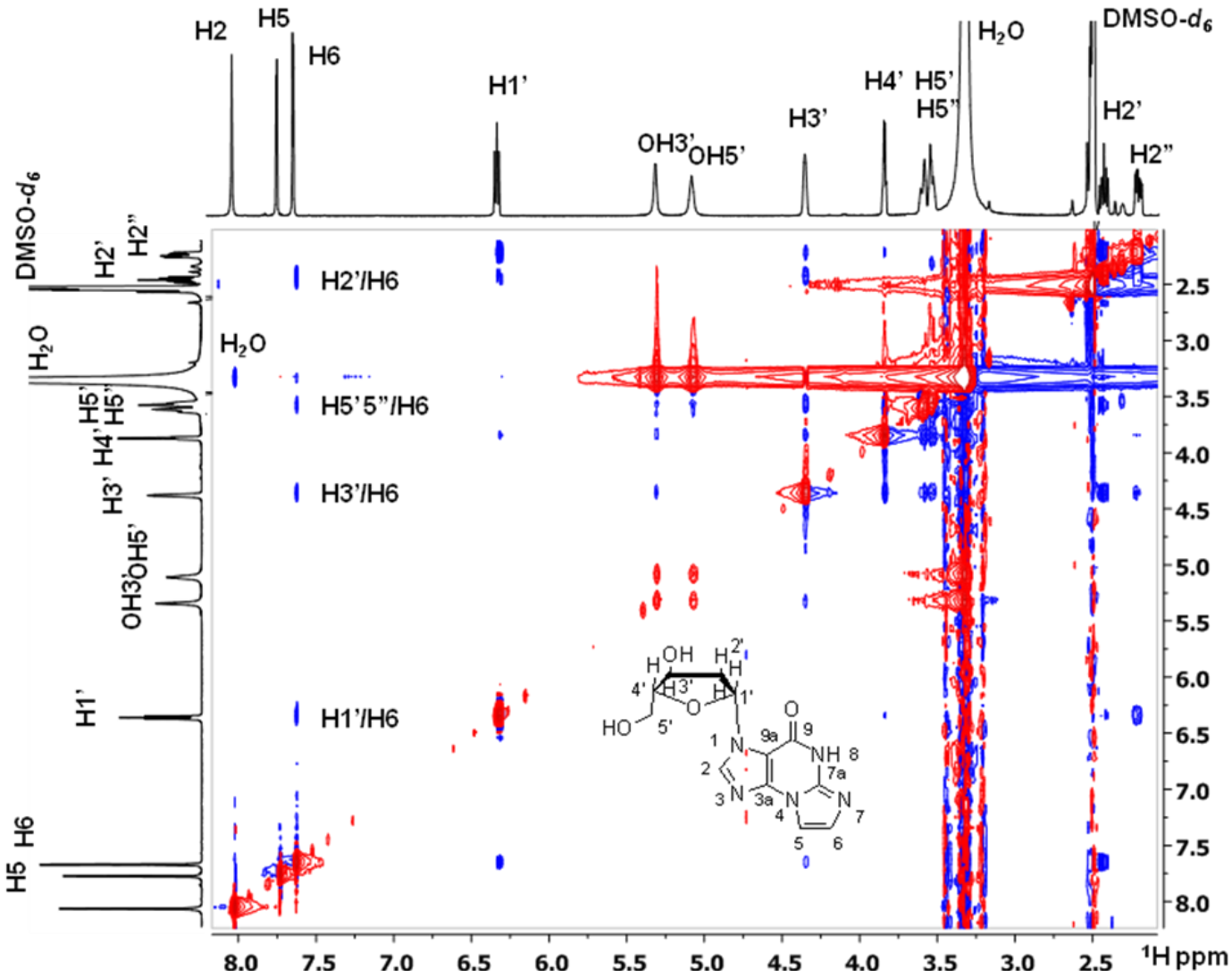

Figure 3.12 NOESY NMR spectrum (DMSO-d_6) of 8,9-dihydro-9-oxo-7-(β-D-2-deoxyribofuranosyl)-imidazo[2,1-*b*]purine spanning the region of H1'-enthenoguanine interaction. Protons are identified on spectrum.

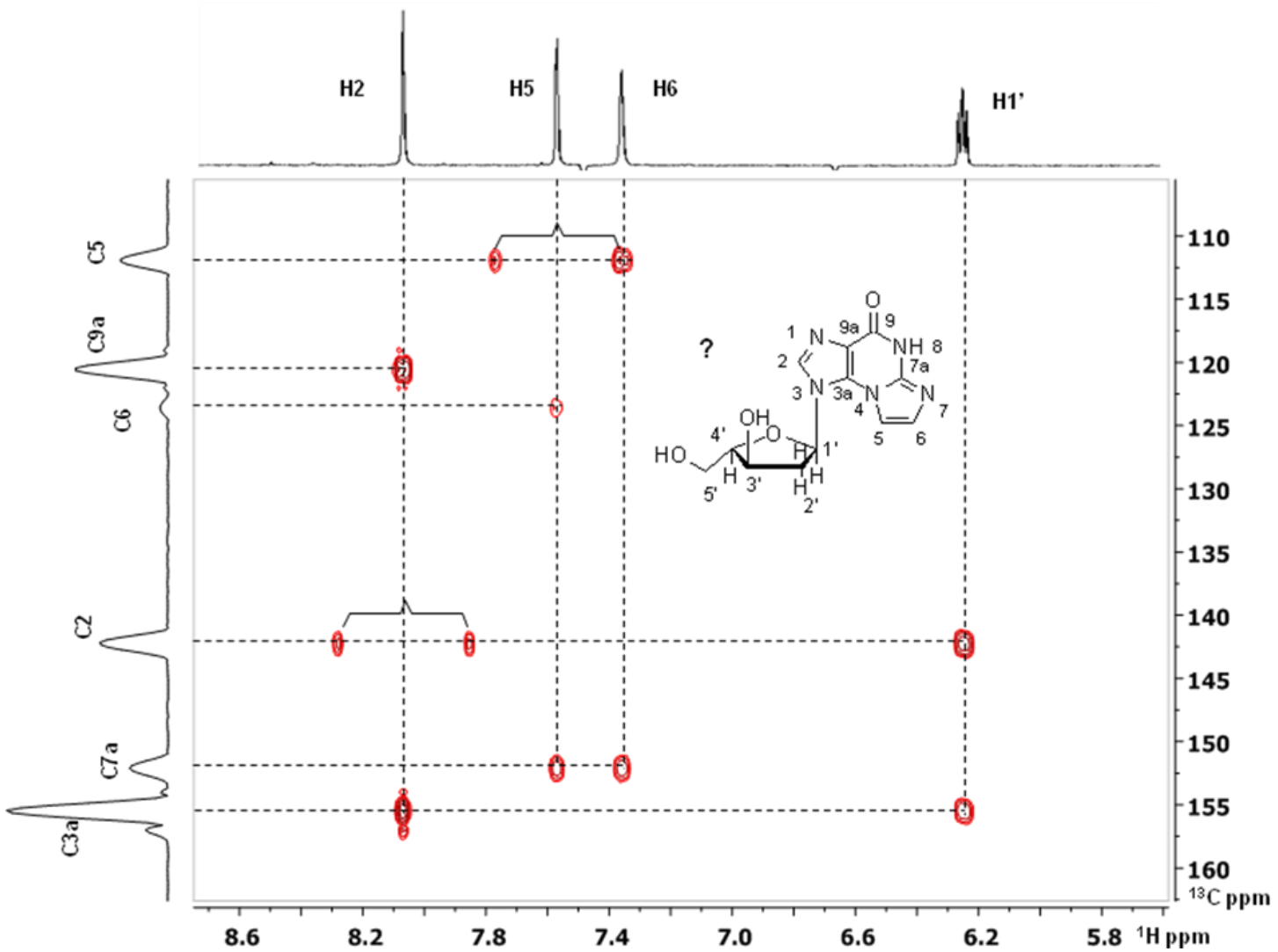

Figure 3.13 HMBC NMR spectrum (DMSO-d_6) of minor product at 18 min. Possible structure: 8,9-dihydro-9-oxo-3-(α-D-2-deoxyribofuranosyl)-imidazo-[2,1-*b*]purine spanning the region of H1'- enthenoguanine interaction. Protons are identified on spectrum. Unsuppressed $^{1}J_{C\text{-}H}$ coupling are indicated by brackets.

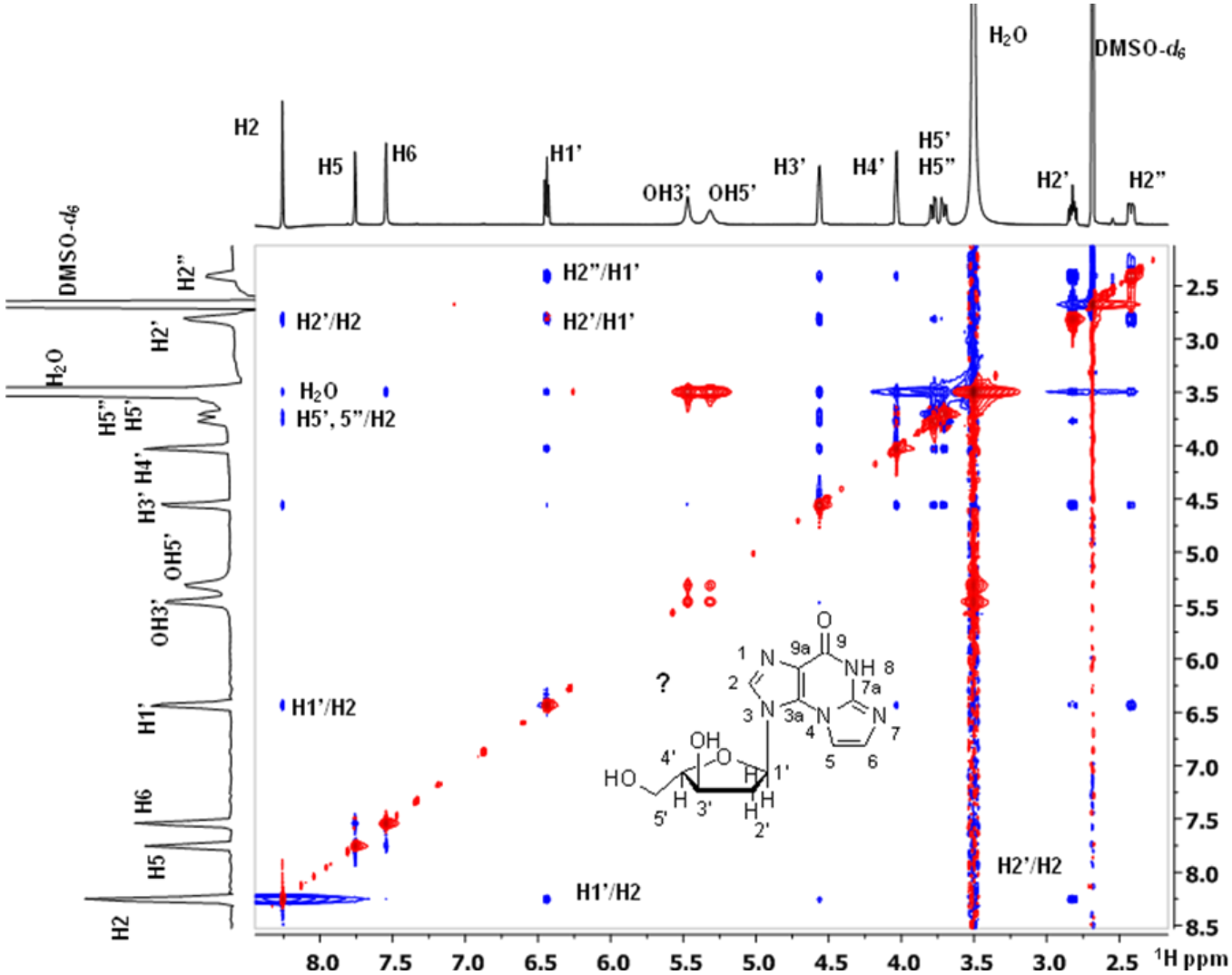

Figure 3.14 NOESY NMR spectrum (DMSO-d_6) of minor product at 18 min. Possible structure: 8,9-dihydro-9-oxo-7-(β-D-2-deoxyribofuranosyl)-imidazo[2,1-*b*]purine spanning the region of H1'-enthenoguanine interaction. Protons are identified on spectrum.

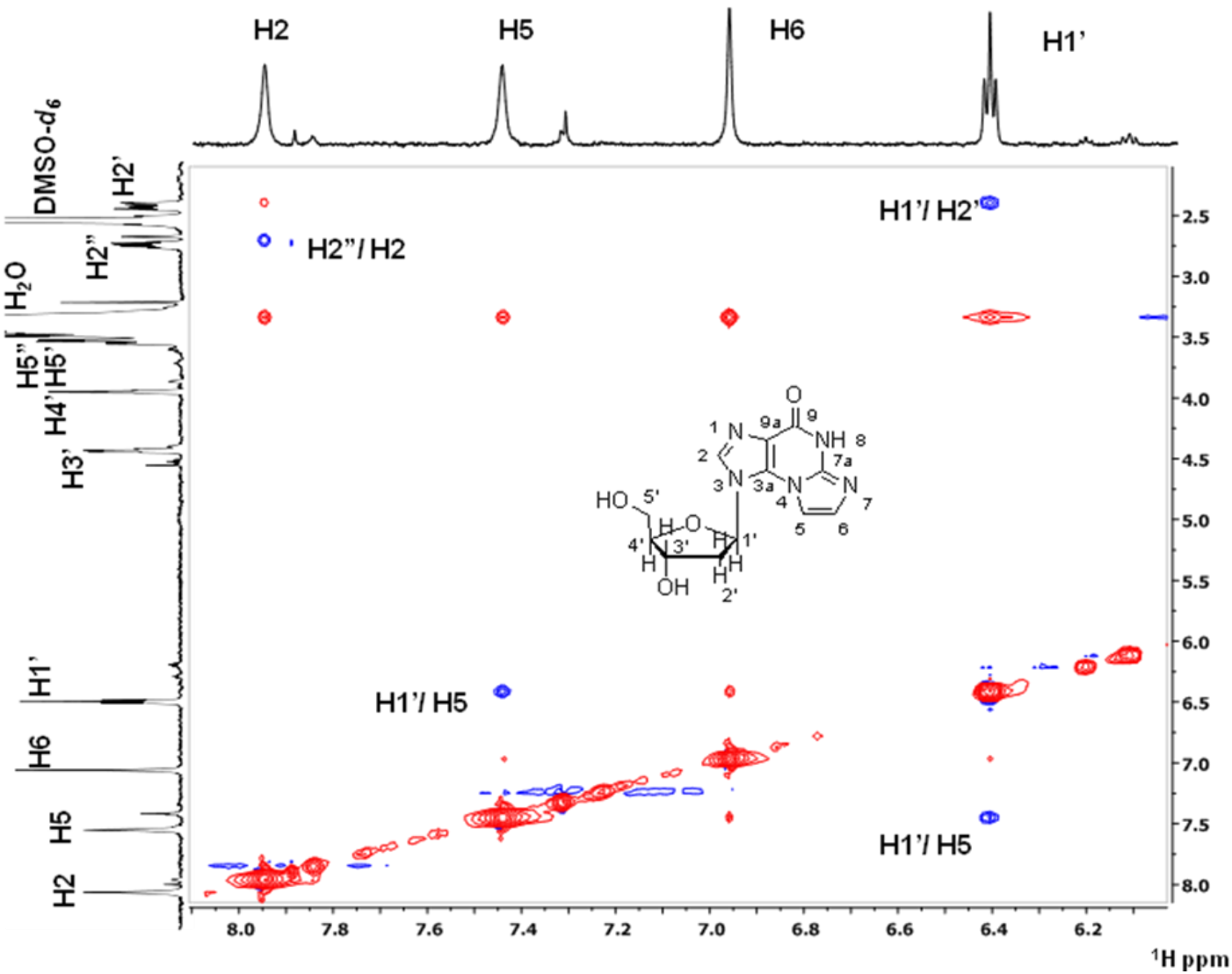

Figure 3.15 NOESY NMR spectrum (DMSO-d_6) of 8,9-dihydro-9-oxo-3-(β-D-2-deoxyribofuranosyl)-imidazo-[2,1-*b*]purine spanning the region of H1'-enthenoguanine interaction. Protons are identified on spectrum.

IV. Discussion and Future Research

Oxidation of DNA leads to the formation of an assortment of oxidation products [Neeley, W. L. et al, 2006]. Relative to the other DNA nucleobases, the oxidation of Gua occurs most readily due to its low oxidation potential. Overall goals of these projects are isolation, identification, characterization and quantitation oxidized Gua adducts both *in vitro* and *in vivo*; furthermore investigate the genotoxic and mutational properties of DNA lesions

4.1 Oxidation of guanine by epoxidizing reagents

Gua + 34 species have been reported from the oxidation of Gua in DNA by a Mn-porphyrin/$KHSO_5$ system, which can function as a monooxygen transfer catalyst [Vialas, C. et al, 2000], and by a dicopper-phenolate complex, via a putative hydroperoxo dicopper(II) transient [Li, L. et al, 2005]. A putative mechanism for the formation of this product with the Mn-porphyrin catalyst has been proposed which involves the trapping of water by a transient guanine cation, formation of dehydrodeoxyspiroiminodihydantoin (N-formylamido-iminohydantoin) followed by hydrolytic opening of the imidazolone ring by breaking the bond between imino carbon and the nitrogen attached to the deoxyribose to give an *N*-formylamido-substituted structure rather than the *N*-formylamino-substituted structure of Scheme 2.2. However, the assignment of the *N*-formyl carboxamido structure was speculative, while we have rigorously established the *N*-formylamino substitution of 2-Ih by a combination of labeling and NMR studies. We therefore suggest the *N*-formylamino structure of 2-Ih as a plausible alternative.

2-Ih has been proved as a stable lesion of Gua oxidation in DNA by epoxidizing reagents which included peracetic acid, mCPBA and DMDO, based on the previous study. In mitochondria, 2-oxoacid decarboxylases have been shown to generate peracids under certain conditions [Abell, L. M. et al, 1991], [Bunik, V. I. et al, 2007], an observation that is significant because mitochondrial DNA repair capability appears to decrease with age [Ledoux, S. P. et al, 2007], [Croteau, D. L. et al, 1999] and accumulated of mutations are implicated in age related neuropathology and the ageing process in general [Dimauro, S. et al, 2005]. Therefore, 2-Ih probably exists in the mitochondrial DNA. If we verified this hypnosis, we can develop an in-depth understanding of the pathology of neurodegenerative diseases and aging though the genotoxicity and mutagenicity of 2-Ih. Furthermore, the 2-Ih base holds promise as a potential biomarker to build up the risk assessment between ROS and mitochondria related diseases. In the further research, we will characterize the genotoxicity and mutagenicity of 2-Ih and whether 2-Ih exists in the mitochondrial DNA

4.1.1 Determination of structures of oxidative lesions in duplex DNA by NMR.

2-Ih has been proved as a stable lesion in single and double stranded DNA, based on the previous study, therefore, next step, the octamer 5′-CCTCGTCC-3′ will be oxidized. This sequence was selected as having a high probability of forming a stable duplex suitable for determination of the molecular structure of the lesion in ds-DNA by NMR. DMDO will be used initially as a model to facilitate characterization of Gua-derived lesions formed by epoxidizing agents. This 2-Ih containing oligonucleotide will be annealed to the complementary partner having C opposite the modified G. ^{13}C, ^{15}N labeled dGuo can be used as a pro-lesion site in the octamer to aid in NMR structure determination. Determination of the molecular structure of the oxidative lesion in a duplex would be the first structure of an

oxidative lesion other than 8-oxodGuo derived from Gua. If this sequence is not suitable for structural determination by NMR, additional duplexes will be investigated, the selection to be determined by the nature of the difficulty encountered.

Preparation of labeled 5'-CCTCGTCC-3' for NMR structure determination of lesion.

The availability of a modified octamer containing a lesion with ^{13}C or ^{15}N label at specific position(s) could be helpful in a structural determination if signal overlap causes uncertainty in establishing connectivity. First, labeled guanine at designated position will be synthesized following the literature [Scheller, N. et al, 1995], and then the isotopomeric nucleobase will be glycosylated enzymatically [Stout, M. D. et al, 2006]. The N^2-isobutyryl-5′-DMT-3′-phosphoramidite derivative of the labeled dGuo will be prepared on a 0.1 mmole scale by standard procedures [Jones, R. A., 1990] and used to for preparation of the labeled octamer.

Determination of structures of oxidative lesions in duplex DNA by NMR

We will begin our structural studies of 2-Ih in duplex DNA with the sequence 5'-d(CCTCG*TCC)-3' / 3'-d(GGAGCAGG)-5', (G* = modified guanine). This sequence was selected with several considerations in mind. (1) The sequence has already been used in a published solution structural study (PDB code 1XRW). (2) The spectral regions of the unmodified duplex shown in citation [Baruah, H. et al, 2005] and supporting information appear to have relatively good chemical shift dispersion and resolution with little overlap. The authors have also listed their nearly complete proton and phosphorus assignments for both the modified and unmodified duplexes. (4) It is a relatively short sequence with a single guanine in the target strand, which should aid our efforts to separate the different

isomers/conformers that are apt to be produced in our synthesis.

Once the individual strands were synthesized and purified, the duplex will be formed by titrating one strand with the other, monitoring single peaks from the separate strands. This would be a check on our calculations of the individual concentrations based on their extinction coefficients. To ensure stable duplex formation, the sample would be heated to ~75 $^{\circ}$C, and then allowed to cool slowly. One-dimensional temperature studies would be performed with the annealed duplex to determine the optimal temperature(s) to record spectra. It remains to be seen if a pH study is also necessary; we would begin at a slightly acidic pH with the intention of slowing exchange.

The assignment procedures for small duplexes are primarily based on NOESY, TOCSY, and DQF-COSY experiments. Phosphorus assignments can be obtained with ^{1}H-^{31}P HETCOR and/or hetero TOCSY experiments.

4.1.2 Whether the DNA lesion, 2-Ih, exist in mitochondrial DNA?

Peracids (RC(O)OOH) have be identified which can cause the Gua form 2-Ih by epoxidation though the completed studies. In mitochondria, three ThDP(Thiamine diphosphate)-dependent enzymes (S. typhimurium ALS II, Baker's yeast pyruvate decarboxylase and Zymomonas mobilis pyruvate decarboxylase) have been shown to catalyze the formation of peracetic acid [$CH_3C(O)OOH$] from pyruvate and O_2 under certain conditions [Abell, L. M. et al, 1991], [Bunik, V. I. et al, 2007], an observation that is significant because mitochondrial DNA repair capability appears to decrease with age [Ledoux, S. P. et al, 2007], [Croteau, D. L. et al, 1999] and accumulated of mutations are

implicated in age related neuropathology and the ageing process in general [Dimauro, S. et al, 2005]. Here we propose a hypothesis that the 2-Ih could exist in the mitochondrial DNA.

Characterization whether 2-Ih can be produced in the system of ThDP-dependent enzymes

Purchased or separated S. typhimurium ALS II will be presented in 0.1 M Tricine-NaOH buffer, pH 7.8, containing 0.1 mM TPP, 0.1 mM FAD, 10 mM MgCl,, and either 30 mM pyruvate, 30 mM a-ketobutyrate, or 5.5 mM acetolactate. The dGuo, dGMP or Gua contained oligonucleotide will be added in to reaction system. The solution will be incubated in 25 °C over night with the bubbling oxygen. Enzymes will be removed by Centricon-10 filtration for 90 min at 4 °C, and the filters rinsed by addition of H_2O followed by centrifugation for a further 90 min. The combined filtrates will be lyophilized and the product analyzed and separated by HPLC coupling with ESI-MS or directly analyzed by LC-MS/MS.

Characterization whether 2-Ih can be produced in the mitochondrial system

Mitochondrial will be separated from cells following the standard procedure, and then be presented in 0.1 M Tricine-NaOH buffer, pH 7.8, containing 0.1 mM TPP, 0.1 mM FAD, 10 mM MgCl,, and either 30 mM pyruvate, 30 mM a-ketobutyrate, or 5.5 mM acetolactate. The solution will be incubated in 25 °C over night with the bu bbling oxygen. The mitochondrial DNA will be extracted and tested by LC-ESI-MS. The low level qualitative or quantitative analysis will be built though this process.

Characterization whether 2-Ih can be generated in cells

If the 2-Ih was been identified in the previous experiment, we can develop the qualitative or quantitative analysis method for the yeast, certain kind of cell line, or the rat tissue to search 2-Ih in the cell. If the 2-Ih existed in the cell, which means 2-Ih is one of the

relative stable DNA adducts oxidized by ROS in vivo. The 2-Ih base thus appears to be a pathway-specific lesion and holds promise as a potential biomarker for epoxidizing agents in vivo.

4.2 Synthesis of *N9*-(β-D-2-deoxyribofuranosyl)-N^2,3-ethenoguanine

4.2.1 Can we increase the overall yield of N9-β-deoxyribosyl-N^2,3-εdGuo?

We investigated both enzymatic glycosylation and chemical glycosylation of N^2,3-εGua as approaches to obtaining this nucleoside adduct under mild conditions, but both routes led to nucleosides having spectroscopic data compatible with ribosylation at positions corresponding to *N*7- and N^2 of Gua as major products. Consequently, I designed an unambiguous route to *N*9-β-deoxyribosyl-N^2,3-εdGuo (8,9-dihydro-9-oxo-3-(β-D-2-deoxyribofuranosyl)imidazo[2,1-*b*]purine) via cycloaddition of bromoacetaldehyde to O^6-benzyl-protected dGuo. Conducted on a small scale, the cycloaddition pathway gave the target compound, albeit in only 6 % overall yield. The overall yields of Kuśmierek's and Khazanchi's synthetic routes are respectively 1% and 4% starting from dGuo [Kuśmierek, J. T. et al, 1989], [Khazanchi R. et al, 1993]. Comparing with these reported synthetic routes, the yield of our method has increased. However there is still intensive potential for improvement, such as the benzylation of 3′,5′-di-*O*-acetyl-2′-deoxyguanosine at O^6 (yield: ~14%) and the cycloaddition of bromoacetaldehyde to O^6-benzyl-protected dGuo (total yield: ~40%). We can improve yields of these two steps in the future.

4.2.2 Whether structures of enzymatic products can provide a tool to demonstrate the structure of active domain and reaction mechanisms?

Enzymatic glycosylation has been widely employed in preparation for the synthesis of isotopically substituted deoxynucleosides, antitumor agents, and biologically active

molecules [Krenitsky, T. A. et al 1986], [Holy, A. et al, 1987], [Müller, M. et al, 1996], [Gaffnev. B. L. et al, 1990]. N^2-(2-oxoethyl)Gua, 5,6,7,9-tetrahydro-7-acetoxy-9-oxoimidazo[1,2-*a*]purine, M1G, 1,N^2-ethenoGua, Xanthine, hypoxanthine, N^1-methylhypoxanthine, uric acid, kinetin, 5-methylCyt, 8-azaAde, 6-mercaptopurine, N^6-methylaminopurine, 2-ethyl-6-hydroxypurine, 5-fluoroUrd, 2-aminopurine and 8-Br-purine are reported substrates for enzymes [Bessman, M. J. et al, 1974], [Sowers, L. C. et al, 1989][Müller, M. et al, 1996]. The first advantage of enzymatic glycosylation is the reaction is under mild pH, since the chemical preparation of certain classes of deoxynucleoside adducts is problematic because of the instability of intermediates to the conditions of synthetic transformations (e.g., the acid lability of purine deoxyribosides). An approach to the synthesis of sensitive deoxynucleosides is coupling of adducted bases to activated deoxyribose derivatives [Srivastava, P. C. et al, 1988]. This approach has found limited application because of problems of yield and stereochemistry and the need for multiple protecting groups. Therefore the other reason is the enzymatic glycosylation would be highly advantageous for synthesis of small scale reactions for labeled standards.

Steven E. Ealick et al. reported that although the PTD is highly selective for purine deoxynucleosides, the transfer of the deoxyribosyl moiety can occur at several positions on the purine base [Anand, R. et al, 2004]. The collection of structures of purine *trans*-deoxyribosylase and purine complexes shows purine bases in the three different orientations, each consistent with one of the *N9*, *N7*and *N3* deoxyribosyl transfer reactions in previous study. Interestingly, two major products, *N*7- and N^2 glycosylated N^2,3-εGua (basing on the Gua numbering system) were characterized in the enzymatic deoxyribosylation, while the target compound *N*9 glycosylated N^2,3-εGua doesn't exist in the reaction mixture. Hence, we

can suppose that the orientations of N^2,3-εGua in purine *trans*-deoxyribosylase will different from purine.

Furthermore, a minor product of the enzymatic ribosylation had a C,H coupling pattern in the HMBC spectrum that was consistent with ribosylation at the target Gua *N*9, but the HPLC retention time and NMR data ruled out the target structure. Thus, this product has tentatively been assigned as the α-anomer of the desired *N*3 riboside. However, the conformation of α-deoxyribosyl-anomer conflicts with the conclusion in Ealick's research [Anand, R. et al, 2004]. They stated that the binding of the deoxyribose has only one possible conformation (β-anomer).

We can understand the structure of this enzyme and catalysis mechanisms further, if the x-ray crystallography is used to get the docking screen of the PDT- N^2,3-εGua complexes. Therefore, we will prepare the crystal of PDT first. After diffusion of N^2,3-εGua into the PDT crystal, an X-ray absorption spectrum will be determined for the PTD- N^2,3-εGua complex crystal by recording the X-ray fluorescence as a function of wavelength, then do the MIRAS phasing, model building and refinement to finally identify the structure and reaction mechanism of the crystal complexes.

REFERENCES

Abell, L. M., Schloss, J. V. (1991) Oxygenase side reactions of acetolactate synthase and other carbanion-forming enzymes. *Biochem. 30*, 7883-7887.

Adam, W., Arnold, M. A., Grüne, M., Nau, W. M., Pischel, U., and Saha-Möller, C. R. (2002) Spiroiminodihydantoin is a major product in the photooxidation of 2′-deoxyguanosine by the triplet states and oxyl radicals generated from hydroxyacetophenone photolysis and dioxetane thermolysis. *Org. Lett. 4*, 537-540.

Adam, W., Arnold, M.A., Nau, W.M., Pischel, U., Saha-Möller, C.R. (2001) Structure-dependent reactivity of oxyfunctionalized acetophenones in the photooxidation of DNA: base oxidation and strand breaks through photolytic radical formation (spin trapping, EPR spectroscopy, transient kinetics) versus photosensitization (electron transfer, hydrogen atom abstraction) *Nucl. Acids Res. 29*, 4955-4962.

Adam, W., Curci, R., Edwards, J. O. (1989) Dioxiranes: A new class of powerful oxidants. *Acc. Chem. Res. 22*, 205-211.

Adam, W., Arnold, M., and Saha-Möller, C. R. (2001) Photooxidative damage of guanine in dG and DNA by the radicals derived from the R cleavage of the electronically excited carbonyl products generated in the thermolysis of alkoxymethyl-substituted dioxetanes and the photolysis of alkoxyacetones. *J. Org. Chem. 66*, 597-604.

Adam, W., Kurz, A., and Saha-Möller, C. R. (1999) DNA and 2′-deoxyguanosine damage in the horseradish peroxidase-catalyzed autoxidation of aldehydes: The search for the oxidizing species. *Free Radical Biol. Med. 26*, 566-579.

Adam, W., Kurz, A., and Saha-Möller, C. R. (2000) Peroxidase-catalyzed oxidative damage of DNA and 2′-deoxyguanosine by model compounds of lipid hydroperoxides: Involvement of peroxyl radicals. *Chem. Res. Toxicol. 13*, 1199-1207.

Adam W., Sahamoller Cr, Schonberger A, Berger M ., Cadet J .(1995) Formation of 7,8-dihydro-8-oxoguanine in the 1,2-dioxetane-induced oxidation of Calf thymus DNA evidence for photosensitized DNA-damage by thermally generated triplet ketones in the dark. *Photochem. Photobiol. 62*, 231-238.

Aikens J., Dix T.A. (1991) Perhydroxyl radical initiated lipid peroxidation. The role of fatty acid hydroperoxides. *J Biol Chem. 266*, 15091-1509.

Anand, R., Kaminski, P. A., and Ealick, S. E. (2004) Structures of purine 2β-deoxyribosyltransferase, substrate complexes, and the ribosylated enzyme intermediate at 2.0 Å resolution. *Biochemistry. 43*, 2384-2393.

Aoshima, H., Satoh, T., Sakai, N., Yamada, M., Enokido, Y., Ikeuchi, T., Hatanaka, H. (1997) Generation of free radicals during lipid hydroperoxide-triggered apoptosis in PC12h Cells.

Biochim. Biophys. Acta. 1345, 35-42.

Bach, R. D., Dmitrenko, O., Adam, W., Schambony, S. (2003) Relative reactivity of peracids versus dioxiranes (DMDO and TFDO) in the epoxidation of alkenes: A combined experimental and theoretical analysis. *J. Am. Chem. Soc. 125*, 924-934.

Barbin, A., Bartsch, H., Leconte, P., Radman, M. (1981) Studies on the miscoding properties of 1,N^6-ethenoadenine and 3,N^4- ethenocytosine, DNA reaction products of vinyl chloride metabolites, during in vitro DNA synthesis. *Nucleic Acids Res. 9*, 375-387.

Barbin, A., Brěsil, H., Croisy, A., Jacquignon, P. , Malaveille, C., Montesano, R., Bartsch, H. (1975) Liver-microsome-mediated formation of alkylating agents from vinyl bromide and vinyl chloride. *Biochem. Biophys. Res. Commun. 67*, 596-603.

Bach, R. D., Dmitrenko, O., Adam, W., Schambony, S. (2003) Relative Reactivity of Peracids versus Dioxiranes (DMDO and TFDO) in the Epoxidation of Alkenes. A Combined Experimental and Theoretical Analysis. *J. Am. Chem. Soc.*, *125*, 924-934.

Barth C., Seitz O., and Kunz, H. (2004) Synthesis of *6-O*-benzyl guanine and its conjugations with linkers. *Z. Naturforsch. 59b,* 802-806.

Bartsch H., Barbin, A., Marion, M.J., Nair, J. , Guichard, Y. (1994) Formation, detection, and role in carcinogenesis of ethenobases in DNA. *Drug Metab. Rev. 26*, 349-371.

Barbin A., Bartsch H. (1986) Mutagenic and promutagenic properties of DNA adducts formed by vinyl chloride metabolites, in: B. Singer, H. Bartsch Eds., *The Role of Cyclic Nucleic Acid Adducts in Carcinogenesis and Mutagenesis*, *70*. IARC Sci. Publ. IARC, Lyon, 345-358.

Bellon, S., Ravanat, J.-L., Gasparutto, D., Cadet, J. (2002) Cross-linked thymine-purine base tandem lesions: Synthesis, characterization, and measurement in γ-irradiated isolated DNA. *Chem. Res. Toxicol. 15,* 598-606.

Bernadou, J., Fabiano, A.-S., Robert, A., and Meunier, B. (1994) "Redox tautomerism" in high-valent metal-oxo-aquo complexes. Origin of the oxygen atom in epoxidation reactions catalyzed by water-soluble metalloporphyrins. *J. Am. Chem. Soc. 116*, 9375-9376.

Bessman, M. J., Muzyczka, N., Goodman, M. F., and Schnaar, R. L. (1974) Studies on the biochemical basis of spontaneous mutation. II. The incorporation of a base and its analogue into DNA by wild-type, mutator and antimutator DNA polymerases. *J. Mol. Biol.* 88, 409-421.

Birdsall, N. J. M., Lee, T.-C., Delia, T. J., and Parham, J. C. (1971) Purine *N*-oxides. XXXV. Alkylated guanine 3-oxides and 3-hydroxy-xanthines. *J. Org. Chem. 36*, 2635-2638.

Boussicault, F., Kaloudis, P., Caminal, C., Mulazzani, Q. G., Chatgilialoglu, C. (2008) The fate of C5′ radicals of purine nucleosides under oxidative conditions. *J. Am. Chem. Soc. 130*, 8377- 8385.

Bravo, A., Bjorsvik, H.-R., Fontana, F., Minisci, F., Serri, A. (1996) Radical versus "oxenoid" oxygen insertion mechanism in the oxidation of alkanes and alcohols by aromatic peracids. New synthetic developments. *J. Org. Chem. 61,* 9409-9416.

Breitmaier, E., Jung, G., Voelter, W., and Pohl, L. (1973) Effect of deuterium isotope on the carbon-13 chemical shift, and hydrogen-deuterium coupling constants in deuterated compounds. *Tetrahedron 29*, 2485-2489.

Bulai, A., Elvira, C., Gallardo, A., Lozano, A., and Román, J.S. (1997) Microstructural analysis of poly(4-*N*-acrylamide-2-hydroxybenzoic acid and poly(5-*N*-acrylamide-2-hydroxybenzoic acid) by ^{13}C NMR spectroscopy. *Polymer. 38*, 3625-3635.

Bulai, A., Jimeno, M. L., De Queiroz, A.-A. A., Gallardo, A., and Roma´n, J. S. (1996) ^{1}H and ^{13}C Nuclear magnetic resonance studies on the stereochemical configuration of bis(*N*,*N*-dimethyl-2,4-di-methylglutarylamide) and poly(*N*,*N*-dimethylacrylamide). *Macromolecules 29*, 3240-3246.

Bunik, V. I., Schloss, J. V., Pinto, J. T., Gibson, G. E., Cooper, A. J. L. (2007) Enzyme-catalyzed side reactions with molecular oxygen may contribute to cell signaling and neurodegenerative diseases. *Neurochem. Res. 32*, 871-891.

Burrows, C. J., Muller, J. G. (1998) Oxidative nucleobase modifications leading to strand scission. *Chem. Rev. 98,* 1109-1151.

Cadet, J., Berger, M., Buchko, G. W., Joshi, P. C., Raoul, S., and Ravanat, J. L. (1994) 2,2-Diamino-4-[(3,5-di-*O*-acetyl-2-deoxy-*β*-D-*erythro*-pentofuranosyl)amino]-5-(2*H*)-oxazolone: A novel and pre-dominant radical oxidation product of 3′,5′-di-*O*-acetyl-2′-deoxy-guanosine. *J. Am. Chem. Soc. 116*, 7403-7404.

Cadet, J., Douki, T., Gasparutto, D., Ravanat, J. L. (2003) Oxidative damage to DNA: formation, measurement and biochemical features. *Mutat. Res. 531*, 5-23.

Choi, S., Cooley, R. B., Hakemian, A. S., Larrabee, Y. C., Bunt, R. C., Maupas, S. D., Muller, J. G., Burrows, C. S. (2004) Mechanism of two-electron oxidation of deoxyguanosine 5'-monophosphate by a platinum(IV) Complex. *J. Am. Chem. Soc.*, *126*, 591-598.

Colson, A.-O., Becker, D. Eliezer, I., Sevilla, M. D. (1997) Application of isodesmic reactions to the calculation of the enthalpies of H• and OH• addition to DNA bases: estimated heats of formation of DNA base radicals and hydrates. *J. Phys. Chem. A. 101*, 8935-8941.

Croteau, D. L.; Stierum, R. H.; Bohr, V. A. (1999) Mitochondrial DNA repair pathways *Mutat. Res. 434*, 137-148.

Davies. J. R., Boyd, D. R., Kumar, S., Sharma, N.D., Stevenson, C. (1990) Prefrential modificatoin of guanine bases in DNA by dimethyldioxirane and its application to DNA sequencing. *Biochem. Biophys. Res. Commun*. *169*, 87-94.

Davies, R. H. J., Stevenson, C., Kumar, S., Lyle, J., Cosby, L., Malone, J., Boyd, F. D. R., Sharma, N. D., Hunter, A. P., and Stein, B. K. (2002) Novel oxidation products from guanine nucleosides reacted with dimethyldioxirane. *Chem. Commun.* 1378-1379.

Davies, R. J. H., Stevenson, C., Kumar, S., Lyle, J., Cosby, L., Malone, J. F., Boyd, D. R., Sharma, N. D., Hunter, A. P., and Stein, B. K. (2003) Oxidation of guanine nucleosides to 4-amidinocarbamoyl-5-hydroxyimidazoles by dimethyldioxirane. *Nucleosides, Nucleotides Nucleic Acid 22*, 1355-1357.

Davies. J. R., Stevenson, C., Kumar, S., Lyle, J., Cosby, L., Malone, J. F., Boyd, D. R., Sharma, N.D., Hunter, A. P., Stein, B.K. (2002) Novel oxidation products from guanine nucleosides reacted with dimethyldioxirane. *Chem. Commun. 13*, 1378-1379.

Dedon, P. C. (2008) The chemical toxicology of 2-deoxyribose oxidation in DNA. *Chem. Res. Toxicol. 21*, 206-219.

Dimauro, S., Davidzon, G. (2005) Temporal changes in cardiovascular autonomic regulation in type II diabetic patients: association with coronary risk variables and progression of coronary artery disease. *Ann. Med*. *37*, 222-232.

Dix, T. A., and Marnett, L. J. (1983) Metabolism of polycyclic aromatic hydrocarbon derivatives to ultimate carcinogens during lipid peroxidation. *Science 221*, 77-79.

Dix, T. A., and Marnett, L. J. (1985) Conversion of linoleic acid hydroperoxide to hydroxy, keto, epoxyhydroxy, and trihydroxy fatty acids by hematin. *J. Biol. Chem. 260*, 5351-5357.

Djordevic V.B. (2004) Free radicals in cell biology. *Int. Rev. Cytol. 237*. 57-89.

Duarte, V., Muller, J. G., and Burrows, C. J. (1999) Insertion of dGMP and dAMP during in vitro DNA synthesis opposite an oxidized form of 7,8-dihydro-8-oxoguanine. *Nucleic Acids Res. 27*, 495-502.

Dul'neva, L. V., Moskvin, A. V. (2005) Kinetics of formation of peroxyacetic acid. *Russ. J. Gen. Chem.75,* 1125-1130.

Evans, M.D. Cooke, MS. (2004) Factors contributing to the outcome of oxidative damage to nucleic acids. *Bioessays 26*, 533-42.

Evans, M. D., Dizdaroglu, M., and Cooke, M. S. (2004) Oxidative DNA damage and disease: induction, repair and significance. *Mutat. Res. 567*, 1-61.

Fang J.L., Vaca, C.E., Valsta, L.M., Mutanen, M. (1996) Determination of DNA adducts of malonaldehyde in humans: effects of dietary fatty acid composition. *Carcinogenesis 17*, 1035-1040.

Fedtke, N., Boucheron,J.A., Walker, V.E. Swenberg, J.A. (1990) Vinyl chloride-induced DNA adducts. II: Formation and persistence of 7-(2'-oxoethyl)guanine and N^2,3-etheno-guanine in rat tissue DNA. *Carcinogenesis 11*, 1287-1292.

Ferris, T. D., Lee, P. T., and Farrar, T. C. (1997) Synthesis of propiolamide and ^{1}H, ^{13}C, and ^{15}N NMR spectra of formamide, acetamide and propiolamide. *Magn. Res. Chem. 35*, 571-576.

Frenkel, K. (1992) Carcinogen-mediated oxidant formation and oxidativeDNA damage. *Pharmacol. Ther. 53,* 127-166.

Gaffnev. B. L., Kune. P. P. and Jones. R. A. (1990) Nitrogen-15-labeled deoxynucleosides. ' 2. Synthesis of [7-^{15} N]-labeleideoxyadenosine, deoxyguanosine, and related deoxynucleosides. J. *Am. Chem. SOC.* 112, 6748-6749.

Garcia-Martín, M. L., Garcia-Espinosa, M. A., Ballesteros, P., Bruix, M., and Cerda´n, S. (2002) Hydrogen turnover and subcellular compartmentation of hepatic [2-^{13}C]glutamate and [3-^{13}C]aspartate as detected by ^{13}C NMR. *J. Biol. Chem. 277*, 7799-7807.

Gates, K. S., Nooner, T., and Dutta, S. (2004) Biologically relevant chemical reactions of *N7*-alkylguanine residues in DNA. *Chem. Res. Toxicol. 17*, 839-856.

Gedick, C. M., Boyle, S. P., Wood, S. G., Vaughan, N. J., Collins, A. R. (2002) Oxidative stress in humans: validation of biomarkers of DNA damage. *Carcinogenesis 23*, 1441-1446.

Greenberg, M. M. (2007) Elucidating DNA damage and repair processes by independently generating reactive and metastable intermediates. *Org. Biomol. Chem. 5*, 18-30.

Gros, L., Ishchenko, A. A., and Saparbaev, M. (2003) Enzymology of repair of etheno-adducts. *Mutat. Res. 531*, 219-229.

Guengerich, F. P., Crawford, W. M., Jr. and Watanabe, P. G. (1979) Activation of vinyl chloride to covalently bound metabolites: Roles of 2-chloroethylene oxide and 2-chloroacetaldehyde. *Biochemistry 18*, 5177-5177.

Guengerich, F. P., Pressmarks, M., and Humphreys, W. G. (1993) Formation of 1,N^2- and N^2,3-Ethenoguanine from 2-Halooxiranes: Isotopic Labeling Studies and Isolation of a Hemiaminal Derivative of N^2-(2-Oxoethyl)guanine. *Chem. Research Toxicol. 6*, 635-648.

Guengerich, F. P. (1992) Roles of the vinyl chloride oxidation products 1-chlorooxirane and 2-chloroacetaldehyde in the in vitro formation of etheno adducts of nucleic acid base. *Chem. Res. Toxicol. 5*, 2-5.

Guy, A., Duplaa, A.-M., Ulrich, J., Teoule, R. (1991) Incorporation by chemical synthesis and characterization of deoxyribosylformylamine into DNA. *Nucl. Acids Res.*, *19*, 5815-5820.

Hall, J.A., Saffhill, R., Green, T., Hathway, D.E. (1981) The induction of errors during in vitro DNA synthesis following chloroacetaldehyde treatment of poly dA-dT. and poly dC-dG. templates. *Carcinogenesis 2*, 141-146.

Halliwell B., Gutterridge J.M.C. (2003) Free radicals in biology and medicine. *Oxford University PressOxford (UK)*. 62–66, 76–78, 247–249, 257, 546-547.

Hamilton, J. G., Ivin, K. J., Kuan-Essig, L. C., and Watt, P. (1976) ^{13}C Nuclear magnetic resonance spectra of poly(N-formylpropylenimine) and some related formamide derivatives. *Macromolecules 9*, 67-71.

Hoeijmakers, J. H. J. (2001) Genome maintenance mechanisms for preventing cancer. *Nature 411*, 366-374.

Hoffer. M. (1960) Alpha thymidin. *Chem. Ber. 93*, 2777-2781.

Hole, E. O., Nelson, W. H. (1987) ESR and ENDOR Study of the Guanine Cation: Secondary Product in 5′-dGMP. *J. Phys. Chem.*, *89*, 5218-5219.

Holy, A., and Votruba, I. (1987) Facile preparation of purine and pyrimidine 2-deoxy-β-D-ribonucleosidbeys biotransformation on encapsulated cells. *Nucleic Acids Symp. Ser.* 18, 69-72.

Hong, I. S., Carter, K. N., Sato, K., Greenberg, M. M. (2007) Characterization and mechanism of formation of tandem lesions in DNA by a nucleobase peroxyl radical. *J. Am. Chem. Soc. 129*, 4089-4098.

IARC (1979) Some Monomers, Plastics and Synthetic Elastomers, and Acrolein. IARC *Monographs on the Evaluation of Carcinogenic Risks to Humans.* Vol. 19. International Agency for Research on Cancer, Lyon, pp. 377-438.

Ippel, J. H., Wijmenga, S. S., de Jong, R., Heus, H. A., Hilbers, C. W., de Vroom, E., van der Marel, G. A., van Boom, J. H. (1996) Heteronuclear scalar couplings in the bases and sugar rings of nucleic acids: Their determination and application in assignment and conformational analysis. *Magn. Reson. Chem. 34*, 156-l76.

Jacobsen, J. S., Humayun, M. Z. (1986) Chloroperbenzoic acid induced DNA damage and peracid activation of alfatoxin B_1. *Carcinogenesis* 7, 491-493.

Jeong, Y. C., Sangaiah, R., Nakamura, J., Pachkowski, B. F., Ranasinghe, A., Gold, A., Ball, L. M., Swenberg, J. A. (2005) Analysis of M_1G-dR in DNA by aldehyde reactive probe labeling and liquid chromatography tandem mass spectrometry. *Chem. Res. Toxicol. 18*, 51-60.

Johnston, E. R., Fortt, R., and Barborak, J. C. (2000) Correlated rotation in a conformationally restricted amide. *Magn. Reson. Chem. 38*, 932-936.

Kanner, J., Rosenthal, I. (1992) An assessment of lipid oxidation in foods. *Pure &Appl. Chem. 64*, 1959-1964.

Khazanchi, R., Yu, P. L., and Johnson, F. (1993) N^2,3-Etheno-2'-deoxyguanosine [8,9-dihydro-9-oxo-3-(β-D-2-deoxyribofuranosyl)-imidazo[2,1-*b*]purine]: A practical synthesis and Characterization. *J. Org. Chem. 58,* 2552-2556.

Kibbe, W. A. (2007) OligoCalc: an online oligonucleotide properties calculator. *Nucl. Acids Res. 35*, W43-6.

Klaunig, J. E., and Kamendulis, L. M. (2004) The role of oxidative stress in carcinogenesis. *Annu. Rev. Pharmacol. Toxicol. 44*, 239-267.

Klein, C. B., Frenkel, K., and Costa, M. (1991). The role of oxidative processes in metal carcinogenesis. *Chem. Res. Toxicol. 4*, 592-604.

Krenitsky, T. A., Rideout, J. L., Chao, E. Y., Koszalka, *G.* W., Gurney, F., Crouch, R. C., Cohn, N. K., Wolberg, *G.,* and Vinegar, R. (1986) Imidazo[4,5-c]pyridines (3-deazapurines) and their nucleosides as immunosuppressive and antiinflammatory agents. J. *Med. Chem.* 29, 138-143.

Kochetkov, N.K., Shibaev, V.N., Kost, A.A. (1971) New reaction of adenine and cytosine derivatives, potentially useful for nucleic acid modifications. *Tetrahedron Lett. 22*, 1993-1996.

Kodama, T., Greenberg, M. M. (2005) Preparation and analysis of oligonucleotides containing lesions resulting from C5'-oxidation. *J. Org. Chem. 70*, 9916-9924.

Kuśmierek, J. T., Folkman, W., and Singer, B. (1989) Synthesis of N^2,3-ethenodeoxyguanosine, N^2,3-ethenodeoxyguanosine 5'-Phosphate, and N^2,3-ethenodeoxyguanosine 5'-Triphosphate. Stability of the Glycosyl Bond in the Monomer and in Poly(dG, εdG-dC). *Chem. Res. Toxicol. 2,* 230-233.

Kyaw M., Yoshizumi M., Tsuchiya K. (2004) Atheroprotective effects of antioxidants through inhibition of mitogen activated kinases. *Acta. Pharmacol. Sin. 25,* 977-985.

Laib, R.J., Bolt, H.M. (1977) Alkylation of RNA by vinyl chloride metabolites in vitro and in vivo: formation of 1, N^6-ethenoadenosine. *Toxicology 8*, 185-195.

Laib R.J., Bolt, H.M. (1978) Formation of 3,N^4-ethenocytidine moieties in RNA by vinyl chloride metabolites in vitro and in vivo. *Arch. Toxicol. 39*, 235-240.

Lang, B., and Maier, P. (1986) Lipid peroxidation dependent aldrin epoxidation in liver microsomes, hepatocytes and granulation tissue cells. *Biochem. Biophys. Res. Commun. 138*, 24-32.

Ledoux, S. P., Druzhyna, N. M., Hollensworth, S. B., Harrison, J. F., Wilson G. L. (2007) Mitochondrial DNA repair: A critical player in the response of cells of the CNS to genotoxic insults. *Neuroscience 145*, 1249-1259.

Li, L., Karlin, K. D., Rokita, S. E. (2005) Changing selectivity of DNA oxidation from deoxyribose to guanine by ligand design and a new binuclear copper complex . *J. Am. Chem. Soc. 127*, 520-521.

Luo, W., Muller, J. G., Burrows, C. (2001) The pH-dependent role of superoxide in riboflavin-catalyzed photooxidation of 8-oxo-7,8-dihydroguanosine. *J.Org. Lett. 3*, 2801-2804.

Luo, W., Muller, J. G., Rachlin, E. M., and Burrows, C. J. (2000) Characterization of spiroiminodihydantoin as a product of one-electron oxidation of 8-oxo-7,8-dihydroguanosine. *Org. Lett. 2*, 613-616.

Luo, W., Muller, J. G., Rachlin, E. M., Burrows, C.J. (2001) Characterization of hydantoin products from one-electron oxidation of 8-oxo-7,8-dihydroguanosine in a nucleoside model. *Chem. Res. Toxicol. 14,* 927-938.

Lupatelli, P., Saladino, R., Minicione, E. (1993) Oxidation of uracil derivatives and pyrimidine nucleosides by dimethyldioxirane: A new and mild synthesis of 5,6-oxiranyl-5,6-dihydro and 5,6-Dihydroxy-5,6-dihydro-derivatives. *Tetrahedron Lett. 34*, 6313-6316.

Mandelker L. (2008) Introduction to oxidative stress and mitochondrial dysfunction. *Vet. Clin. Small Anim*. *38*, 1-30

Marnett, L. J. (1987) Peroxyl free radicals: Potential mediators of tumor initiation and promotion. *Carcinogenesis 8*, 1365-1373.

Maufrais, C., Fazakerley, G. V., Cadet, J., Boulard, Y. (2003) Structural study of DNA duplex containing an N-(2-deoxy-beta-D-erythro-pentofuranosyl) formamide frame shift by NMR and restrained molecular dynamics. *Nucl. Acids Res. 31*, 5930-5940.

McCallum, J. E. B., Kuniyoshi, C. Y., and Foote, C. S. (2004) Characterization of 5-hydroxy-8-oxo-7,8-dihydroguanosine in the photosensitized oxidation of 8-oxo-7,8-dihydroguanosine and its rearrangement to spiroiminodihydantoin. *J. Am. Chem. Soc. 126*, 16777-16782.

Miyamoto, S., Martinez, G.R., Medeiros, M. H. G., Di Mascio, P. (2003) Singlet molecular oxygen generated from lipid hydroperoxides by the russell mechanism: studies using ^{18}O-labeled linoleic Acid hydroperoxide and monomol light emission measurements. *J. Am. Chem. Soc. 125*, 6172-6179.

Miyamoto, S., Martinez, G. R., Rettori, D., Augusto, O., Medeiros, M. H. G., Di Mascio, P. (2006) Linoleic acid hydroperoxide reacts with hypochlorous acid, generating peroxyl radical intermediates and singlet molecular oxygen. *Proc. Natl. Acad. Sci. USA*, *103*, 293-298.

Müller, M., Hutchinson, L. K., and Guengerich, F. P. (1996) Addition of deoxyribose to guanine and modified bases by *lactobacillus helveticus trans-N*-deoxyribosylase *Chem. Res. Toxicol. 9*, 1140-1144.

Murray, R. W. (1989) Dioxiranes. *Chem. Rev.89*, 1187-1201.

Murray, R. W., and Jeyaraman, R. (1985) Dioxiranes: Synthesis and reactions of methyldioxiranes. *J. Org. Chem. 50*, 2847-2853.

Nackerdien, Z., Kasprzak, K. S., Rao, G., Halliwell, B., and Dizdaroglu, M. (1991). Nickel(II)- and cobalt(II)-dependent damage by hydrogen peroxide to the DNA bases in isolated human chromatin. *Cancer Res. 51,* 5837-5842.

Nair, J., Barbin A., Velic, I., Bartsch, H. (1999) Etheno DNA-base adducts from endogenous reactive species. *Mut. Res. 424*, 59-69

Nair, J., Sone, H., Nagao, M., Barbin, A., Bartsch, H. (1996) Copperdependent formation of miscoding etheno-DNA adducts in the liver of Long Evans Cinnamon LEC. rats developing hereditary hepatitis and hepatocellular carcinoma. *Cancer Res. 56*, 1267-1271.

Nair, J., Vaca, C.E., Velic, I., Mutanen, M., Valsta, L.M,. Bartsch, H. (1997) High dietary v-6 polyunsaturated fatty acids drastically increase the formation of etheno-DNA base adducts in white blood cells of female subjects. *Cancer Epidemiol. Biomarkers Prev. 6*, 597-601.

Nam, W., Kim, H., Hoon J. S., Raymond, K., Ho, Y. N., Valentine, J. S. (1996) Nickel complexes as antioxidants. Inhibition of aldehyde autoxidation by nickel(II) tetraazamacrocycles. *Inorg. Chem. 35,* 1045-1049.

Neeley, W. L., Essigmann, J. M. (2006) Mechanisms of formation, genotoxicity, and mutation of guanine oxidation Products. *Chem. Res. Toxicol. 19*, 491-505.

Niles, J. C., Wishnok, J. S., and Tannenbaum, S. R. (2001) Spiro-iminodihydantoin is the major product of the 8-oxo-7,8-dihydro-guanosine reaction with peroxynitrite in the presence of thiols and guanosine photooxidation by methylene blue. *Org. Lett. 3*, 963-966.

Olofson, A., Yakushijin, K., and Horne, D. A. (1998) Unusually large ^{13}C NMR chemical shift differences between neutral and protonated glycocyamidines. New insights on previously reported chemical shift assignments and chemical properties. *J. Org. Chem. 63*, 5787-5790.

Otting, G., Messerle, B. A., and Soler, L. P. (1996) ^{1}H-Detected, gradient-enhanced ^{15}N and ^{13}C NMR experiments for the measurement of small heteronuclear coupling constants and isotopic shifts. *J. Am. Chem. Soc. 118*, 5096-5102.

Pratviel, G., Meunier, B. (2006) Guanine oxidation: one- and two-electron reactions. *Chem. Eur. J. 12*, 6018-6030.

Ravanat, J. L., Douki, T., Incardona, M. F., and Cadet, J. (1993) HPLC separations of normal and modified nucleobases and nucleosides on an amino silica gel column. *J. Liq. Chromatogr. 16*, 3186-3202.

Ravanat, J. L., and Cadet, J. (1995) Reaction of singlet oxygen with 2′-deoxyguanosine and DNA. isolation and characterization of the main oxidation products. *Chem. Res. Toxicol. 8*, 379-388.

Read, J. M., and Goldstein, J. H. (1965) The proton magnetic resonance and ^{13}C-H satellite spectra of aqueous purine, and their pH dependence. *J. Am. Chem. Soc. 87*, 3440-3445.

Reed, G. A., and Ryan, M. J. (1990) Peroxyl radical-dependent epoxidation of cyclopenteno[c,d]pyrene. *Carcinogenesis 11*, 1825-1829.

Reuben, J. (1985) Isotopic multiplets in the carbon-13 NMR spectra of polyols with partially deuterated hydroxyls. 5. *β*-Diols. *J. Am. Chem. Soc. 107*, 1756-1759.

Porter, N. A., Yin, H., Pratt, D. A. (2000) The peroxy acid dioxirane equilibrium: base-promoted exchange of peroxy acid oxygens. *J. Am. Chem. Soc. 122*, 11272-11273.

Russell, G. A. (1957) Deuterium-isotope Effects in the Autoxidation of Aralkyl Hydrocarbons. Mechanism of the Interaction of Peroxy Radicals. *J. Am. Chem. Soc. 79*, 3871-3877.

Ryu, E. K., MacCoss, M. (1981) New procedure for the chlorination of pyrimidine and purine nucleosides. *J. Org. Chem. 46*, 2819-2823.

Sattsangi, P. D., Leonard N. J., and Frihart, C. R. (1977) 1,N^2-Ethenoguanine and N^2,3-ethenoguanine, synthesis and comparison of the electronic spectral properties of these linear and angular triheterocycles related to the Y bases. *J. Org. Chem. 42*, 3292-3296.

Scheller, N., Sangaiah, R., Ranasinghe, A., Amarnath, V., Gold, A., and Swenberg, J. A. (1995) Synthesis of [4,5,6,8-^{13}C4]guanine, a reagent for the production of internal standards of guanyl DNA adducts. *Chem. Res. Toxicol. 8*, 333-337.

Sheu, C., Foote, C. S. (1993) Endoperoxide formation in a guanosine derivative, *J. Am. Chem. Soc. 115*, 10446-10447.

Sheu, C., Foote, C. S. (1995) Photosensitized oxygenation of a 7,8-dihydro-8-oxoguanosine derivative. formation of dioxetane and hydroperoxide intermediates. *J. Am. Chem. Soc. 117*, 474-477.

Simakov, P. A., Choi, S.-Y., and Newcomb, M. (1998) Dimethyl-dioxirane hydroxylation of a hypersensitive radical probe: Supporting evidence for an oxene insertion pathway. *Tetrahedron. Lett. 39*, 8187-8190.

Sowers, L. C., Mhaskar, D. N., Khwaja, T. A., and Goodman, M. F. (1989) Preparation of imino and amino N-15 enriched 2-aminopurine deoxynucleoside. *Nucleosides Nucleotides* 8, 23-34.

Spengler, S., Singer, B. (1981) Transcriptional errors and ambiguity resulting from the presence of 1,N^6-ethenoadenosine or 3,N^4-ethenocytidine in polyribonucleotides, *Nucleic Acids Res. 9*, 365-373.

Srivastava, P. C., Robins, R. K., and Meyer, R. B. (1988) Synthesis and properties of purine nucleosides and nucleotides. In *Chemistry of nucleosides and nucleotides* (Townsend, L. B., Ed.) pp 113-281, Plenum Press, New York.

Standeven, A. M., and Wetterhahn, K. E. (1991). Is there a role for reactive oxygen species in the mechanism of chromium(VI) carcinogenesis? *Chem. Res. Toxicol. 4*, 616-625.

Stothers, J. B. (1972) A survey of ^{13}C spin-spin couplings. *In Carbon-13 NMR Spectroscopy*, Academic Press, New York. pp331-385

Sugden, K. D., Martin, B. D. (2002) Guanine and 7,8-Dihydro-8-Oxo-Guanine–Specific Oxidation in DNA by Chromium(V). *Environ. Hlth. Persp. 110* , 725-728.

Suzuki, T., Friesen, M. D., Ohshima, H. (2003) Formation of a Diimino-Imidazole Nucleoside from 20-Deoxyguanosine by Singlet Oxygen Generated by Methylene Blue Photooxidation. *Bioorg. Med. Chem.*, *11*, 2157-2162.

Swenberg, J. A., La, D. K., Scheller, N. A., Wu, K.Y. (1995) Dose-response relationships for carcinogens, *Toxicol. Lett. 82/83*, 751-756.

Tomasz, M., Lipman, R., Lee, M. S., Verdine, G. L., and Nakanishi, K. (1987) Reaction of acid-activated mitomycin C with calf thymus DNA and model guanines: Elucidation of the base-catalyzed degradation of *N7*-alkylguanine nucleosides. *Biochemistry 26*, 2010-2027.

Tudek, B. (2003) Imidazole ring-opened DNA purines and their biological significance. *Journal of Biochemistry and Molecular Biology 36*, 12-19.

Valko, M., Morris, H., Cronin, M.T. (2005) Metals, toxicity and oxidative stress. *Curr. Med. Chem. 12*, 1161-208.

Vialas, C., Claparols, C., Pratviel, G., and Meunier, B. (1998) Efficient oxidation of 2′-deoxyguanosine by Mn-TMPyP/KHSO5 to imidazolone dIz without formation of 8-oxo-dG. *J. Am. Chem. Soc. 120*, 11548-11553.

Vialas, C., Claparols, C., Pratviel, G., and Meunier, B. (2000) Guanine oxidation in double-stranded DNA by Mn-TMPyP/KHSO5: 5,8-dihydroxy-7,8-dihydroguanine residue as a key precursor of imid-azolone and parabanic acid derivatives. *J. Am. Chem. Soc. 122*, 2157-2167.

Williams G. M., Jeffrey A. M. (2000) Oxidative DNA Damage: Endogenous and chemically induced. *Regulatory Toxicology and Pharmacology 32*, 283-292.

Xu, X., Muller, J. G., Ye, Y., Burrows, C. J. (2008) DNA−Protein Cross-links between Guanine and Lysine Depend on the Mechanism of Oxidation for Formation of C5 vs C8 Guanosine Adducts. *J. Am. Chem. Soc. 130*, 703-709.

Ye, W., Sangaiah, R., Degen, D. E., Gold, A., Jayaraj, K., Koshlap, K. M., Boysen, G., Williams, J., Tomer K. B., Ball, L. M. (2006) A 2-Iminohydantoin from the Oxidation of Guanine. *Chem. Res. Toxicol. 19*, 506-510.

Yen, T.Y., Christova-Gueoguieva, N.I., Scheller,N., Holt, S., Swenberg, J.A., Charles, M.J. (1996) Quantitative analysis of DNA adduct N^2,3-ethenoguanine using liquid chromatography/electrospray ionisation mass spectrometry. *J. Mass Spectrom. 311,* 1271-1276.

Yin, H., Porter, N. (2005) A. New Insights Regarding the Autoxidation of Polyunsaturated Fatty Acids. *Antioxid. Redox. Signal. 7*, 170-184.